Aspects of Cyclodextrin Host-Guest Complexes in Mass Spectrometry

Inauguraldissertation

der Philosophisch-naturwissenschaftlichen Fakultät

der Universität Bern

vorgelegt von

Pia Simona Bruni

von Stocken-Höfen BE

Leiter der Arbeit:

Prof. Dr. Stefan Schürch

Departement für Chemie, Biochemie und Pharmazie

Universität Bern

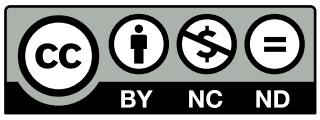

Aspects of Cyclodextrin Host-Guest Complexes in Mass Spectrometry

Inauguraldissertation
der Philosophisch-naturwissenschaftlichen Fakultät
der Universität Bern

vorgelegt von

Pia Simona Bruni

von Stocken-Höfen BE

Leiter der Arbeit:

Prof. Dr. Stefan Schürch
Departement für Chemie, Biochemie und Pharmazie
Universität Bern

Von der Philosophisch-naturwissenschaftlichen Fakultät angenommen.

Bern, 29. April 2022 Der Dekan:

Prof. Dr. Zoltan Balogh

But I don't see myself as a woman in science.
I seem myself as a scientist.

Donna Strickland (1959–present)

Acknowledgment

First of all, I want to thank Prof. Dr. Stefan Schürch for giving me the possibility to carry out my thesis in his research group. I had the chance to learn a lot during these four years, not only from a scientific but also from a personal point of view. I want to thank Prof. Dr. Britta Lundström-Stadelmann for taking over the role of the co-supervisor of my thesis for the last year. My thank also goes to Prof. Dr. Götz Schlotterbeck for accepting to be my co-referee and for reviewing my PhD thesis, and to Prof. Dr. Robert Häner for chairing the examination committee.

I am very thankful for the support I received from the members of the research group, namely Rahel Eberle, Claudia Bühr, Urs Kämpfer, Andrea Bill, and Thomas Muggli, as well as all Bachelor and Master students I've had the pleasure to work with in the last years. I greatly appreciated the many professional and personal discussions we had.

I would also like to express my gratitude to my family for their constant support, and my friends for accepting my limited time and the canceled appointments. I'm looking forward to spending more time with you! Finally, a special thank goes to Florian. This work would not have been successfully accomplished without his constant support and patience.

Abstract

Cancer is a widely spread disease leading to uncontrolled cellular replication that caused 9.6 million deaths worldwide in 2018. One approach in cancer treatment is inhibiting the replication process by the administration of organometallic compounds that bind to DNA. Cisplatin is one of the most prominent organometallic compounds that reached clinical approval. However, it suffers from severe side effects (e.g., nephrotoxicity) and causes the development of resistance. Various other metallorganic drugs have been evaluated for their potential in cancer treatment. Thereof, titanocene dichloride had entered clinical trials, but showed only low patient efficacy. Titanocene dichloride is a representative of the class of the bent metallocene dihalides that comprise a tetrahedral structure with two cyclopentadienyl and two halogenide ligands and a metal ion as central atom. Hydrolysis of the halogenide ligands is a crucial step in the activation of the metallocene, allowing for the interaction with its biological target. Unfortunately, extensive hydrolysis of the halogenide and the cyclopentadienyl ligands is detected for titanocene in aqueous environment at physiological conditions, leading to its inactivation. One approach for increasing the hydrolytic stability of titanocene is its inclusion within the cavity of a macrocyclic host structure. Cyclodextrins are such macrocyclic compounds composed of six to eight 1,4-linked α-D-glucopyranose units that are considered nontoxic upon oral administration. Therefore, several aspects of cyclodextrin host-guest complexes in mass spectrometry have been investigated and are discussed in this thesis.

In the first section, the mass spectrometric behavior of cyclodextrins is discussed. The central part of this project was the elucidation of the fragmentation mechanism underlying the decomposition of protonated cyclodextrins. Linearization of the macrocyclic structure upon charge-induced cleavage of a glycosidic bond has been revealed as the initial dissociation step. Further decomposition of the linearized structure is characterized by neutral loss of glucose subunits. This dissociation step has been stated to occur upon charge-remote cleavage of other glycosidic bonds, leading to the elimination of a zwitterionic moiety which is potentially internally rearranged.

In the second section, the focus is laid on the interaction between titanocene and cyclodextrins elucidated from mass spectrometric experiments. The obtained data indicated the formation of covalent bonds between titanium and the hydroxy groups

at the rim of cyclodextrins rather than the formation of an inclusion complex. Consequently, improvement of the hydrolytic stability of titanocene at physiological pH was not obtained by the interaction of titanocene with cyclodextrins.

In-source fragmentation has been found to contribute considerably to the ions detected in full scan mass spectrometry. Therefore, the effect of instrumental parameters on the quality of the obtained full scan mass spectra has been evaluated. While the capillary voltage showed only minor effects, proper adjustment of the capillary temperature and the tube lens voltage significantly improved the quality of the obtained data.

In conclusion, diverse aspects of cyclodextrin host-guest complexes have been successfully investigated using mass spectrometry showing the potential of this analytical technique for various applications.

Table of Contents

1 Introduction

Cancer is a widely spread disease diagnosed to one in five people globally within their lifetime. In 2018, 18.1 million new cases were reported globally, and it caused one in six deaths worldwide, corresponding to 9.6 million deaths. Thereof, lung (18.4%), colorectal (9.2%), and stomach cancer (8.2%) are the leading causes of death.

Cancer can affect any part of the body, leading to uncontrolled cellular replication. This is caused by accumulated DNA mutation, leading to disturbed processes during cell replication or missing reparation mechanisms. External influences, such as exposure to UV light or smocking, may increase cancer risk. The abnormal cancer cells can also spread throughout the body, affecting other tissues (metastasis) [1–3].

1.1 Cancer Treatment

Disturbance of cellular replication is a defining feature of cancer. As many cellular processes are involved in the replication process, as many potential targets are present to tackle for treatment [2, 4]. Chemotherapy makes use of this approach. The administered drugs interact with endogenous compounds in order to reduce cell replication and destroy affected tissue [2, 4].

Frequently targeted endogenous compounds are DNA and proteins related to cell replication [3–5]. One approach in targeting DNA is the delivery of modified nucleosides, such as gemcitabine (2',2'-difluordesoxycytidine). During the cell replication process, the activated gemcitabine is integrated instead of cytidine, which interrupts the DNA synthesis and induces cell death [6]. Another approach is the administration of drugs binding to DNA (e.g., metallodrugs). Due to this interaction, the structure of DNA is altered, hampering its replication and transcription [5].

A major drawback of these approaches is their systemic effect. This means not only cancerous cells are targeted, but the entire organism, which may cause severe side effects, such as toxicity [4, 7].

1.1.1 Organometallic Drugs

Organometallic compounds are promising drugs for anticancer treatment. One of the most famous of those is cisplatin (*cis*-diammineplatinum(II) dichloride). After its first synthesis in 1845, Rosenberg discovered in 1965 the antiproliferative potential of cisplatin, which led to its clinical approval for cancer treatment in 1978 [8–10]. Cisplatin comprises a square planar structure with a platinum(II) coordination center surrounded by two ammine and two chloro ligands in cis position (figure 1.1) [10].
In aqueous environment, the two chloro ligands undergo rapid hydrolysis, leading to the active form of cisplatin. This results in activation of the complex and allows for interaction with biomolecules [10–12]. Its anticancer activity occurs due to the formation of inter- and intra-strand crosslinks of the activated cisplatin between two adjacent guanines in double stranded DNA, inhibiting the replication process [8, 12–16]. Cisplatin is mainly used in the treatment of solid-organ cancer, such as lung, ovarian, and breast cancer [16]. However, treatment with cisplatin causes severe side effects, such as nephrotoxicity and the development of resistance of certain tumors. Nephrotoxicity is caused by the accumulation of cisplatin within the kidney upon its excretion. It interacts with the DNA of renal epithelial cells, inducing cell death [16]. Interaction of cisplatin with biomolecules other than DNA, is a plausible explanation for the development of resistance as the overexpression of the cellular compartments dedicated to the excretion of biomolecule-xenobiotic assemblies also leads to impelled excretion of cisplatin [7, 10].

To overcome the drawbacks of cisplatin, over 30 different modified platin-based drugs have been developed that comprise modified ligands (figure 1.1) [7]. Thereof, only carboplatin and oxaliplatin, in addition to cisplatin, became globally used as anticancer agents. Other platin-based drugs have been locally approved, such as nedaplatin in Japan, lobaplatin in China, and heptaplatin in Korea (figure 1.1) [7, 12]. Compared to cisplatin, carboplatin and nedaplatin retain the ammine ligands, whereas the two chloro ligands are exchanged by a bidentate cyclobutane dicarboxylato or a glycolato ligand, respectively. In case of oxaliplatin, lobaplatin, and heptaplatin, the chloro ligands are exchanged by a bidentate oxalato, oxidopropanoato, and malonato ligand, respectively, and the two ammine-ligands are linked by a cyclohexane, cyclobutandimethyl, or isopropyl dioxolane dimethyl, respectively [7, 8, 12, 14, 15, 17]. With these alterations of the labile ligands of cisplatin to more stable alternatives, rapid interaction with biomolecules other than the desired target is decreased, and toxicity could be reduced [7].

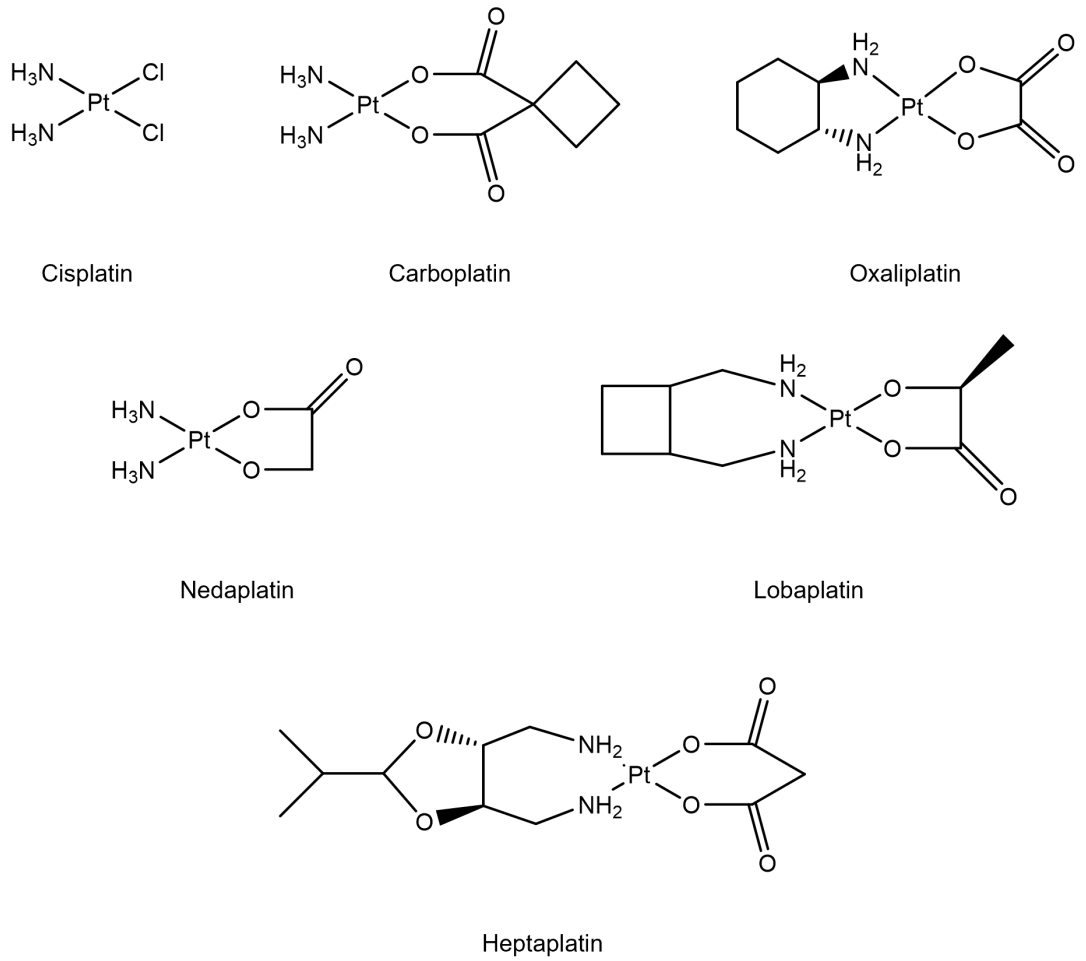

Figure 1.1: Structures of the platinum based anticancer agents cisplatin, oxaliplatin, carboplatin, nedaplatin, lobaplatin, and heptaplatin.

Besides modifying ligands of platinum complexes, organometallic complexes containing various other metals (Ru, Fe, Co, Cu, Au, Ag, Pd, Ga, Rh, Sn, Os, Ir) have been examined for their potential as cytostatics [8, 15, 18–24]. Thereof, ruthenium, gold, and silver complexes are briefly discussed in the next paragraphs.

Ruthenium

Ruthenium-based complexes with Ru(II) or Ru(III) as coordination centers have been discovered and have shown anticancer activity [23, 24]. Representatives of ruthenium(III) complexes are *fac*-$[Ru(Cl)_3(NH_3)_3]$ and NAMI-A (*trans*-[tetrachloro(dimethylsulfoxide)(imidazole)-ruthenate(III)]) (figure 1.2). The *fac*-$[Ru(Cl)_3(NH_3)_3]$ complex showed activity, but was not applicable for clinical use due to its low aqueous solubility [25]. NAMI-A, on the other hand, entered clinical trials and is used in the treatment of metastatic non-small-cell lung carcinoma

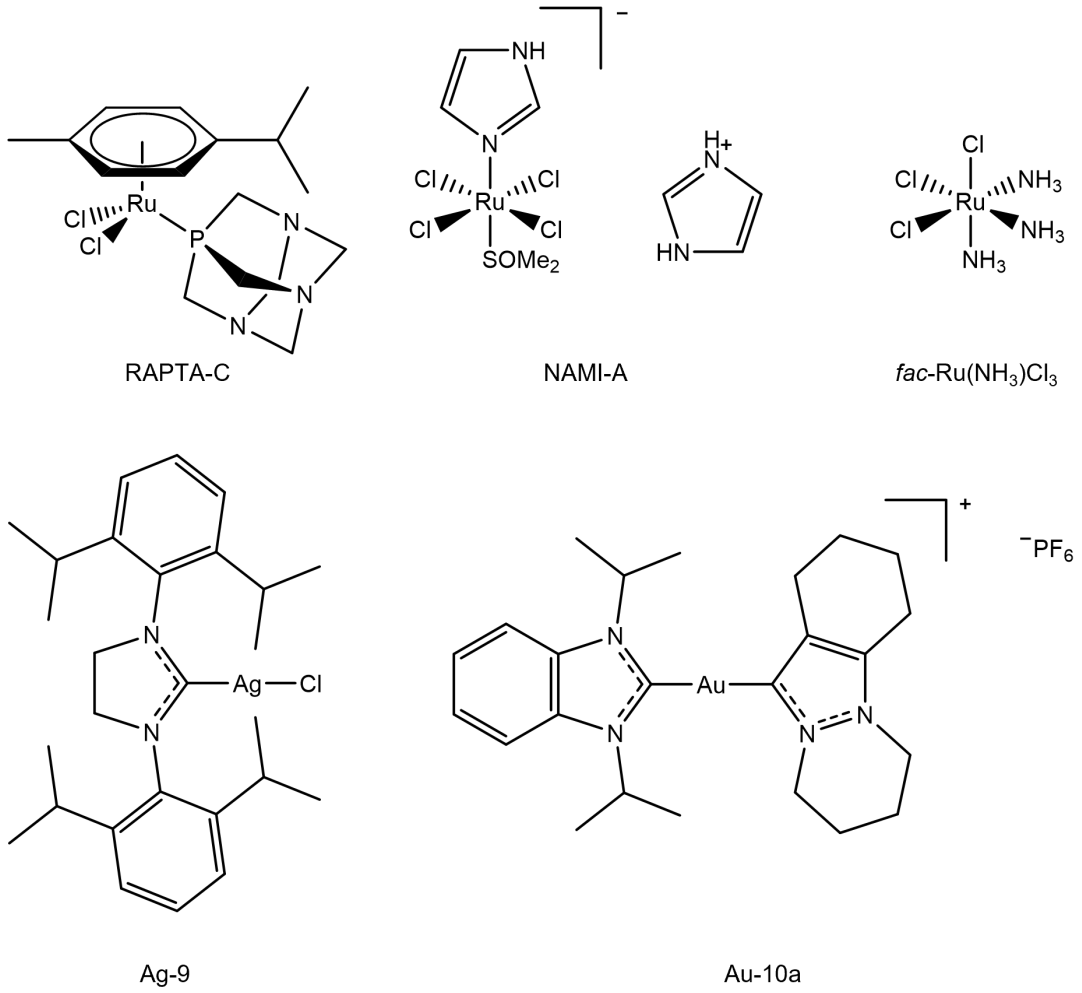

Figure 1.2: Examples of ruthenium-, silver-, and gold-based drugs: NAMI-A, *fac*-$Ru(NH_3)_3Cl_3$, RAPTA-C, Ag-9, and Au-10a.

[8, 18, 19, 25]. Ruthenium(II) complexes with η^5-cyclopentadienyl and η^6-arene ligands showed promising results against diverse human cancer cell lines [20, 25]. The class of η^6-arene ruthenium(II) anticancer compounds includes the RAPTA complexes, containing a 1,3,5-triaza-7-phosphaadamantane (PTA) group. The RAPTA-C complex ($Ru(\eta^6-p-cymene)(pta)Cl_2$), for example, showed inhibition of lung metastasis in CBA mice bearing the MCa mammary carcinoma (figure 1.2) [8, 18–20, 25].

Silver and Gold

Silver- and gold-based N-heterocyclic carbenes have already found application in treatment of bacterial infections or rheumatoid arthritis. Subsequently, they have been examined for anticancer activity [19, 23, 24]. A series of silver- and gold complexes have been described by Hackenberg and Tacke [19]. In comparison

to cisplatin, the silver(I) complex "Ag-9" (figure 1.2) shows a 350-fold increased activity against a breast cancer cell line (MCF-7) and the gold(I) complex "Au-10a" (figure 1.2) shows higher activity against non-small lung cancer cells [19].

1.1.2 Metallocene Dihalides

With the development of the anticancer properties of titanocene dichloride by Köpf and Köpf-Maier in 1979, the field of bent metallocene dihalides as potential anticancer agents emerged [9, 10, 21, 24, 26]. Bent metallocene dihalides comprise a tetrahedral structure with a metal center, two halogenide (mainly chloride), and two cyclopentadienyl ligands (figure 1.3A). In these so-called sandwich complexes, the cyclopentadienyl ligands are bound in a η^5-manner with an angle of $< 180\,^\circ$ between each other, and the coordination center is usually a transition metal (e.g., Ti, V, Nb, Mo, Zr, Ta, W, Hf) in the +IV oxidation state [10, 18, 27].

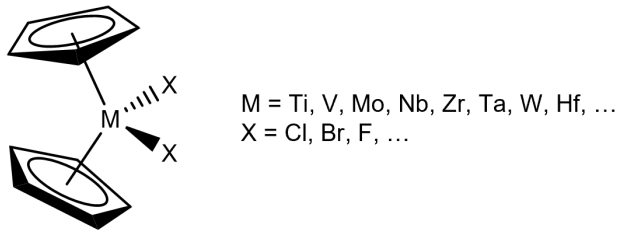

Figure 1.3: General structure of bent metallocene dihalides.

Research on the anticancer activity of bent metallocene dihalides even led to the entrance of titanocene dichloride into phase I clinical trials, revealing nephrotoxicity, hypoglycemia, and pain during infusion, among others, as dose-limiting side effects [28]. However, some phase II clinical trials for treatment of advanced renal cell carcinoma [29] and breast metastatic carcinoma [30] have been carried out, showing low patient efficacy [9, 10, 15, 21, 22, 31]. Other metallocene dihalides have been found to show anti-proliferative effects *in vivo* and *in vitro* [27, 32]. Titanocene(IV)dichloride has been shown to have anti-proliferative effects on human ovarian carcinoma cell lines (A2780, CH1) and, especially, on the platinum-resistant variants (2780CP, CH1 cisR) [9, 33]. Molybdenocene(IV)dichloride has also been investigated against breast cancer (MCF-7) and colon cancer (HT-29) cell lines [34, 35], and vanadovene inhibits the proliferation of human breast cancer cells (BT-20) and glioblastoma cells (U373) [36]. The anticancer activity of further metallocnes have been summarized by Harding and Mokdsi [27], including the *in vitro* activity of highest concentrations of zirconocene(IV)dichloride and hafnocene(IV)dichloride, or lowest concentration of vanadocene(IV)dichloride against Ehrlich ascites tu-

mours. As chlorides are the most frequently used halogenide ligands in metallocenes dihalides, they are usually not mentioned explicitly. Therefore, if the halogenide ligands are not stated, the respective metallocene dichloride is meant.

Hydrolysis

Analogously to platinum compounds, the hydrolysis of metallocene ligands plays a crucial role in the activation and the degradation of these metallocene anticancer agents. The hydrolysis rates of the halogenide and cyclopentadienyl ligands are dependent on the identity of the transition metal, the halogenide ligand, and the pH of the solution [27]. Hydrolysis of the first chloro ligand of metallocenes (M = Ti, V, Mo, Zr) occurs immediately after getting in contact with water, leading to aqua- and hydroxo-species (figure 1.4) [22, 27, 31, 36–40]. The second chloro ligand is dissociated with a half-live of about 50 min for titanocene, 30 min for vanadocene, 24 min for zirconocene, and 6.7 min for molybdenocene [9, 27]. With the hydrolysis of the chloro ligands, the pH decreases to acidic condition (pH $\sim$ 3) [27]. At this pH, the cyclopentadienyl ligands remain bound to the metal center for 14 h up to 4 weeks (Zr < Ti < V < Mo) [22, 27, 34, 41]. At a higher pH ($\sim$ 7) hydrolysis of the cyclopentadienyl ligands is induced, leaving behind insoluble metal oxide species that precipitate and are biologically inactive [9, 21, 27, 42, 43]. A general hitch in the pharmaceutical application of metallocenes is their poor solubility and stability, resulting in a low bioavailability [21, 37].

1.1.2.1 Modified Metallocene Dihalides

In order to improve solubility, stability, and activity, and reduce side effects of metallocenes, alteration of the halogenide ligands and modification of the cyclopentadienyl ligands are promising approaches [9, 21, 31, 37, 39, 43]. As the lability of the chloride ligand is mandatory for its anticancer activity, alteration of this part of the metallocene will undoubtedly affect its biological activity [21]. Replacement of the chloride with other halogenides (bromine, iodine [44]), or organic structures have been investigated [21]. Experiments on a derivative having a chloride exchanged by a dibenzothiophene (figure 1.5A), for example, showed activity against human colon cancer cell lines [21].

Modifications at the cyclopentadienyl ligands can alter the interaction strength between the ligand and the central ion [21]. This decelerates the hydrolysis rate of the cyclopentadienyl ligands at physiological pH, which stabilizes the metallocene complex against degradation. Furthermore, modifications introducing electron-withdrawing groups may alter the acidity of the central atom, and, as a

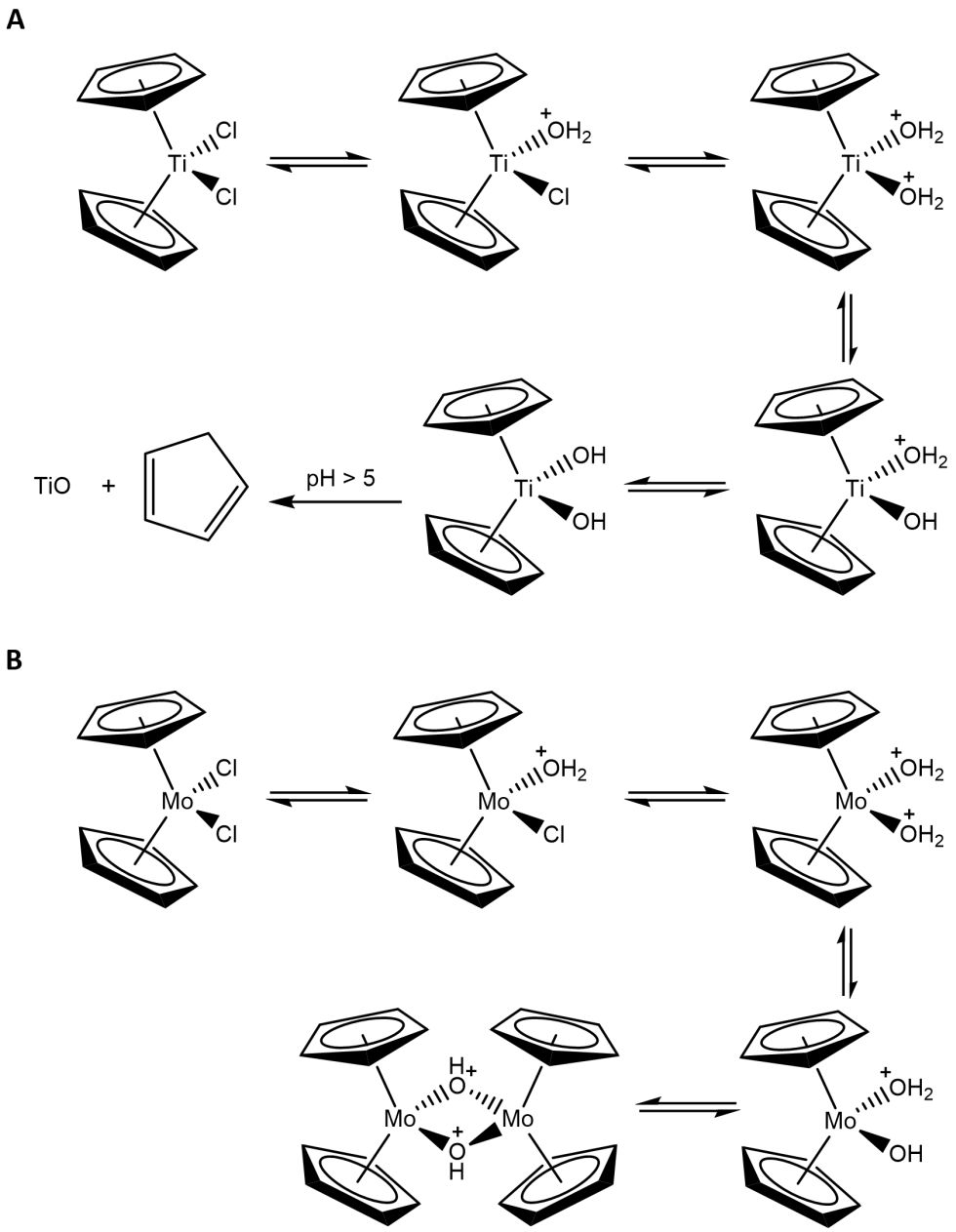

Figure 1.4: Hydrolysis products of A) titanocene dichlodride [27, 37, 42] and B) molybdenocene dichloride [21, 27, 40, 42].

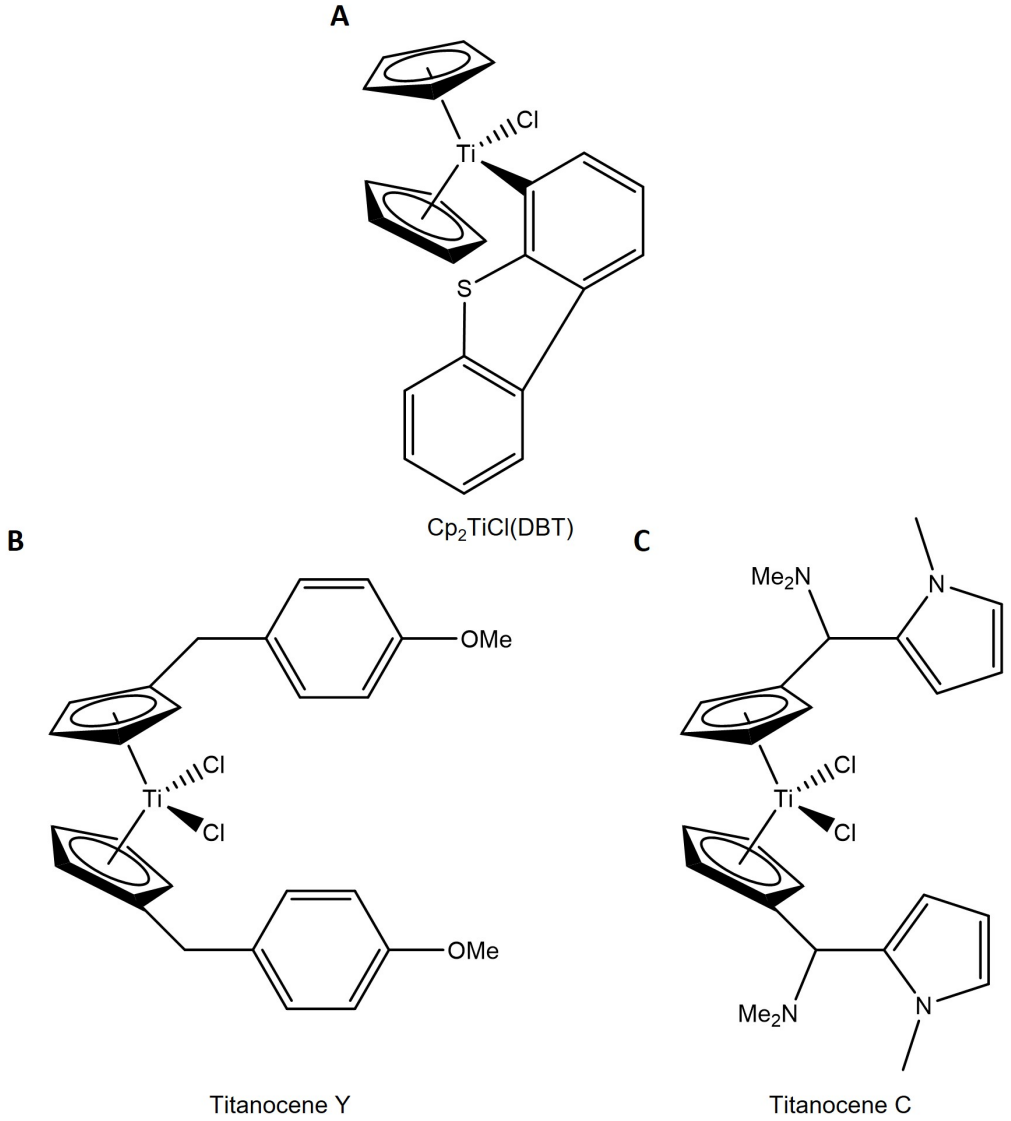

Figure 1.5: Examples of modified metallocenes: A) $Cp_2TiCl(DBT)$, B) titanocene Y, C) titanocene C.

consequence, also its interaction strength with biomolecules [21, 45, 46]. Several reviews [9, 10, 15, 39, 47] and studies on different series of modified metallocenes [35, 37, 46, 48, 49] cover the synthesis and evaluation of their toxicity. For example, modifications of the cyclopentadienyl ligands of titanocene have been studied by the research group of Matthias Tacke [31, 43, 50–52]. They synthesized, among others, titanocene Y (bis-[(p-methoxybenzyl)cyclopentadienyl] titanium(IV) dichloride, (figure 1.5B) and titanocene C (bis-(N,N-dimethylamino-2(N-methyl- pyrrolyl)-methyl-cyclopentadienyl) titanium(IV) dichloride (figure 1.5C). Titancoene Y has shown activity on long-life epithelial pig kidney cell lines (LLC-PK) [51], and stronger antiproliferative effects than titanocene dichloride against breast cancer

(MCF-7) and colon carcinoma (HT-29) cell lines [45]. Titanocene C has been tested for cytotoxic activity against a panel of cell lines, showing particularly high activity against small cell lung cancer (SCLC) cell lines [53].

1.1.3 Interaction with Biomolecules

As already mentioned for platinum compounds, the interaction of anticancer drugs with biomolecules is mandatory for their activity. Titanium deriving from titanocene dichloride has been found to accumulate in the nucleic acid-rich region of tumor cells, indicating DNA as target [22, 27, 54–56]. As a consequence, various studies focused on the interaction of bent metallocene dichlorides with DNA, oligonucleotides, and nucleobases [10, 22, 27, 36, 40, 57]. Using nuclear magnetic resonance (NMR) experiments, the interaction of titanocene with phosphate groups of nucleotides was revealed [44, 55, 58]. Further, mass spectrometric experiments showed an interaction with oxygen in phosphate groups of the oligonucleotide backbone and nucleobases [56, 59, 60]. Molybdenocene, on the other hand, interacts with nitrogen-containing nucleobases, with a preference for $G > A \sim C >> T$, as well as phosphate oxygens [56]. NMR experiments on niobocene showed no interaction with nucleosides and the nucleotides of guanine (dGMP), cytosine (dCMP), and uracil (dUMP), but with deoxyadenosine monophosphate (dAMP) [44]. This preference of metallocenes for specific interaction partners is in agreement with the Pearson hard-soft Lewis acid-base concept (HSAB) [56, 59, 61]. Titanium(IV) and niobium(IV) bear high charge densities, resulting in a hard Lewis acid character. Molybdenum(IV) is classified as intermediate, and platinum(II) as a soft Lewis acid [56]. In general, the higher the charge density on the transition metal, the harder its Lewis acid character. Hard Lewis acids preferably bind to hard Lewis bases, such as oxygen or fluoride, whereas soft Lewis acids rather interact with soft Lewis bases (e.g., Nitrogen, Sulphur), according to the Pearson concept [55].

Biomolecules other than DNA are also expected as targets for organometallic drugs, including proteins, peptides, and amino acids [18, 21]. These interactions can lead to stabilization, transport, or inactivation of the metallocenes, or even cause undesired side effects by impairing the biological function of the endogenous compounds [10, 21, 60–62]. Frequently investigated biomolecules are glutathione, serum albumin, and transferrin.

Glutathione is an ubiquitous protein in biological fluids, occurring in concentrations in the range of 1–10 mM. It is a tripeptide with the composition γ-Glu-Cys-Gly [63, 64]. Experiments on the interaction of titanocene, molybdenocene, and niobocene with glutathione at different pH showed no or little interaction for titanocene and

niobocene, respectively. In contrast, molybdenocene strongly interacts with the sulfur atom and the carboxy group of glycine [64], which is consistent with its intermediate Lewis acid character. This strong interaction with glutathione leads to the inactivation of the molybdenocene.

Human serum albumin (HSA) is the most abundant protein in human blood and is involved in metal transport [25, 27, 34, 65]. It is composed of 585 amino acids and has a molecular mass of 66.5 kDa. Studies on the interaction of molybdenocene dichloride towards HSA and DNA showed significantly more binding towards HSA [66]. Experiments evaluating the cellular uptake of titanocene derivatives in cancer cells in the presence or lack of serum albumin in media were performed. They showed increased uptake of a titanocene Y complex in the absence of serum albumin, whereas the cellular levels of a titanium-salan complex decreased in media lacking serum albumin [45].

Transferrin has a molecular mass of 80 kDa and occurs in a concentration of about 35 µM in the blood plasma. It is responsible for the endogenous transport of iron(III) [21, 27, 67]. Due to the similarity of titanium(IV) to iron(III), its transport via transferrin is frequently proposed. This hypothesis is supported by the demonstrated uptake of titanium(IV) within the iron(III) binding site of transferrin (figure 1.6) [9, 10, 21, 32, 65, 67–69]. In order to bind to the iron pocket of transferrin, the cyclopentadienyl ligands have to be abstracted from titanocene. This is easily feasible, as loss of the cyclopentadienyl ligands occurs rapidly in an aqueous environment at physiological pH [27, 67, 68].

These results show the potential of biomolecules as targets for metallocenes. The interaction of metallocenes with biomolecules can increase their stabilization and mediate their transport towards their target. However, irreversible binding to endogenous compounds may also cause the inactivation of the metallocenes.

In addition to these previously discussed plasma constituents, also other biomolecules such as ubiquitin [32, 35] and the DNA processing proteins protein kinase C and topoisomerase II [22, 27, 32, 36, 40] have been discussed as targets for metallcenes. These interactions may also be responsible for stabilization and transport, but metallation of proteins may induce loss of function, which serves as an alternative mechanism of action [10, 22, 32, 61].

Drawbacks of Metallocenes

The instability at physiological conditions and poor solubility of metallocenes is a mayor challenge in the formulation and administration of these drugs [18, 21, 46, 70]. Besides the discussed approaches of structural modification targeting

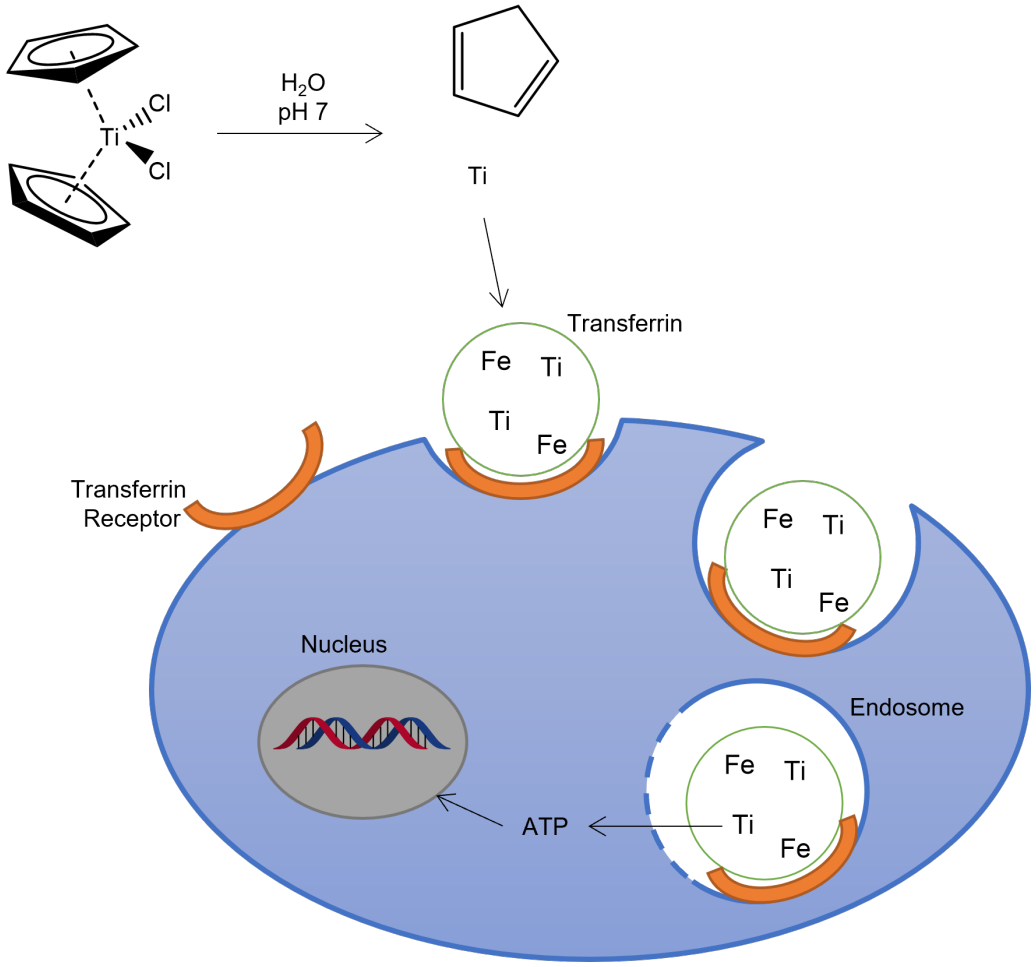

Figure 1.6: Proposed transferrin-mediated transportation of titan towards the cell nucleus according to Abeysinghe and Harding [21].

these drawbacks, the inclusion of metallocenes within host molecules has found application.

1.2 Host-Guest Complexes

Macrocyclic compounds are capable of acting as hosts for smaller guest compounds by incorporating them into their structure. The formation of host-guest complexes has found application in diverse fields [71].

In the pharmaceutical industry, the host-guest approach is, for example, used to control the transport and release of drugs [72, 73]. The ability of host molecules to stabilize volatile compounds by changing their physicochemical properties upon inclusion, or mask undesired flavors, odors, or bitterness, are beneficial for the application of host-guest complexes in the food and beverage industry [74]. The textile industry also made use uf host-guest complexes. First, as auxiliaries in the

dyeing process. Later, permanent fixation of hosts (e.g., cyclodextrins) on the fiber surface also allowed for generation of intelligent textiles [75]. Other applications are the extraction of metals, or as analytical separators (e.g., as stationary phase in chromatography) [71, 76–79].
In order to form such inclusion complexes, a guest molecule with hydrophobic properties is partially or entirely incorporated within the host structure [70, 80].

1.2.1 Hosts

In general, host molecules are composed of multiple subunits, forming macrocyclic structures. Depending on the character and the number of subunits forming the macrocycle, the properties and potential applications of the host are different. The subunits themselves can occur, for example, in linear, cyclic, or bicyclic forms. Examples of host molecules that are frequently used are cyclodextrins, cucurbiturils, calixarenes, and crown ethers.

1.2.1.1 Cyclodextrins

Cyclodextrins are macrocyclic oligosaccharides produced from natural degradation of starch [70, 81–83]. They are composed of 1,4-linked α-D-glucopyranose units, that are shaped like a truncated cone (figure 1.7A) [70–72, 80, 81, 84–87]. Due to the chair conformation of the sugar subunits, the primary hydroxy groups (located at the C6) are oriented towards the smaller rim, and the secondary hydroxy groups (located at the C2 and C3) are oriented towards the larger rim. The skeletal carbon atoms, on the other hand, point towards the interior of the cone, forming the hydrophobic cavity of the cyclodextrins [82, 85]. The most common cyclodextrins are α-, β-, and γ-cyclodextrin, that are composed of six, seven, or eight subunits, respectively [80–82, 84, 85, 87]. Depending on the number of subunits comprised in the macrocycle, the size of the cavity changes. The cavity diameter of α-cyclodextrin is ≈5.2 Å, whereas β- and γ-cyclodextrin have a diameter of ≈6.6 Å and ≈8.4 Å, respectively [81].
For some applications of cyclodextrin as a host, appropriate solubility is an essential factor for their use. With an aqueous solubility of 0.016 M, β-cyclodextrin is significantly less soluble than α- (0.12 M) and γ- (0.17 M) cyclodextrin [81, 85]. This phenomenon can be explained with the intramolecular hydrogen bonds formed between the hydroxy groups at the rims of cyclodextrin [80, 81, 85]. In aqueous solutions, the formation of aggregates through the self-assembly of cyclodextrins has been observed. These aggregates are either of transient nature, reducing

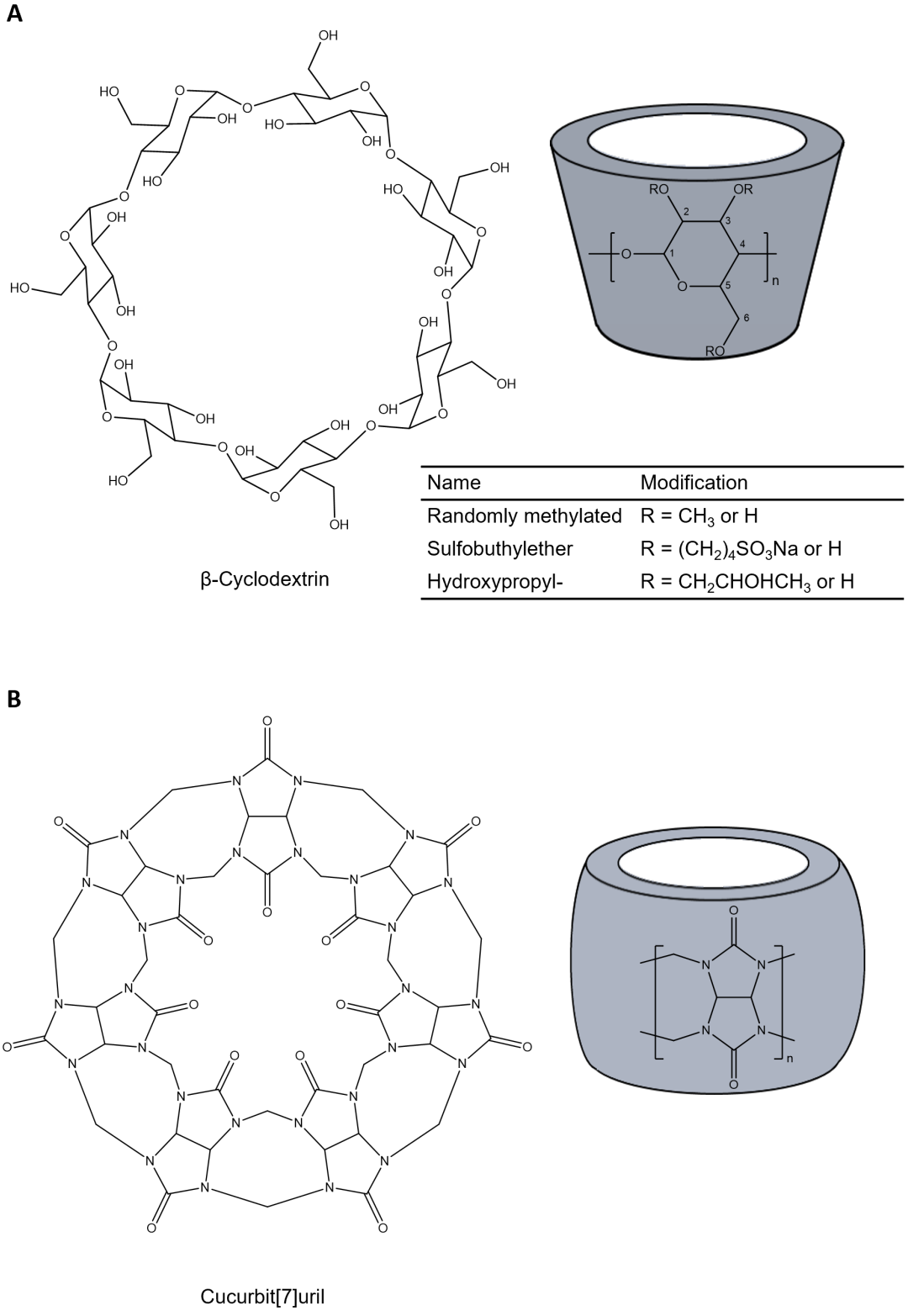

Figure 1.7: Examples of host structures: A) Chemical structure and sketch of the formed cone of β-cyclodextrin with examples of established modifications; B) Chemical structure and depiction of the cucurbit-like structure of cucurbit[7]uril.

their capability to act as host, or are of more persistent nature, resulting in poor solubility and their precipitation from the solution [85, 86]. Modifications of the hydroxy groups are implemented in order to disrupt the intramolecular hydrogen bonding and, therefore, increase solubility [80–82, 84, 87]. Random methylation, for example, increases the solubility of β-cyclodextrin to 0.38 M, which corresponds to a factor > 20. This is somewhat surprising since a reduced number of hydroxy groups is expected to result in a reduced solubility as well [85]. However, the modification of the hydroxy groups lowers their potential for intramolecular hydrogen bonding, which increases their ability to interact with the surrounding water. Other modified cyclodextrins showing increased solubility, are for example sulfobuthyl ether-β-cyclodextrin with a solubility of more than 0.23 M [70], or hydroxypropyl-β-cyclodextrin with 0.43 M [70, 80, 81, 84–86].
A significant advantage of the clinical applications of cyclodextrins is their relatively high stability against degradation after administration. Therefore, they are not absorbed through the gastrointestinal tract and, consequently, are considered nontoxic when administered orally. Together with the ability of cyclodextrins to improve the aqueous solubility and reduce toxic side effects of guests, these are great advantages for various applications, especially in the pharmaceutical, and the food and beverage industry [42, 84, 85, 88–90].

1.2.1.2 Cucurbiturils

Cucurbiturils are composed of glycoluril units, that are linked by two methylene groups (figure 1.7B) [42, 91]. Their name derives from their barrel shaped structure, that resembles the shape of a cucurbit, with the carbonyl groups arranged at two rims of identical size, and a hydrophobic cavity [92, 93] They are composed of five to ten subunits, and comprise cavity diameters ranging from ~ 2.4 Å to ~ 10.6 Å, depending in the number of subunits [42, 93, 94]. Cucurbiturils are produced synthetically by polymerization reactions. Cucurbit[6]uril, for example has been formed via condensation of glycoluril and formaldehyde under acidic condition [91, 93]. Interestingly, the solubility of cucurbiturils is dependent on the number of glycoluril subunits: comprising an odd number of subunits results in moderate solubility (~ 0.02–0.03 M), whereas cucurbiturils with an even number of subunits are less soluble ($< 10^{-5}$ M) [91, 93]. An advantage of cucurbiturils over other host molecules is their increased rigidity, resulting from the two linkages between neighboring subunits [72].
Cucurbiturils are able to include hydrophobic guests within their cavity, but also electrostatic interaction with the carbonyl groups at the portals is possible [42, 91].

Therefore, they have found application as reaction chambers for chemical reactions or drug carrier [42, 91].

1.2.1.3 Calixaranes and Analogs

Calix[n]arenes and their analogs are composed of n (usually 4–8) phenol groups, linked by methylene bridges (figure 1.8A). In case of calixarene, the linkage is located at the 2- and 6-position (meta). This results in a bowl-shaped structure, with a π-electron rich cavity. However, calixarenes may also exist as partial cone, 1,3 alternate, or 1,2 alternate [72], which significantly alters the structure of the cavity (figure 1.8A). Pillar[n]arenes are structurally related to calixarenes, but the linkage occurs at the 2- and 5-position (para), resulting in a more symmetrical structure (figure 1.8B) [95].
Calixarenes and pillararenes are suitable hosts for sugars, amino acids, and other biomolecules [96], as well as organometallic structures and diverse drug molecules [96–98].

1.2.1.4 Crown Ether

Crown ethers are rather simple macrocycles, comprising the repetitive pattern $(CH_2{-}CH_2{-}O{-})_n$ (figure 1.8C) [72]. Their nomenclature contains the number of atoms included in the macrocycle, and the number of involved oxygen atoms. Therefore, the name of the crown ether corresponds to 3n-crown-n, with n as number of subunits. In contrast to the other described host molecules, the cavity of crown ethers is hydrophilic due to the arrangement of the oxygen atoms towards the cavity. Crown ethers have found application as phase transfer reagents or extractants in liquid extraction [79, 99], as well as hosts for protonated amines [100].

1.2.2 Principle of Host-Guest Complexes

The common feature of these host molecules is the depiction of a cavity that allows for the inclusion of a guest molecule or ion [70, 101]. In order to allow for (partial) incorporation of guests, the cavity has to be of appropriate size to fit the guest [70, 80, 81, 85, 88, 89, 101–103]. With too little cavity size, guest molecules will not fit in, whereas a too wide cavity does not allow for sufficient interaction between the host and guest to form a complex [101]. For example, the cavity size of α-cyclodextrin is appropriate for smaller structures with, e.g., an aliphatic side chain, whereas β-cyclodextrins are able to incorporate aromatic and heterocyclic

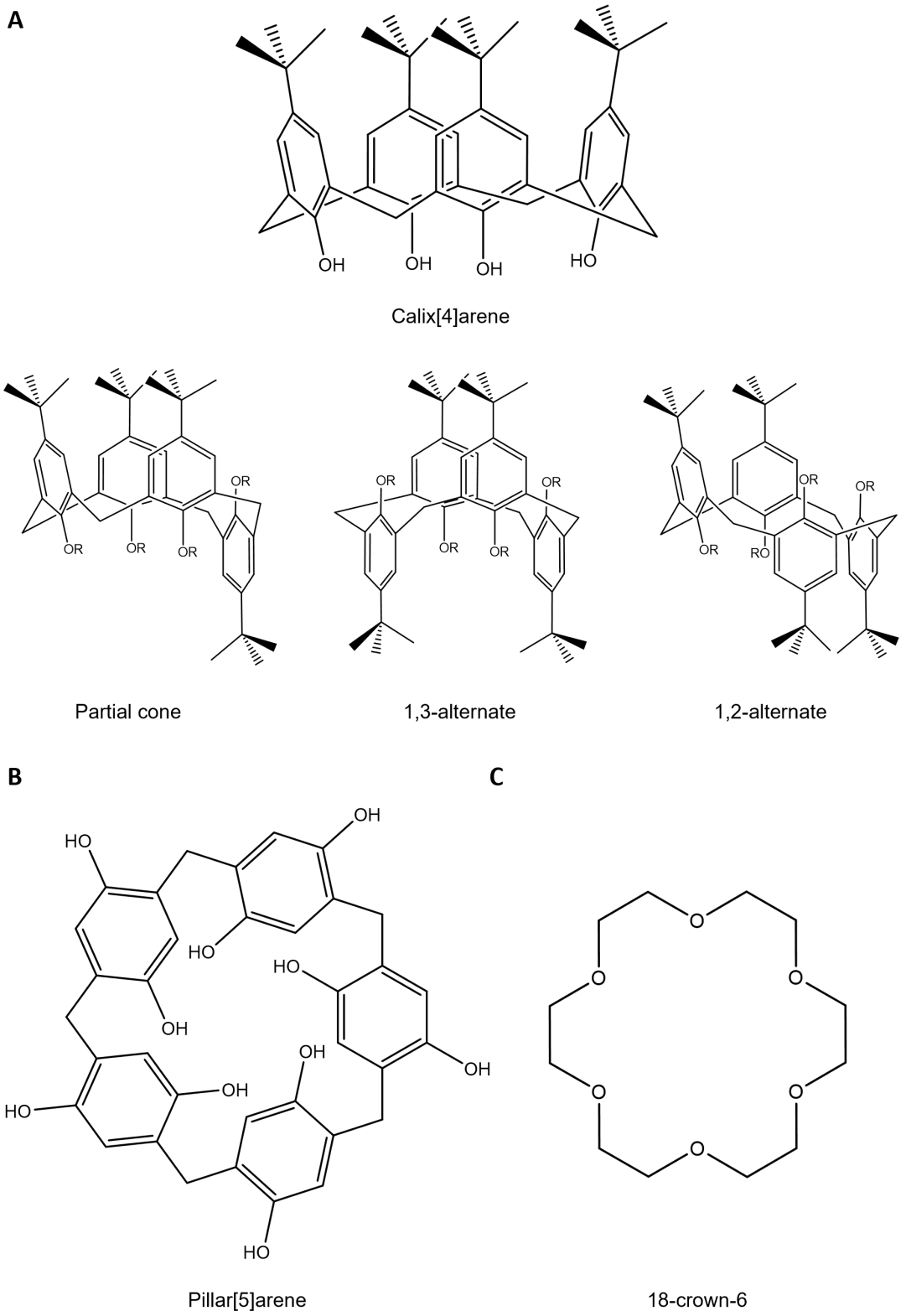

Figure 1.8: Examples of host structures: A) Calix[4]arene with its possible conformations (cone, partial cone, 1,2-alternate, and 1,3-alternate), B) Pillar[5]arene, and C) 18-crown-6.

molecules. Even bigger structures, such as steroids, can be included within the cavity of γ-cyclodextrin. Besides the size of the cavity, the steric properties of host molecules are also affected by modifications at the aperture of the cavity [85, 89, 104]. For example, the addition of hydroxypropyl groups to the rim of β-cyclodextrin improves its aqueous solubility but also increases the steric hindrance for inclusion of guests, as it obstructs the portal [89].

The interactions involved in host-guest complexes are exclusively of non-covalent nature, such as Van der Waals interaction, electrostatic interactions (e.g., hydrogen bonding), or hydrophobic effects. Due to the hydrophobic cavity exploited by several host structures, the inclusion of guest structures comprising hydrophobic elements (e.g., aromatic structures) is a driving factor for host-guest complex formation. The other non-covalent interactions can also occur at the rim of host structures. Hydrogen bonds that are formed at the rim of cyclodextrins, for example, are the reason for the self-association and the poor solubility of β-cyclodextrin. Furthermore, the interaction of guest molecules with the rims of hosts is also possible due to electrostatic interactions. This interaction is possible in addition to the incorporation of the guest within the cavity, leading to further stabilization of the complex. However, the non-covalent interaction of guests with the edges of hosts is also possible without its inclusion within the cavity, which may result in non-specific binding [42, 91, 105]. In general, the non-covalent character of the interaction between the host and guest molecules is a prerequisite for forming an inclusion complex. This means no covalent bonds are newly formed or dissociated during complex formation [72, 80, 81, 85]. However, this criterion does not bijectively indicate the formation of an actual host-guest complex, as unspecific binding does also not involve covalent interactions. In solution, the non-covalent interactions result in a dynamic equilibrium between the host-guest complex and the individual molecules [80, 81, 84, 85, 88, 101]. The interaction stoichiometry of host-guest complexes is usually 1:1, but also 1:2, 2:1 and 2:2 stoichiometries (figure 1.9) have been described [74, 81, 88].

Complex Formation

In an aqueous solution, cyclodextrins and appropriate guest molecules spontaneously form inclusion complexes that are in equilibrium with the unbound host and guest molecules [81, 103, 106]. The driving force for this interaction is the oust of enthalpy-rich water molecules from the cavity by incorporating a hydrophobic guest [103]. In order to get the inclusion complex in solid form, coprecipitation, physical mixing, freeze-drying, kneading, and several other methods have been

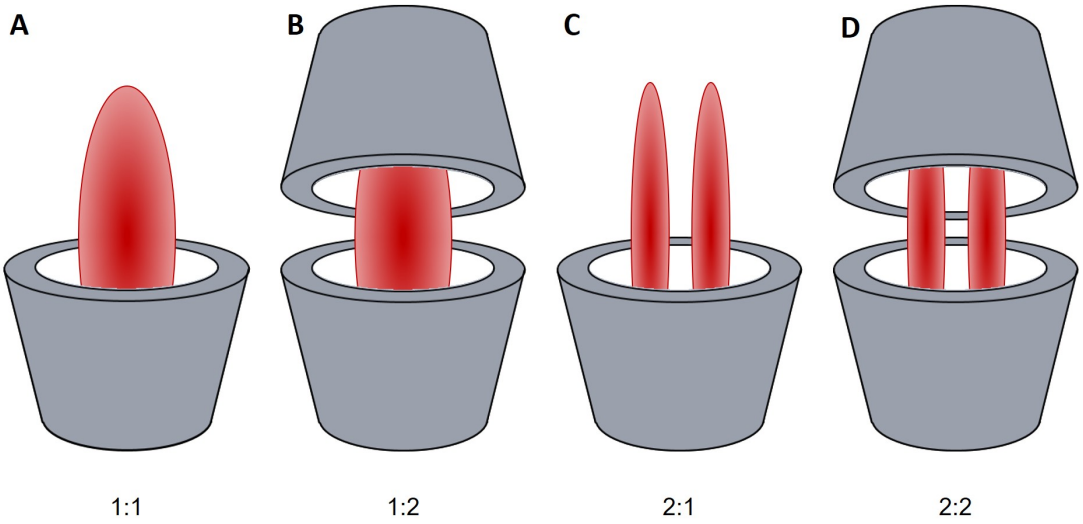

Figure 1.9: Schematic illustration of host-guest stoichiometries at the example of cyclodextrin: A) 1:1, B) 1:2, C) 2:1, and D) 2:2.

used, depending on the properties of the host and guest [103, 106, 107]. The coprecipitation method is easily used on a laboratory scale. To a solution of a host, the guest is added while stirring. With appropriate conditions, the complex will precipitate. This method is, however, not applicable for large-scale usage in the industry due to the high demand for water and required wastewater disposal [103, 106]. For freeze-drying, a similar approach was used. An equimolar solution of the guest is added to a host solution while stirring. The resulting mixture is then filtrated, and the filtrate further lyophilized [108] In physical mixing, 1:1 molar ratios of host and guest compounds are mixed with mortar and pestle. The kneading method is similar, but small amounts of solvent are added prior to the mixing, which is evaporated later [109].

1.2.3 Applications of Host-Guest Complexes

As mentioned previously, host-guest complexes have found application in various fields. Therefore, the interactions of hosts with diverse classes of guest molecules have been described in the literature. Besides this research, the interaction of model compounds with hosts is investigated to study different properties affecting the host-guest interaction.

1.2.3.1 Organic Molecules

Using organic molecules comprising hydrophobic structural elements (e.g., styrene, phenol, benzoic acid, borneol), the structure and interaction properties of host-guest

complexes have been investigated [110–112]. Tang et al. [110], for example, examined the inclusion of L-borneol in β-cyclodextrin, hydroxypropyl-β-cyclodextrin, cucurbit[7]uril, and cucurbit[8]uril in aqueous solution. A higher affinity of L-borneol was detected towards the cucurbiturils than the cyclodextrins. This system also showed that the stoichiometry of a host-guest complex might be affected by the cavity size of the host molecule: While the two β-cyclodextrins and cucurbit[7]uril showed a 1:1 stoichiometry, inclusion of two guests within one host was observed for cucurbit[8]uril.

Plant-based substances with biological activity have been subject to inclusion complex formation to improve their aqueous solubility [108, 109, 113, 114]. Recently, the effect on the anti-inflammatory activity of amyrin [109] or the antioxidant activity of cannabidiol [108] after their inclusion within cyclodextrins have been evaluated. Low bioavailability is a drawback of both compounds that is approached by changing their physicochemical properties by forming a host-guest complex using physical mixing and kneading methods [109], or freeze-drying [108], respectively. In both studies, the formation of 1:1 inclusion complexes could be confirmed, accompanied by increased antioxidant and anti-inflammatory activity, respectively.

Amino Acids

Amino acids differ from each other by their side chains. They are subdivided into non-polar, uncharged polar, acidic, and basic residues. Furthermore, every amino acid except glycine can occur as a D- or L-isomer. Due to this broad range of properties in the side chain together with the steady amino and carboxyl groups, amino acids have found application as model compounds for the evaluation of inclusion complex formation with cyclodextrins [115–123]. It has been shown that the incorporation of amino acid side chains is affected by the size of the host cavity. β- and γ-cyclodextrins, for example are more suitable for the inclusion of amino acids than α-cyclodextrin [116, 119–121]. Furthermore, differences depending on the amino acid residue have been revealed. Ramanathan and Prokai [119] evaluated the preference for complexation for L-amino acids as Trp > Phe > Tyr > Val in β-cyclodextrin. This means that the inclusion of aromatic non-polar (Trp, Phe) residues is favored over aromatic polar (Tyr) and small non-polar residues (Val). Similar results were obtained by Roy et al. [121], comparing the inclusion of glutamic acid, lysine, and phenylalanine in β-cyclodextrin. They elucidated a preference of Phe > Lys > Glu, showing a favored inclusion of aromatic non-polar amino acids over basic and acidic side chains. In this publication, the molecular structures of the resulting inclusion complexes have been proposed schematically. All three

amino acids are proposed to enter the cavities from the bigger rim residue first. Additionally, the amino and carboxylic groups are suggested to interact with the hydroxy groups at the rim of the cyclodextrins. Investigation of the interaction of Gly, L-Leu, L-Phe with α- and β-cyclodextrin by Chen et al. [116] also proposed the interaction of the amino and carboxylic groups with the hydroxy groups and formation of inclusion complexes with β-cyclodextrin. Due to the smaller cavity size, only Gly is proposed to form an inclusion complex with α-cyclodextrin, whereas L-Leu and L-Phe are expected to form exclusion complexes, with the residues pointing away from the cavity. On the other hand, Rudolph, Riedel, and Henle [122] were able to show that even bulkier amino acid tryptophan forms an inclusion complex with β-cyclodextrin, using 2D-NMR experiments. Additionally, different studies were able to show differences in the interaction between several D- and L-amino acids [115, 118, 123]. These results on the inclusion of amino acids within cyclodextrins highlight their potential to evaluate the effect of different properties of guest molecules and the size of hosts on the complex formation.
The inclusion of amino acid side chains also occurs when the amino acids are located in longer chains, as in peptides or proteins [124], such as ubiquitin [125], insulin [126], or substance P [127]. This inclusion allows for the protection of proteins and peptides against degradation (if the point of attack is masked), aggregation, or folding [124, 125, 127]. In addition, masking of undesired properties, such as the bitter taste of rice protein hydrolysate, is enabled by host-guest complexation [122].

1.2.3.2 Metalorganic Compounds

In order to increase the solubility, stability, and bioavailability of organometallic drugs, approaches using the formation of host-guest complexes have been studied. Cisplatin and its analogs oxaliplatin, carboplatin, and nedaplatin have been found to form stable inclusion complexes in α- and β-cyclodextrins, and cucurbit[7]urils [17, 128–131]. The cisplatin inclusion complex in cucurbit[7]uril has been shown to have comparable efficacy on a human ovarian cancer cell line as free cisplatin. In addition, the complex showed an effect on the tumor growth of cisplatin-resistant cell lines. This is a remarkable improvement occurring due to the host-guest complex formation, as cucurbit[7]uril itself had shown no effect on the cell lines [129]. In contrast, experiments on the activity of oxaliplatin incorporated in cucurbit[7]uril showed loss of antitumor activity towards human non-small cell lung (A549) and human ovarian (SKOV-3) cancer cell lines [130]. However, the inclusion of oxaliplatin in β- and 2-hydroxypropyl-β-cyclodextrin showed almost twofold higher cytotoxicity against human colon cancer (HCT116) and human

breast cancer (MCF-7) cells, compared to free oxaliplatin [131].

Metallocenes

Inclusion complexes of bent metallocene dihalides have also been investigated to improve their stability. Experiments on the interaction of molybdenocene with β-cyclodextrin and its derivatives gave evidence for the inclusion of Cp_2MoCl_2 rather than its hydrolysed forms $Cp_2Mo(H_2O)Cl^+$ or $Cp_2Mo(H_2O)_2^{2+}$ [132, 133]. This is also proposed for the inclusion complex of vanadocene as Cp_2VCl_2 [134] and titanocene as Cp_2TiCl_2 [135] within cyclodextrins. In contrast, niobocene dichloride is found to be included as Cp_2NbCl_2OH within cyclodextrins [136]. Theoretical studies of complexes formed by titanocene derivatives and cyclodextrins also propose enhanced cytotoxic activity [137]. Indeed, cytotoxicity studies revealed increased anti-tumor activity of molybdenocene interacting with cyclodextrins [133]. Cucurbiturils have also shown their potential for inclusion of hydrolyzed forms of molybdenocene ($Cp_2Mo(OH)(H_2O)$) and titanocene ($Cp_2Ti(OH)_2$) [42]. Inclusion of molybdenocene leads to alteration of cell growth in cell proliferation assays, whereas the inclusion of titanocene decelerates the hydrolysis of its cyclopentadienyl-ligands [42]. Further, theoretical studies gave evidence for the inclusion of four metallocene dichlorides (Cp_2MCl_2) or dications (Cp_2M^{2+}, M = Ti, V, Nb, Mo), within cucurbiturils [138].

Generally, two inclusion geometries have been proposed for the inclusion of metallocenes within cyclodextrins: Either one or both cyclopentadienyl-ligands is located within the cavity (figure 1.10 left) [132, 136]. Similar inclusion geometries are proposed to occur with cucurbiturils. Although the inclusion of only one cyclopentadienyl-ligand is not expected, their orientation relative to the aperture of the cucurbituril leads to two different inclusion geometries: either horizontally or vertically (figure 1.10 right) [138]. Due to the identical size of the two rims, these two entrances are not differentiated.

1.3 Analysis of Host-Guest Complexes

Various techniques have been used for the analysis of potential host-guest complexes. In general, one single analysis is not sufficient for unambiguous confirmation and characterization of the inclusion. Therefore, different analytical techniques or complementary experiments were applied to get reliable data to confirm or reject the formation of inclusion complexes.

The properties of the complex can also vary depending on whether the sample is

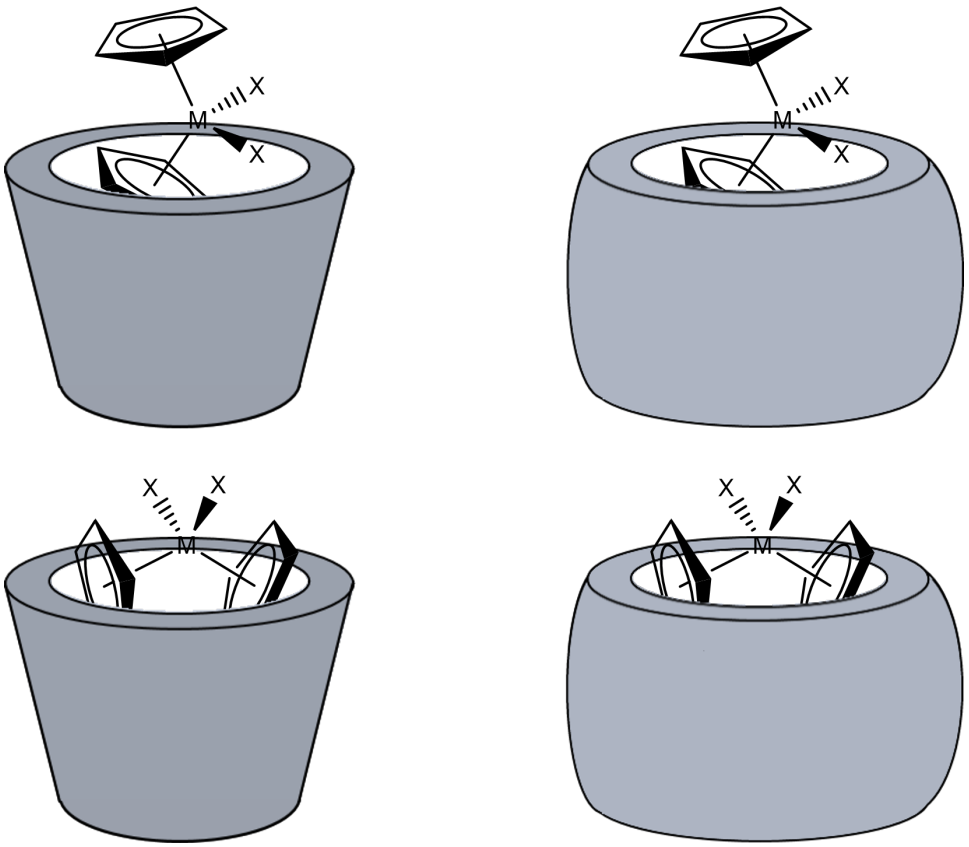

Figure 1.10: Proposed inclusion geometries of metallocene dichlorides in cyclodextrins and cucurbiturils.

examined in the solid state, in solution, or in the gas phase. Therefore, complementary analytical techniques can highlight different aspects for the characterization of the complex.

1.3.1 Solid State Analysis

X-Ray Diffraction

X-ray diffraction is a common approach for characterizing inclusion complexes in the solid state. Single crystal analysis requires a single, stable crystal of appropriate size, which is not easily feasible for all host-guest complexes. However, this approach results in data that allow for the determination of the position of atoms, bond-lengths, and bond-angles of the analyte. These three-dimensional information give insight into the conformation and packing of complexes [139]. A series of crystal structure determinations of host-guest complexes in cyclodextrins has been published by Harata [140] between 1975 and 1990 in the *Bulletin of the Chemical Society of Japan*.

By contrast, powder X-ray diffraction only requires powder of the homogenized

sample, making it significantly more applicable for the analysis of inclusion complexes. Diffraction patterns of the single components and the proposed inclusion complex are compared, expecting new diffraction peaks as well as the disappearance of characteristic peaks of the guest molecule [139]. Morales, Struppe, and Meléndez [136], for example, compared the diffraction patterns of a physical mixture and a freeze-dried complex of cyclodextrins and niobocene or vanadocene, respectively. Physical mixture of the sample compounds resulted for both guest structures in overlapping host and guest signals. In contrast, the analysis of the freeze-dried mixtures showed different characteristics, depending on the size of the host molecule. For both metallocenes, the spectra with α-cyclodextrin showed peaks attributed to free cyclodextrin and metallocene, whereas the spectra with β-cyclodextrin comprised significantly different peaks. These data allowed to conclude that physical mixture is not sufficient for inclusion complex formation, and the cavity of α-cyclodextrin is not of sufficient size to host these metallocenes. However, complexation within β-cyclodextrin is confirmed, based on these data [134, 136].

Thermal Analyses

Thermal gravimetric analysis (TGA) and differential scanning calorimetry (DSC) are thermal analysis techniques used to characterize host-guest complexes. Using TGA, the weight loss of the sample depending on the temperature change is recorded. Weight loss profiles of cyclodextrins, for example, are characterized by a mass loss deriving from the loss of water at temperatures up to 100°C and a second mass reduction upon melting and degradation of the macrocycle at higher temperature. In the analysis of complexes, the weight loss profiles of the single components are compared to the profile of the interaction compounds to identify differences caused by the interation. Upon inclusion, the thermal stability of the guest should be increased, which results in an altered profile [139]. Furthermore, decomposition of β-cyclodextrin occurs at a lower temperature when part of a host-guest complex [132]. The analysis of a lyophilized mixture of molybdenocene and β-cyclodextrin, for example, showed different profiles for the mere compounds and their physical mixture [132].

DSC provides information about the physical and energetic properties of the sample. Comparable to TGA, the curves obtained from single compounds are compared to those of mixtures. By simply mixing of the host and guest compounds, no interaction is expected to occur, resulting in a curve representing the sum of the two compounds. By inclusion of the guest within the host, its melting peak disappears [139].

Spectroscopy

Fourier-transform infrared (FT-IR) and Raman spectroscopy of host-guest complexes are based on the comparison of the spectra deriving from the sole compounds and their mixture. In contrast to FT-IR, which detects the absorption of an analyte, Raman relies on the light scattering of the sample. Therefore, sample preparation is significantly facilitated as Raman does not require the preparation of a pellet of the sample mixed with potassium bromide [139]. Disappearance, shift, or broadening of characteristic bands of the guest molecule may hint at the formation of inclusion complexes. These alterations are proposed to be the result of restrictions in the vibrations of the guest molecule caused by its inclusion [139]. Mangolim et al. [141] investigated the complex of curcumin and β-cyclodextrin formed by co-precipitation. Indeed, the FT-IR and Raman spectra of the complex show shifted peaks compared to the physical mixture of the two compounds.

1.3.2 Theoretical Approaches

Theoretical approaches frequently complement the conclusions drawn from the previously described experimental approaches [97, 123, 132] Other studies are entirely based on calculational methods [17, 137, 138]. Molecular modeling and conformational analysis, for example, are applied to propose the inclusion of modified titanocene dichlorides within cyclodextrins [137]. Furthermore, Senthilnathan et al. [138] concluded the preferred inclusion of bent metallocene dichlorides within cucurbit[7]uril over cucurbit[6]uril based on computations.

1.3.3 Nuclear Magnetic Resonance Spectroscopy

Nuclear magnetic resonance (NMR) spectroscopy covers various experiments, providing complementary information about the analyte. Usually, NMR experiments are performed in solution with deuterated solvents, but also ^{13}C experiments in solid-state are possible. As the behavior of a complex is expected to be different in solution than in solid phase, data derived from these experiments may differ from the previously described methods that have been exclusively performed in solution. Similar to other spectroscopic methods, comparing the spectra of the pure involved compounds with the mixtures allows for drawing conclusions about the complexation. Using 1D experiments, such as ^{1}H or ^{13}C NMR leads to a shift of individual signals upon complex formation [142]. In the case of cyclodextrins, the signal of the H3 and H5 protons, which are located at the interior of the cavity, will be affected by guest molecules in ^{1}H NMR experiments, leading to a shift of their

signal [110, 112]. Using 2D experiments (e.g., NOESY, COSY), the proximity of atoms of the host and guest molecules can be distinguished, allowing for even more precise allocation of the guest within the cavity. Further details on NMR experiments used for the analysis of cyclodextrins and their complexes are summarized in the review of Schneider et al. [142]. NMR techniques have been used in addition to other techniques for investigating different host-guest complexes. For example, Buck et al. [42] used ^{1}H- and NOESY-NMR experiments to confirm the formation of inclusion complexes between cucurbiturils and molybdenocene and titanocene, whereas Rudolph, Riedel, and Henle [122] evaluated the interaction of the aromatic amino acids with cyclodextrins using ^{1}H- and ROESY-NMR experiments.

1.4 Mass Spectrometry of Host-Guest Complexes

Mass spectrometry is an analytical technique with high advantages over other techniques, such as sensitivity and speed [107, 143]. It has found broad applications in different fields, and the development of soft ionization techniques, such as electrospray ionization (ESI) and matrix assisted laser desorption ionization (MALDI), has opened an even broader field of applications. These techniques allow for the transfer of molecules and complexes to the gas phase, remaining their native structure [72, 143–145]. This preservation of the native structure of the analyte enables for the analysis of the quarternary structure of DNA, or the interaction between proteins and other proteins, drugs, or nucleic acids [144, 146]. Furthermore, the application of mass spectrometry for the analysis of non-covalent host-guest complexes has been discussed in several reviews [71, 72, 147].

In comparison to the previously described methods for the analysis of host-guest complexes, mass spectrometry does not require the analysis of neat components to draw conclusions from the data acquired from the analysis of the mixture. Mass spectrometry detects the mass-to-charge (m/z) ratios of the ions present in the sample. As the m/z ratio of the monoisotopic peak is identical for a singly charged ion and a doubly charged ion of twice the mass, these two cannot be directly distinguished. Using high-resolution mass spectrometry, the detected signals are resolved into their isotopic pattern. This even allows for differentiation of singly and doubly charged ions of the same m/z ratio, as the isotopic peaks are $m/z = 1$ apart for singly charged ions, whereas they differ by $m/z = 0.5$ for doubly charged ions. Based on the knowledge of the sample composition, the m/z ratios expected for the complex can be calculated and serve as a reference for the data interpretation.

Ramanathan and Prokai [119], investigated the interaction between amino acids and cyclodextrins using electrospray ionization mass spectrometry. The addition of equimolar amounts of α-, β-, and γ-cyclodextrin to L-Trp resulted in signals assigned as the protonated interaction species $[Trp + \alpha CD + H]^+$, $[Trp + \beta CD + H]^+$, and $[Trp + \gamma CD + H]^+$, respectively, as well as the protonated host and guest molecules. Based on these results, they concluded the preference for the inclusion of Trp into cyclodextrins with appropriate cavity size based on the intensities of the respective ions. By adding equimolar amounts of different amino acids to β-cyclodextrin, they further postulated the order of Trp > Phe > Tyr > Val for their encapsulation preference. In a third experiment, tandem mass spectrometric experiments of the inclusion complexes were examined to determine their gas phase stability. Although Ramanathan and Prokai [119] showed the potential of different experiments on the analysis of host-guest complexes, Cunniff and Vouros [148] tempered the enthusiasm on the conclusions drawn on host-guest complexes by mass spectrometry. Their experiments on the interaction of amino acids with cyclodextrins showed inclusion complex-like interactions between cyclodextrins and amino acids that do not comprise the required hydrophobic side chains to undergo encapsulation. They concluded that these interactions are electrostatic adducts rather than host-guest complexes [148]. This opened the question of how the character of the interaction is altered upon the transfer into the gas phase.

Non-Covalent Interactions in the Gas Phase

Different intra- and intermolecular interactions occur in solution and in gas phase. In both environments, several non-covalent interactions contribute to the stabilization of the non-covalent complexes.

In solution, they are usually stabilized by weak interactions, such as van der Waals forces, hydrophobic interactions, hydrogen bonding, or electrostatic interactions. With the transfer of these non-covalent interactions in the gas phase, most of them are probably retained, but their relative contribution is altered [144]. For example, the propensity of ionic interactions is increased in the gas phase compared to the solution, whereas hydrophobic interactions contribute less in the gas phase [144, 149]. Guest molecules containing polar groups can form hydrogen bonds or dipole-dipole interactions with polar parts of the host structure, for example, the hydroxy groups at the cyclodextrin rims [107]. These interactions become even stronger in the gas phase, leading to non-specific adducts in addition to the formation of inclusion complexes [148, 149]. On the other hand, nonpolar interactions are more robust in solution than in gas phase [149]. Consequently, host-guest complexes

that are stabilized exclusively by hydrophobic interactions that have been detected by other analytical techniques (e.g., NMR) might be decomposed upon transfer into the gas phase, preventing their detection by mass spectrometry. Therefore, mainly inclusion complexes comprising polar interactions are detectable in mass spectrometry [107].

In order to differentiate between "real" inclusion complexes and non-specific interactions, two approaches have been proposed. One is the comparison of the relative intensities of the interaction species with cyclodextrins and linear oligosaccharides. If "real" inclusion complexes are formed, higher signal intensities are expected for the interaction of the guest with cyclodextrins than with linear oligosaccharides. In contrast, non-specific binding would lead to similar intensities for adducts with cyclodextrins and linear oligosaccharides [107, 150]. This direct comparison of the intensities requires comparable ionization efficiencies for the participating compounds, or the intensities have to be corrected for different ionization efficiencies [143].

A second method for determining the interaction characteristics is the recording of the survival yield [151–155]. This displays the relative intensity of the precursor ion as a function of the collision energy applied in tandem mass spectrometric experiments.

Different approaches have been used for the determination of this survival yield (SY). Ma et al. [156] calculated the survival yield on the basis of the signal intensity of the precursor ion. Without any energy applied, the intensity (I_0) corresponds to a survival yield of 100%. With increasing collision energy, the intensity of the precursor decreases (I_{CE}). The survival yield is, therefore, calculated as the fraction of the remaining precursor ion intensity of its initial intensity (equation 1.1). Gabelica, Galic, and De Pauw [150] calculated the relative intensity of the precursor ($I_{P^{2-}}$) ion as its percentage of the sum of the precursor and the free host (I_{H^-}) and guest (I_{G^-}) ions (equation 1.2). As the precursor ion in this example occurs in doubly charged form and decomposes to singly charged host and guest ions, their relative intensity has to be divided by the factor two. Another approach is used by Memboeuf et al. [152]. Here, the fraction of the precursor ion (I_P) of the sum of the intensities of the precursor and all fragment ions (I_F) is calculated (equation 1.3). This approach is also applicable for the determination of the breakdown curves. In breakdown curves, not only the progression of the precursor, but also of the fragment ions is determined. Therefore, the breakdown curve of a specific ion (BDC_X) is determined by the fraction of the intensity of an individual fragment ion

(I_X) of the total intensity of all detected precursor and fragment ions (equation 1.4) [107, 150, 151]. The energy at which the intensity of the precursor ion declined to 50% is called the CE_{50} value. In general, higher CE_{50} values indicate for stronger interaction [151, 156, 157].

$$SY = \frac{I_0 - I_{CE}}{I_0} \tag{1.1}$$

$$SY = \frac{I_{P^{2-}}}{I_{P^{2-}} + \frac{I_{H^-} + I_{G^-}}{2}} \tag{1.2}$$

$$SY = \frac{I_P}{I_P + \sum I_F} \tag{1.3}$$

$$BDC_X = \frac{I_X}{I_P + \sum I_F} \tag{1.4}$$

This method allows for differentiation between non-specific interactions and inclusion complexes by compairing the CE_{50} of the interaction with linear and cyclic oligosaccharides [107, 150]. If the interaction of a guest is exclusively of non-specific character, no difference is expected. On the other hand, differing interactions occurring from inclusion, lead to differences in the survival yield [150].
In this thesis, a particular focus is put on the behavior of cyclodextrin host-guest complexes in mass spectrometry. Therefore, the analysis of saccharides serves as a profound basis for their investigation.

1.5 Saccharides in Mass Spectrometry

Cyclodextrins are composed of several saccharides arranged in a macrocycle. These saccharides are also appearing in linear and branched forms of different lengths. Mono- and disaccharides, for example, are built of one or two subunits, oligosaccharids are composed of up to ten subunits, and polysaccharides comprise more than ten subunits [158]. The analysis of saccharides is also of importance due to their wide occurrence in biomolecules, including glycoproteins, gangliosides, glycolipids, glycosphingolipids, or glycodendrimers [158–162].
With the development of fast atom bombardment (FAB) [160, 163–166] and liquid secondary ion mass spectrometry (LSIMS) [167–170], the possibility for analysis of even bigger oligosaccharides and glycoconjugates without derivatization found application [171]. Earlier, alkylation or esterification was a prerequisite in order

to increase the volatility and thermal stability to make these structures accessible for the analysis with electron impact (EI) or chemical ionization (CI) methods [169, 171]. Another approach is the addition of salts in order to increase the signal intensities, e.g., thiocyanate in negative mode and ammonium in positive mode, making even large permethylated oligosaccharides accessible to analysis [172]. Since the development of FAB and LSIMS, various other ionization techniques have been used to analyze oligosaccharides in positive and negative mode, of which ESI and MALDI are the most frequently used [158, 159, 173–183], but newer methods, such as ion mobility mass spectrometry, are used as well [184–187].

1.5.1 Ionization

Using these diverse ionization techniques, the quasi-molecular ions $[M + H]^+$, $[M + Na]^+$, $[M + NH_4]^+$, and $[M + K]^+$ of saccharides are frequently detected in positive mode. Furthermore, ions derived from the addition of multiply charged metal ions can lead either to quasi-molecular ions of the same charge as the metal ion (e.g., $[M + Ca]^{2+}$) or the charge is partially compensated by the abstraction of protons from the molecule (e.g., $[M - H + Ca]^+$). Additionally, combinations of charge-carrying species can also lead to multiply charged quasi-molacular ions (e.g., $[M + 2\,Na]^{2+}$). In negative mode, $[M - H]^-$ occur from abstraction of a proton, or molecules that cannot lose protons can be detected in the form of species like $[M + Cl]^-$ [160, 182]. By adding certain salts and additives to the sample the ionization efficiency could be enhanced and, consequently, the abundances of the respective quasi-molecular ions increase. With these increased abundances, the selection of these quasi-molecular ions as precursor for tandem mass spectrometric experiments is promoted, as the resulting fragment ions are of higher intensity as well [160, 175, 176].

The size of the saccharide, as well as the type of the charge-carrying species, significantly affect the ionization efficiency and the resulting fragment ions. Generally, bigger saccharides are more easily ionized, as they provide more coordination sites for metal ions [175].

In addition, the size of the charge carrier affects the resulting fragmentation. In the case of small charge carriers (e.g., H^+) more fragmentations take place than in the case of bigger (alkali-)metal ions acting as charge carriers [174, 188]. This effect is caused by the multi-dentate interaction of bigger charge carriers with saccharides. With this wider distribution of the charge, the quasi-molecular ions are stabilized, resulting in less fragmentation [175, 188–190].

1.5.2 Fragmentation

The fragmentation of quasi-molecular ions reveals further structural information of the analyte. Two prevalent techniques are collision-induced dissociation (CID) and higher energy collision-induced dissociation (HCD). In both techniques, acceleration of the selected precursor ion leads to its collision with an inert gas (e.g., N_2, He, Ar, Xe). These collisions increase the internal energy of the precursor ion, subsequently inducing its dissociation. The energy applied in these processes can be given in the laboratory (LAB) or center-of-mass (COM) frame of reference [191, 192]. Only a fraction of the LAB frame energy is available for the precursor ion, which is considered in the COM energy, displaying the maximum available energy that can be converted into internal energy [191, 193]. Therefore, the conversion of LAB to COM energy takes the mass of the collision gas and the mass of the precursor ion into account, as shown in equation 1.5 [191, 194].

$$E_{COM} = \left(\frac{m_{gas}}{m_{ion} + m_{gas}}\right) E_{LAB} \tag{1.5}$$

In ion-trap CID, resonance excitation of the precursor ion is induced by applying a specific radiofrequency (RF) voltage. This causes its movement and consequently its collision and dissociation. As the RF amplitude required for the dissociation is in relation to the RF voltage required for the trapping of the resulting fragment ions, ions with about 25–30% of the precursor's m/z cannot be detected in ion-trap CID experiments [191, 195]. This so-called "low-mass cut-off" is a significant limitation of ion-trap CID that can be overcome using HCD. Acceleration of precursor ions in HCD is non-resonant, occurring due to application of a direct current (DC) voltage [191].

In addition to ion-trap CID and HCD, decomposition of ions can already occur within the ionization source. In the case of an electrospray ionization source, the ions are generated at atmospheric pressure and are transferred to the first vacuum stage of the mass spectrometer. In-source fragmentation is caused by the collision of the analyte ions with the residual gas in this region of the mass spectrometric instrument [193].

1.5.2.1 Nomenclature

In 1987, Dell [160] postulated different fragmentation pathways (A to E) that have been found as common patterns for the decomposition of polysaccharides and glycoconjugates (figure 1.11). Pathway A derives from the cleavage of the glycosidic

bond, forming an oxonium ion with the charge retained at the non-reducing end. This pathway is only possible in positive mode. Dissociation of the glycosidic bond with a hydrogen transfer from an adjacent carbon towards the non-reducing end corresponds to pathway B. In this case, the charge is retained at the reducing end, and it can occur in positive and negative ionization mode. On the contrary, pathway C results from glycosidic bond cleavage with a hydrogen transfer from an adjacent carbon towards the reducing end, resulting in the charge being located at the non-reducing end. Pathways D and E are two types of cross-ring cleavage with the charge either retained on the reducing, or the non-reducing end.

Domon and Costello [196] summarized in 1988 the ions observed in FAB-MS and MS/MS experiments and introduced a systematic nomenclature for the assignment of these ions analogously to the nomenclature system used for peptides (figure 1.12A). A_i-, B_i-, and C_i-fragments are defined to contain the non-reducing end, whereas X_j-,Y_j-, and Z_j-fragments comprise the reducing sugar unit and the subscripts indicate the position of cleavage relative to the termini. Formation of B- and Y-fragments originates from the cleavage of a glycosidic bond closer to the non-reducing end, C- and Z-ions result from the cleavage of a glycosidic bond nearer to the reducing end. A- and X-fragments are formed by cross-ring cleavage, with superscripts indicating the position of the cleaved bond (e.g., ^{2,4}A or ^{1,5}X). The bond between the ring oxygen and the C1 is defined as position 0, the bond between C1 and C2 as position 1, and so on. This nomenclature can even be extended for branched oligosaccharides by greek letters as subscripts. Hence, the largest branch (or antenna) obtains the addition of an $\alpha$to the subscript, the second largest a β, and so forth (figure 1.12B) [196].
Experiments performed in the positive and negative mode indicated possible cleavage at every glycosidic bond. However, the resulting ions did not allow for drawing any conclusion regarding the sequence of the oligosaccharide. Due to their high symmetry, it is not possible to differentiate from which terminus or even from the internal part the fragment ions derive [160, 171]. For example, a B_3-ion cannot be distinguished from a Z_3-ion only from its m/z if there are no modifications, aglycone moieties, or isotopic labeled moieties allowing for identification of the end [181, 197–199]. Additionally, consecutive fragmentation mechanisms can result in formation of internal fragmentation [160, 171]. In order to improve the sequential information of the fragment ions, derivatization (e.g., permethylation, peracetylation) of the oligosaccharide is needed to tag the reducing or non-reducing end [171, 198, 200].

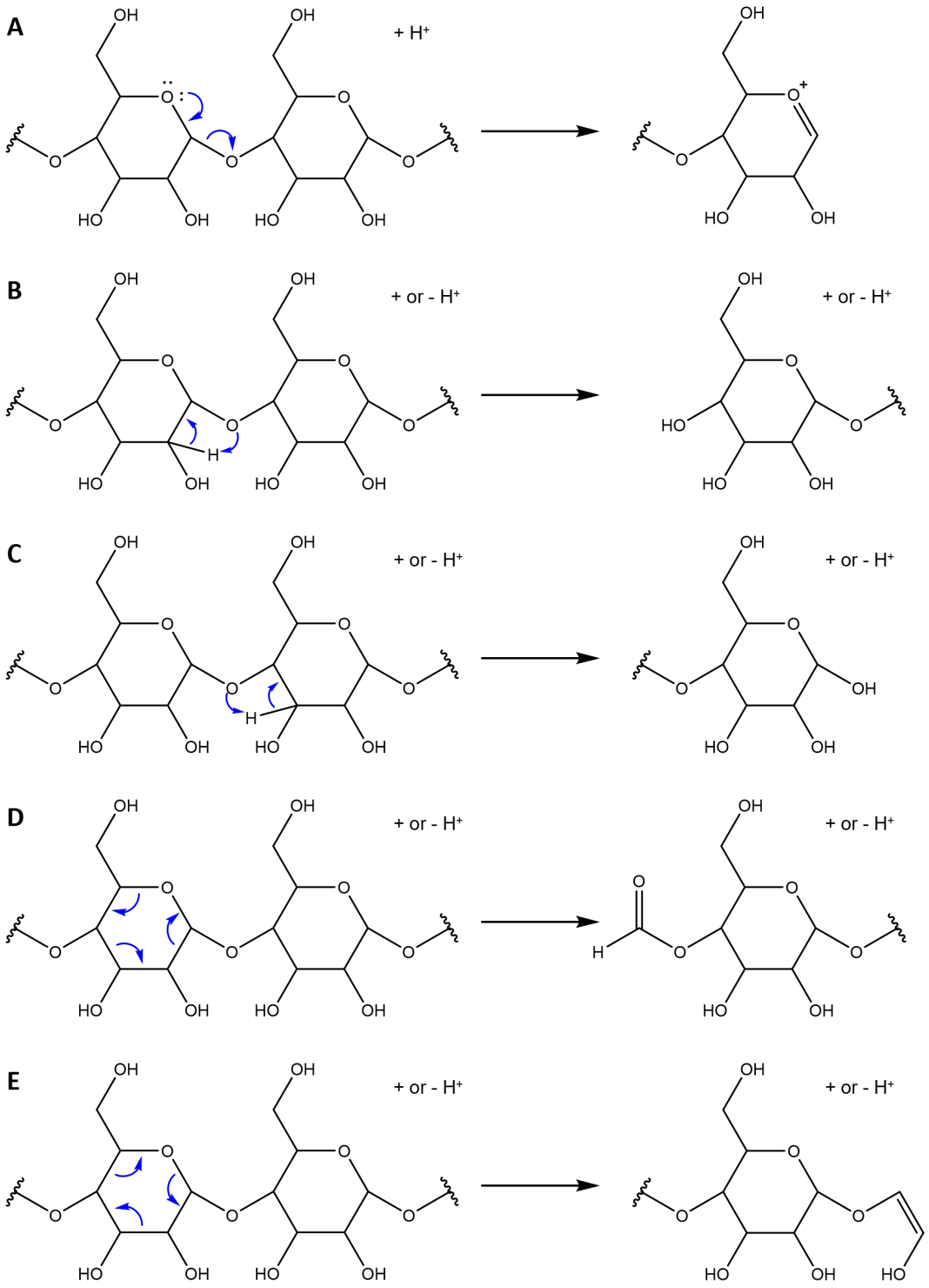

Figure 1.11: Fragmentation pathways A to E proposed by Dell [160].

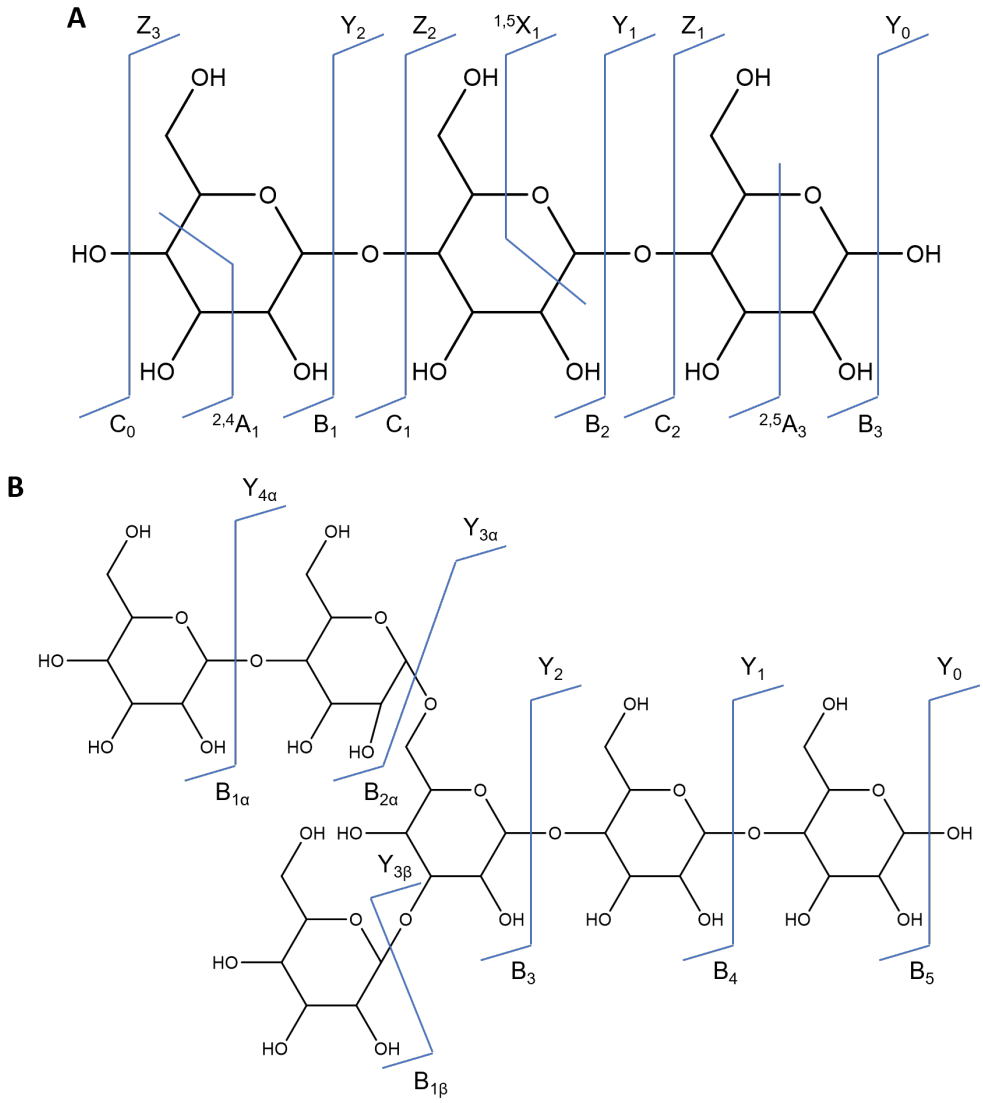

Figure 1.12: Nomenclature of saccharide fragmentation proposed by Domon and Costello [196] for A) linear saccharides and B) branched saccharides.

1.5.2.2 Dissociation Patterns

Since the implementation of this systematic nomenclature, it is used to assign fragment ions in order to explain the decomposition patterns of diverse saccharides. Oligosaccharides comprise various structural features affecting the formation of fragment ions, independent of the ionization mode. They can be built of different subunits with identical formulas (e.g., glucose, galactose). Furthermore, the anomeric carbons of these subunits occur in α- of β-form and can be linked to different hydroxyl groups of another sugar [187]. These features are called the composition, connectivity, and configuration of saccharides. In addition, the location and identity of the charge-carrying moiety also have an impact on the detected

fragment ions [144, 174, 177, 181, 186, 187, 201–203].

Differentiation of Isomers

Comparison of the detected fragment ions of various saccharide isomers has revealed significant dissimilarities occurring from their distinct composition, connectivity, and configuration. The ability to discriminate between different linkage positions using mass spectrometry has been shown by the investigation of saccharides of identical composition with altered linkage positions [185, 204–211]. Lemoine et al. [204] and Hsu et al. [205], for example, have examined saccharides comprising distinct linkages between the mannose subunits. CID mass spectra of the respective sodium adducts show distinct fragment ions, mainly occurring from cross-ring fragmentation, that allowed for differentiation of 1,2-, 1,3-, 1,4-, and 1,6-linkage.

Other research showed the effect of the anomeric configuration on the formation and intensity of certain fragment ions [185, 188, 197, 205, 209, 212–215]. One example is the comparison of the fragment ions obtained from the dissociation of maltohexaose (1,4-linked α-glucopyranose) and cellohexaose (1,4-linked β-glucopyranose), showing distinct spectra from each other [188, 215].

In addition to differences in linkage position and anomeric configuration, Asam and Glish [209] investigated the fragmentation occurring from lithium an sodium adducts of lactose (galactosyl-β-$(1 \rightarrow 4)$glucose) and cellobiose (glucosyl-β-$(1 \rightarrow 4)$glucose), among others. For both adducts, the relative intensities of the B_1- and Y_1-ions, and the fragment ions occurring from loss of H_2O, $C_2H_4O_2$, and $C_4H_8O_4$ are significantly different.

As mentioned previously, the charge density of alkali metal ions results in multidentate interaction with oligosaccharides. This does not only result in altered stability compared to protonated oligosaccharides but also affects the fragmentation patterns [190]. In general, protonation leads mainly to loss of a water molecule and cleavage of the glycosidic bonds, whereas the addition of an alkali metal also promotes cross-ring fragmentation [188, 190]. Therefore, analysis of sodium, potassium, or lithium adducts, for example, may provide even more structural information.

A particular type of fragmentation, occurring mainly in protonated saccharides comprising an aglycone unit, is the internal residue loss (or rearrangement) [163, 164, 166, 216–219]. In this case, not a terminal but an internal residue of the oligosaccharide is eliminated, and the remaining structures are recombined. This rearrangement enormously exacerbates the structural elucidation of oligosaccharides and may lead to misinterpretation of the obtained data [216, 217]. Therefore, analysis of the sodium adducts is favorable for sequence determination, as internal

residue loss is not occurring [165, 218–220].
The differences in fragment ions obtained from different saccharide isomers have also found application in the identification of carbohydrates by comparing relative intensities of detected fragment ions with reference spectra [210, 221, 222]. Based on this, fragmentation libraries have been established [186, 187, 223, 224].

1.5.3 Mechanisms

In order to explain the formation of fragment ions, diverse mechanisms have been proposed explaining their formation in positive and negative ionization modes. These mechanisms are either kept rather general, leaving structural features of the saccharides out of consideration or refraining from precise allocation of the charge, or very specific, considering the particular structural properties of the respective saccharide.
Mechanisms proposed for the fragmentation of protonated saccharides have the proton located either at the glycosidic oxygen [174, 189, 190, 196, 225], or the location is not specified [215, 225]. Domon and Costello [196] propose a mechanism for the formation of B-ions, in which the protonation at the glycosidic oxygen induces cleavage of the glycosidic bond adjacent to the C1 and the formation of an oxonium-ion (figure 1.13A). This mechanism coincides with mechanisms proposed by Ngoka, Lebrilla, and Gal [189], Cancilla et al. [174], and Bythell et al. [190]. However, alternative mechanisms resulting in the formation of B-ions have been suggested. Bythell et al. [190], for example, also discussed the formation of a 1,6-anhydrogalactose ion as B-ion, resulting from the nucleophilic attack of the C6 oxygen onto the C1 carbon, inducing subsequent glycosidic bond cleavage (figure 1.13B). A corresponding charge-independent mechanism was proposed by Zhu et al. [225]. Fentabil et al. [215] did also not include the proton in their mechanism. The formation of an oxonium ion by the formation of a new double bond from a electron lone pair of the ring-oxygen is comparable to the previously described mechanisms. However, proton transfer from the adjacent hydroxy group at C2 to the glycosidic oxygen results in the formation of a negatively charged oxygen. This is compensated either by the binding to C1, forming an epoxide, or the uptake of the initially not allocated proton (figure 1.13C). A similar mechanism was proposed by Zhu et al. [225]. Up to the zwitterionic structure, these two mechanisms are identical, but the compensation of the charge leads to a ring contraction (figure 1.13D). Furthermore, Zhu et al. [225] proposed glycosidic bond cleavage upon the abstraction of the C2 hydrogen by the glycosidic oxygen with subsequent formation of a double bond (figure 1.13E). In general, the formation of the corresponding

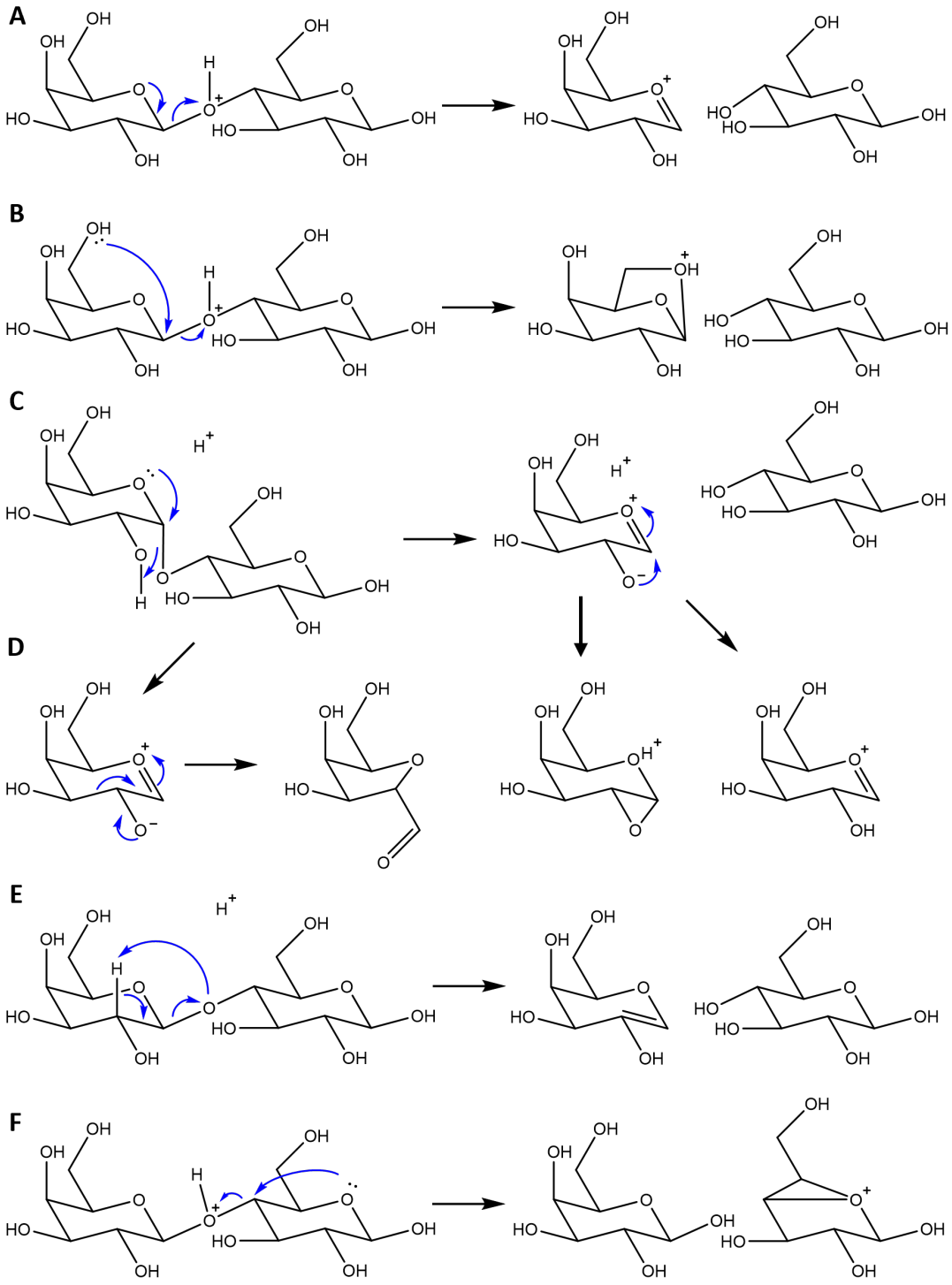

Figure 1.13: Overview of fragmentation mechanisms of protonated saccahrides resulting in B-/Z- and C-/Y-fragments.

Y-ions occurs from proton transfer simultaneously to the glycosidic bond cleavage, if the charge is contributing to the mechanism. If the location of the proton is not specified, its final location defines whether the B- or Y-ion is formed. Formation of Z- and C-ions has been proposed by Bythell et al. [190] (figure 1.13F). Nucleophilic attack of the ring-oxygen electron lone pair to C4 induces the cleavage of the adjacent glycosidic bond and the formation of a bicyclic Z-ion. Subsequent proton transfer leads to the corresponding C-ion.

Interestingly, despite internal residue loss is occurring mainly for protonated saccharides, the location of the proton is not defined in the mechanisms proposed by Brüll et al. [163] (figure 1.14A) and Van Der Burgt et al. [164] (figure 1.14B), for 1,4- and 1,6-linked saccharides, respectively. In both mechanisms, two nucleophilic attacks of glycosidic oxygens on the C1 carbons lead to the exclusion of bridged saccharide residues and reconnection of the remaining structures.

Fragmentation mechanisms of metallated saccharides in positive mode generally bear resemblances to the previously described mechanisms for protonated saccharides [190, 211, 214]. For example, a suggested mechanism of Bythell et al. [190] (figure 1.16A) is analogous to the glycolysis proposed by Zhu et al. [225] (figure 1.13D). However, the multidentate interaction of metal ions with saccharide oxygens can result in reduced cleavage of the glycosidic bond due to its stabilization (figure 1.15) [174, 226, 227]. This stabilization promotes cross-ring fragmentation, following mechanisms proposed by König and Leary [211] (figure 1.16B), Bythell et al. [190] (figure 1.16 C, D), and Tüting, Adden, and Mischnick [199] (figure 1.16E).

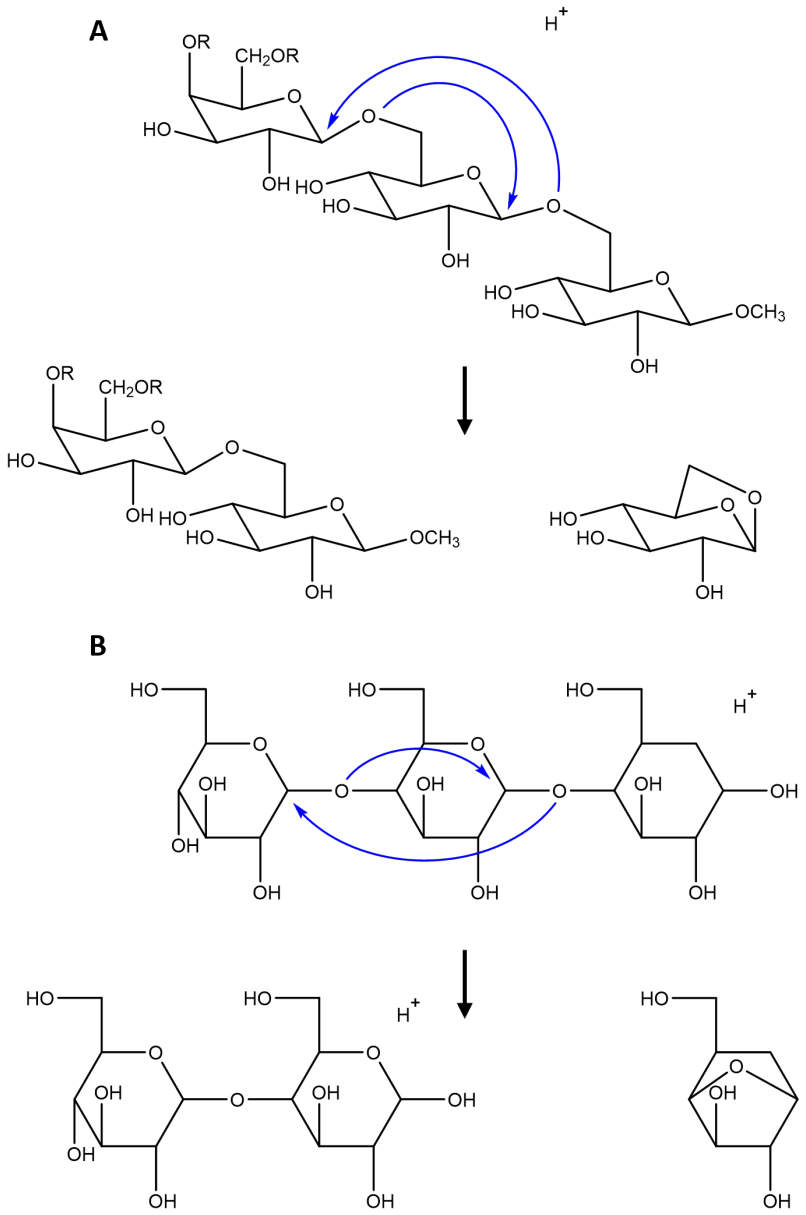

Figure 1.14: Fragmentation mechanism explaining the internal residue loss in A) 1,6- and B) 1,4-linked saccharides.

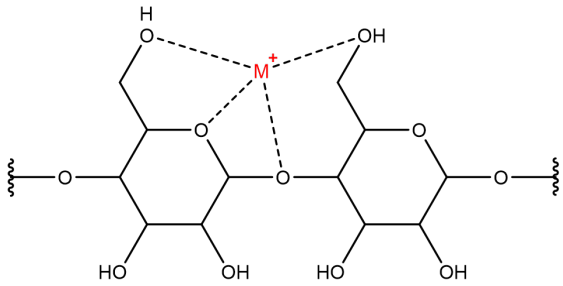

Figure 1.15: Illustration of the multidentat interaction of metal ions with saccharides.

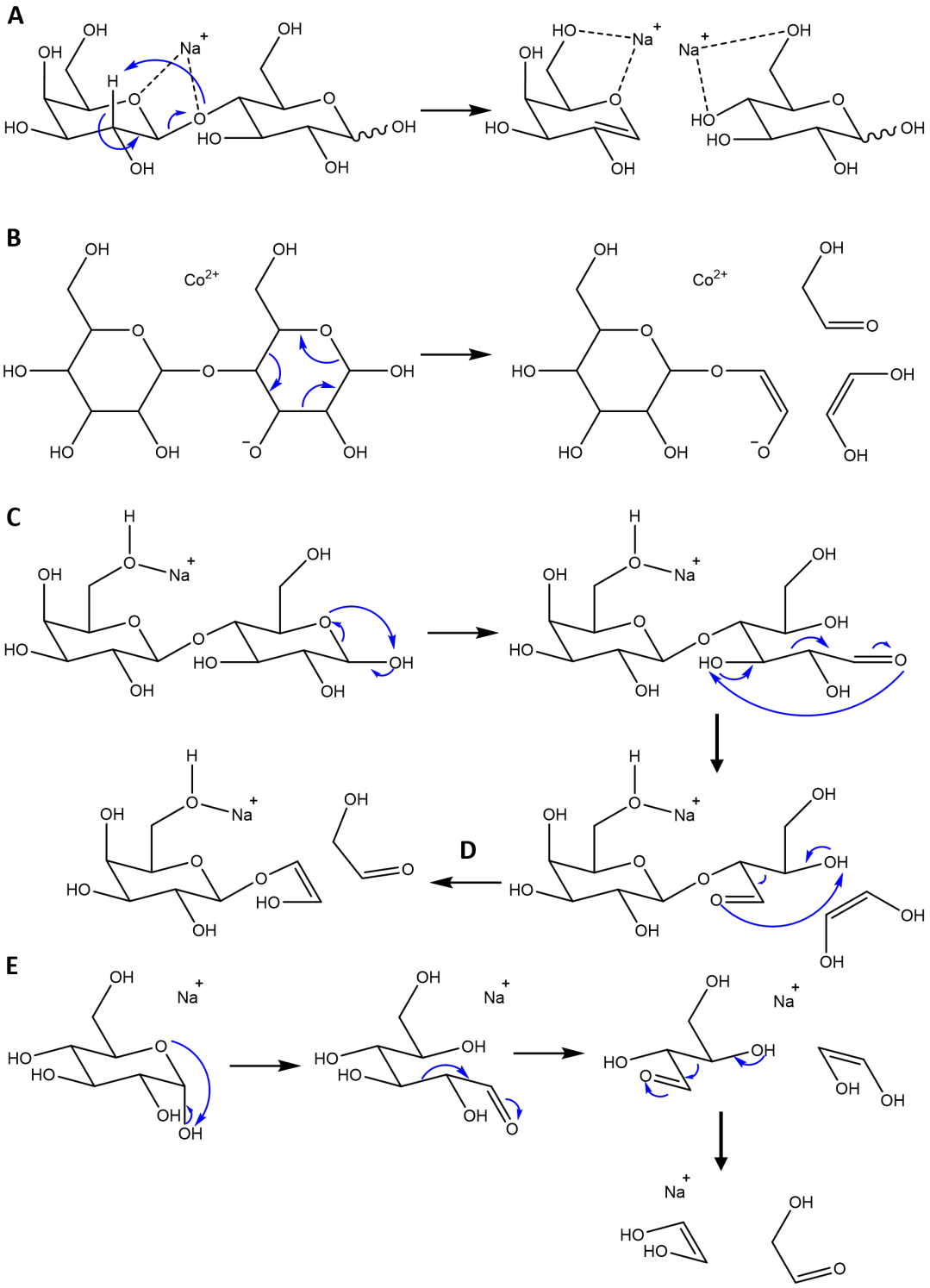

Figure 1.16: Proposed fragmentation mechanisms of metallated saccharides.

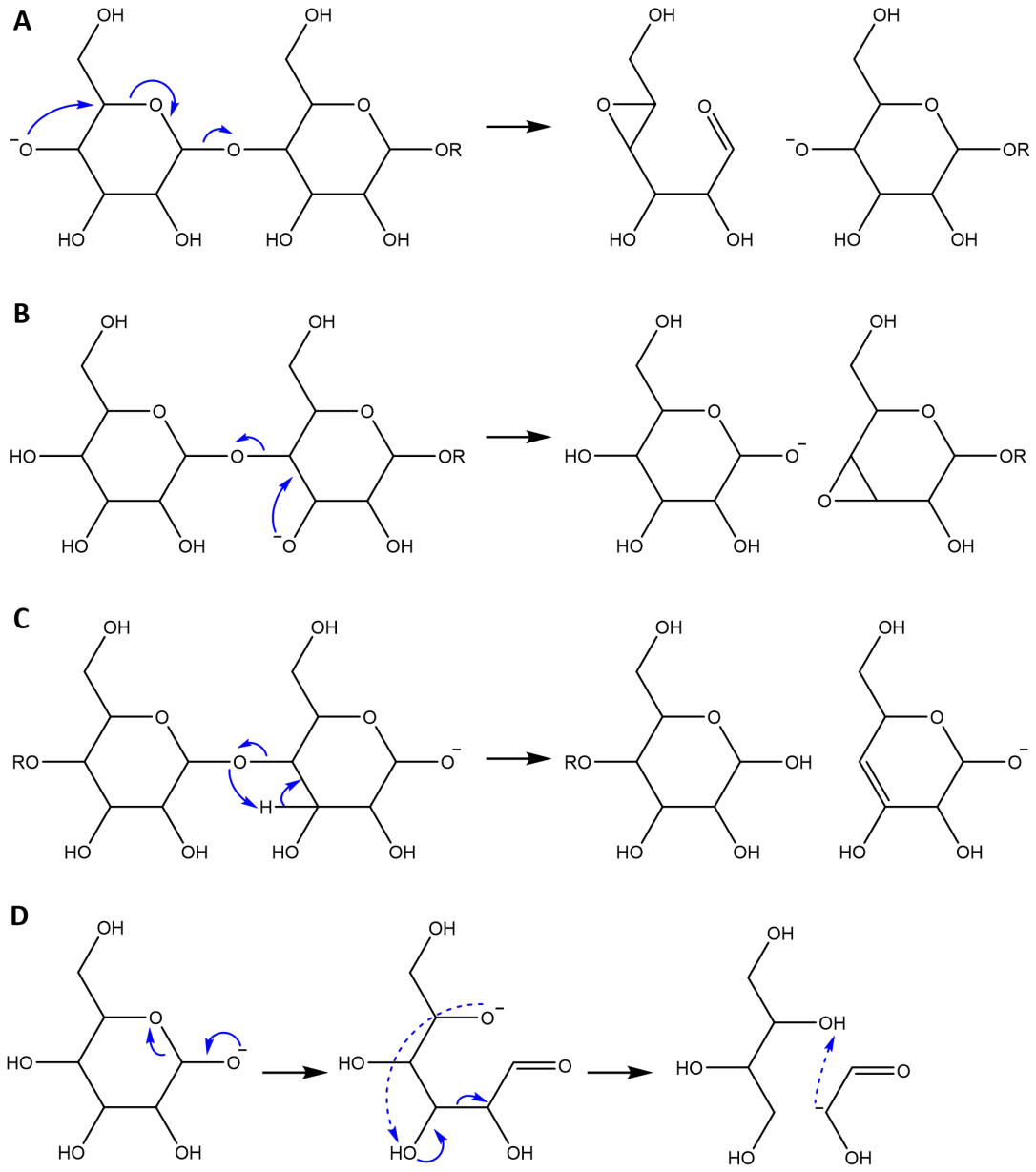

Figure 1.17: Fragmentation mechanisms proposed for deprotonated saccharides. Dashed arrows represent a proton migration.

In the negative ionization mode, the deprotonation site strongly affects the fragmentation mechanism. A selection of those mechanisms is discussed in the following. Domon and Costello [196] proposed a mechanism with deprotonation site located at the non-reducing end leading to Y-ions (figure 1.17A). In contrast, deprotonation at the C3 hydroxy group leads to the formation of a C-ion (figure 1.17B). In both cases, the corresponding B- and Z-ions are formed from subsequent proton transfer. Deprotonation at the reducing end can either result in cleavage of the glycosidic bond, leading to B- and Y-ions (figure 1.17C) [168, 189], or induce cross-ring fragmentation (figure 1.17D) [168].

1.5.4 Cyclodextrins

Similar to linear saccharides, positive ionization of cyclodextrins can lead to the formation of quasi-molecular ions with protons, ammonium, alkali metals (M^+), or alkaline earth metals (M^{2+}) [154, 155, 175, 228–231]. As mentioned earlier, the formation of clusters occurring from unmodified cyclodextrins can lead to signals assigned as $[2\,CD + 2\,H]^{2+}$, for example, which overlap with the signal of the corresponding singly charged monomer $[CD + H]^+$ [228, 232]. Again, metal ions can interact with multiple sites of cyclodextrins and have been found to interact preferentially with the narrow rim of cyclodextrins [154, 230, 233]. Lithium (Li^+), for example, can interact with up to four oxygen atom in its proximity when interacting with α- or β-cyclodextrin, and its methylated analogs [233], whereas Fe^{2+} was found to undergo five interactions with α-cyclodextrin, four with β-cyclodextrin, and three with γ-cyclodextrin [154]. These trends are affected by the size of cyclodextrins as well as the radii of the metal ions [154, 230]. On the other hand, protonation of cyclodextrins occurs at a glycosidic oxygen due to its basic properties [188, 234].

Dissociation Patterns

Upon decomposition of singly positive charged cyclodextrins, consecutive loss of 162 Da is consistently described in several publications [155, 157, 228, 229, 231–235]. In the case of doubly charged precursor ions, loss of $m/z = 81$ (162 Da / 2) is documented [157, 231, 232]. This mass differences correspond to a glucopyranose subunit ($C_6H_{10}O_5$), deriving from cleavage of two glycosidic bonds [229]. It has to be emphasized that these losses are detected for protonated cyclodextrins and cyclodextrins with alkali metal adducts.

Rabus et al. [229] and Przybylski and Bonnet [157] investigated the fragmentation of sodiated β-cyclodextrin ($[\beta CD + Na]^+$). Both detected a series of fragment ions

differing from each other by 162 Da. Based on these data, it cannot be differentiated whether the dissociation occurs consecutively or simultaneously. In addition, Rabus et al. [229] detected a signal occurring from the loss of 264 Da from the precursor ion, indicating cross-ring fragmentation. Furthermore, Frański et al. [231] assigns fragment ions deriving from β-cyclodextrin ionized with diverse metal ions (Na^+, Mg^{2+}, Ca^{2+}, Cd^{2+}, Co^{2+}, Cu^{2+}, and Pb^{2+}) to one series differing by $m/z = 81$ from each other and from the doubly charged precursor, and up to three series of ions being 162 Da apart. Those occur from charge-separation reactions from the doubly charged precursor, leading to singly charged fragment ions. Thereof, one is the direct loss of 162 Da, whereas the other two occur from the initial loss of a cross-ring fragment with 264 Da or water (18 Da), respectively, and subsequent loss of the subunits with 162 Da.

Dissociation patterns are frequently explained by marking the cleavage site in the macrocyclic structure, as shown in figure 1.18 [228, 231, 236], whereas, in other publications, the fragment ions deriving from cyclodextrins are assigned as B-, Y-, or Z-ions [155, 157, 229]. However, the definition of Domon and Costello [196] regarding this nomenclature includes whether the fragment ions contain the reducing or non-reducing end. As discussed by Chizhov, Tsvetkov, and Nifantiev [228], the lack of any beginning or end within cyclodextrin macrocyclic structure hampers the application of this nomenclature.

Comparable fragmentation pathways have also been found for modified cyclodextrins comprising side chains. One ion series is occurring from the loss of subunits of cyclodextrin and a second series of ions is assigned to the decomposition of the side chains. These two series have also been found to overlap, leading to the characteristic pattern of the loss of subunits shifted by the m/z ocurring from the decomposition of the sidechains [228, 235, 236]. Aditionally, cleavage of the entire modified subunits has been detected [155, 228, 233, 237, 238]. In the case of methylations, fragments of 176 Da, 190 Da, or 204 Da are lost from mono-, di-, or trimethylated subunits, respectively. This trait has been used by Sforza et al. [238] for investigating regioisomers of diamino- and ditosyl-β-cyclodextrins. The regioisomers comprise the two modifications either at neighboring subunits (AB), or one (AC) or two (AD) subunits apart, as depicted in figure 1.19. By determining the relative intensities of the resulting tetrameric fragment ions containing no, one, or two modifications differentiation of these isomers was possible. For example, the AB isomer can form three tetrameric fragments containing two modifications, two with one, and two without any modification, leading to a proportion of 3:2:2. This

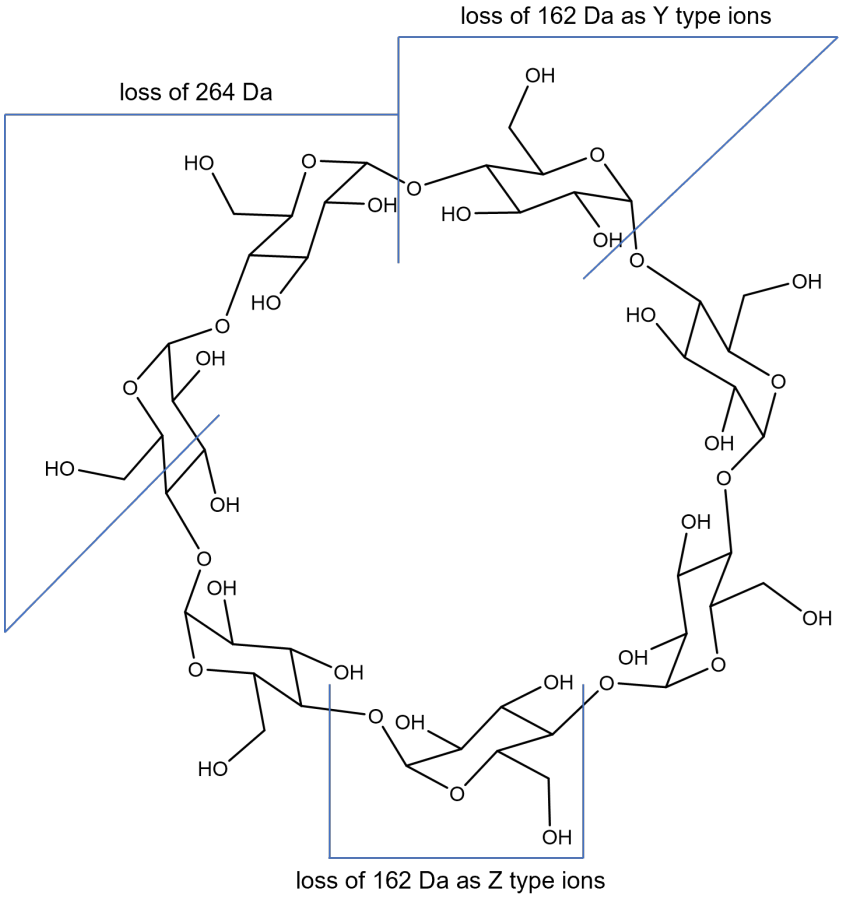

Figure 1.18: Example of the indication of cleavage sites in cyclodextrins.

is clearly distinguishable from the 2:4:1 and 1:6:0 patterns expected from the AC and AD isomers, respectively.

Fragmentation Mechanism

Although dissociation patterns are frequently used to describe the decomposition of cyclodextrins, only sparse information is available on the structure of fragment ions and the mechanisms leading to those. Donkuru et al. [235] stated that the loss of glucopyranose subunits accompanies ring-opening of the macrocyclic structure of a doubly charged modified β-cyclodextrin. They also proposed the structure shown in figure 1.20A for the resulting ion, but did not discuss the underlying mechanism. Rabus et al. [229] evaluated four different structures for dimeric sodiated fragment ions based on simulations: three are B-ions and one is a Z-ion (figure 1.20B). Of those, the 2-ketone fragment ion (blue) is identified as the lowest energy structure. Furthermore, they proposed the fragmentation mechanism shown in figure 1.20B for the formation of this B-ion. Dossmann et al. [154] proposed a fragmentation mechanism for divalent metal adducted cyclodextrins (figure 1.20C). It includes

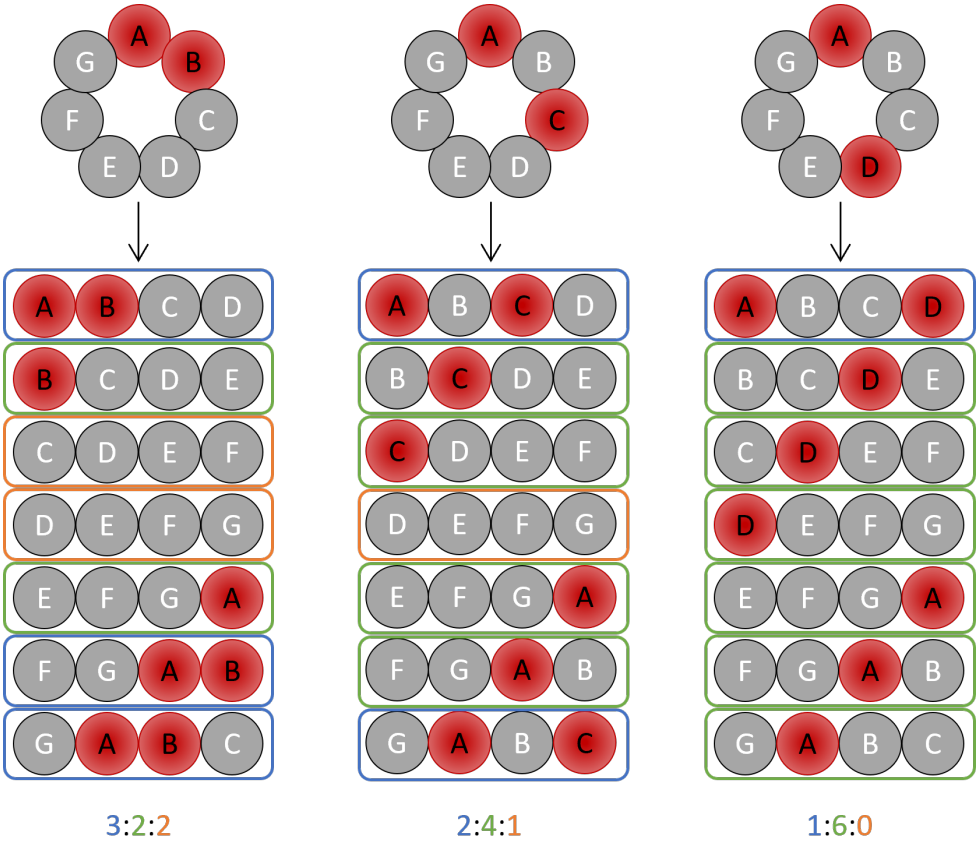

Figure 1.19: Trameric fragments occurring from the decomposition of AB, AC, and AD regioisomers, according to Sforza et al. [238].

simultaneous cleavage of two glycosidic bonds and exclusion of a zwitterionic glucose subunit. In a second step, the remaining cyclodextrin fragment ion undergoes recyclization. Jang and Choi [234] characterized the dissociation of protonated α-cyclodextrin by two pathways. The first is the linearization of the macrocyclic structure and subsequent loss of subunits (figure 1.20D), whereas the second is the direct decomposition of the macrocyclic α-cyclodextrin. Although both mechanisms lead to ions of the same m/z ratio, their structure and stability, based on energy-minimized structure calculations, are not the same.

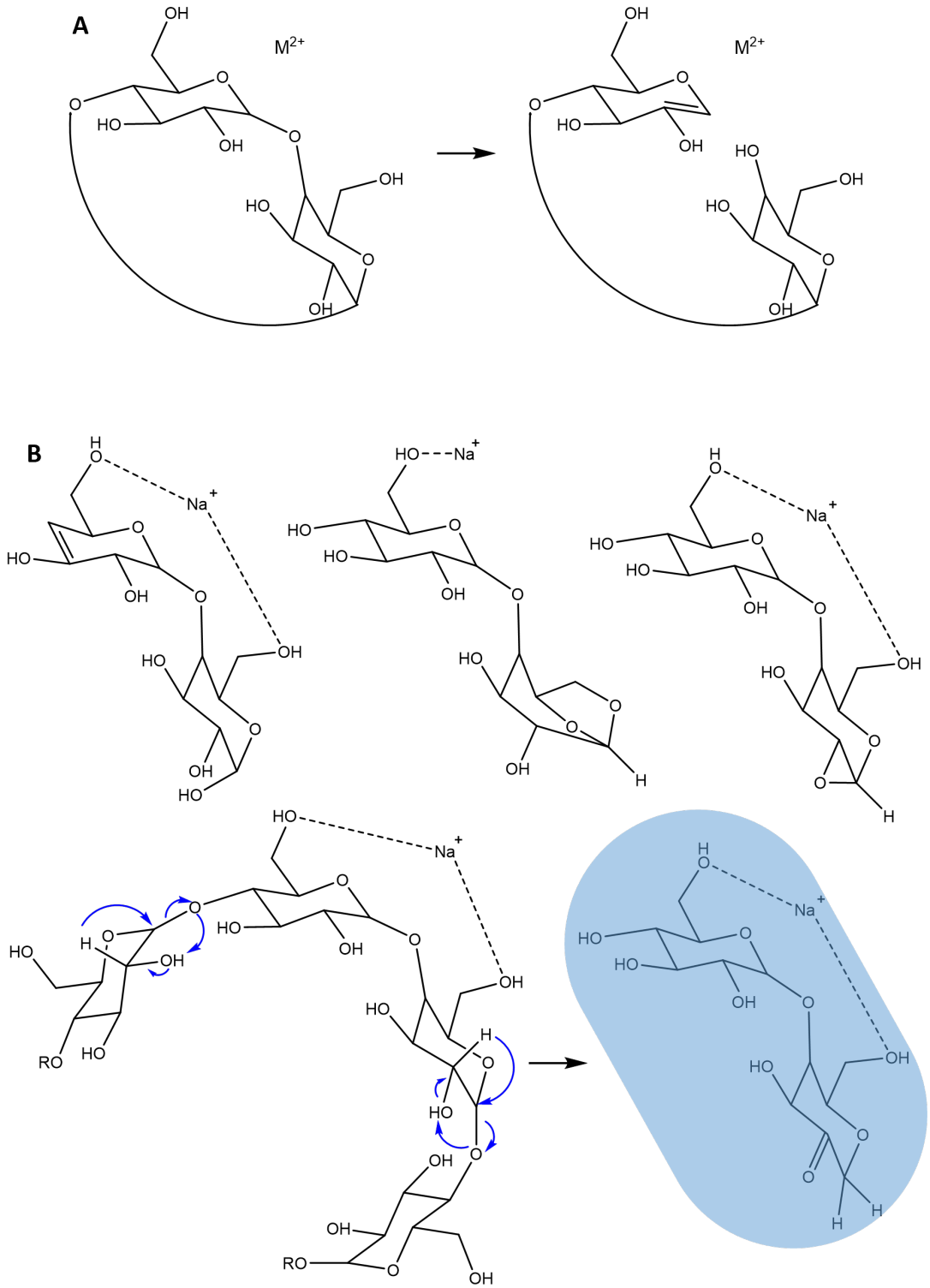

Figure 1.20: Fragment ion structures and fragmentation mechanisms of cyclodextrins proposed by A) Donkuru et al. [235], B) Rabus et al. [229], C) Dossmann et al. [154], and D) Jang and Choi [234].

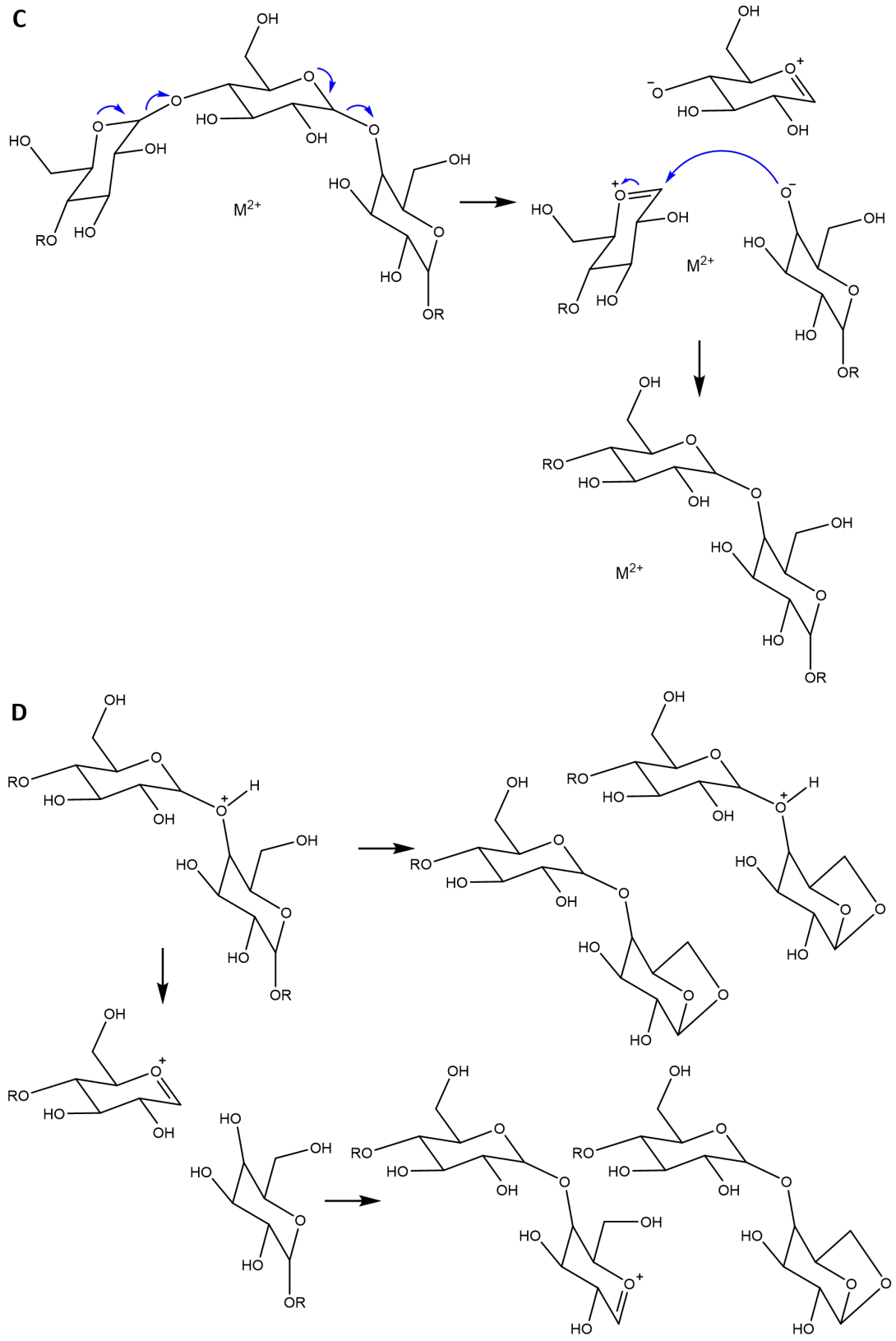

Figure 1.20: (continued) Fragment ion structures and fragmentation mechanisms of cyclodextrins proposed by A) Donkuru et al. [235], B) Rabus et al. [229], C) Dossmann et al. [154], and D) Jang and Choi [234].

2 Fragmentation of Cyclodextrins in Mass Spectrometry

A first step towards the comprehension of the mass spectrometric behavior of cyclodextrin host-guest complexes is the analysis of cyclodextrins individually. This allows for the identification of signals independent of an interaction. Furthermore, understanding of the fragmentation mechanisms underlying the decomposition of cyclodextrins provides information on the potential effects of the inclusion of a guest on the fragmentation of the complex. Although several publications discuss the fragmentation mechanism of linear and branched oligosaccharides, only a few focus on the dissociation mechanisms or structure of fragment ions of cyclodextrins. [154, 229, 234, 235]. To fill this gap, the fragmentation patterns occurring from collisional activation of protonated cyclodextrins of different sizes are investigated. Furthermore, methylated derivatives of β-cyclodextrins are examined to get a more in-depth insight into the effect of the numerous hydroxy groups.

2.1 α-, β-, and γ-Cyclodextrins

The analysis of α-, β-, and γ-cyclodextrin in 50/50 H_2O/MeCN showed comparable results for all three host structures. The intact cyclodextrins are detected as proton (m/z 973.325, m/z 1135.380, m/z 1297.432), sodium (m/z 995.305, m/z 1157.360, m/z 1319.413), potassium (m/z 1011.279, m/z 1173.334, m/z 1335.388), and ammonium (m/z 990.351, m/z 1152.406, m/z 1314.459) adducts, respectively (figure 2.1).

The formation of ammonium adducts is frequently mentioned in the literature using ammonium-containing additives during the analysis. However, these adducts are also mentioned in publications that did not use any of those additives [155, 157, 239]. Yet, the authors of these publications did not clarify the origin of this NH_4^+ cation. In order to rule out the cyclodextrin raw material as the ammonium source, its composition is determined by thermal elemental analysis. For β-cyclodextrin, a composition of 38.28% carbon, 6.73% hydrogen, and 0.00% nitrogen was detected. This composition is in agreement with the molecular formula of β-cyclodextrin ($C_{43}H_{70}O_{35}$) including the declared water content of 10–13%. Also, the lack of any nitrogen excluded the sample as an ammonium source. Possible external sources

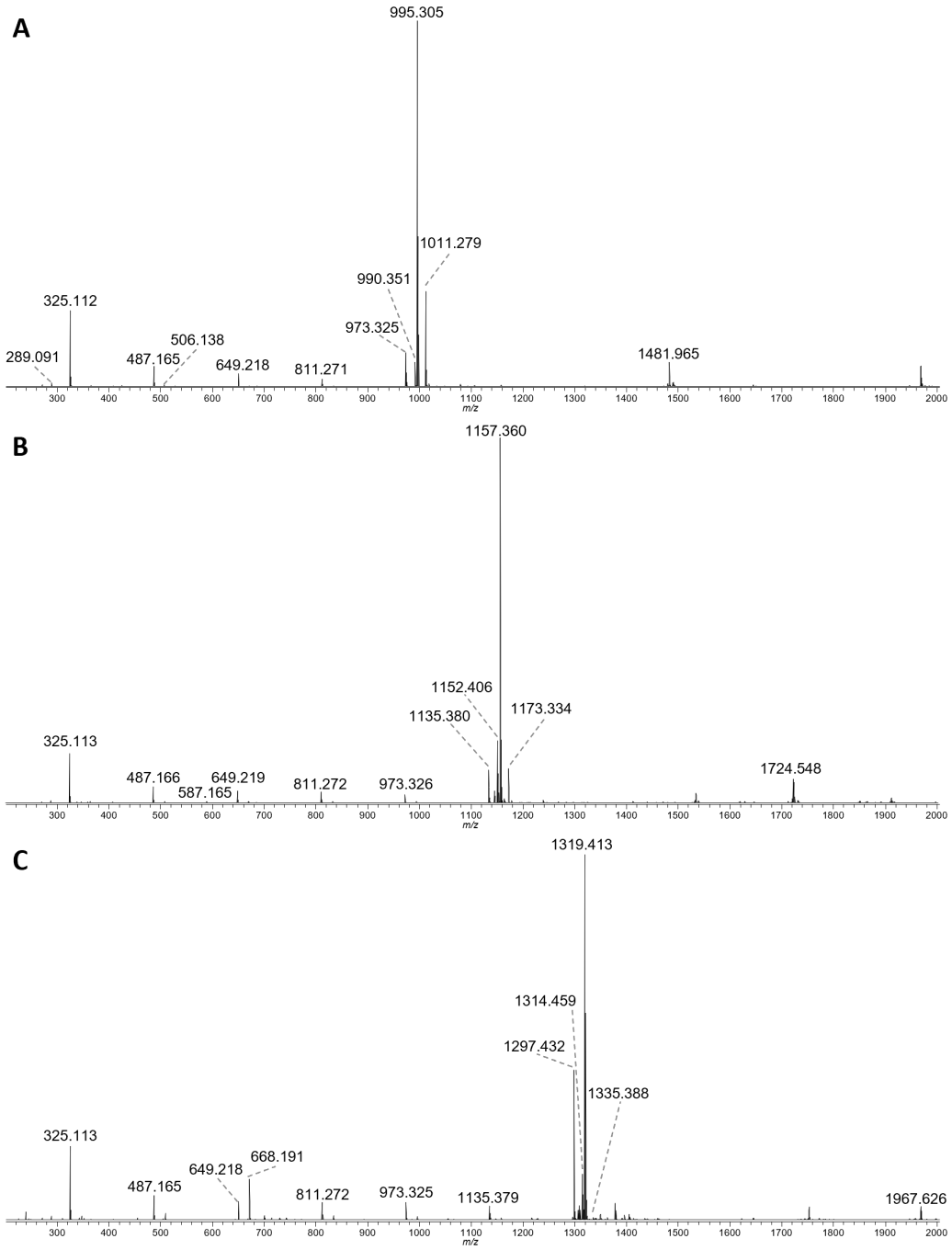

Figure 2.1: Full scan electrospray ionization mass spectra of A) α-; B) β-; and C) γ-cyclodextrin recorded in positive mode.

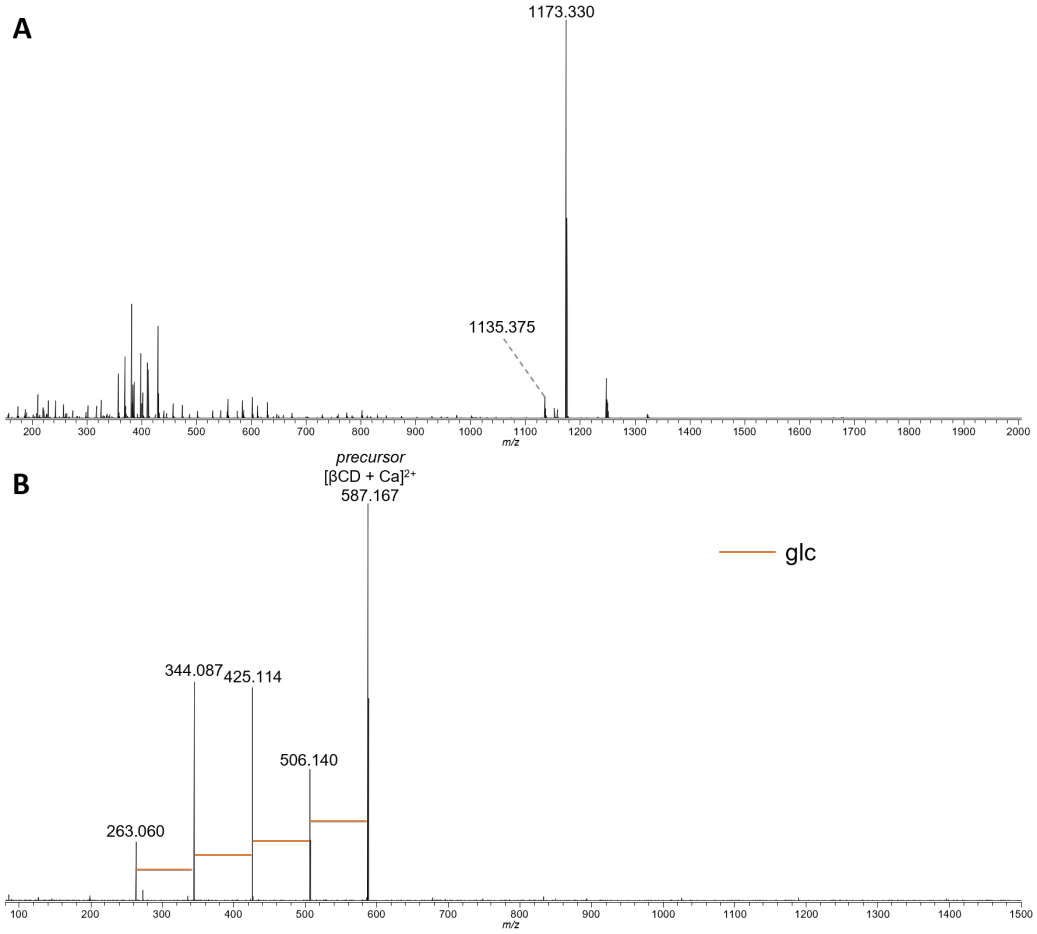

Figure 2.2: A) Full scan electrospray ionization mass spectrum of β-cyclodextrin after the addition of KCl, B) tandem mass spectrum of $[\beta\mathrm{CD} + \mathrm{Ca}]^{2+}$.

have been mentioned in the literature. Selva et al. [240] explained the occurrence of ammonium adducts from "residual ammonium contamination of the instrument", whereas Blades, Ikonomou, and Kebarle [241] declared the origin of NH_4^+ from "NH_3 gas impurity present in atmospheric air". In our experiments, no further effort was made to ascertain the source of ammonium.

In addition to singly charged ions, doubly charged species could be assigned as clusters of cyclodextrins with different types of charge carriers, e.g., $[3\,\mathrm{CD} + 2\,\mathrm{Na}]^{2+}$ at m/z 1481.465, m/z 1724.548, and m/z 1967.626 for α-, β-, and γ-cyclodextrin, respectively. Signals of other clusters are overlapping with the peaks of singly charged species, for example, the signals deriving from $[\beta\mathrm{CD} + \mathrm{Na}]^+$ are overlapping with the signals of $[2\,\beta\mathrm{CD} + 2\,\mathrm{Na}]^{2+}$, resulting in a mixed isotopic distribution. Another species of doubly charged ions is the adduct of Ca^{2+}, resulting in the signals at m/z 506.138, m/z 587.165, and m/z 668.191, respectively.

This doubly charged ion is of special interest, as it has been found misassigned in some publications as $[CD + H + K]^{2+}$ [155, 157]. Regarding the mass deviation in ppm, this assignment would result in a deviation of approximately 11 ppm, which significantly exceeds the accepted deviation of ±5 ppm [242]. Nevertheless, further experiments were performed to reject the assignment of the signal as $[\beta CD + H + K]^{2+}$. By adding KCl to a sample of β-cyclodextrin, a significant increase of the singly charged potassium adduct $[\beta CD + K]^{+}$ at *m/z* 1173.330 occurred, but not of the doubly charged signal at *m/z* 587.166 (figure 2.2A). Additionally, collisional activation of the doubly charged ion of interest leads exclusively to doubly charged fragment ions that correspond to $[glc_n + Ca]^{2+}$ with n = 3–6, (*m/z* 263.060, 2.6 ppm; *m/z* 344.087, 2.2 ppm; *m/z* 425.114, 1.6 ppm; *m/z* 506.140, 1.4 ppm) as shown in figure 2.2B. Therefore, the assignment of these doubly charged ions as calcium adducts is confirmed.

In all three full scan mass spectra, two series of peaks shifted by 162 Da are detected, what coincides with the subunits of cyclodextrins ($C_6H_{10}O_5$). The first series coincides with the molecular formula $[(C_6H_{10}O_5)_n + H]^{+}$ with n = 2–5 (α-cyclodextrin), n = 2–6 (β-cyclodextrin), and n = 2–7 (γ-cyclodextrin), whereas the less intense series represents the corresponding sodium adducts. These classes of fragment ions have been expected to occur upon in-source decomposition of the respective cyclodextrins. As $[\alpha CD + H]^{+}$ and $[glc_5 + H]^{+}$, as well as $[\beta CD + H]^{+}$ and $[glc_6 + H]^{+}$ comprise the same molecular formula and occur at the same *m/z* ratios, sample contamination with other cyclodextrins represented a potential source of these ions. However, the lack of potassium and ammonium adducts and the altered relative intensities of the proton and sodium adducts point to in-source fragmentation rather than contamination with other cyclodextrins. In the *m/z* range lower than 300, even smaller fragments have been detected, assumed to derive from the further decomposition of the subunits.

Effect of Formic Acid

The peak intensities of the proton adducts of cyclodextrins are relatively small compared to the sodium and potassium adducts, which hampered their selection for further tandem mass spectrometric experiments. Therefore, formic acid has been added as a proton donor to the sample [243]. As shown at the example of β-cyclodextrin, the relative intensity of $[\beta CD + H]^{+}$ was increased compared to the experiment without formic acid (figure 2.3). With the addition of an acid, the

Table 2.1: Comparison of the relative ion intensities of the intact β-cyclodextrin and its fragments obtained from full experiments with an without formic acid in two time ranges.

	No Formic Acid		Formic Acid	
Time / min	0.02–0.16	7.90–8.18	0.01–0.32	6.35–6.98
Intact β-Cyclodextrin	89.53%	59.73%	90.46%	76.27%
$[\beta CD + H]^+$	5.69%	29.75%	36.70%	21.53%
$[\beta CD + Na]^+$	60.62%	11.00%	33.93%	13.01%
$[\beta CD + K]^+$	5.99%	1.37%	2.19%	1.22%
$[\beta CD + NH_4]^+$	17.23%	17.60%	14.59%	18.68%
$[\beta CD + Ca]^{2+}$	0.00%	0.00%	3.05%	21.83%
β-Cyclodextrin Fragments	10.47%	40.27%	9.54%	23.73%

question arose if degradation due to acid hydrolysis of the cyclodextrin occurs, impeding the analysis. Experimental data did not confirm an increased degradation of the β-cyclodextrin in presence of formic acid compared to the experiments performed without formic acid (table 2.1). The relative intensities of the signals assigned as fragment ions of β-cyclodextrin showed an increase from 10.47% in the first minute of the experiment without formic acid to 40.27% after ∼8 min, whereas in presence of formic acid, the signal intensity increased from 9.54% in the first minute to 23.73% after ∼7 min. These findings are in agreement with the literature, proposing that even α-cyclodextrin, the least stable of the three cyclodextrins against acid hydrolysis, does not show any indication for degradation after 3 h at 100 °C in an acidic solution of pH 2.4 [83].
As the identity of the signals is independent of the presence of formic acid, no differentiation is made between those two condiditons in the following experiments.

2.1.1 Collisional Activation of α- , β- , and γ-Cyclodextrin

The collsional activation of $[\alpha CD + H]^+$, $[\beta CD + H]^+$, and $[\gamma CD + H]^+$ at *m/z* 973.4, *m/z* 1135.4, and *m/z* 1297.4, respectively, showed also the consecutive loss of $C_6H_{10}O_5$, as detected from in-source fragmentation in full scan experiments. The corresponding signals are assigned as $[glc_n + H]^+$ with n = 2–5, 6, or 7, respectively. In ion-trap CID experiments, the low-mass cut-off only allowed for detection of ions greater than *m/z* 265, *m/z* 310, or *m/z* 355, respectively. Detection of the glucose monomer or smaller fragments was, therefore, not possible. Using HCD as an activation method, the monomer $[glc + H]^+$ as well as multiple loss of H_2O moieties from the glucose mono- and dimer are detected (figure 2.4). Ion-trap CID

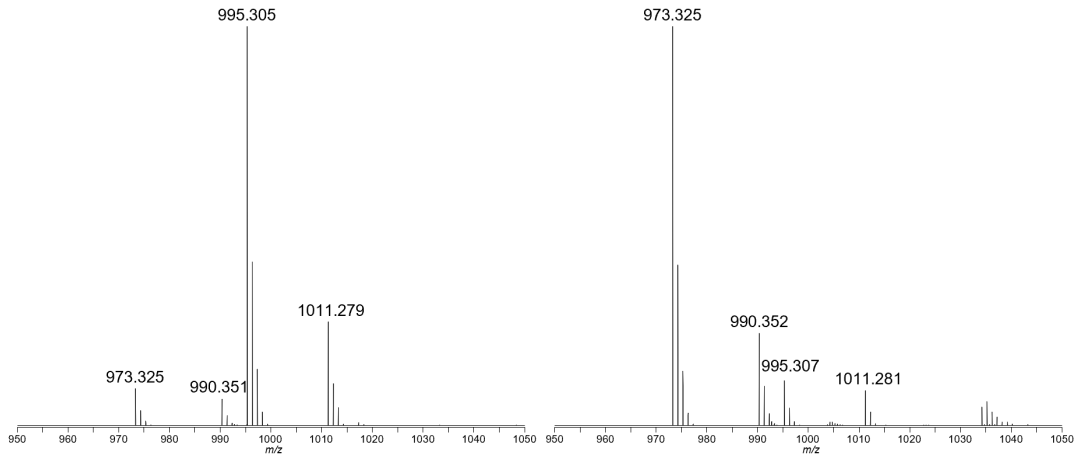

Figure 2.3: Different intensities of the quasi-molecular ions with proton, sodium, ammonium and potassium adducts of α-cyclodextrin measured without (left) and with the addition of formic acid (right).

and HCD experiments, therefore, result in comparable ions, despite the small ions missing in CID data due to low-mass cut-off. These fragment ions coincide with the ions detected in full scan experiments, supporting their assignment as in-source fragments.

Additional tandem mass spectrometric experiments of $[\beta CD + H]^+$ and its in-source fragments using ion-trap CID and HCD revealed an even broader range of fragment ions. These ion activation experiments can be performed consecutively, but in-source fragmentation can be only used as first stage, and HCD only as last stage. The number (n) of consecutively applied mass spectrometric experiments resulting in a mass spectra is indicated by a superscript (MS^n). Thus, a full scan mass spectra results from an MS^1 experiment, and a collisional dissociation mass spectrum results from a MS^2 experiment. If an in-source fragment is subject to an additional collisional activation, it is referred to as pseudo-MS^3 experiment. With every ion activation process, the intensity of the fragment ions decreases. As shown in figure 2.5A, MS^3 fragmentation of $[glc_6 + H]^+$ originating from $[\beta CD + H]^+$ results in comparable fragment ions, but of significantly less intensity than the pseudo-MS^3 fragmentation of $[glc_6 + H]^+$ generated by in-source fragmentation (figure 2.5B). The resulting fragmentation patterns are not affected by the number of consecutively performed fragmentation experiments [222, 244]. Pseudo-MS^3 experiments of the glucose dimer $[glc_2 + H]^+$ also allowed for the identification of fragment ions occurring from the decomposition of the subunits down to a m/z of 85 (figure 2.5C). This gives even more structural information of the fragment ions deriving from cyclodextrins.

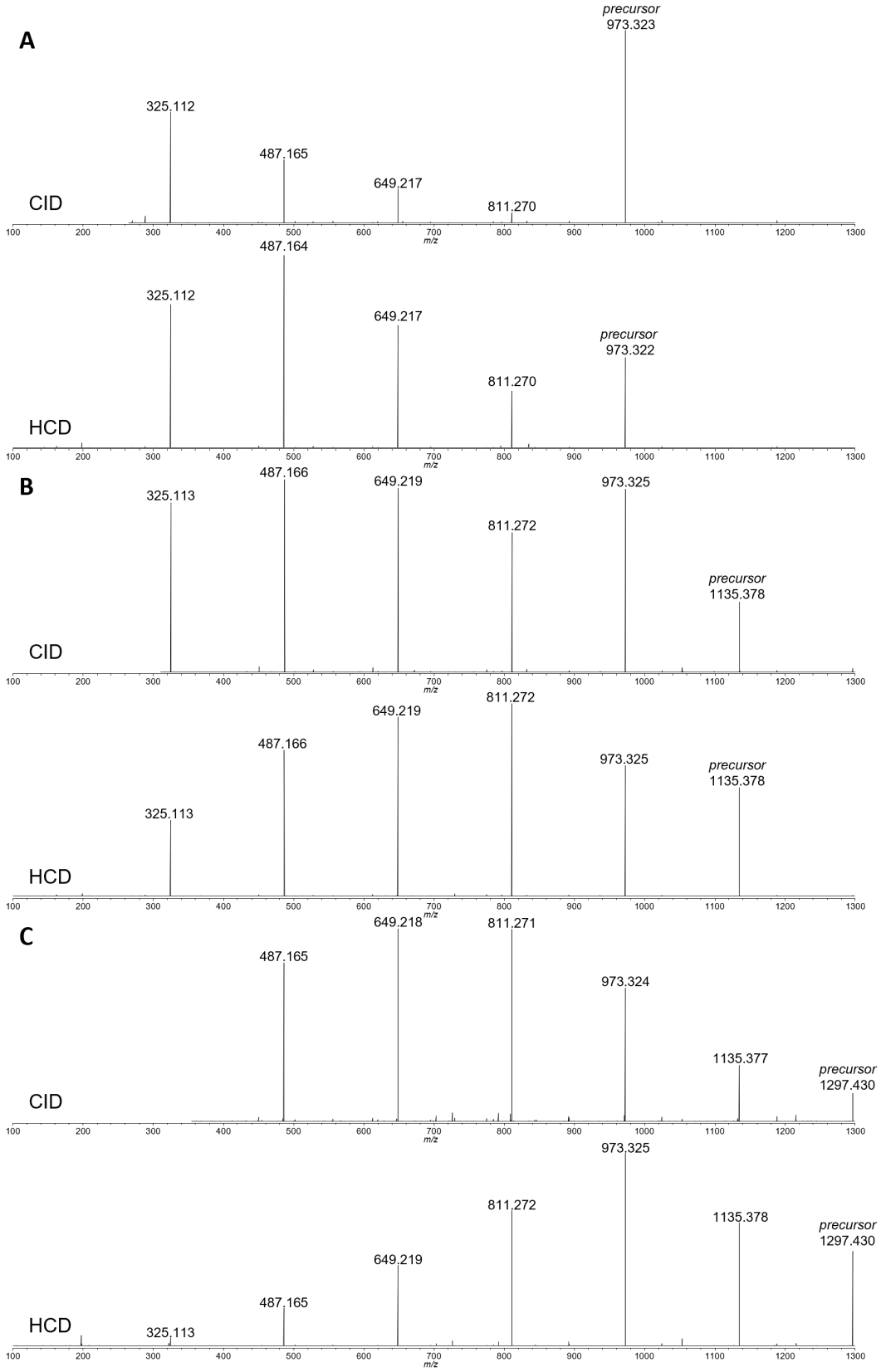

Figure 2.4: Tandem mass spectra of A) ion-trap CID (upper) and HCD (lower) activation of $[\alpha\text{CD} + \text{H}]^+$, B) ion-trap CID (upper) and HCD (lower) activation of $[\beta\text{CD} + \text{H}]^+$, and C) ion-trap CID (upper) and HCD (lower) activation of $[\gamma\text{CD} + \text{H}]^+$.

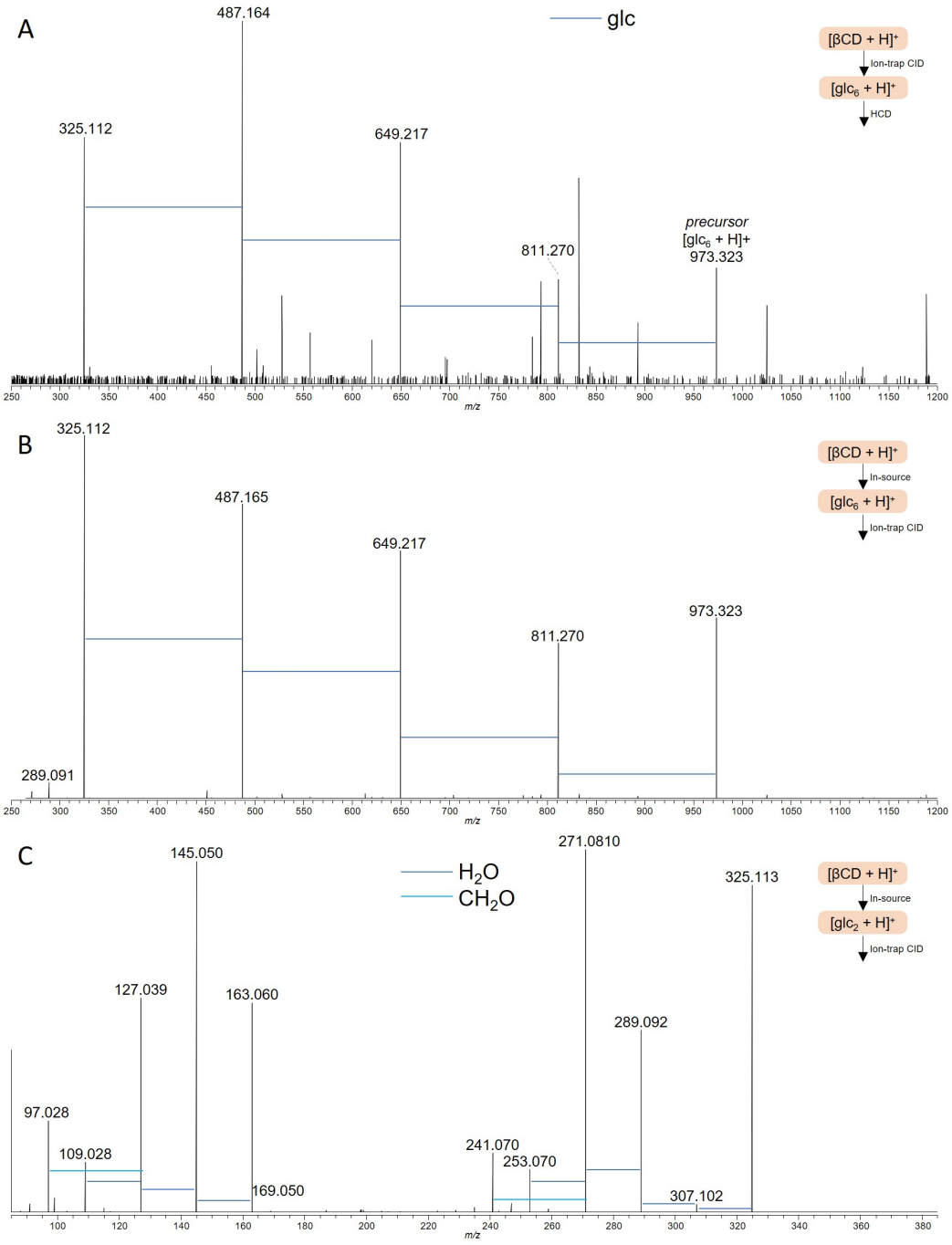

Figure 2.5: A) MS^3 and B) pseudo-MS^3 mass spectra of $[glc_6 + H]^+$ deriving from $[\beta CD + H]^+$; C) pseudo-MS^3 mass spectrum of $[glc_2 + H]^+$.

2.2 Methylated Cyclodextrins

In several fragmentation mechanisms proposed for linear saccharides, hydroxy groups are stated to contribute to the decomposition. Therefore, their effect on the fragmentation of cyclodextrins is evaluated by examination of di- and trimethylated analogs of β-cyclodextrin. Dimethyl-β-cyclodextrin comprises methoxy groups at the 2 and 6 position, whereas trimethyl-β-cyclodextrin is methoxylated at the 2, 3, and 6 position (figure 2.6).

Full scan mass spectrometric experiments of dimethyl- and trimethyl-β-cyclodextrin show peaks of protonated and sodiated compounds of various degrees of methylation (figure 2.7). The spectra of trimethylated β-cyclodextrin shows its proton (m/z 1429.710), sodium (m/z 1451.691), potassium (m/z 1467.665), and ammonium (m/z 1446.735) adducts, with 21 methoxy groups, as well as respective adducts deficient up to eight methyl groups ($-$OH instead of $-OCH_3$). These series of ions exhibit a mass difference of 14 Da overlap with the series of ions originating from the consecutive loss of trimethylated glucose units (204 Da). Therefore, $[TMglc_n - (CH_2)_x + H]^+$ (n = 2–6, x = 4–7) fragment ions are also detected in the full scan. In the context of methylated cyclodextrins, the terms " $+ CH_2$" or " $- CH_2$" represents the difference in the chemical formula between a hydroxy and a methoxy group. It has to be emphasized that, although ions with different degrees of methylation are detected as a result of in-source fragmentation of trimethylated-β-cyclodextrin, no signal with more than three methoxy group per subunit is detected. Therefore, it can be concluded that no transfer of methoxy or methyl groups occurs during the decomposition of the macrocyclic structure. This fact becomes important later in the discussion of fragmentation mechanisms.

In the full scan mass spectrum of dimethylated β-cyclodextrin signals assigned as

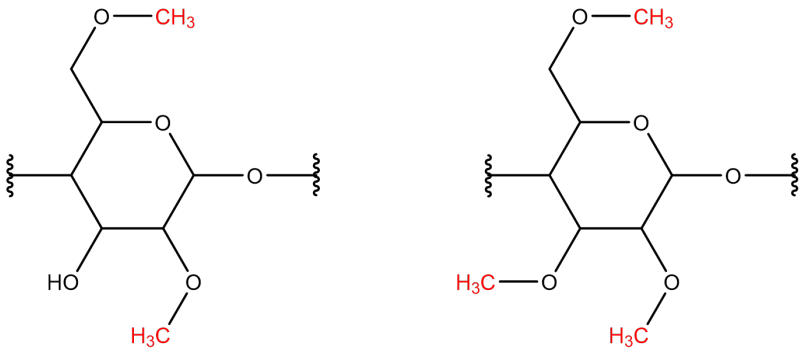

Figure 2.6: Indication of the position of methoxylation of dimethyl- and trimethyl-β-cyclodextrin.

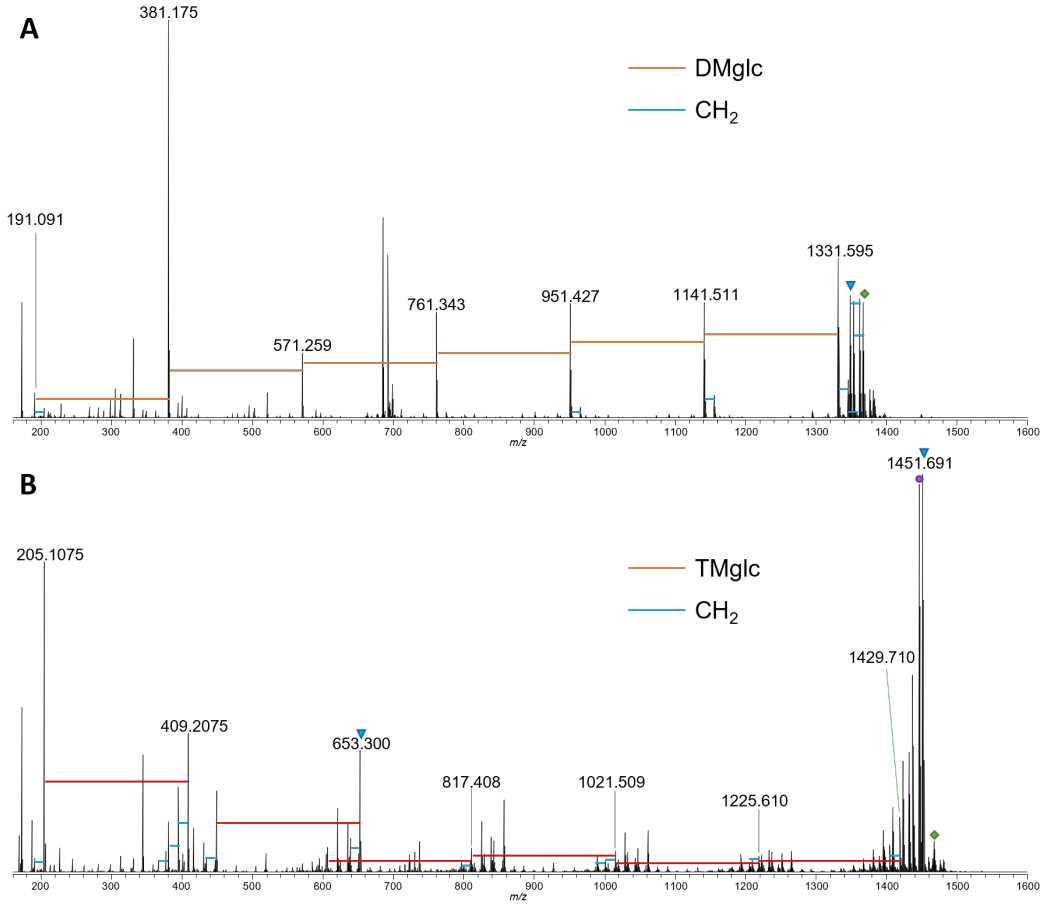

Figure 2.7: Full scan mass spectra of A) dimethyl-, and B) trimethyl-β-cyclodextrin. Sodium adducts are indicated with a triangle, potassium adducts with a rhombus, and ammonium adducts with a circle.

the proton (m/z 1331.597), sodium (m/z 1353.578), potassium (m/z 1369.552), and ammonium (m/z 1348.623) adducts, with a total of 14 methoxy-groups (two per subunit) are recorded. Similar to the experiments with trimethylated β-cyclodextrin, a series of signals differing by 14 Da is detected, ranging from a total of 13–17 methoxy groups is also observed for dimethylated β-cyclodextrin, giving evidence for the presence of the cyclodextrin with altered degree of methylation. Also, these different degrees of methylation lead to signals differing by 14 Da occurring from the loss of dimethylated glucose subunits (190 Da). Proper isolation of precursor ions is aggravated due to the overlapping signals. These incomplete methylations also tremendously complicate the interpretation of spectra. For example, the decomposition (also in-source) of a dimethyl-β-cyclodextrin with an additional methoxy group ($[\mathrm{DM\beta CD} + \mathrm{CH_2} + \mathrm{H}]^+$) can result in two different hexameric ions, depending on the identity of the cleaved subunit, as shown in equation 2.1 and 2.2. This is even more amplified by the broad range of methylation detected for these

samples. As with two additional methylations, also different regioisomers are possible, which lead to different patterns of fragment ions [238].

$$[\mathrm{DM\beta CD} + \mathrm{CH_2} + \mathrm{H}]^+ \xrightarrow{\text{-DMglc}} [\mathrm{DMglc_6} + \mathrm{CH_2} + \mathrm{H}]^+ \tag{2.1}$$

$$[\mathrm{DM\beta CD} + \mathrm{CH_2} + \mathrm{H}]^+ \xrightarrow{\text{-TMglc}} [\mathrm{DMglc_6} + \mathrm{H}]^+ \tag{2.2}$$

Despite the overlapping signals, the dimethylated glucose dimer $[\mathrm{DMglc_2} + \mathrm{H}]^+$ and the trimethylated glucose monomer $[\mathrm{TMglc} + \mathrm{H}]^+$ could be isolated as precursors from their full scan experiments, respectively. Comparable to the decomposition of the unmodified glucose monomer deriving from β-cyclodextrin, consecutive losses of $\mathrm{H_2O}$ and $\mathrm{CH_2O}$ are detected for $[\mathrm{DMglc_2} + \mathrm{H}]^+$, as well as the loss of $\mathrm{CH_3OH}$ (figure 2.8A). While $\mathrm{H_2O}$ is cleaved from protonated hydroxy groups, the loss of $\mathrm{CH_3OH}$ occurs from protonated methoxy groups. Interestingly, the same pattern is detected for the decomposition of $[\mathrm{TMglc} + \mathrm{H}]^+$, including the loss of a $\mathrm{H_2O}$ (figure 2.8B, red). This is surprising, as all initially present hydroxy groups are exchanged by methoxy-groups. Therefore, the presence of the ion $[\mathrm{TMglc} - \mathrm{H_2O} + \mathrm{H}]^+$ at *m/z* 187.096 indicates that a hydroxy group had to be formed in a previous fragmentation step.

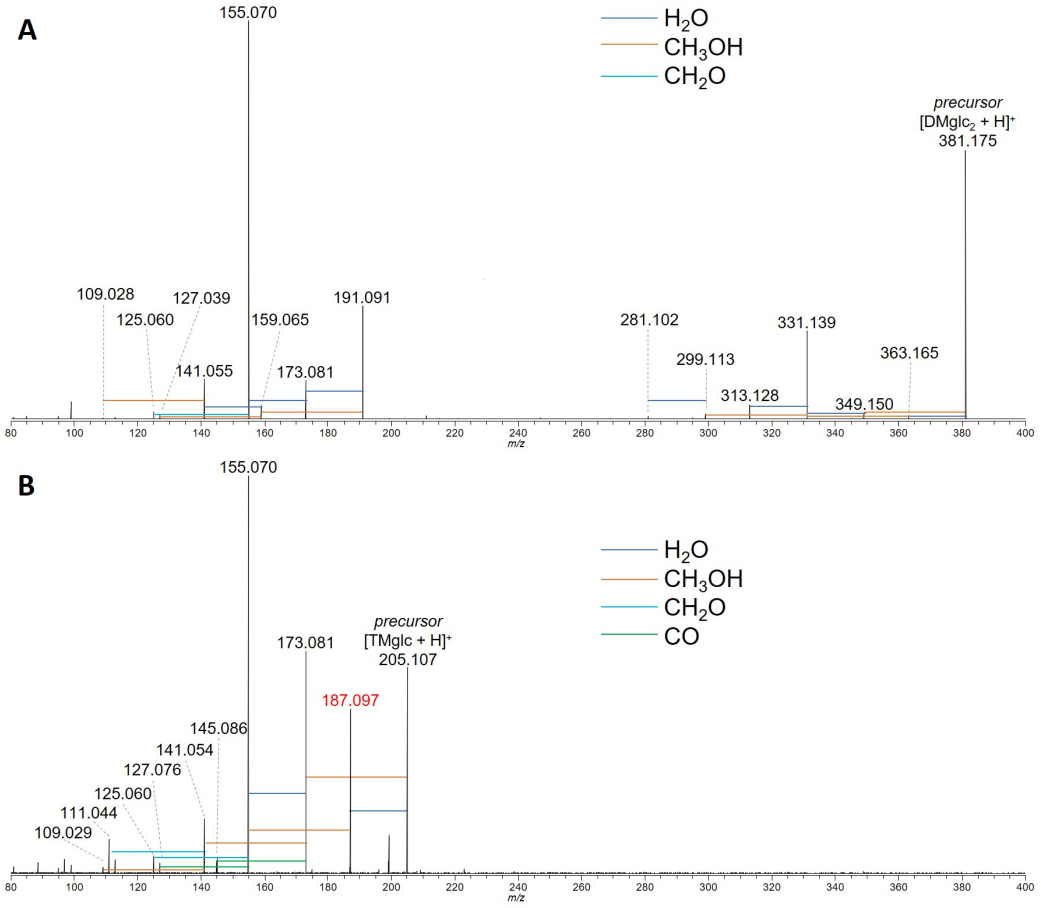

Figure 2.8: Tandem mass spectra obtained by A) HCD activation of $[DMglc_2 + H]^+$ and B) ion-trap CID activation of $[TMglc + H]^+$, with the loss of H_2O indicated in red.

2.3 Fragmentation Pathways

The detected fragment ions of α-, β-, γ-, as well as dimethyl- and trimethyl-β-cyclodextrin are summarized in the fragmentation pathway shown in figure 2.9. They coincide with signals described in literature [155, 157, 221, 228, 229, 231–235]. The sequential loss of neutral glucose subunits is the main identified fragmentation pathway down to glucose dimers. From this point, consecutive losses of H_2O and CH_2O are detected in the case of unmodified cyclodextrins, and H_2O, CH_2O, and CH_3OH in the case of methylated cyclodextrins. Special attention should be paid to the loss of H_2O from the trimethylated glucose monomer, as it implies that a hydroxy group had to be formed during previous fragmentation steps. Based on these fragmentation pathways, the underlying fragmentation mechanism has been proposed.

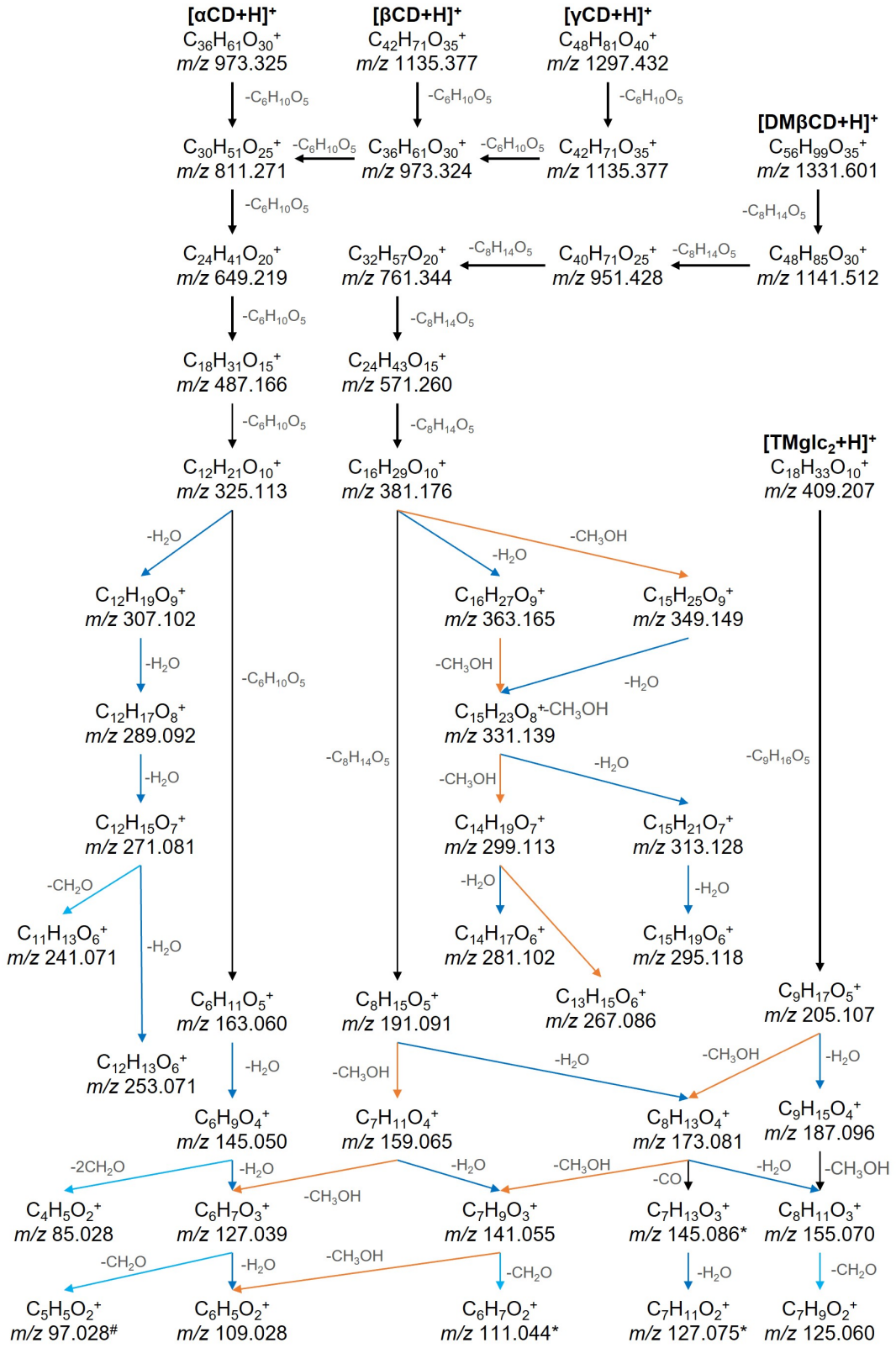

Figure 2.9: Combined fragmentation pathways of α-, β, γ-cyclodextrin, and the di- and trimethylated derivatives of β-cyclodextrin. # Fragment ions exclusively detected for β-cyclodextrin. * Fragment ions exclusively detected for trimethylated β-cyclodextrin.

2.4 Fragmentation Mechanism

Of the previously mentioned publications which address the decomposition of cyclodextrins in more detail, Donkuru et al. [235] and Jang and Choi [234] proposed a structure of the fragment ions, however, without further discussion of the mechanisms. Rabus et al. [229] and Dossmann et al. [154], on the other hand, proposed fragmentation mechanisms, but of sodium adducts. Those two have been published after the submission of our own publication on this topic. Therefore, they have not been considered in the deduction of our published mechanism. Nevertheless, they will be compared to our mechanism at the end of this section.

As only sparse information is available on the fragmentation of cyclodextrins, the mechanisms known for linear and branched oligosaccharides are used as the basis for proposing mechanisms applicable to protonated cyclodextrins. Therefore, cyclodextrins are treated as an internal part of a linear oligosaccharide of infinite length. Although the nomenclature proposed by Domon and Costello [196] is not strictly applicable to cyclodextrins due to the lack of a reducing or non-reducing end, it can be used to label the fragmentation site relative to the rest of the structure (figure 2.10). B-/Y- and C-/Z-ions differ in the location of the glycosidic oxygen, whereas B-/C- and Y-/Z-ions differ in the charge location after the fragmentation. Therefore, if the glycosidic oxygen remains bound to C1, B-/Y-fragments are formed, whereas C-/Z-fragments are formed when the oxygen remains bound to C4.

In linear oligosaccharides, the first cleavage results in two fragments of different lengths, depending on the cleavage site. In cyclodextrins, the first cleavage results in only one fragment ion, independent of the cleavage site, as the macrocycle gets linearized. At this point, the mechanism inducing the first cleavage and the structure of the linearized cyclodextrin is not known. However, the structure of the linearized cyclodextrin has to be appropriate for further loss of $C_6H_{10}O_5$ as the primary fragmentation step. Furthermore, at any point, a new hydroxy group has to be formed, indicated by the loss of a H_2O from the trimethylated glucose monomer. Based on these criteria, fragmentation mechanisms of linear saccharides are evaluated for their applicability to protonated cyclodextrins.

In general, fragmentation mechanisms are either charge-induced or charge-remote. This means the charge-carrying proton is either located at a specific site, inducing fragmentation, or its location is not affecting the cleavage. If the first cleavage is charge-remote, the proton remains mobile on the resulting fragment ion. Therefore,

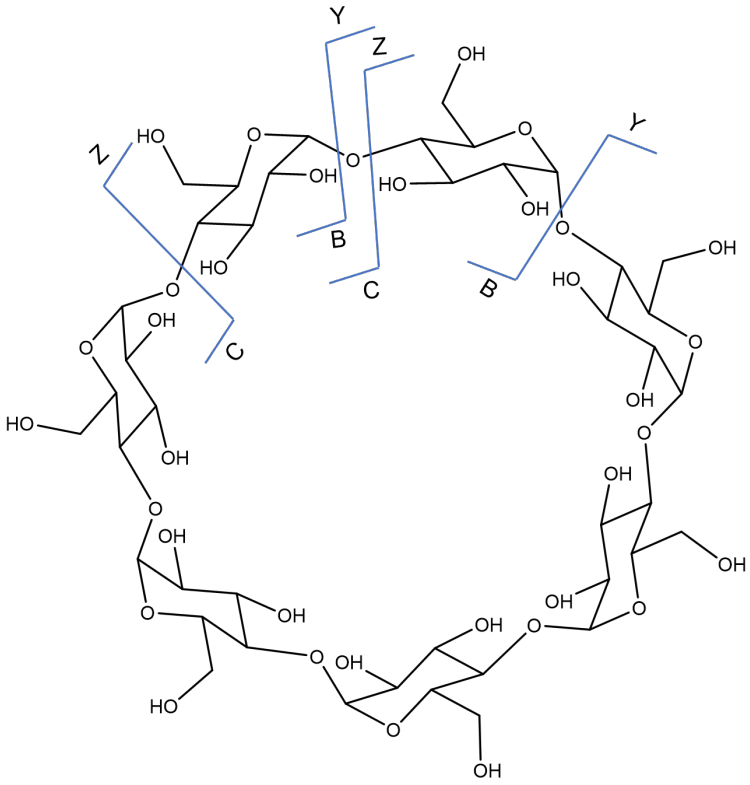

Figure 2.10: Application of the nomenclature proposed by Domon and Costello [196] on cyclodextrins.

loss of water (from any hydroxy group) is expected, as described in several publications [188, 190, 215, 245]. As loss of H_2O is not detected in our experiments, the first cleavage has to be charge-induced, and the proton has to be consumed in this linearization step. The glycosidic oxygens are the most acidic sites within the macrocyclic structure. The charge-carrying proton is, therefore, bound to any of these glycosidic oxygens [188, 234]. This is also a common feature of various fragmentation mechanisms of linear and branched oligosaccharides [174, 189, 190, 196, 225].

Protonation at the glycosidic oxygen can induce cleavage either next to the C1 or next to C4, resulting in B-/Y- or C-/Z-fragments, respectively. As discussed previously, the composition, connectivity, and configuration of saccharides significantly affect the fragmentation mechanisms, limiting the number of mechanisms applicable to the structure of cyclodextrins, due to steric effects. A single mechanism for the formation of C-/Z- ions is proposed by Bythell et al. [190] (figure 1.13F). This mechanism fulfills the requirements of forming a new hydroxy group and consuming the proton. However, the consecutive loss of glucose subunits as the predominant fragmentation step is not achievable from these C- and Z-fragment ion structures. Of the mechanisms leading to B- and Y- ions, the formation of a

1,6-anhydrogalactose proposed by Bythell et al. [190] and Zhu et al. [225] (figure 1.13B) matches the formation of a new hydroxy group and the ability to lose further glucose subunits. However, the mobilized proton at the C6 hydroxy group will be able to induce the loss of H_2O, which is contradictory with our results. Furthermore, the 1,6-anydrogalactose structure of the B-ion is also disproved by the fragmentation observed in methylated cyclodextrins, as they comprise a methoxy group at the C6 position. Therefore, not a proton but a CH_3^+ would be mobilized. In further dissociation steps, this CH_3^+ would induce glycosidic bond cleavage, leading to its transfer to either a hydroxy or a glycosidic oxygen. As no fragments of the trimethylated β-cyclodextrin are detected that comprise more than three methylations per subunit, this mechanism is also rated as implausible. The mechanisms proposed by Fentabil et al. [215] and Zhu et al. [225] (figure 1.13C and D) both include the transfer of the hydrogen of the C2 hydroxy group to the glycosidic oxygen. Comparable to the previously discussed mechanism, this is not in accordance with the fragments observed for methylated cyclodextrins, as no transfer of a methyl group is detected. The transfer of the C2 hydrogen, as suggested by Zhu et al. [225] (figure 1.13E) is not affected by the methylation. However, steric effects hinder this proton transfer. In the structure proposed by Zhu et al. [225], the C2 hydrogen is in the equatorial position and the glycosidic oxygen is in β-position (equatorial). Therefore, they are in proximity, enabling their interaction (figure 2.11 left). In cyclodextrins, the α-position of the glycosidic oxygen (axial) and the equatorial position of the C2 hydroxy group prevent such interaction (figure 2.11 right).

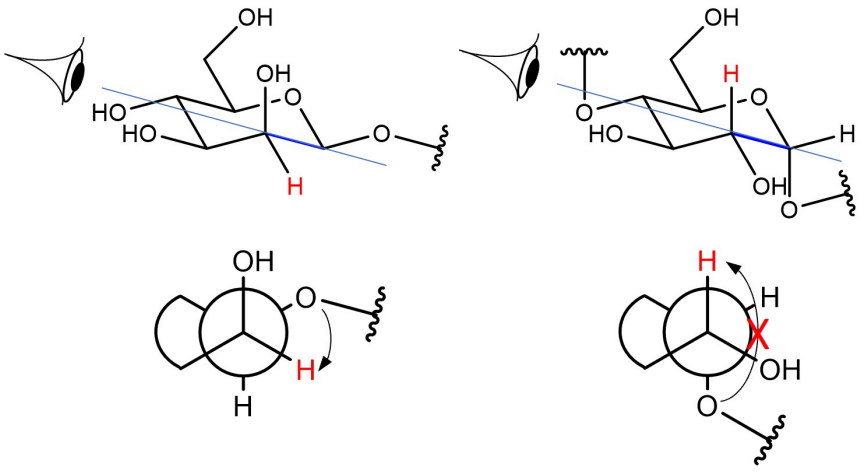

Figure 2.11: Steric hindrance preventing the transfer of the C2 hydrogen to the glycosidic oxygen in cyclodextrins (right), compared to the conformation described by Zhu et al. [225] (left).

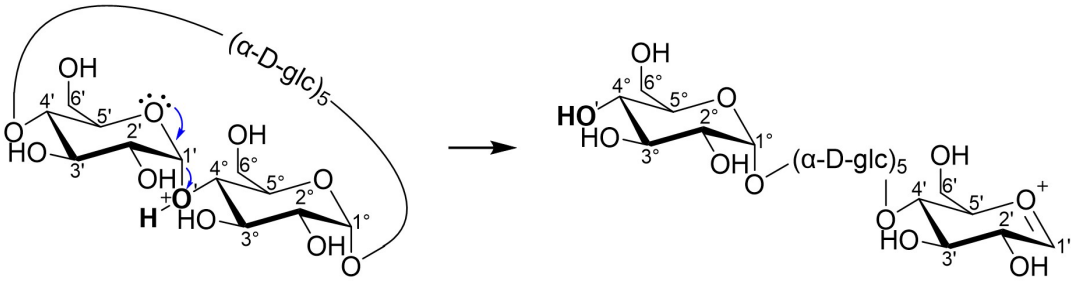

Figure 2.12: Proposed mechanism inducing the linearization of the macrocyclic structure of β-cyclodextrin. Reprinted from [246].

The charge-induced cleavage of the glycosidic bond by protonation of the glycosidic oxygen and formation of a double bond from an electron lone pair of the ring-oxygen, as shown in figure 1.13A is also applicable to cyclodextrins. It fulfills all requirements on the first fragmentation step: a new hydroxy group is formed, no proton gets mobilized, and loss of other $C_6H_{10}O_5$ moieties is possible. Therefore, this formation of an oxonium-ion is proposed as the first step, inducing the linearization of the macrocyclic structure. With the formation of the new hydroxy group at the C4, a non-reducing end is introduced (figure 2.12). Consequently, the resulting linearized structure is identical to a B-ion deriving from a linear saccharide. The formation of the corresponding Y-ion is declined, as Y-ions are proposed to decompose to B- and smaller Y-ions, leading to two series of fragment ions, whereas B-ions only form other B-ions [215].
This resulting B-ion undergoes further cleavage of glycosidic bonds, following a similar mechanism. Delocalization of the electron lone pair towards the antibonding orbital of the glycosidic bond induces its cleavage (figure 2.13). Due to the lack of a proton at the glycosidic oxygen, it retains a negative charge. Together with the previously formed oxonium ion, the fragment is lost either as a zwitterion (L1), as a 1,4-anhydroglucose (L2) if one subunit is lost, or as a macrocyclic unit (L3) if several subunits are cleaved in one step (figure 2.14).

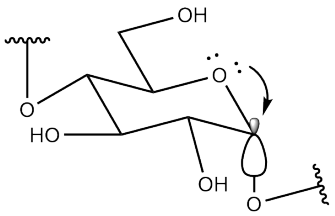

Figure 2.13: Illustration of the delocalization of the electron lone pair from the ring oxygen towards the antibonding orbital of the glycosidic bond in the α-configuration.

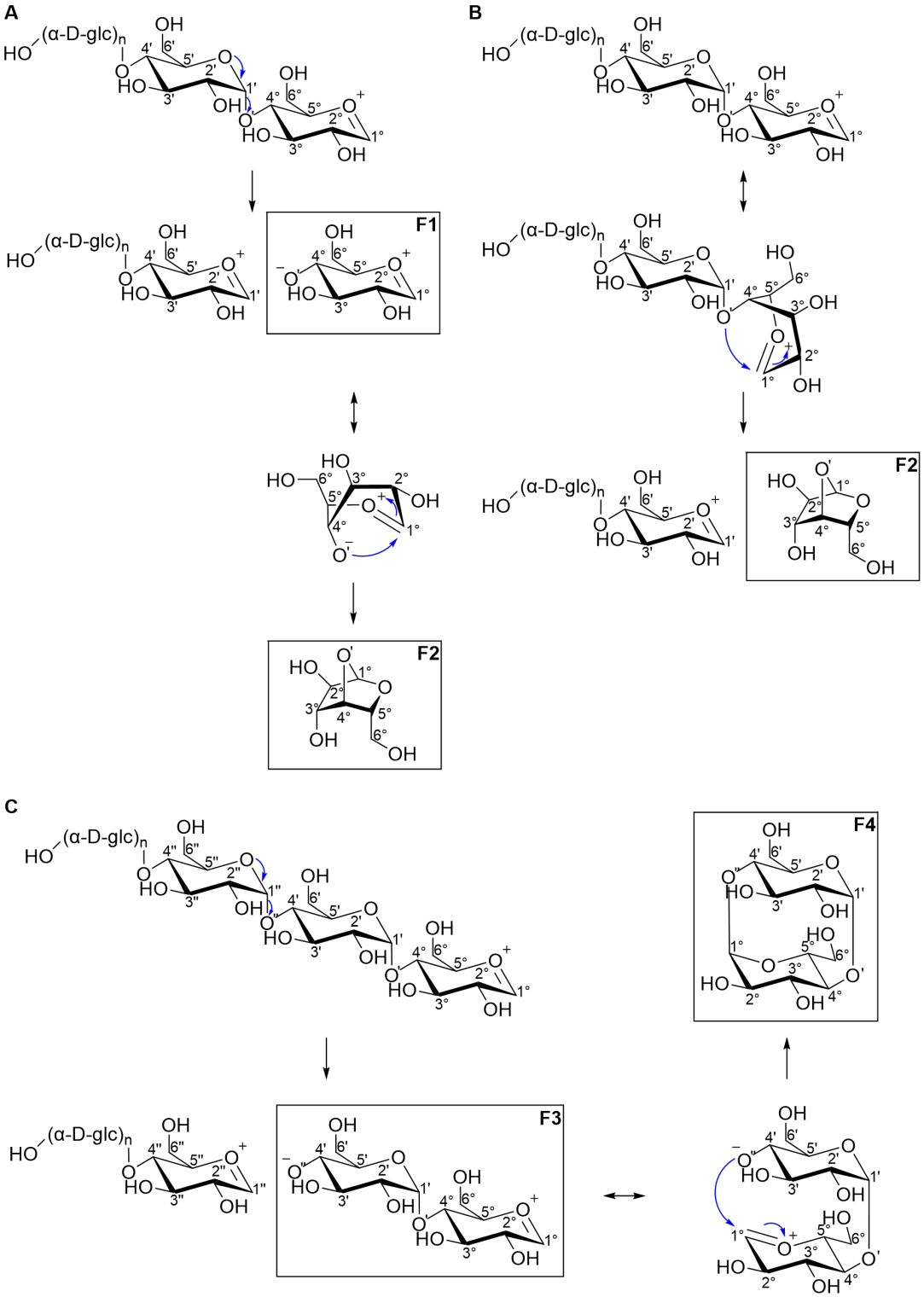

Figure 2.14: Proposed fragmentation mechanism explaining the consecutive loss of glucose subunits from the linearized β-cyclodextrin. Reprinted from [246].

The structure of fragment ions proposed by Donkuru et al. [235] do not coincide with our results but correspond to the transfer of a C1 hydrogen, as proposed by Zhu et al. [225]. However, this mechanism can be ruled out due to steric hindrance. Also, hydrogen transfer from the skeletal carbons is proposed by Rabus et al. [229] in addition to the transfer of the proton from the C2 hydroxy group to the glycosidic bond. As discussed previously, these transfer reactions are implausible due to steric hindrance. Additionally, the fragments obtained from trimethylated derivatives contradicts the transfer of protons at hydroxy groups, as this would induce the transfer of a CH_3^+ from a methoxy group, which is not detected. Furthermore, the mechanism proposed by Rabus et al. [229] is generally questionable, as the arrows indicating the movement of electrons are not drawn correctly in the transfer of the skeletal hydrogen. Jang and Choi [234] postulated two different pathways leading to ions of the same m/z ratio. Their proposed structure of the fragment ions deriving from cleavage of the linearized macrocycle coincides with our results. However, the structure of the neutral fragment comprises a 1,6-bridged subunit, which is not expected based on our findings on methylated cyclodextrins. Also, their second mechanism that describes the direct cleavage of two glycosidic bonds from the macrocyclic structure postulates the formation of 1,6-bridged glucose subunits. Therefore, this mechanism also does not coincides with our results. Although the mechanism suggested by Dossmann et al. [154] describes the dissociation of the doubly charged metal adducts of cyclodextrins, their mechanism is highly similar to our suggested mechanism. Consecutive cleavage of two glycosidic bonds leads to the exclusion of a zwitterionic glucose subunit, which coincides with our neutral fragment. As the second step, recyclization of the fragment ion is suggested. The mechanism for this recyclization is identical to cyclization process postulated in our own mechanism to occur on the neutral fragment.

The elucidated fragmentation mechanism underlying the decomposition of protonated cyclodextrins was published in *Carbohydrate Research* in 2021.

Carbohydrate Research 504 (2021) 108316

Contents lists available at ScienceDirect

Carbohydrate Research

journal homepage: www.elsevier.com/locate/carres

Fragmentation mechanisms of protonated cyclodextrins in tandem mass spectrometry

Pia S. Bruni, Stefan Schürch *

Department of Chemistry, Biochemistry and Pharmaceutical Sciences, University of Bern, Freiestrasse 3, CH-3012 Bern, Switzerland

ARTICLE INFO

Keywords:
β-cyclodextrin
Methylated cyclodextrin
Gas-phase fragmentation
Dissociation mechanism
Mass spectrometry

ABSTRACT

Tandem mass spectrometry has found widespread application as a powerful tool for the characterization of linear and branched oligosaccharides. Though the technique has been applied to the analysis of cyclic oligosaccharides as well, the underlying fragmentation mechanisms have hardly been investigated. This study focuses on the mechanistic aspects of the gas-phase dissociation of protonated β-cyclodextrins. Elucidation of the dissociation mechanisms is supported by tandem mass spectrometric experiments and by experiments on di- and trimethylated cyclodextrin derivatives. The fragmentation pathway comprises the linearization of the macrocyclic structure as the initial step of the decomposition, followed by the elimination of glucose subunits and the subsequent release of water and formaldehyde moieties from the glucose monomer and dimer fragment ions. Linearization of the macrocycle occurs due to proton-driven scission of the glycosidic bond adjacent to carbon atom C1 in conjunction with the formation of a new hydroxy group. The resulting ring-opened structure further decomposes in charge-independent processes forming either zwitterionic fragments, a 1,4-anhydroglucose moiety, or a new macrocyclic structure, that is lost as a neutral, and an oxonium ion. Since the hydroxy group formed at the ring-opening site can be regarded as the non-reducing end of the linearized structure, the fragment ion nomenclature commonly used for linear and branched oligosaccharides, which relies on the designation of a reducing and a non-reducing end, can also be applied to the description of fragment ions derived from cyclic structures.

1. Introduction

Carbohydrates are a family of highly abundant biopolymers that play essential roles in nature. Structural polysaccharides provide the basis for the formation of plant cell walls and exoskeletons of animals, whereas starch and glycogen are involved in energy storage in living organisms. Additionally, glycoconjugates fulfill indispensable tasks in various biological processes, such as intercell signaling and recognition. Oligo- and polysaccharides are composed of furanose or pyranose units that can adopt different conformations and offer several linkage positions. This results in a wide structural diversity comprising linear, branched, and cyclic motifs [1,2].

Cyclodextrins are cyclic oligosaccharides composed of α-(1→4) linked glucose subunits that are formed in nature by bacterial degradation of starch. The abundant native cyclodextrins consist of six, seven, or eight subunits and are referred to as α-, β-, and γ-cyclodextrin, respectively. Cyclodextrins can form supramolecular assemblies with hydrophobic guest molecules, which increase the solubility and stability of the encapsulated moieties in aqueous environment. Therefore, cyclodextrins have found applications in the food and beverage industry as carriers for additives, and the pharmaceutical industry takes advantage of cyclodextrins in drug formulations to increase the stability and bioavailability of drugs. To improve complex formation, tailored cyclodextrin derivatives with modifications at the hydroxy groups (e.g., alkylation) are synthesized (Fig. 1). The resulting structural diversity of cyclodextrin-based compounds created a need for their structural elucidation, and mass spectrometry has become a major pillar for such analyses [2–5]. However, structural alteration, the binding of metal ions, and the formation of host-guest inclusion complexes may affect the pathways of fragment ion generation in tandem mass spectrometric experiments [5,6]. Therefore, knowledge about the underlying dissociation mechanisms is crucial as it provides the basis for unambiguous data interpretation and the further investigation of cyclodextrin-based supramolecular assemblies.

* Corresponding author.
E-mail addresses: pia.bruni@dcb.unibe.ch (P.S. Bruni), stefan.schuerch@dcb.unibe.ch (S. Schürch).

https://doi.org/10.1016/j.carres.2021.108316
Received 5 November 2020; Received in revised form 5 March 2021; Accepted 6 April 2021
Available online 20 April 2021
0008-6215/

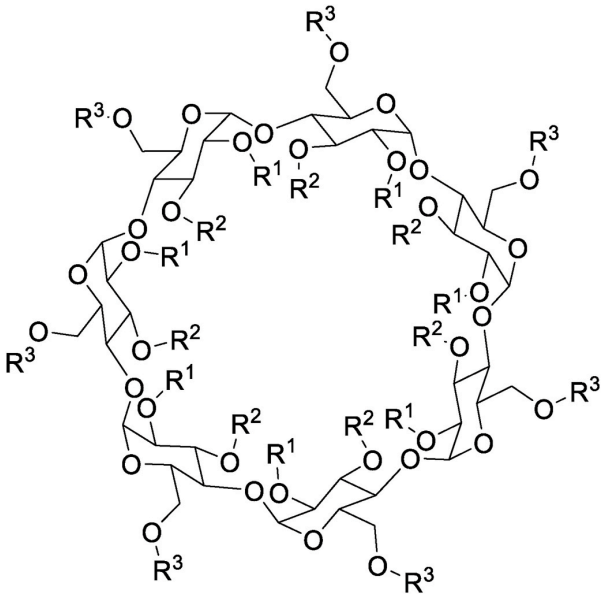

Fig. 1. Structure of β-cyclodextrin (R^1=R^2=R^3=H) and its methylated derivatives dimethyl-β-cyclodextrin (R^1=R^3=CH_3; R^2=H), and trimethyl-β-cyclodextrin (R^1=R^2=R^3=CH_3).

1.1. Mass spectrometry of linear oligosaccharides

Oligosaccharides are an extremely heterogeneous class of biopolymers. Unlike peptides, proteins, and oligonucleotides, which are mainly characterized by a linear sequence of clearly defined building blocks, oligosaccharide structures distinguish themselves from each other by the linkage positions, the composition, and additionally, their anomeric configuration. Such structural diversity is reflected by a multitude of dissociation pathways of oligosaccharide ions in the gas phase and renders structure elucidation by tandem mass spectrometry (MS/MS) a challenging task [7–11]. Already in the 1980s, studies based on fast atom bombardment and liquid secondary ion mass spectrometry revealed the complexity of carbohydrate structural analysis by mass spectrometry, but also demonstrated the potential of the method as a highly sensitive analytical tool [12,13].

A systematic nomenclature of oligosaccharide fragment ions was introduced by Domon and Costello, who applied fast atom bombardment for ionizing linear and branched glycoconjugates (Fig. 2) [14]. Fragment ions containing the non-reducing end of the sugar are referred to as A-, B-, and C- fragments, whereas X-, Y-, and Z-fragments contain the reducing end. B-/Y- and C-/Z-ion pairs both derive from cleavage of a bond next to the glycosidic oxygen. ^{m,n}A-/^{m,n}X-fragment ions are formed by cross-ring cleavage, with the cleaved bonds indicated by the superscripts. The authors also postulated mechanisms for the cleavage of the glycosidic bond, whereof one includes protonation at the glycosidic oxygen that leads to the formation of a B-type oxonium ion and its complementary Y-ion.

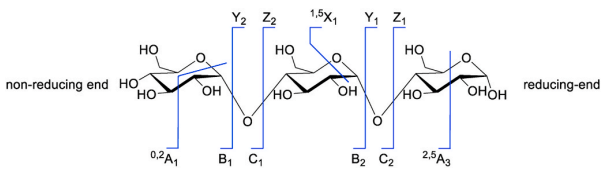

Fig. 2. Nomenclature of oligosaccharide fragments according to Domon and Costello [14].

In the following years, linear and branched oligosaccharides have been investigated in protonated, deprotonated, and metallated form by various mass spectrometric techniques as summarized in several reviews [1,3,7–10,15–18]. Studies focused on the products of metastable decay of oligosaccharide ions formed by infrared laser desorption [19], liquid secondary ion mass spectrometry [13,20], as well as MALDI [21–24], and on the products generated by blackbody infrared radiative dissociation [25] and collision induced dissociation (CID) of electrosprayed oligosaccharides [26]. These investigations disclosed the distinct differences in the dissociation of oligosaccharide anions, cations, and metallized species.

Studies on the dissociation of oligosaccharide cations revealed the strong influence of the charge-carrying coordinating ion. Protonation at the glycosidic oxygen was found to directly induce extensive cleavage of the glycosidic bond, whereas the weaker binding alkali metal ions rather generate cross-ring cleavage products of lower abundance [13]. Beside charge-induced mechanisms, alternative dissociation pathways independent from the location of the charge were proposed, which suggest the cleavage of the glycosidic bond occurring in conjunction with proton transfer either from the nearby C3 atom [13] or from the hydroxy-group bound to the C2 atom to the glycosidic oxygen [25]. The general consent of the findings from these investigations is that fragment ion formation is significantly influenced by the sugar species, the linkage position between the subunits, their anomeric configuration, the adduct species, and the polarity of mass spectrometric analysis. These characteristics were taken advantage of by further studies focusing on the elucidation of oligosaccharide conformations based on the relative intensities of specific fragment ions [20,27,28]. Also, the rearrangement of glycan subunits and the release of internal sugar moieties are specific phenomena contributing to the gas phase chemistry of protonated carbohydrate structures, mainly if an aglycone part or deoxyhexoses are involved. Such processes have been observed upon CID of protonated oligosaccharides and represent a potential cause for misinterpretation of MS/MS data, potentially compromising a correct sequence assignment [29–31].

1.2. Mass spectrometry of cyclodextrins

In contrast to the extensively investigated linear oligosaccharides, a limited number of studies focused on the dissociation of cyclic structures [5,32–35]. Though the loss of neutral subunits has been reported to be the prevalent fragmentation channel, the underlying mechanistic aspects and the elucidation of the corresponding fragment ion structures have not been described in detail.

A major challenge regarding the structural assignment of cyclodextrin fragments is the repetitive pattern of the macrocyclic structure as well as the wealth of hydroxy groups potentially participating in dissociation events. These ambiguities can at least partly be circumvented by including methylated cyclodextrin derivatives in the study, as the decreased number of hydroxy protons enables a more precise identification of functional groups involved in the fragmentation steps. Studies on the dissociation of cyclic oligosaccharides raised the question of how to denominate the fragment ions generated in the gas-phase [5]. The Domon and Costello nomenclature commonly applied to linear oligosaccharides is based on distinct reducing and non-reducing ends [14], which are obviously absent in cyclic structures.

To the best of our knowledge, there is a lack of mechanistic information regarding the fragmentation of cyclic oligosaccharides. In this study, we investigate the collision-induced dissociation of protonated β-cyclodextrins in the gas phase. Based on the obtained results, fragmentation mechanisms accounting for ring-opening and truncation of the linearized structure are proposed and supported by experiments on methylated cyclodextrins.

2. Experimental

Stock solutions at a concentration of 1 mM β-cyclodextrin (Fluka,

Buchs, Switzerland), heptakis(2,6-di-*O*-methyl)-β-cyclodextrin (DMβ-cyclodextrin, Sigma-Aldrich, Buchs, Switzerland), and heptakis(2,3,6-tri-*O*-methyl)-β-cyclodextrin (TMβ-cyclodextrin, Sigma-Aldrich, Buchs, Switzerland) in LC-MS grade H_2O (Merck KGaA, Darmstadt, Germany) were prepared. For mass spectrometric analysis, H_2O (Merck KGaA, Darmstadt, Germany), acetonitrile (MeCN, Biosolve, Dieuze, France), and formic acid (Honeywell, Steinheim, Germany), were used as solvents. Samples at a concentration of 0.02 μM in 50/50 H_2O/MeCN or 50/50 H_2O/MeCN + 1% formic acid were prepared from the stock solutions for electrospray ionization (ESI) mass spectrometry measurements.

ESI mass spectrometry was performed on an LTQ Orbitrap XL instrument (Thermo Fisher Scientific, Bremen, Germany) equipped with a nanoESI source. All measurements were performed in positive mode with a spray voltage of 0.8–1.3 kV. The capillary temperature was set to 200 °C, the capillary voltage to 20 V and the tube lens to 250 V. All mass spectra were acquired in FTMS mode with a resolution of 100000 in a mass range of *m/z* 50–2000. Ion trap CID and higher-energy C-trap dissociation (HCD) measurements were performed with a precursor ion selection window of 2–5 *m/z* with an activation time of 30 ms and helium (for ion trap CID) or nitrogen (for HCD) as collision gas, depending on the activation mode. External calibration was performed using the Pierce LTQ ESI Positive Ion Calibration Solution. Data proceeding was performed using the Xcalibur Software Suite including Qualbrowser ver. 2.2 (Thermo Fisher Scientific).

3. Results and discussion

The full scan ESI mass spectrum of β-cyclodextrin depicted in Fig. 4A gives evidence for adduct formation of oligosaccharides with various species. Besides the peak of the protonated β-cyclodextrin (*m/z* 1135.378), additional signals corresponding to the sodium (*m/z* 1157.360), ammonium (*m/z* 1152.405), and the potassium adduct (*m/z* 1173.334) appear. In addition to the intact β-cyclodextrin, fragments pointing to a series of one to six protonated glucose subunits are detected (*m/z* 163.060, 325.113, 487.166, 649.219, 811.273, and 973.326), whereas similar signals of the corresponding sodium adducts are hardly visible. Despite ESI being classified as a soft ionization technique, this ion series is expected to be generated by in-source dissociation of protonated β-cyclodextrin, as evidenced by tandem MS (MS/MS, MS^2) experiments using CID of isolated protonated β-cyclodextrin, which results in identical fragment ions (Fig. 4B). Additional collisional activation of the cyclodextrin fragment ions in MS^3 experiments by subjecting ions generated by ion trap CID to activation by HCD leads to the consecutive loss of glucose subunits from the precursor ions and the MS^3 spectrum of the hexameric glucose precursor ion $[glc_6+H]^+$ (Fig. 4C) closely resembles the MS/MS spectrum of β-cyclodextrin.

The effect of different fragmentation energies on the detected fragment ions are shown in the HCD breakdown curve of $[\beta CD+H]^+$ (Fig. 3) and $[glc_6+H]^+$ (supplementary material, Figure S3). Normalized collision energies (NCE) applied during the experiment are converted to eV for HCD measurements [35,36].

Experiments on chemically altered compounds greatly assist in mechanistic studies, as selective blocking of proton donors and acceptors reveals their role in dissociation pathways. Hydroxy groups represent proton sources that potentially participate in cleavage reactions

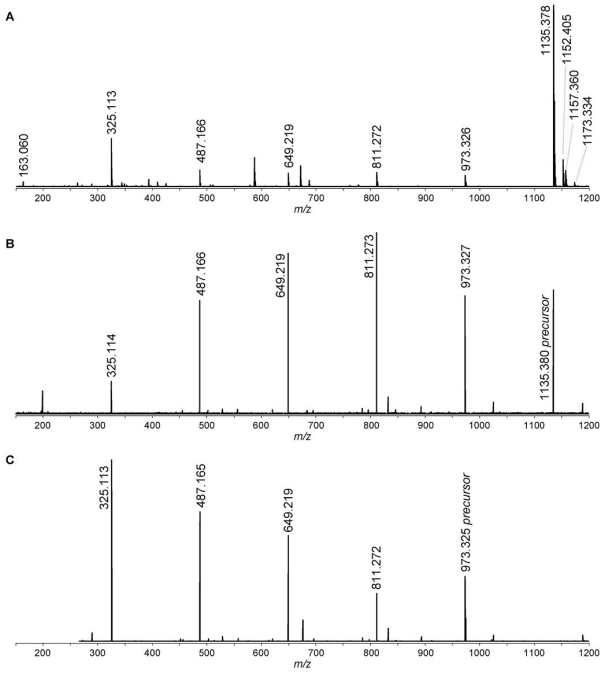

Fig. 4. ESI mass spectra of β-cyclodextrin. A) Full scan spectrum. B) HCD spectrum of $[\beta CD+H]^+$ (20.0 eV). C) ion trap CID spectrum of the hexameric glucose ion $[glc_6+H]^+$ (20% NCE, 30 ms activation time).

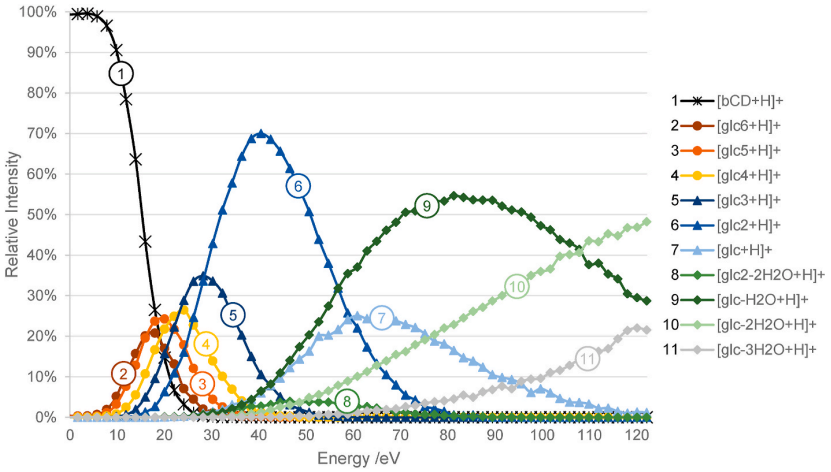

Fig. 3. HCD breakdown curve of $[\beta CD+H]^+$. Fragments with a maximum relative intensity <2% are not displayed.

upon collisional activation of biopolymers, and such approach also turned out to be beneficial for the elucidation of the mechanisms responsible for the dissociation of protonated cyclodextrins.

Analysis of DM- and TMβ-cyclodextrin reveals mixtures with different methylation degrees, causing the series of peaks spaced by 14 mass units and leading to higher spectral complexity. The spectrum of DMβ-cyclodextrin indicates the presence of protonated derivatives comprising 13 to 15 methyl groups (*m/z* 1317.586, 1331.601, and 1345.617) (Fig. 5A and B, supplementary material Figure S2). Though the corresponding ammonium and sodium adducts are detected, the abundant fragment ion peaks at *m/z* 191.092, 381.176, 571.261, 761.346, 951.431, and 1141.516 exclusively refer to the series of up to six dimethylated glucose subunits originating from in-source dissociation of the protonated precursor ion, whereas fragments derived from ammonium adducts or sodiated cyclodextrin are not observed. As for the protonated unmodified β-cyclodextrin, additional collisional activation of in-source generated fragment ions in pseudo-MS^3 experiments results in signals differing by 190 Da, corresponding to dimethylated glucose subunits (Fig. 5C).

While the dissociation of longer linearized oligosaccharide ions is mainly characterized by the release of glucose moieties, a different picture is obtained from fragment ions consisting of one or two subunits only. Collisional activation of the glucose dimer $[glc_2+H]^+$ derived from β-cyclodextrin shows repetitive losses of H_2O and CH_2O (supplementary material, Figure S1A), whereas collisional activation of the dimethylated glucose dimer $[DMglc_2+H]^+$ (supplementary material, Figure S1B) and the trimethylated glucose monomer $[TMglc+H]^+$ result in consecutive losses of H_2O, CH_2O, and CH_3OH moieties in various combinations (Fig. 6). The loss of H_2O from the trimethylated glucose monomer should be highlighted as this fragment (*m/z* 187.097) gives evidence for a newly formed hydroxy group in a previous fragmentation step and is indicative for the underlying dissociation mechanism.

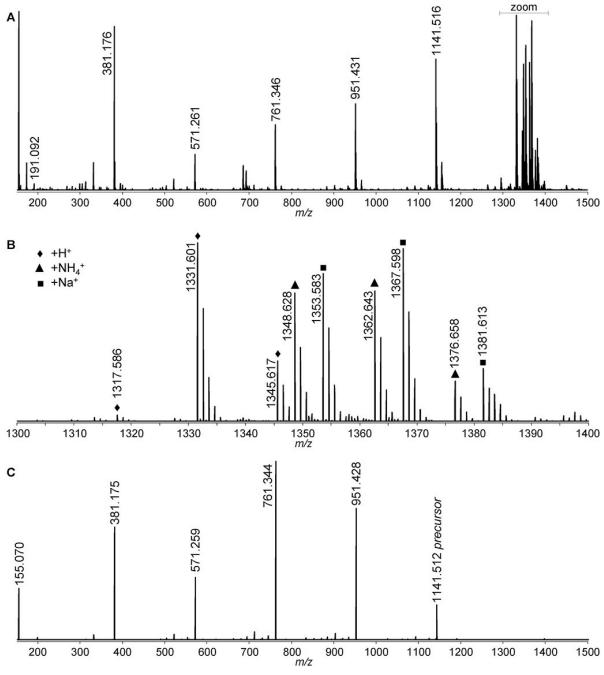

Fig. 5. ESI mass spectra of DMβ-cyclodextrin A) Full scan mass spectra of DMβ-cyclodextrin with B) zoom of the *m/z* range 1300–1400. Protonated fragments are indicated by a rhomb, ammonium adducts by a triangle, and sodiated fragments by a square. C) Collisional activation of the dimethylated hexameric fragment ion $[DMglc_6+H]^+$ (HCD, 20.1 eV) showing the repetitive loss of 190 Da, corresponding to dimethylated glucose subunits.

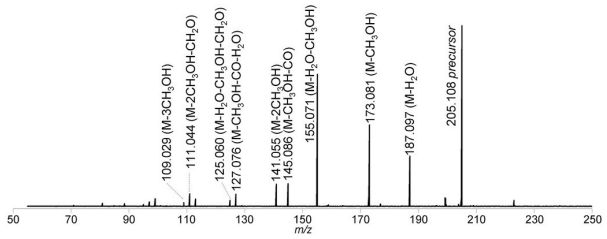

Fig. 6. ESI mass spectrum of the collisionally-activated trimethylated glucose monomer fragment $[TMglc+H]^+$ (CID, 10% NCE, 30 ms activation time).

An overview of all detected ions with formula, calculated and experimental *m/z* and ppm error, as well as a fragmentation pathway is provided in Table S1 and Figure S4 in the supplementary material.

3.1. Fragmentation mechanism

The dissociation of collisionally-activated cyclic oligosaccharides comprises opening of the macrocycle as a first step, which is subsequently followed by the decomposition of the linearized structure and the further decomposition of the subunits.

3.1.1. Linearization of the macrocycle

Protonation of cyclodextrins takes place at one of the glycosidic oxygen atoms, as these are the most basic oxygen in the structure [37]. This is supported by the lack of any signal pointing to a loss of H_2O from $[\beta\text{-cyclodextrin}+H]^+$, which would arise as a consequence of the protonation of a hydroxy group upon in-source fragmentation or collisional activation experiments (Fig. 4). The lone pair electrons of the ring-oxygen are delocalized to the antibinding orbital of the

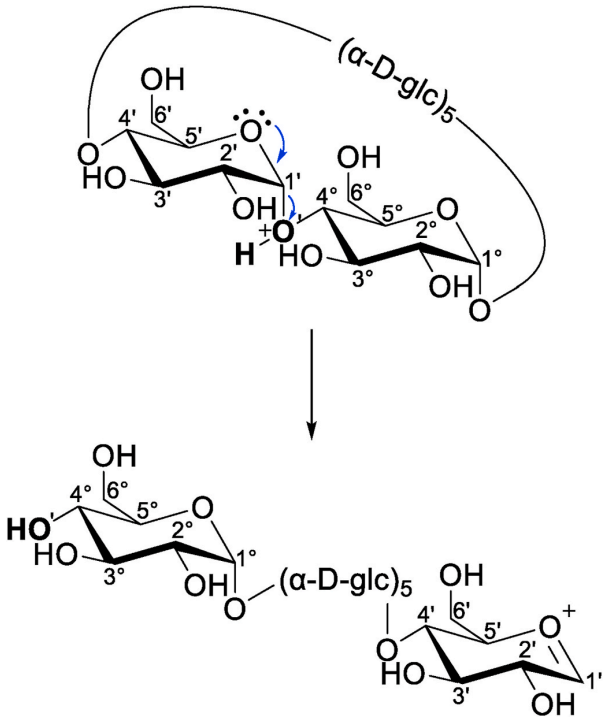

Scheme 1. Proposed mechanism for the charge-induced ring-opening and linearization of protonated β-cyclodextrin, resulting in formation of a new non-reducing end (bold).

C1′-glycosidic oxygen bond [38], resulting in cleavage of the glycosidic bond and therefore, linearization of the macrocyclic structure (Scheme 1). Consistent to the fragmentation of linear oligosaccharides, scission of the glycosidic bond adjacent to C1′ is preferred over cleavage next to C4° and the resulting linearized oligosaccharide bears a newly formed hydroxy and an oxonium group. The localization of the charge on the ring-oxygen can be proven by the lack of H_2O loss from the linearized cyclodextrin, which would arise as a consequence of the presence of a free proton.

The two series of complementary fragments derived from linear and branched oligosaccharides are referred to as A-, B-, C- and X-, Y-, Z-ions, depending on whether they comprise the reducing or the non-reducing end of the sugar, respectively [14]. The validity of such nomenclature to cyclic oligosaccharides has raised controversy, due to the lack of clearly

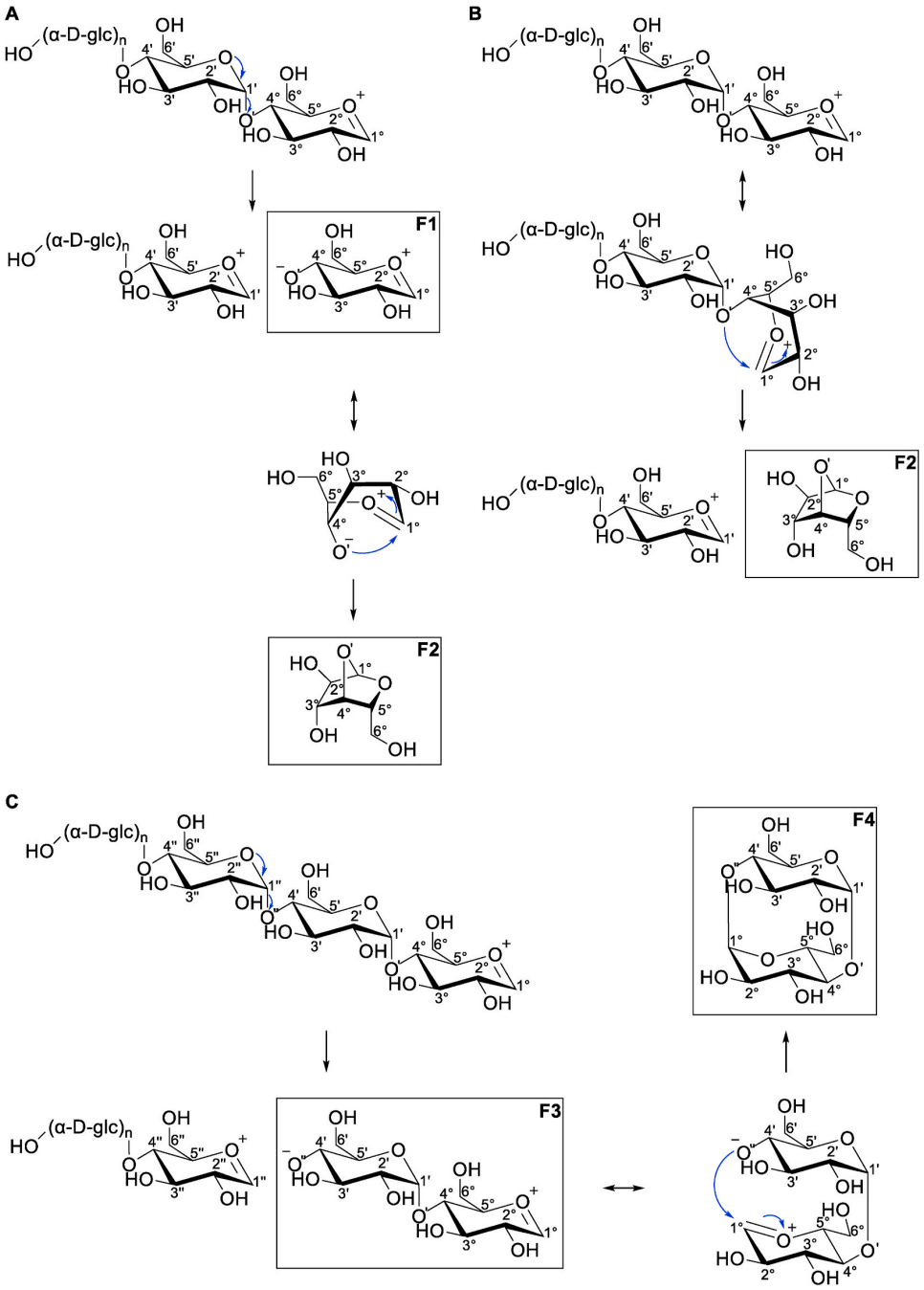

Scheme 2. Proposed mechanism for the loss of neutral glucose subunits from linearized cyclodextrins. A) Two-step reaction resulting in the loss of either a zwitterion (**F1**) 1,4-anhydroglucose **F2**. B) Direct loss of 1,4-anhydroglucose **F2** via a concerted reaction. C) Two-step reaction leading to the release of two glucose subunits, either as the zwitterion **F3** or the macrocyclic unit **F4**.

assignable ends [5]. Though no reducing and non-reducing end can be assigned to cyclic oligosaccharides, the fragment ion nomenclature of Domon and Costello is nevertheless applicable, as the hydroxy group formed in the linearization step represents a new non-reducing end. In combination with the oxonium ion at the opposite end of the linearized cyclodextrin (Scheme 1), the structure is identical to a B-ion originating from the decomposition of a native linear oligosaccharide. The formation of the corresponding Y-ion from protonated cyclodextrin is excluded, as the transfer of a proton to any hydroxy group, would promote the loss of H_2O, which is not detected from collisional activation of β-cyclodextrin. The same mechanism must apply to the fragmentation of DMβ- and TMβ-cyclodextrins, as the consecutive loss of $C_8H_{14}O_5$ and $C_9H_{16}O_5$ units, respectively, is detected without any indication for the transfer of methyl groups or neutral loss of CH_3OH (Fig. 5).

3.1.2. Decomposition into subunits

The occurrence of a linearization step as the initial dissociation event of cyclic oligosaccharides significantly affects their further decomposition. Decay of the protonated precursor ion must follow a two-step pathway involving ring opening and linearization of the macrocyclic structure followed by the cleavage of a second glycosidic bond in order to consecutively lose glucose subunits. In contrast to the dissociation of native linear oligosaccharides, the charging proton has been consumed in the linearization step and consequently, is not available for participating in further cleavage reactions anymore. Nevertheless, the fragment ions resulting from collisional activation of protonated β-cyclodextrin (in-source dissociation or ion trap CID/HCD) show exclusively the consecutive loss of 162 Da ($C_6H_{10}O_5$), corresponding to neutral glucose subunits (Fig. 4). No signals pointing to cross-ring cleavage (A- or X-ions) or neutral loss of other moieties are detected. This observation supports the hypothesis that the structure of the linearized macrocycle is identical to a B-ion, as the fragmentation of B-ions leads to other B-ions only, whereas the fragmentation of Y-ions would result in the formation of new B- and Y-ions [25].

As a result of the cleavage of the glycosidic bond, an oxonium-ion is formed at the ring-oxygen of the fragment ion. Consequently, a negative charge resides at the glycosidic oxygen of the released glucose subunit, which is either released as this zwitterionic species **F1**, which further rearranges to 1,4-anhydroglucose **F2** via a conformational change in combination with the nucleophilic attack of the negatively charged O′ on C1° (Scheme 2A), or decomposes directly into **F2** in a concerted reaction (Scheme 2B). Both mechanisms are indistinguishable by mass spectrometry, as the mass of the resulting ions is identical.

Since this mechanism is charge-independent, delocalization of the ring-oxygen lone pairs can occur next to any glycosidic bond and lead to the loss of larger fragments (Scheme 2C). The loss of multiple glucose moieties differs from the release of a single glucose inasmuch as the charges of the zwitterion **F3** reside on different glucose moieties. Analogous to the loss of one glucose residue, the negatively charged O″ can attack on C1°, resulting in a new glycosidic bond and cyclisation of the fragment (**F4**). Furthermore, direct loss of fragment **F4** in a concerted reaction leads to indistinguishable fragments.

In contrast, attack of O″ electrons on C1′ can be excluded due to mechanistic aspects. Compared to the sp^2-hybridized C1° at the terminal glucose unit comprising an oxonium ion, C1′ located within the chain is sp^3-hybridized. Consequently, attack of the O″ electrons on the antibonding orbital inducing cleavage of the glycosidic bond is precluded due to the three-dimensional arrangement, and therefore inhibits the loss of an internal glucose residue.

Although the structures of the fragments lost as neutrals are different in the proposed mechanisms (Scheme 2), the structure of the detected fragment ions is identical and a combination of the three mechanism is likely to apply. The proposed mechanisms are applicable to methylated oligosaccharide derivatives as well, as no hydroxy groups are involved.

These mechanisms are opposed to the pathways proposed in literature so far for linear oligosaccharides. The alternative charge-remote mechanism proposed by Ngoka et al. [13], involving the transfer of the C3° hydrogen from the adjacent sugar towards the oxonium ion, can be excluded as it would lead to the loss of a neutral $C_6H_{12}O_6$ (180 Da) moiety instead of $C_6H_{10}O_5$ (162 Da), as demonstrated in Fig. 4. Transfer of the C2′ hydrogen from the adjacent sugar towards the non-reducing end, as proposed by Zhu et al. [39] for β-(1→4)-linked glucose in cellulose is precluded as well, as steric hindrance inhibits the access to this hydrogen for the lone pair electrons of this hydrogen.

Further mechanistic evidence was gained by experiments on DM- and TMβ-cyclodextrin. Due to the substitution of hydroxy protons by methyl groups, dissociation mechanisms involving proton transfer reactions would either be disabled due to masking of the hydroxy protons, or result in the migration of methyl groups which would be recognizable by the corresponding mass shift of 14 Da. The fact that the product ion spectra of DM- and TMβ-cyclodextrin show the fragments with the corresponding degree of methylation only (e.g. *m/z* 381.175 for the dimethylated glucose dimer in Fig. 5C) contradicts the occurrence of methyl transfer reactions, thus, indicating that the decomposition of linearized structures does not involve any hydroxy groups of the glucose subunits. The release of H_2O from glucose subunits was observed regardless whether they are in methylated form or not (Fig. 6). Consequently, the loss of H_2O has to originate from the hydroxy group newly formed during the linearization step, as all initially available hydroxy groups are methylated in the case of the trimethylated glucose monomer.

4. Conclusion

The gas-phase dissociation of protonated β-cyclodextrins has been examined by ESI-MS/MS. Fragmentation was found to be initiated by cleavage of the macrocyclic structure at the protonated glycosidic oxygen atom. The dissociation of the linearized oligosaccharides distinguishes itself from linear structures as the charging proton is abstracted upon macrocyclic ring opening and is not available for inducing subsequent bond cleavages. Thus, linearization of the macrocycle is followed by the release of neutral glucose subunits following charge-independent mechanisms. The individual dissociation steps do not comprise transfer of hydroxy groups and are supported by the data obtained by the analysis of methylated cyclodextrin derivatives. Due to the formation of a new hydroxy group in the linearization step, the established nomenclature of oligosaccharide fragment ions nomenclature can be applied to linearized oligosaccharides as well.

Funding

This research did not receive any specific grant from funding agencies in the public, commercial, or not-for-profit sector.

Declaration of competing interest

The authors declare that they have no known competing financial interests or personal relationships that could have appeared to influence the work reported in this paper.

Appendix A. Supplementary data

Supplementary data to this article can be found online at https://doi.org/10.1016/j.carres.2021.108316.

References

[1] G.L. Sassaki, L.M. de Souz, Mass spectrometry strategies for structural analysis of carbohydrates and glycoconjugates, in: A.V. Coelho (Ed.), Tandem Mass Spectrometry - Molecular Characterization, InTech, 2013, https://doi.org/10.5772/55221.

[2] S.S. Braga, Cyclodextrins: emerging medicines of the new millennium, Biomolecules 9 (2019) 801, https://doi.org/10.3390/biom9120801.

[3] L. Szente, J. Szemán, T. Sohajda, Analytical characterization of cyclodextrins: history, official methods and recommended new techniques, J. Pharmaceut. Biomed. Anal. 130 (2016) 347–365, https://doi.org/10.1016/j.jpba.2016.05.009.
[4] C. Peptu, M. Danchenko, L. Škultéty, J. Mosnáček, Structural architectural features of cyclodextrin oligoesters revealed by fragmentation mass spectrometry analysis, Molecules 23 (2018) 2259, https://doi.org/10.3390/molecules23092259.
[5] A.O. Chizhov, Y.E. Tsvetkov, N.E. Nifantiev, Gas-phase fragmentation of cyclic oligosaccharides in tandem mass spectrometry, Molecules 24 (2019) 2226, https://doi.org/10.3390/molecules24122226.
[6] C. Przybylski, J.M. Benito, V. Bonnet, C.O. Mellet, J.M. García Fernández, Revealing cooperative binding of polycationic cyclodextrins with DNA oligomers by capillary electrophoresis coupled to mass spectrometry, Anal. Chim. Acta 1002 (2018) 70–81, https://doi.org/10.1016/j.aca.2017.11.034.
[7] M.J. Kailemia, L.R. Ruhaak, C.B. Lebrilla, I.J. Amster, Oligosaccharide analysis by mass spectrometry: a review of recent developments, Anal. Chem. 86 (2014) 196–212, https://doi.org/10.1021/ac403969n.
[8] Y. Park, C.B. Lebrilla, Application of Fourier transform ion cyclotron resonance mass spectrometry to oligosaccharides, Mass Spectrom. Rev. 24 (2005) 232–264, https://doi.org/10.1002/mas.20010.
[9] J. Zaia, Mass spectrometry of oligosaccharides, Mass Spectrom. Rev. 23 (2004) 161–227, https://doi.org/10.1002/mas.10073.
[10] E. Mirgorodskaya, N.G. Karlsson, C. Sihlbom, G. Larson, C.L. Nilsson, Cracking the sugar code by mass spectrometry: an invited perspective in honor of dr. Catherine E. Costello, recipient of the 2017 ASMS distinguished contribution award, J. Am. Soc. Mass Spectrom. 29 (2018) 1065–1074, https://doi.org/10.1007/s13361-018-1912-3.
[11] E. Mucha, A. Stuckmann, M. Marianski, W.B. Struwe, G. Meijer, K. Pagel, In-depth structural analysis of glycans in the gas phase, Chem. Sci. 10 (2019) 1272–1284, https://doi.org/10.1039/c8sc05426f.
[12] A. Dell, Mass spectrometry of carbohydrates, Adv. Carbohydr. Chem. Biochem. 45 (1987) 19–72, https://doi.org/10.1016/S0065-2318(08)60136-5.
[13] L.C. Ngoka, C.B. Lebrilla, J.F. Gal, Effects of cations and charge types on the metastable decay rates of oligosaccharides, Anal. Chem. 66 (1994) 692–698, https://doi.org/10.1021/ac00077a018.
[14] B. Domon, C.E. Costello, A systematic nomenclature for carbohydrate fragmentations in FAB-MS/MS spectra of glycoconjugates, Glycoconj. J. 5 (1988) 397–409, https://doi.org/10.1007/BF01049915.
[15] D.J. Harvey, Matrix-assisted laser desorption/ionization mass spectrometry of carbohydrates, Mass Spectrom. Rev. 18 (1999) 349–450, https://doi.org/10.1002/(sici)1098-2787.
[16] D.J. Harvey, Analysis of carbohydrates and glycoconjugates by matrix-assisted laser desorption/ionization mass spectrometry: an update covering the period 1999-2000, Mass Spectrom. Rev. 25 (2006) 595–662, https://doi.org/10.1002/mas.20080.
[17] D.J. Harvey, Analysis of carbohydrates and glycoconjugates by matrix-assisted laser desorption/ionization mass spectrometry: an update for 2013–2014, Mass Spectrom. Rev. 37 (2018) 353–491, https://doi.org/10.1002/mas.21530.
[18] D.J. Harvey, Carbohydrate analysis by ESI and MALDI, in: R.B. Cole (Ed.), Electrospray and MALDI Mass Spectrometry: Fundamentals, Instrumentation, Practicalities, and Biological Applications, second ed., John Wiley and Sons Inc., 2012, pp. 723–769, https://doi.org/10.1002/9780470588901.ch19.
[19] B. Spengler, J.W. Dolce, R.J. Cotter, Infrared laser desorption mass spectrometry of oligosaccharides: fragmentation mechanisms and isomer analysis, Anal. Chem. 62 (1990) 1731–1737, https://doi.org/10.1021/ac00216a004.
[20] J.A. Carroll, D. Willard, C.B. Lebrilla, Energetics of cross-ring cleavages and their relevance to the linkage determination of oligosaccharides, Anal. Chim. Acta 307 (1995) 431–447, https://doi.org/10.1016/0003-2670(94)00514-M.
[21] S.G. Penn, M.T. Cancilla, C.B. Lebrilla, Collision-induced dissociation of branched oligosaccharide ions with analysis and calculation of relative dissociation thresholds, Anal. Chem. 68 (1996) 2331–2339, https://doi.org/10.1021/ac960155i.
[22] T. Yamagaki, H. Suzuki, K. Tachibana, Semiquantitative analysis of isomeric oligosaccharides by negative-ion mode UV-MALDI TOF postsource decay mass spectrometry and their fragmentation mechanism study at N-acetyl hexosamine moiety, J. Mass Spectrom. 41 (2006) 454–462, https://doi.org/10.1002/jms.1001.
[23] B. Guan, R.B. Cole, MALDI linear-field reflectron TOF post-source decay analysis of underivatized oligosaccharides: determination of glycosidic linkages and anomeric configurations using anion attachment, J. Am. Soc. Mass Spectrom. 19 (2008) 1119–1131, https://doi.org/10.1016/j.jasms.2008.05.003.
[24] S.G. Penn, M.T. Cancilla, C.B. Lebrilla, Fragmentation behavior of multiple-metal-coordinated acidic oligosaccharides studied by matrix-assisted laser desorption ionization Fourier transform mass spectrometry, Int. J. Mass Spectrom. 195–196 (2000) 259–269, https://doi.org/10.1016/S1387-3806(99)00169-4.
[25] M.A. Fentabil, R. Daneshfar, E.N. Kitova, J.S. Klassen, Blackbody infrared radiative dissociation of protonated oligosaccharides, J. Am. Soc. Mass Spectrom. 22 (2011) 2171–2178, https://doi.org/10.1007/s13361-011-0243-4.
[26] B.J. Bythell, M.T. Abutokaikah, A.R. Wagoner, S. Guan, J.M. Rabus, Cationized carbohydrate gas-phase fragmentation chemistry, J. Am. Soc. Mass Spectrom. 28 (2017) 688–703, https://doi.org/10.1007/s13361-016-1530-x.
[27] H.C. Hsu, C.Y. Liew, S.P. Huang, S.T. Tsai, C.K. Ni, Simple approach for de novo structural identification of mannose trisaccharides, J. Am. Soc. Mass Spectrom. 29 (2018) 470–480, https://doi.org/10.1007/s13361-017-1850-5.
[28] J. Xue, L. Song, S.D. Khaja, R.D. Locke, C.M. West, R.A. Laine, K.L. Matta, Determination of linkage position and anomeric configuration in Hex-Fuc disaccharides using electrospray ionization tandem mass spectrometry, Rapid Commun. Mass Spectrom. 18 (2004) 1947–1955, https://doi.org/10.1002/rcm.1573.
[29] M. Wuhrer, A.M. Deelder, Y.E.M. Van Der Burgt, Mass spectrometric glycan rearrangements, Mass Spectrom. Rev. 30 (2011) 664–680, https://doi.org/10.1002/mas.20337.
[30] E. Mucha, M. Lettow, M. Marianski, D.A. Thomas, W.B. Struwe, D.J. Harvey, G. Meijer, P.H. Seeberger, G. von Helden, K. Pagel, Fucose migration in intact protonated glycan ions: a universal phenomenon in mass spectrometry, Angew. Chem. Int. Ed. 57 (2018) 7440–7443, https://doi.org/10.1002/anie.201801418.
[31] Y.E.M. Van Der Burgt, J. Bergsma, I.P. Bleeker, P.J.H.C. Mijland, A. Van Der Kerk-Van Hoof, J.P. Kamerling, J.F.G. Vliegenthart, FAB CIDMS/MS analysis of partially methylated maltotrioses derived from methylated amylose: a study of the substituent distribution, Carbohydr. Res. 329 (2000) 341–349, https://doi.org/10.1016/S0008-6215(00)00187-7.
[32] R. Frański, B. Gierczyk, G. Schroeder, S. Beck, A. Springer, M. Linscheid, Mass spectrometric decompositions of cationized β-cyclodextrin, Carbohydr. Res. 340 (2005) 1567–1572, https://doi.org/10.1016/j.carres.2005.03.014.
[33] M. Donkuru, J.M. Chitanda, R.E. Verrall, A. El-Aneed, Multi-stage tandem mass spectrometric analysis of novel β-cyclodextrin-substituted and novel bis-pyridinium gemini surfactants designed as nanomedical drug delivery agents, Rapid Commun. Mass Spectrom. 28 (2014) 757–772, https://doi.org/10.1002/rcm.6827.
[34] A.O. Chizhov, M.L. Gening, O.A. Pinsker, O.N. Yudina, Y.E. Tsvetkov, N. E. Nifantiev, Gas-phase fragmentation studies of cyclic oligo-β-(1→6)-D-glucosamines by electrospray ionization mass spectrometry using a hybrid high-resolution mass spectrometer, Russ. Chem. Bull. 67 (2018) 144–149, https://doi.org/10.1007/s11172-018-2050-6.
[35] C. Przybylski, V. Bonnet, Discrimination of cyclic and linear oligosaccharides by tandem mass spectrometry using collision-induced dissociation (CID), pulsed-Q-dissociation (PQD) and the higherenergy C-trap dissociation modes, Rapid Commun. Mass Spectrom. 27 (2013) 75–87, https://doi.org/10.1002/rcm.6422.
[36] D. Szabó, G. Schlosser, K. Vékey, L. Drahos, Á. Révész, Collision energies on QTof and Orbitrap instruments: how to make proteomics measurements comparable? J. Mass Spectrom. 56 (2021), e4693 https://doi.org/10.1002/jms.4693.
[37] S. Pasanen, J. Jänis, P. Vainiotalo, Cello-, malto- and xylooligosaccharide fragmentation by collision-induced dissociation using QIT and FT-ICR mass spectrometry: a systematic study, Int. J. Mass Spectrom. 263 (2007) 22–29, https://doi.org/10.1016/j.ijms.2006.12.002.
[38] H. Suzuki, A. Kameyama, K. Tachibana, H. Narimatsu, K. Fukui, Computationally and experimentally derived general rules for fragmentation of various glycosyl bonds in sodium adduct oligosaccharides, Anal. Chem. 81 (2009) 1108–1120, https://doi.org/10.1021/ac802230a.
[39] C. Zhu, C. Krumm, G.G. Facas, M. Neurock, P.J. Dauenhauer, Energetics of cellulose and cyclodextrin glycosidic bond cleavage, React. Chem. Eng. 2 (2017) 201–214, https://doi.org/10.1039/c6re00176a.

2.5 Breakdown Curves

In breakdown curves, the relative intensities of precursor and fragment ions are plotted against the applied energy of the collisional activation. This energy can be depicted either in the percentage of the normalized collision energy (NCE) or, depending on the dissociation technique, in electron volts (eV) or the applied RF amplitude in volts (V). In HCD experiments, the Xcalibur software directly provides the applied energy in eV, whereas in ion-trap CID experiments, 100% NCE is stated to correspond to a RF amplitude of 5 V [247]. The relative intensities of the ions are defined as their fraction of the total intensity of all identified ions, corresponding to the formula shown in equation 1.4 on page 28. The breakdown curves determined for protonated β-cyclodextrins differ significantly in their respective shape, depending on the dissociation technique. While ion-trap CID results in a sharp decomposition profile, and the resulting fragment ions remain at constant intensities (figure 2.15A), HCD leads to a slower decomposition of the precursor, and the fragment ions are further decomposed at higher energy (figure 2.15B). This difference is explainable by the excitation processes in these two techniques. The resonance excitation in ion-trap CID only activates the ions in the selected precursor m/z range, preventing further dissociation of the fragment ions. On the other hand, the non-resonance excitation in HCD allows for secondary fragmentation. Therefore, the intensities of the signals assigned as fragment ions subsequently decrease as they are further decomposed.

2.5.1 Semi-Automated Signal Assignment

As the relative ion intensities are defined by the intensity of all assigned ions, variances in the signal assignment strongly affect the resulting breakdown curves. Therefore, the signal assignment should be conducted with the same criteria throughout the series of experiments. Especially with the large size of the dataset required for the determination of breakdown curves, manual signal assignment is very time-consuming and prone to errors. Therefore a semi-automated approach was established.

The OMA & OPA software has been developed in our research group for automated interpretation of oligonucleotide fragmentation spectra [248]. It is composed of two parts: The oligonucleotide mass assembler (OMA) and the oligonucleotide peak analyzer (OPA). OMA is able to calculate possible precursor and fragment ions of an inserted oligonucleotide and save them in a reference data file. OPA compares the peaks detected in a mass spectrum with the reference list and assigns

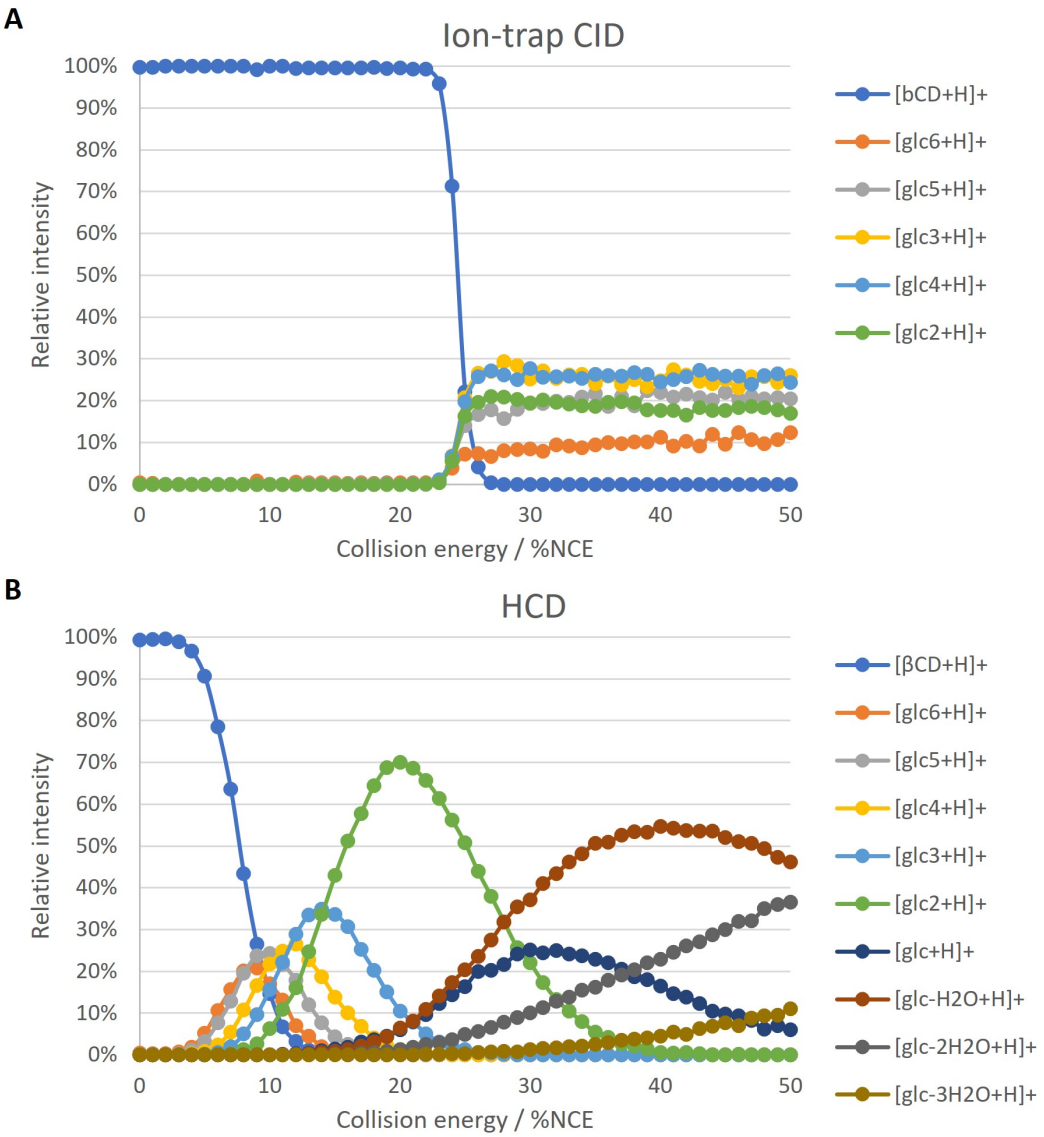

Figure 2.15: Comparison of breakdown curves of $[\beta CD + H]^+$ obtained by A) ion-trap CID and B) HCD.

the signals matching the selected criteria (e.g., ppm deviation). For the analysis of cyclodextrins, the reference list had to be prepared manually, as OMA can only generate fragments of oligonucleotides. For that purpose, potential fragment ions with different adducts are proposed, based on literature and our experimentally established fragmentation pathways, and listed with their respective monoisotopic mass. As α-, β-, and γ- cyclodextrins differ only in the number of subunits and have most of their fragment ions in common, great parts of their reference lists are congruent. OPA can then be used to assign detected peaks using these reference lists. Although the assignment had to be checked manually, especially for signals occurring with low intensity, the time saving and increased consistency is still significant.

2.5.2 Survival Yield

One part of the breakdown curve is the progression of the precursor ion decomposition, also referenced as the survival yield. The collision energy, at which the precursor ion intensity contributes 50% of the intensity of all detected ions, is called the CE_{50} energy. Also, other approaches are used to determine this CE_{50} energy, as shown in equation 1.1 and 1.2 on page 28. However, these approaches are not well applicable to our experiments. The formula used by Gabelica, Galic, and De Pauw [150] (equation 1.2 on page 28) is adapted to host-guest complexes and not directly applicable to the decomposition of cyclodextrins. The main issue in using the formula used by Ma et al. [156] is the definition of the intensity of the precursor ion without applied energy as 100%. Using the nano-electrospray source for ionization leads to fluctuations of the ion current, which has a tremendous effect on the survival yield, as shown in figure 2.16. Determination of the survival yield using the same formula as for breakdown curves suffers from the dependence on the detection of the formed fragment ions. If the signal intensity is too low, its assignment to a fragment ion is not possible and, therefore, not considered in the determination of the survival yield. However, fragment ions that are not assigned due to their low intensity contribute only little to the total signal intensity. Therefore, its effect on the survival yield is only minor.
As previously mentioned, $[\beta CD + H]^+$ and $[glc_6 + H]^+$ cannot be differentiated by their m/z, as they are isobaric. However, determination of the survival yield can be used to distinguish between such isobaric compounds [153, 249, 250]. Therefore, the CE_{50} values are determined for α-, β-, and γ-cyclodextrin. Furthermore, MS^3 and pseudo-MS^3 experiments are used to determine the CE_{50} values of the isobaric fragment ions. In order to compare the applied dissociation energies throughout

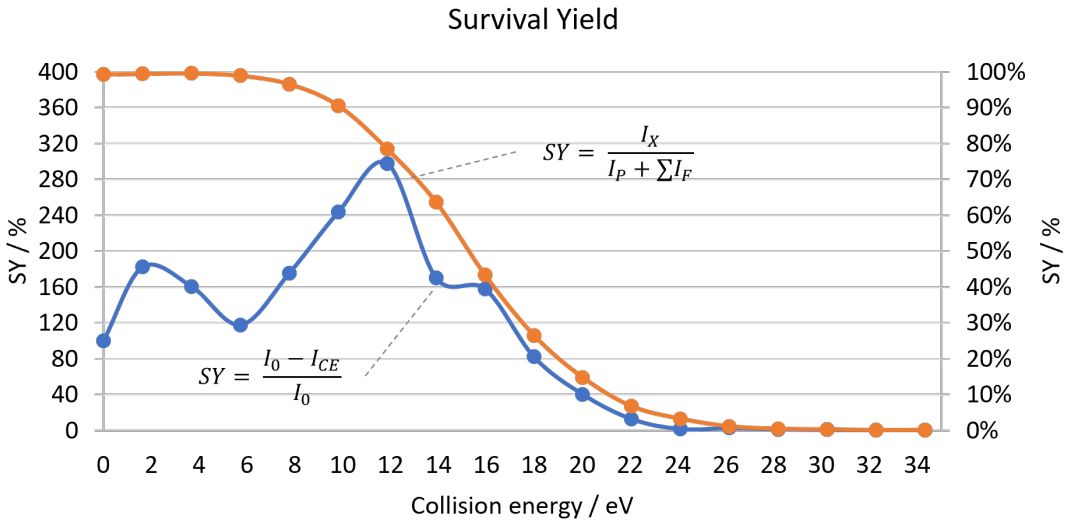

Figure 2.16: Comparison of the survival yield curves of $[\beta CD + H]^+$ obtained from HCD experiments calculated using equation 1.2 (orange) and equation 1.1 (blue).

different experiments, the energies are converted from the lab frame into the center-of-mass frame of reference, according to formula 1.5 on page 30. The target gas in ion-trap CID is helium (He, 4.0 Da) and nitrogen (N_2, 28.0 Da) in HCD experiments.

In the case of protonated α-cyclodextrin, the CE_{50} value obtained from MS^2 HCD experiments of $[\alpha CD + H]^+$ is higher than the CE_{50} obtained for $[glc_6 + H]^+$ deriving from pseudo-MS^3 experiments of β- and γ-cyclodextrin, as well as of maltoheptaose (table 2.2). These differences in the CE_{50} values are evidence for the linearized structure formed from decomposition of β- and γ-cylodextrin in contrast to the macrocyclic structure of α-cyclodextrin. In the case of β-cyclodextrin, the energies are relatively close to each other, and no distinct difference occurs from MS^2 and pseudo-MS^3 experiments.

Table 2.2: CE_{50} values in center-of-mass (or laboratory) frame of reference of HCD experiments.

Compound	$[glc_6 + H]^+$ or $[\alpha CD + H]^+$	$[glc_7 + H]^+$ or $[\beta CD + H]^+$	$[glc_8 + H]^+$ or $[\gamma CD + H]^+$
αCD	0.46* (16.27)*		
βCD	0.36 (12.92)	0.36* (15.01)*	
γCD	0.35 (12.41)	0.34 (14.26)	0.39* (18.36)*
maltodextrin	0.37 (13.08)	0.35 (14.49)	

*MS^2 experiments of the macrocyclic structure.

A possible explanation for this is that relatively little energy is required for the linearization of protonated β-cyclodextrin, due to its low flexibility caused by the intramolecular hydrogen bonds [107]. The CE_{50} energy around 15 eV in the LAB-frame of reference is higher than the 10 eV determined by Przybylski, Bonnet, and Cézard [155] for the HCD decomposition of $[\beta CD + H]^+$. This deviation can be explained by the different approaches used to calculate the survival yield. Przybylski, Bonnet, and Cézard [155] utilized equation 1.1, that uses only the signal intensity of the precursor ion.

3 Host-Guest Complexes

Due to the poor aqueous solubility and stability of bent metallocene dichlorides, their inclusion inside host molecules has been proposed as a promising approach to overcome these drawbacks. While such inclusion complexes have been characterized by theoretical approaches, solid-state analysis, and NMR studies [42, 97, 132–134, 136, 137], only little data from mass spectrometric experiments have been shown [42, 135]. This gap is going to be narrowed with the experiments described in the following.

Although the comparison of the neat compounds is not a prerequisite for the analysis of host-guest complexes using mass spectrometry, it facilitates the correlation of signals to the individual compounds and their interaction products. As the behavior of cyclodextrin host molecules in mass spectrometry has already been discussed in the previous chapter, they are not further discussed in this chapter. Nevertheless, additional experiments of guest compounds were performed before analyzing their mixtures with cyclodextrins.

3.1 Guests

Only a few published data on the inclusion of bent metallocenes within cyclodextrins are available. Therefore, other guest molecules with more extensively investigated interactions with cyclodextrins are used as references. Phenylalanine and oxaliplatin are examined as guests in addition to metallocenes.

Phenylalanine

The full scan mass spectrum of phenylalanine showed signals assigned as the protonated phyenylalanine $[\text{Phe} + \text{H}]^+$ (m/z 166.086, −4.0 ppm) and the corresponding sodium and potassium adducts $[\text{Phe} + \text{Na}]^+$ and $[\text{Phe} + \text{K}]^+$ at m/z 188.068 (−3.0 ppm) and m/z 204.042 (−2.9 ppm), respectively (figure 3.1A). Furthermore, the immonium ion of phenylalanine $[\text{Imm(Phe)}]^+$ is detected at m/z 120.080 (−4.1 ppm). The formation of this immonium ion in mass spectrometry has also been detected by Rogalewicz, Hoppilliard, and Ohanessian [251] as a dominant fragment ion.

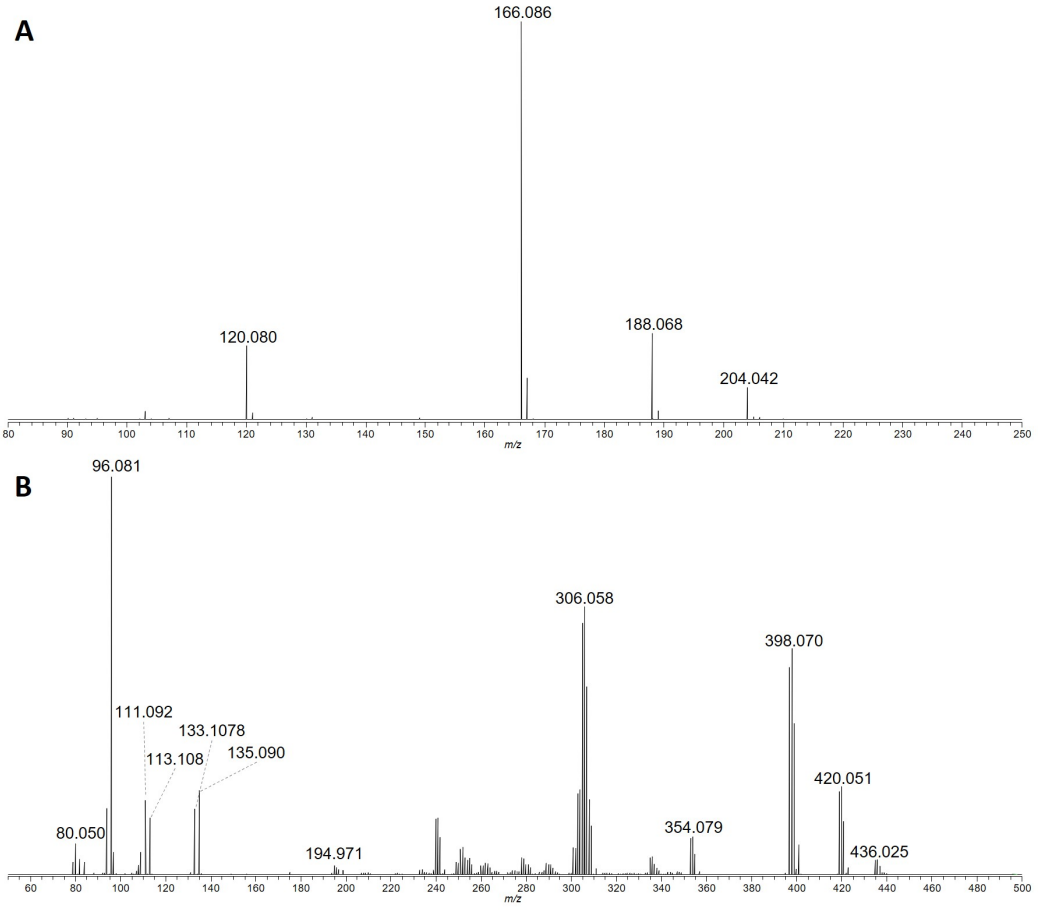

Figure 3.1: Full scan mass spectra of guest molecules: A) phenylalanine, B) oxaliplatin.

Oxaliplatin

In the full scan mass spectrum of the platinum anticancer agent oxaliplatin (figure 3.1B), the proton, sodium, and potassium adducts of intact oxaliplatin are detected ($[\text{oxaliPt} + \text{H}]^+$ *m/z* 398.070, 5.3 ppm; $[\text{oxaliPt} + \text{Na}]^+$ *m/z* 420.051, 4.8 ppm; and $[\text{oxaliPt} + \text{K}]^+$ *m/z* 436.025, 4.4 ppm). Additionally, in-source fragment ions could be assigned to loss of a CO_2 moiety ($[\text{oxaliPt} - CO_2 + \text{H}]^+$, *m/z* 354.078, 5.1 ppm) and loss of the oxalato-ligand ($[\text{oxaliPt} - C_2H_4O_4 + \text{H}]^+$, *m/z* 306.056, 5.9 ppm), respectively, as well as bare platinum (Pt^+, *m/z* 194.964, 5.6 ppm). All these signals show the characteristic isotopic pattern of platinum. At lower *m/z* ratio, signals assigned to fragment ions corresponding to the diamino cyclohexan-ligand are detected. In literature, loss of CO_2 and $C_2H_4O_4$ has also been described for oxaliplatin interacting with biomolecules [252–254]. However, other fragments of oxaliplatin have not been discussed.

Metallocenes

The two metallocenes Cp_2TiCl_2 and Cp_2MoCl_2 are investigated as potential guest molecules as well. In both cases, the exchange of chloro ligands with hydroxo ligands is detected.

Full scan mass spectrometric experiments of Cp_2MoCl_2 show various signals that depict the isotopic pattern of molybdenum (figure 3.2A). Thereof, $[Cp_2MoCl]^+$ (m/z 262.952, 1.1 ppm) and $[Cp_2MoOH]^+$ (m/z 244.986, 1.6 ppm) occur with molybdenum in the +IV oxidation state (Mo^{IV}), whereas $[Cp_2MoO]^+$ (m/z 243.986, 1.6 ppm) contain molybdenum in the oxidation state +V (Mo^{V}). Furthermore, the signal occurring at m/z 227.983 could be assigned to $[Cp_2Mo^{III}]^+$ (1.3 ppm). The signals at m/z 164.908 and m/z 179.895 also showed the characteristic isotopic distribution occuring from molybdenum and correspond to the formula $[H_3O_4Mo]^+$ (0.6 ppm) and $[H_2O_5Mo]^+$ (0.6 ppm), respectively.

The analysis of titanocene dichloride leads to several signals associated to hydrolysis of the chloro ligands (figure 3.2B). This includes $[Cp_2Ti(OH)(H_2O)]^+$ (m/z 213.038, −2.7 ppm), $[Cp_2TiCl]^+$ (m/z 212.994, −2.3 ppm), and $[Cp_2Ti(OH)]^+$ (m/z 195.028, −3.1 ppm), as well as $[Cp_2Ti(COOH)]^+$ (m/z 223.023, −2.7 ppm) in the presence of formic acid. In addition, hydrolysis of one or two cyclopentadienyl ligands resulted in the signals assigned as $[CpTi(OH)_2(H_2O)]^+$ (m/z 165.002, −3.0 ppm), $[CpTi(OH)_2]^+$ (m/z 146.992, −3.4 ppm), and $[Ti(OH)_3(H_2O)]^+$ (m/z 116.966, −4.3 ppm), respectively. In contrast to molybdenocene, no change in the oxidation state is observed for titanocene. This observation is explainable by the stability of the different oxidation states of these two metals. Titanium is occurring in the +II, +III, and +IV oxidation state, whereof, Ti^{IV} is the most stable form [255]. As titanium already occurs in the most stable +IV oxidation state in titanocene dichloride, change in its oxidation state is not favored. On the other hand, molybdenum occurs as Mo^{II}, Mo^{III}, Mo^{IV}, Mo^{V}, and Mo^{VI}. Of those, Mo^{VI} is the most stable form [255]. Changes in the oxidation state of the less stable form Mo^{IV}, present in molybdenocene dichloride, are therefore, plausible.

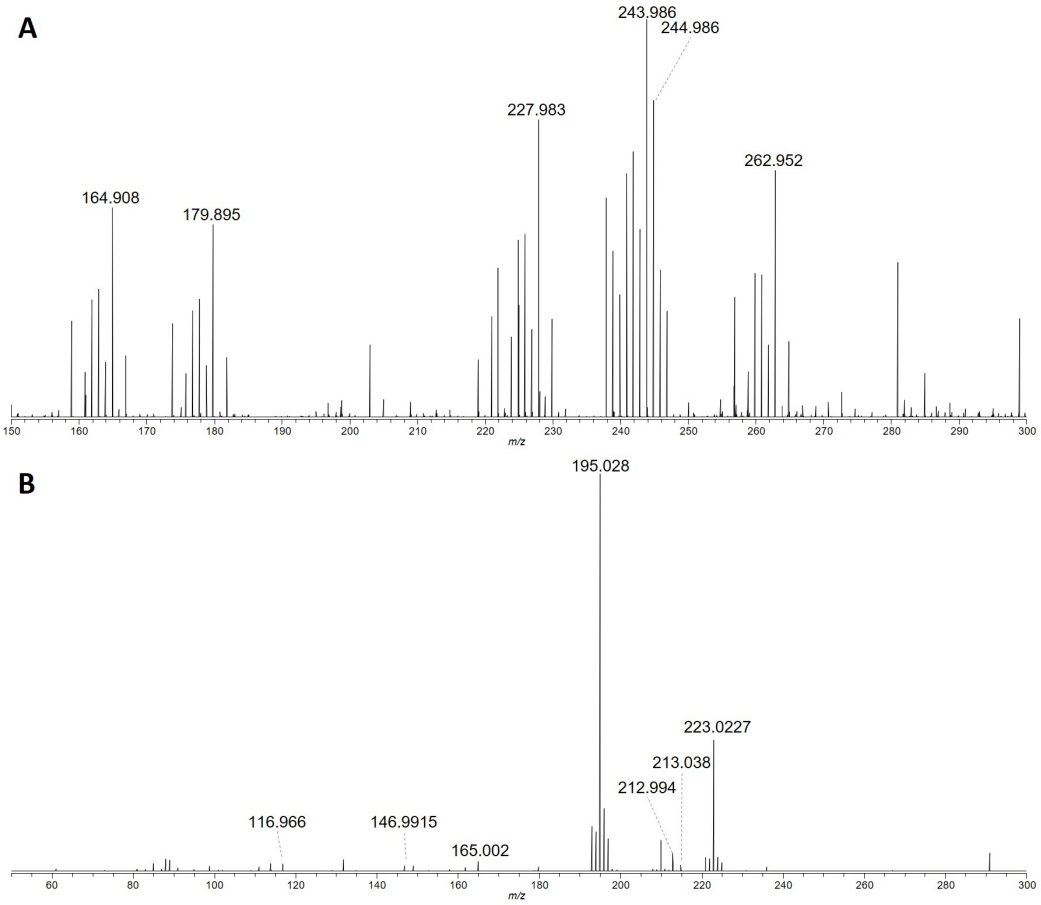

Figure 3.2: Full scan mass spectra of A) Cp_2MoCl_2 and B) Cp_2TiCl_2 in positive ion mode showing signals assigned to hydrolysis products of the respective metallocene.

3.2 Host-Guest Mixtures

In order to examine the interaction between the previously described guest molecules and cyclodextrins, 1:1 stoichiometric mixtures have been prepared and analyzed in the positive ion mode. The experiments have been performed immediately after mixing the two compounds to prevent the degradation of metallocenes, which could potentially occur upon storage of the sample over longer period of time.

3.2.1 Phenylalanine

In case of phenylalanine, an interaction has been detected with α-, β-, and γ-cyclodextrin, corresponding to $[\alpha CD + Phe + H]^+$ (m/z 1138.404, 0.9 ppm), $[\beta CD + Phe + H]^+$ (m/z 1300.458, 1.2 ppm), and $[\gamma CD + Phe + H]^+$ (m/z 1462.509, 0.1 ppm), respectively (figure 3.3). Additionally, the corresponding sodium adducts have been detected for β- and γ-cyclodextrin (figure 3.3).

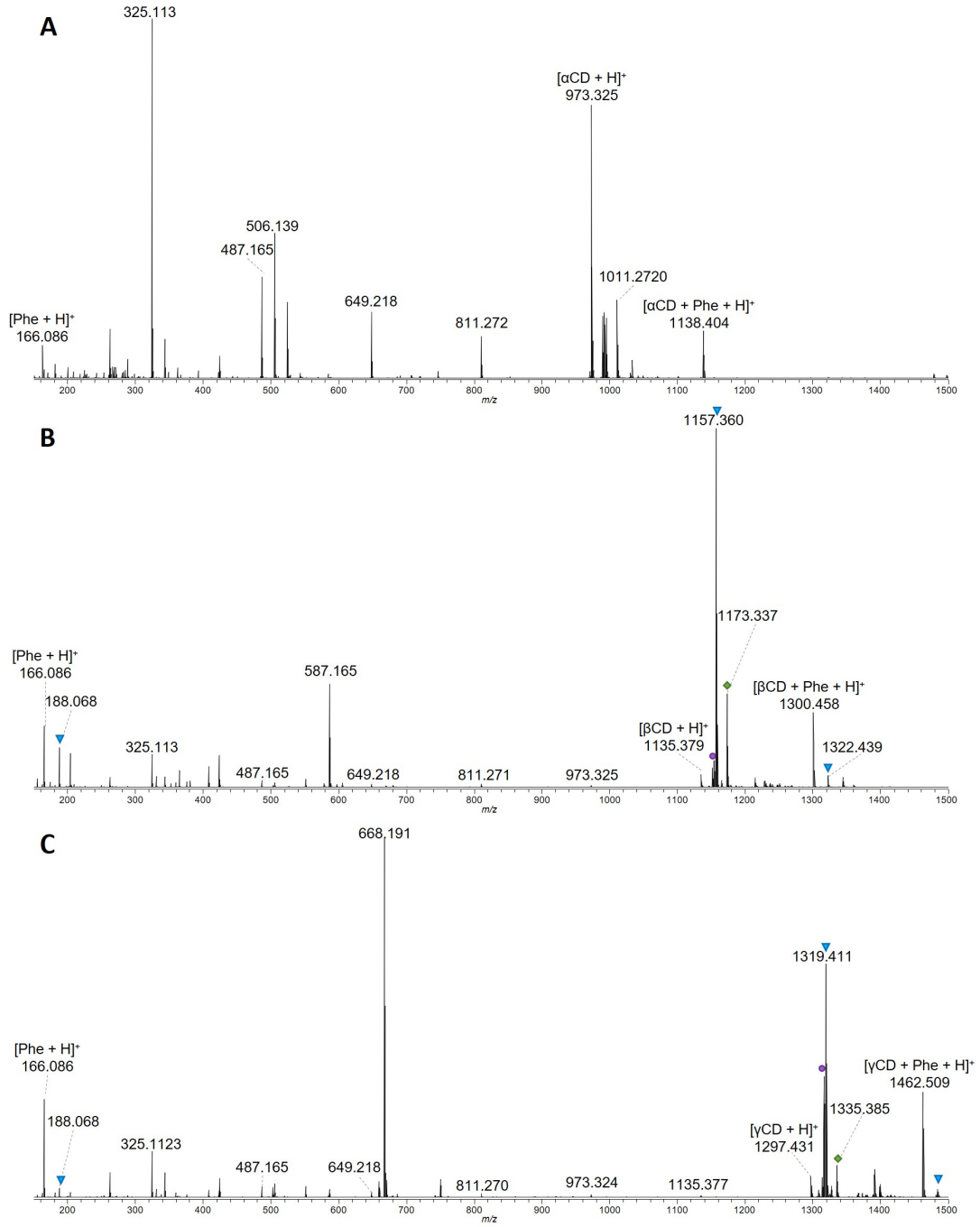

Figure 3.3: Full scan mass spectra of the mixture of phenylalanine with A) α-, B) β-, and C) γ-cyclodextrin.

Further experiments have been performed by Lara Maeder during her bachelor thesis [256]. She added an excess of phenylalanine to an equimolar mixture of α-, β-, and γ-cyclodextrin to determine the preference of this amino acid for a host with appropriate cavity size. By calculating the ratio of the host to the host-guest complex using the absolute peak intensities for each cyclodextrin, a higher preference for the inclusion of phenylalanine in α-cyclodextrin than in β- and γ-cyclodextrin has been found. This is surprising, as the cavity of α-cyclodextrin has been stated in literature to be less suitable for the incorporation of amino acids side chains [116, 119–121].
In general, our results coincide with literature proposing an electrostatic interaction to occur between cyclodextrin hydroxy groups and amino acids [148]. However, different interaction preferences detected for α-, β-, and γ-cyclodextrin indicate that the cavity size affects the interaction. Therefore, at least a part of the guest compound is expected to interact with the cavity of the cyclodextrins [119, 122].

3.2.2 Oxaliplatin

The interaction of oxaliplatin with β-cyclodextrin is represented by the signals detected at m/z 1532.439 ($[\beta CD + oxaliPt + H]^+$, 1.1 ppm) and m/z 1544.421 ($[\beta CD + oxaliPt + Na]^+$, 1.0 ppm), occurring with rather low intensity (figure 3.4). Host-guest interaction between these two compounds has been discussed in literature [17, 131]. However, the low intensity of these complexes is surprising. A potential explanation is the rather intense in-source fragmentation observed in this experiment, preventing the formation of inclusion complexes. Furthermore, a reduced ionization efficiency of the complex compared to neat cyclodextrin and oxaliplatin leads to suppression of the complex signal.

3.2.3 Metallocenes

3.2.3.1 Molybdenocene

Full scan mass spectrometric experiments of the mixture of molybdenocene with α-, β-, and γ-cyclodextrin lead to signals of rather low intensity at higher m/z ratio depicting the characteristic isotopic pattern of molybdenum (figure 3.5).
In case of α-cyclodextrin, the signal at m/z 1235.268 has been assigned as $[\alpha CD + Cp_2MoCl]^+$ (−0.5 ppm), indicating the inclusion of the positively charged Cp_2MoCl^+. Furthermore, at m/z 1199.292, another signal occurred that corresponds to a structure containing molybdenum whose elemental composition was determined as $C_{30}H_{69}O_{46}Mo^+$ (−0.3 ppm). This corresponds to $[\alpha CD + Cp_2Mo - H]^+$, pointing

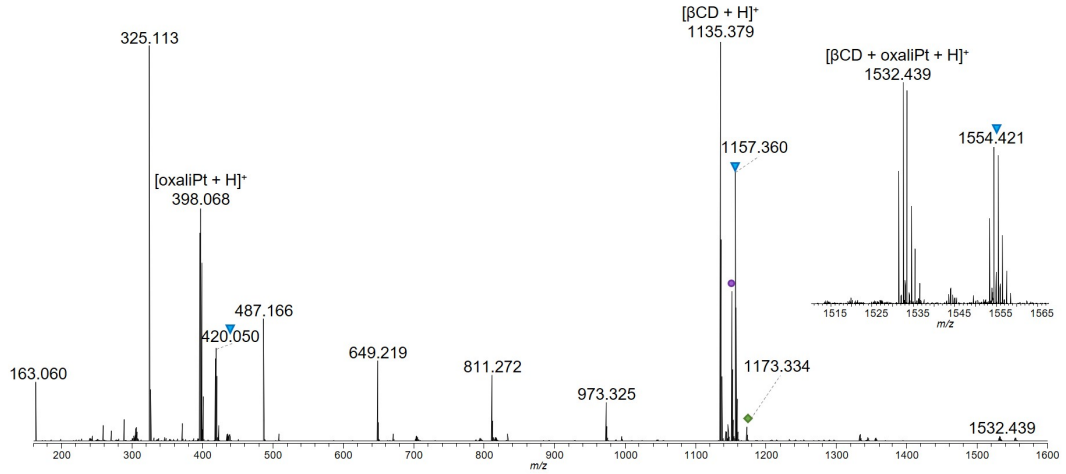

Figure 3.4: Full scan mass spectrum of the mixture of oxaliplatin with β-cyclodextrin.

to the loss of a proton and interaction with the doubly charged Cp_2Mo^{2+}. In case of β- and γ-cyclodextrin, only $[\beta CD + Cp_2Mo - H]^+$ (m/z 1361.348, 1.9 ppm) and $[\gamma CD + Cp_2Mo - H]^+$ (m/z 1523.399, 0.5 ppm) could have been detected with very low intensity, but not the corresponding adducts of Cp_2MoCl^+. These results do not coincide with the inclusion of Cp_2MoCl_2 rather than its hydrolysis products ($Cp_2Mo(OH)Cl$ or $Cp_2Mo(OH)_2$) suggested by Braga et al. [132, 133] from solid-state experiments.

This difference is caused by the rapid hydrolysis of the chloro ligands upon contact with water. In our sample solution, Cp_2MoCl_2 is not present anymore to undergo inclusion.

The interaction of cyclodextrins with molybdenocene is significantly less prominent than with phenylalanine and even oxaliplatin. As our results do not indicate a non-covalent interaction unambiguously, the HSAB concept seems to affect the interaction. The intermediate Lewis acid character of molybdenum explains the low interaction with cyclodextrin, as its oxygens are of hard Lewis base character.

3.2.3.2 Titanocene

Experiments on the mixture of α-, β- and γ-cyclodextrin with titanocene showed signals assigned as $[\alpha CD + Cp_2Ti - H]^+$ (m/z 1149.333, −1.2 ppm), $[\beta CD + Cp_2Ti - H]^+$ (m/z 1311.391, 2.8 ppm), and $[\gamma CD + Cp_2Ti - H]^+$ (m/z 1473.437, −2.6 ppm), respectively, which indicate an interaction (figure 3.6). These signals are analogous to the signals detected for molybdenocene, but of significantly higher intensity. The hard Lewis acid character of titanium explains this increased interaction with the oxygen atoms in cyclodextrins.

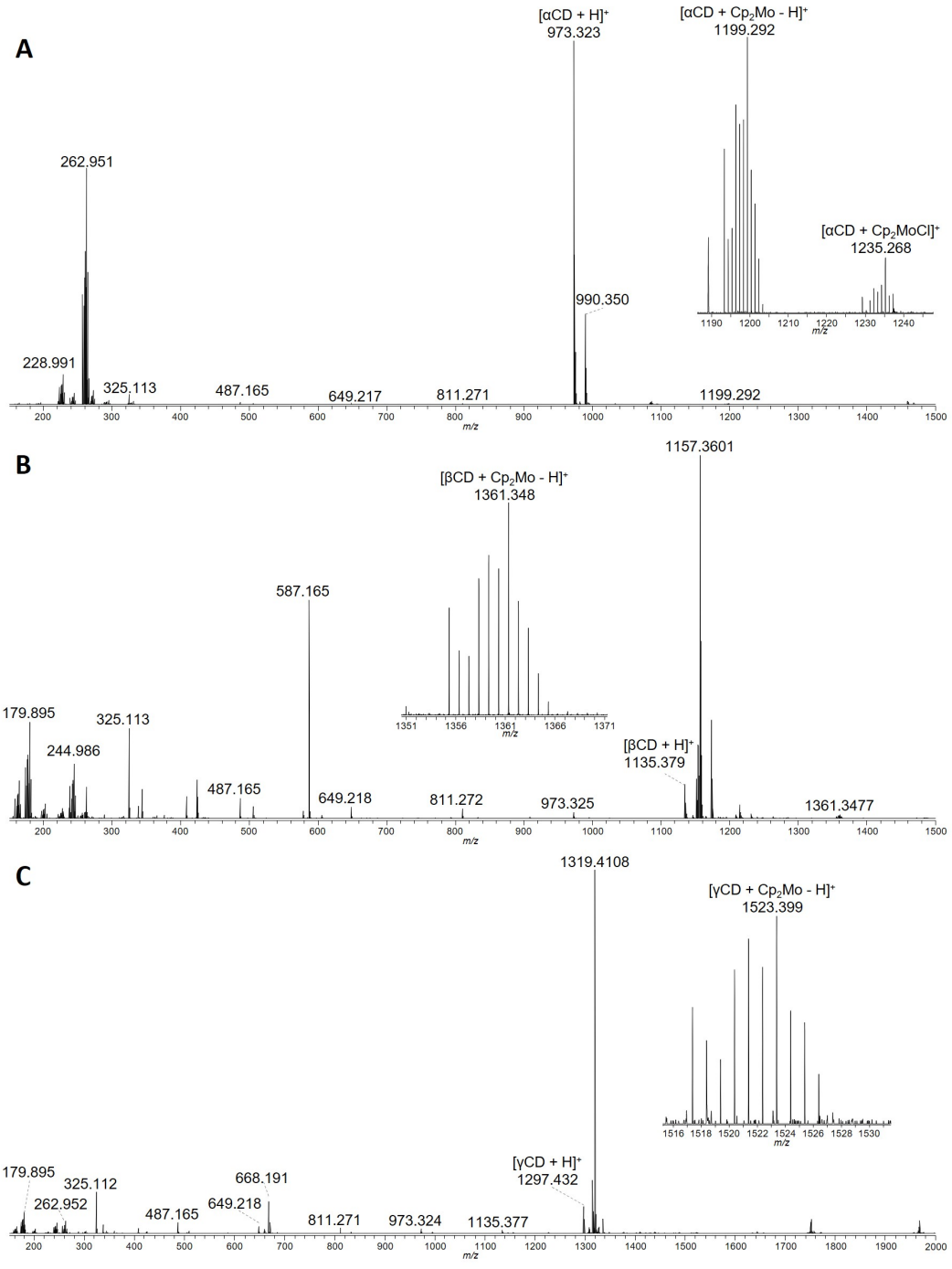

Figure 3.5: Full scan mass spectra of the mixture of molybdenocene with A) α-, B) β-, and C) γ-cyclodextrin.

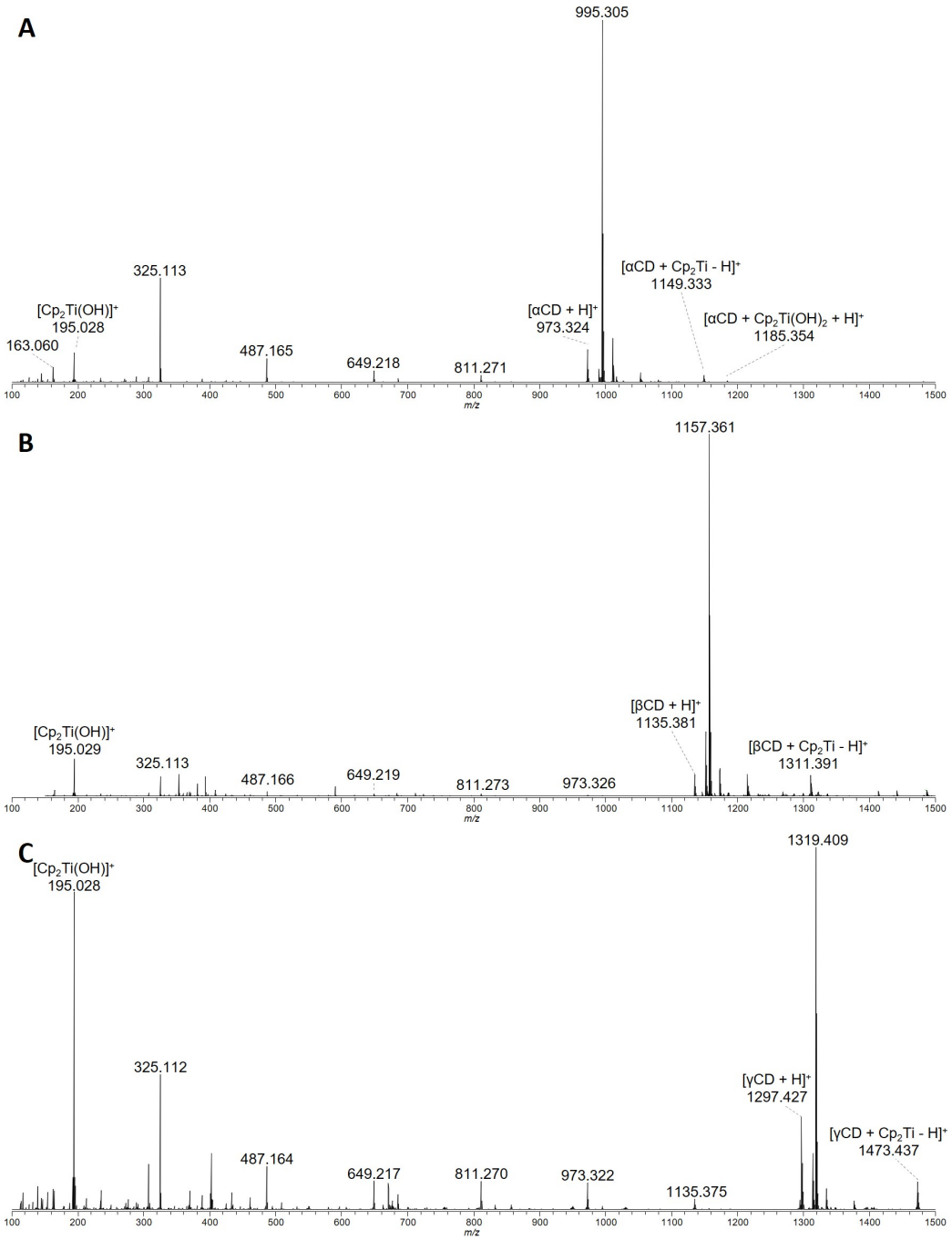

Figure 3.6: Full scan mass spectra of the mixture of titanocene with A) α-, B) β-, and C) γ-cyclodextrin.

In case of α- and γ-cyclodextrin, $[\alpha\text{CD} + \text{Cp}_2\text{Ti(OH)}_2 + \text{H}]^+$ (m/z 1185.354, −1.3 ppm) and $[\gamma\text{CD} + \text{Cp}_2\text{Ti(OH)}_2 + \text{H}]^+$ (m/z 1509.457, −2.9 ppm) have also been detected with low peak abundance. These signals point to the inclusion of hydrolyzed titanocene ($\text{Cp}_2\text{Ti(OH)}_2$) within the cavity of the two cyclodextrins. Surprisingly, this type of interaction has not been detected for β-cyclodextrin, although its cavity size is more appropriate for inclusion than α-cyclodextrin. Unfortunately, the low intensity of these signals did not have allowed further investigation using tandem mass spectrometric experiments. Since one goal of the inclusion of titanocene is to improve its stability, the low intensity of the signal observed for the suspected inclusion complex is not expected to achieve the desired improvement.

Stability at Neutral pH

Although the results obtained so far do not indicate a host-guest interaction, any different interaction might nevertheless increase the aqueous stability of titanocene at physiological pH.

Therefore, the pH of a mixture of β-cyclodextrin and Cp_2TiCl_2 has been raised to approximately seven by adding an ammoinumacetate solution. Immediately after the preparation of the sample, the full scan mass analysis has been started. In the case of an increased stabilization of titanocene due to its interaction with cyclodextrin, the corresponding signal intensity will not be significantly affected by the increased pH, whereas the signals of unbound titanocene will decrease. However, already within the first minutes of the experiment, the signal of $[\text{Cp}_2\text{TiH}]^+$ has decreased significantly, and the signal of $[\beta\text{CD} + \text{Cp}_2\text{Ti} - \text{H}]^+$ has disappeared. These results imply that in solution, the degradation of titanocene is not prevented by interaction with β-cyclodextrin. According to literature, host-guest interaction is in equilibrium with the individual host and guest compounds (equation 3.1) [80, 81, 84, 85, 88, 101]. Therefore, precipitation of titanium-species shifts the equilibrium towards the separated compounds (equation 3.2). This leads to a further separation of the assembly and, consequently, further precipitation of titanium. In conclusion, the degradation of titanocene in aqueous environment at approximately neutral pH cannot be prevented by its interaction with cyclodextrins.

$$\text{Host} + \text{Guest} \rightleftharpoons \text{Host:Guest} \tag{3.1}$$

$$\beta\text{CD} + \text{Ti}-\text{species}\downarrow \rightleftharpoons \beta\text{CD:Ti}-\text{species} \tag{3.2}$$

3.3 Character of the Interaction

Based on the obtained data, it can be stated that the interaction of cyclodextrins with molybdenocene and titanocene is of a different character than with phenylalanine and oxaliplatin. The signals assigned as $[CD + Cp_2Ti - H]^+$ point to the loss of a proton compensating one charge of the doubly charged Cp_2Ti^{2+} and formation of a covalent bond (figure 3.7A). Alternatively, loss of two protons would lead to a neutral assembly with Cp_2Ti^{2+} (figure 3.7B), requiring the addition of an ancillary charge. The considerable amount of sodium and ammonium that form adducts with cyclodextrins would be expected to also form adducts with the assembly, which has not been detected. Therefore, the charge is expected to be located at the titanium atom and not due to adduct formation. Potential deprotonation sites are the abundant hydroxy groups at the rims of cyclodextrins. To evaluate the effect of these hydroxy groups on the interaction with titanocene, supplementary experiments utilizing methylated β-cyclodextrins were conducted. In a second step, the effect of the cavity was elucidated by investigating the interaction between titanocene and linear saccharides. Finally, the breakdown curves and the survival yield of the interaction species have been recorded to elucidate differences in the interaction strength between these assemblies. For comparison, the same experiments have been additionally conducted with phenylalanine.

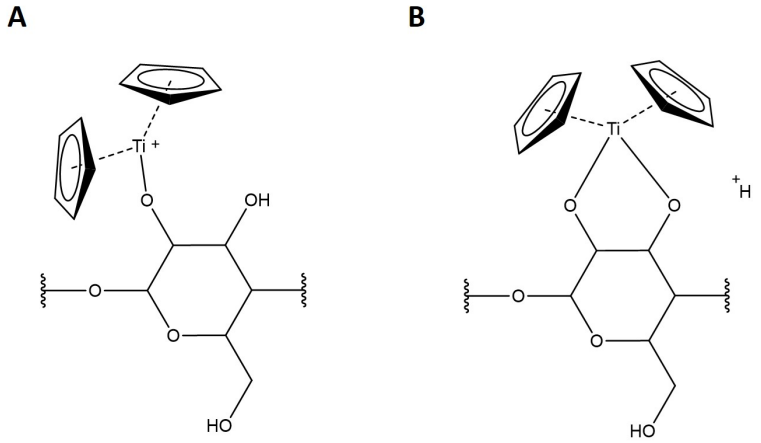

Figure 3.7: Proposed interaction types of titanium with β-cyclodextrin corresponding to $[\beta CD + Cp_2Ti - H]^+$. Reprinted from [257].

3.3.1 Methylated Cyclodextrins

Full scan mass spectrometric experiments of the mixture of phenylalanine with di- and trimethylated β-cyclodextrin resulted in signals assigned the correspond-

ing inclusion complexes $[DM\beta CD + Phe + H]^+$ (m/z 1496.675, −0.1 ppm) and $[TM\beta CD + Phe + H]^+$ (m/z 1594.787, 1.1 ppm), respectively. Furthermore, the corresponding ammonium adducts $[DM\beta CD + Phe + NH_4]^+$ and $[TM\beta CD + Phe + NH_4]^+$ have been detected at m/z 1513.700 (−1.5 ppm) and m/z 1597.796 (0.1 ppm), respectively. Apparently, the methoxylation of the hydroxy groups of β-cyclodextrin did not hinder the inclusion of phenylalanine.

The wide-ranging degree of methylation of the β-cyclodextrin derivatives complicates the unambiguous elucidation of their effect on the interaction with titanocene. If β-cyclodextrin is fully methylated, $[TM\beta CD + Cp_2Ti(OH)_2 + H]^+$ (m/z 1641.740, 1.6 ppm) and $[TM\beta CD + Cp_2Ti(OH)]^+$ (m/z 1623.730, 1.8 ppm) have been detected. With a total of 14, 15, and 16 methoxy groups, inclusion of $Cp_2Ti(OH)_2$ has been detected as well at m/z 1543.625 ($[DM\beta CD + Cp_2Ti(OH)_2 + H]^+$, −1.9 ppm), m/z 1557.641 ($[DM\beta CD + CH_2 + Cp_2Ti(OH)_2 + H]^+$, −1.9 ppm), and m/z 1571.656 ($[DM\beta CD + 2\,CH_2 + Cp_2Ti(OH)_2 + H]^+$, −2.0 ppm), respectively. Additionally, the same type of interaction as detected for unmodified β-cyclodextrin has been found for trimethylated β-cyclodextrin comprising one unmodified hydroxy group ($[TM\beta CD - CH_2 + Cp_2Ti - H]^+$, m/z 1591.704, 1.9 ppm), as well as for dimethylated β-cyclodextrins comprising a total of 13–16 methoxy groups. These results clearly indicate the effect of the hydroxy groups on the interaction of cyclodextrins with titanocene. Furthermore, these findings support the hypothesis of the covalent binding of titanocene to the rim of cyclodextrin.

3.3.2 Interaction with Linear Saccharides

A second approach to prove the covalent interaction of titanocene with the hydroxy rim of cyclodextrins is to evaluate their interaction with linear saccharides. Therefore, mixtures of titanocene with sucrose (glucose-α-(1→2)-fructose), maltose (glucose-α-(1→4)-glucose), and maltoheptaose ((glucose-α-(1→4))$_6$-glucose) have been examined. Sucrose and maltose are dimeric saccharides comprising hydroxy groups that serve as possible targets for the interaction with titanocene. Maltoheptaose comprises seven α-1,4-linked glucose subunits, which is the same number of subunits as than in β-cyclodextrin.

In full scan analysis of the titanocene mixtures with sucrose and maltose signals assigned as $[sugar + Cp_2Ti - H]^+$ (m/z 519.131, −5.1 ppm and m/z 519.133, −3.1 ppm) and $[sugar + Cp_2Ti(OH)_2 + H]^+$ (m/z 555.153, −5.0 ppm and m/z 555.153, −3.6 ppm), respectively, have been detected (figure 3.8). For the interaction of titanocene with maltoheptaose, analogous signals have been detected. This includes $[malto_7 + Cp_2Ti - H]^+$ at m/z 1329.395 (−2.4 ppm), $[malto_7 + Cp_2TiOH]^+$

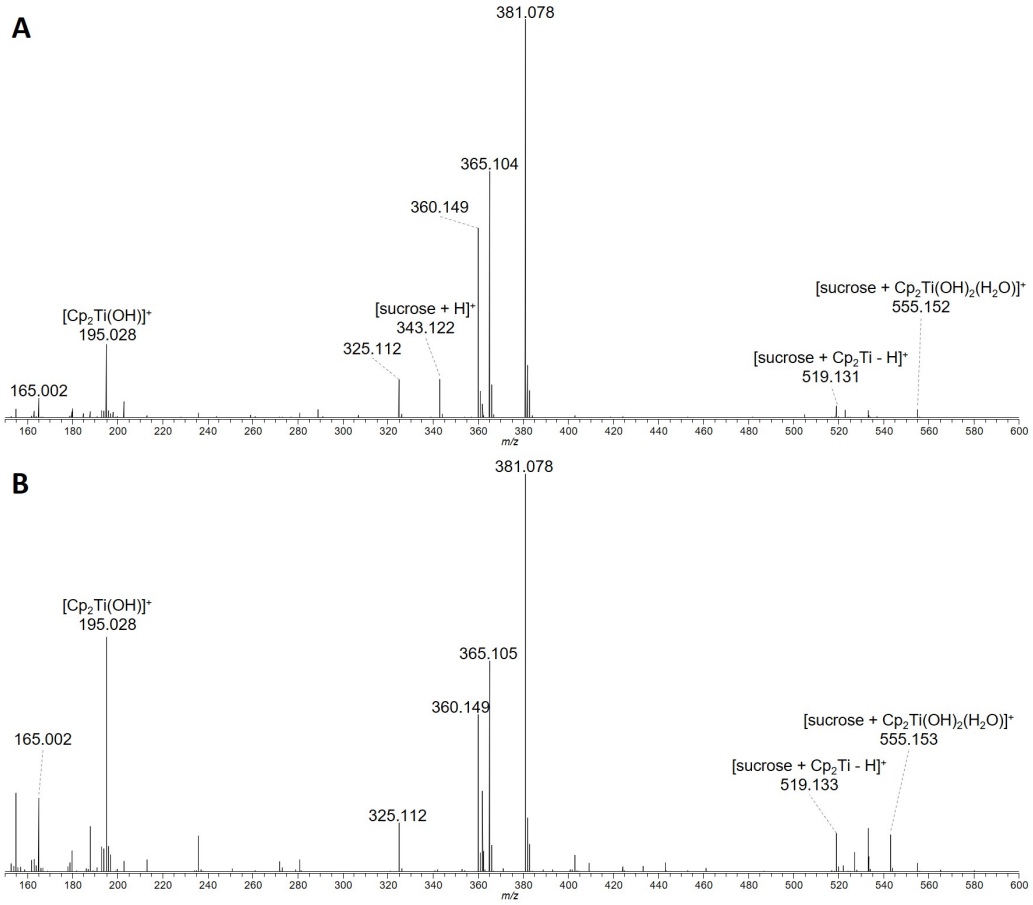

Figure 3.8: Full scan mass spectra of the mixture of titanocene with A) sucrose and B) maltose.

at m/z 1347.406 (-1.7 ppm), and $[\text{malto}_7 + \text{Cp}_2\text{Ti(OH)}_2 + \text{H}]^+$ at m/z 1365.416 (-2.4 ppm) as well as the corresponding sodium and potassium adducts (figure 3.9). Therefore, it is concluded that the proposed covalent interaction between titanocene and hydroxy groups of saccharides occurs also with linear saccharides. However, the assigned signals also suggest a non-covalent interaction, comparable to the minor signals detected for α- and γ-cyclodextrin. The full scan experiment of the mixture of maltoheptaose and phenylalanine also show peaks indicating a non-covalent interaction that have been assigned as $[\text{malto}_7 + \text{Phe} + \text{H}]^+$ and $[\text{malto}_7 + \text{Phe} + \text{Na}]^+$ (figure 3.9). Due to the linear structure of maltoheptaose, no cavity is present that allows for the incorporation of a host compound. Consequently, these interactions point to unspecific binding between the saccharides and the host compounds [107, 150, 258]. An alternative explanation for the interaction of these compounds is the formation of "quasi-inclusion" complexes, as discussed by Lebrilla [118]. The flexible structure of maltoheptaose enabling its wrapping around guest compounds, building a cavity-like structure.

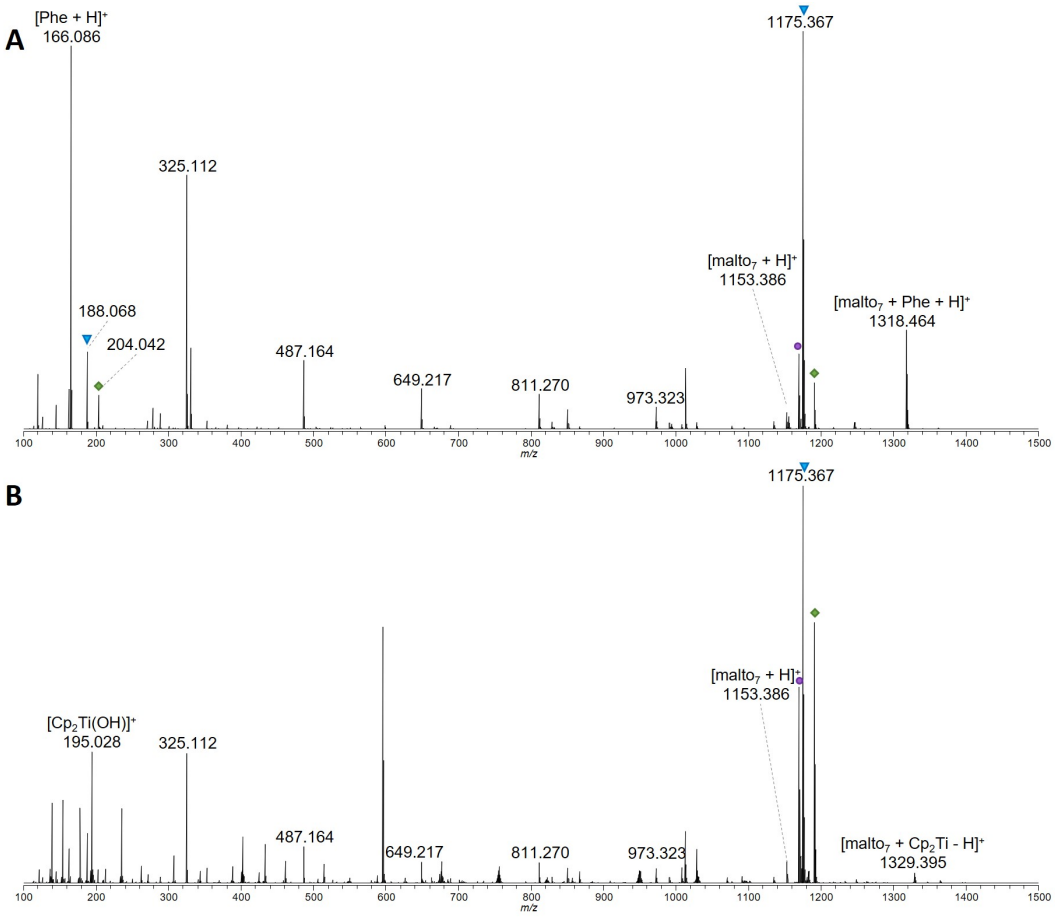

Figure 3.9: Full scan mass spectra of the mixture of maltoheptaose with A) phenylalanine and B) titanocene.

3.3.3 Tandem Mass Spectrometry

Collisional activation of the host-guest assemblies may give further insight into the character of the interaction. Tandem mass spectrometric experiments of $[\beta CD + Phe + H]^+$ led to separation of the two compounds and further dissociation of β-cyclodextrin (figure 3.10A). Similar behavior has been found for the decomposition of $[DM\beta CD + Phe + H]^+$ (figure 3.10B), $[TM\beta CD + Phe + H]^+$ (figure 3.10C), and $[malto_7 + Phe + H]^+$ (figure 3.10D). Although the signal of phenylalanine and the intact saccharides was not detected in all spectra, no fragments indicating a preserved interaction between the host and guest compound have been detected. Upon separation of the complex, the host and guest structures compete for the charge. If one compound has a higher proton affinity, it suppresses the ionization of the other compound [156].

In contrast to the separation of phenylalanine and saccharides, collisional activation of $[\beta CD + Cp_2Ti - H]^+$, $[DM\beta CD + Cp_2Ti - H]^+$, and $[malto_7 + Cp_2Ti - H]^+$ led

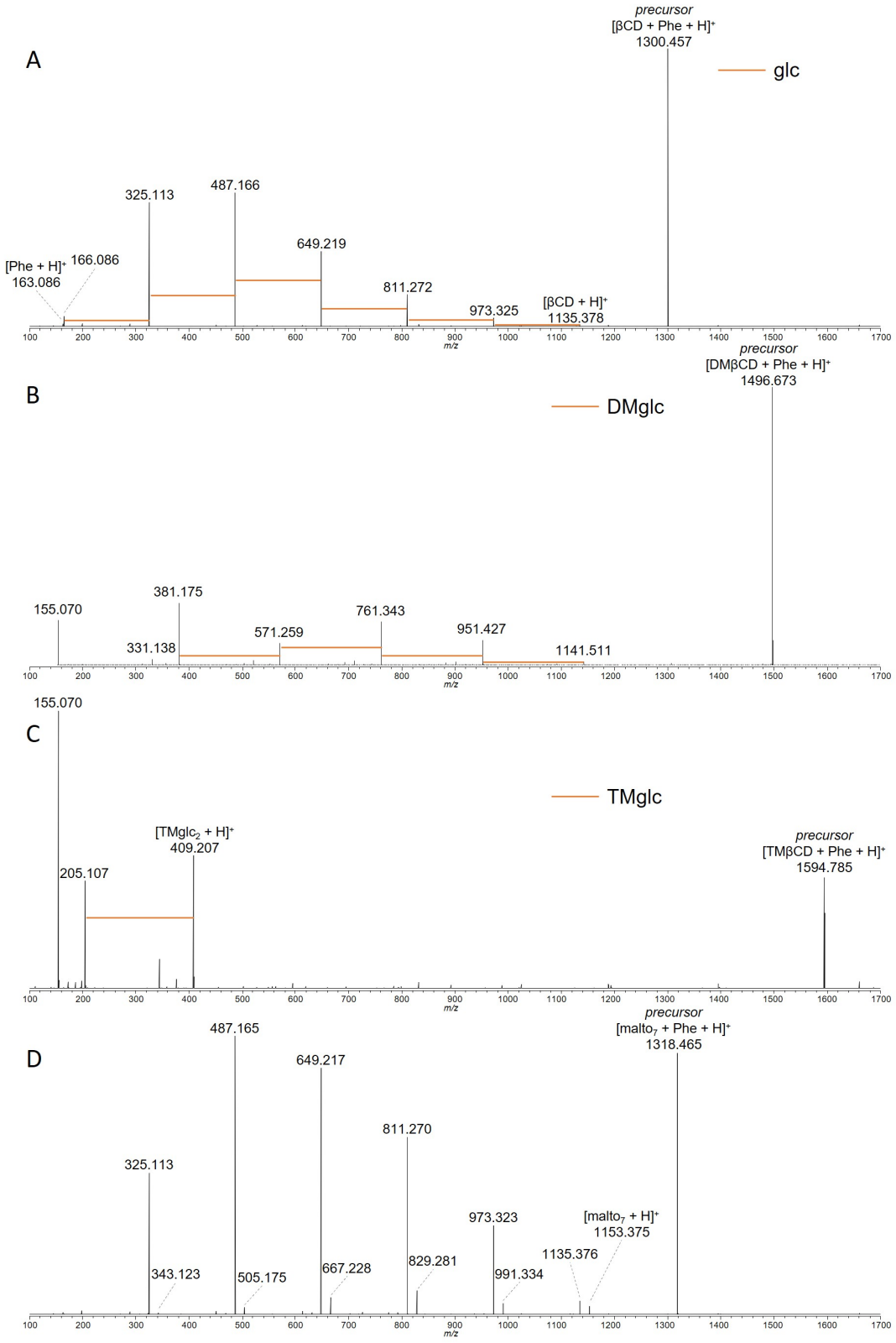

Figure 3.10: Tandem mass spectra obtained from HCD experiments of A) [βCD + Phe + H]$^+$, B) [DMβCD + Phe + H]$^+$, C) [TMβCD + Phe + H]$^+$, and D) [malto$_7$ + Phe + H]$^+$.

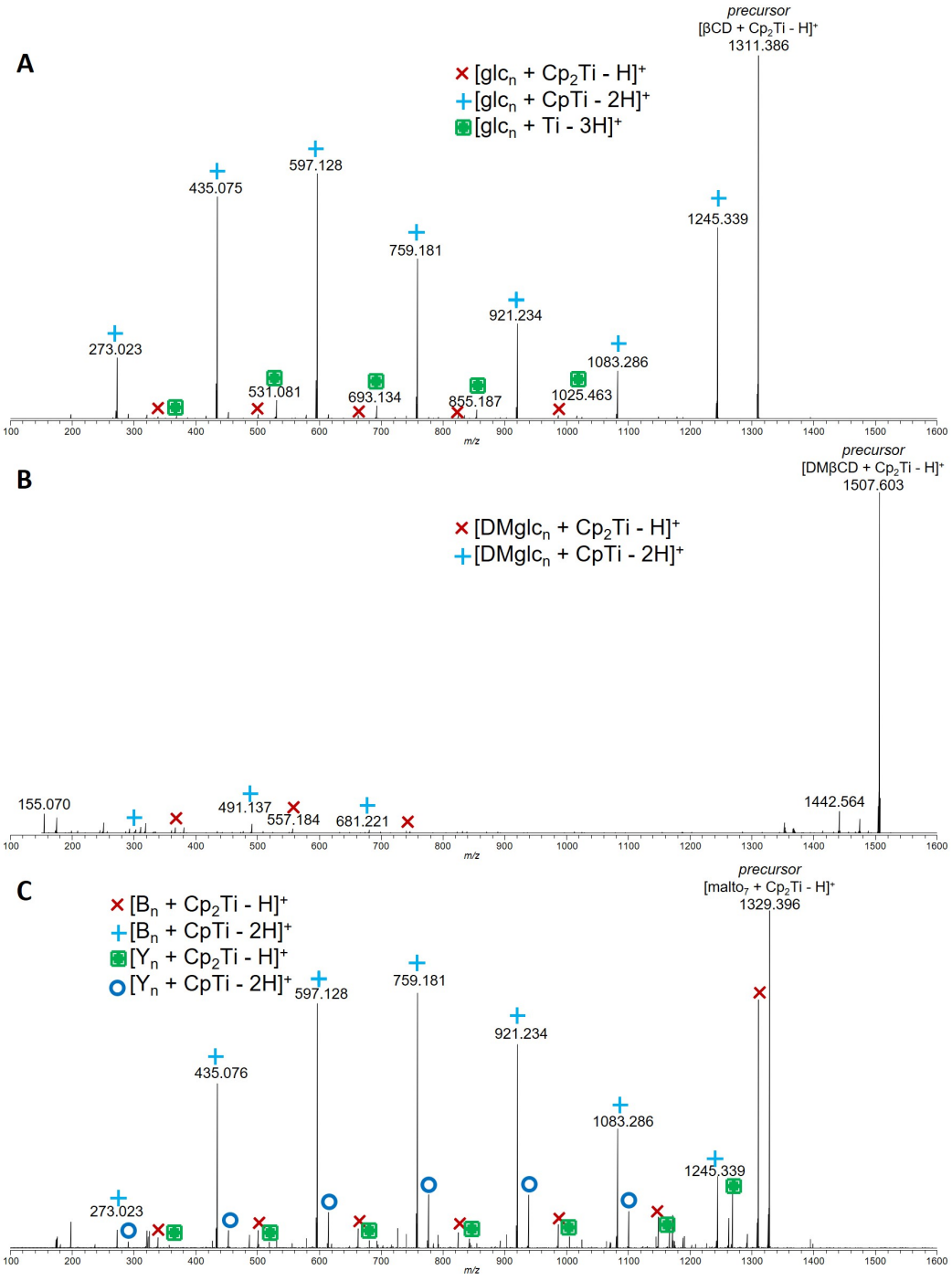

Figure 3.11: Tandem mass spectra obtained from HCD experiments of A) [βCD + $Cp_2Ti - H]^+$, B) [DMβCD + $Cp_2Ti - H]^+$, and C) [$malto_7$ + $Cp_2Ti - H]^+$.

to signals assigned as fragment ions that still preserve an interaction between the two compounds (figure 3.11). These fragment ions are characterized by the loss of one or both cyclopentadienyl ligands as C_5H_6 and loss of neutral glucose subunits, resulting in signals assigned as $[glc_n + Cp_2Ti - H]^+$ (n = 1–6), $[glc_n + CpTi - 2\,H]^+$ (n = 1–6), and $[glc_n + Ti - 3\,H]^+$ (n = 2–6), for the decomposition of $[\beta CD + Cp_2Ti - H]^+$. Dissociation of $[DM\beta CD + Cp_2Ti - H]^+$ led to the comparable signals assigned as $[DMglc_n + Cp_2Ti - H]^+$ (n = 1–3) and $[DMglc_n + CpTi - 2\,H]^+$ (n = 1–3), respectively. The rather low intensity of the fragment ions prevented the detection of $[DMglc_n + Ti - 3\,H]^+$ fragment ions. Collisional activation of $[malto_7 + Cp_2Ti - H]^+$ also resulted in B- and Y-ions comprising Cp_2Ti and CpTi, respectively (figure 3.11).

Although signals occurring from the interaction between cyclodextrins and titanocene have been detected that point to a non-covalent interaction, elucidation of their fragmentation patterns was not possible do to insufficient signal intensity. The low intensity of the signals assigned to the proposed non-covalent assemblies also implies little formation of this interaction species in solution. Therefore, hardly any improvement of the hydrolytic stability of titanocene is expected from its interaction with cyclodextrin.

3.3.3.1 Survival Yield

From the breakdown curves of obtained from HCD experiments of the protonated complexes of phenylalanine and cyclodextrins or maltoheptaose, the survival yield curves have been plotted against the applied collision energy (E_{LAB}) in eV (figure 3.12). From these curves, the characteristic CE_{50} energies have been determined and converted to the center-of-mass frame of reference for better comparability (table 3.1). The highest CE_{50} has been detected for $[\beta CD + Phe + H]^+$ with 0.76 eV, followed by $[DM\beta CD + Phe + H]^+$ (0.71 eV) and $[\gamma CD + Phe + H]^+$ (0.69 eV). With a CE_{50} of 0.62 and 0.63 eV, the weakest interaction has been detected for $[\alpha CD + Phe + H]^+$ and $[malto_7 + Phe + H]^+$, respectively. These variances indicate the effect of the cavity size on the strength of the interaction.

The CE_{50} energies determined for the dissociation of the titanocene assemblies with cyclodextrins and maltoheptaose are generally higher (0.75 – 0.85 eV). This implies a stronger interaction, which coincides with the proposed formation of a covalent bond. The highest CE_{50} has been detected for $[\beta CD + Cp_2Ti - H]^+$ (0.85 eV), followed by $[\gamma CD + Cp_2Ti - H]^+$ (0.80 eV), $[\alpha CD + Cp_2Ti - H]^+$ (0.77 eV), and $[malto_7 + Cp_2Ti - H]^+$ (0.75 eV).

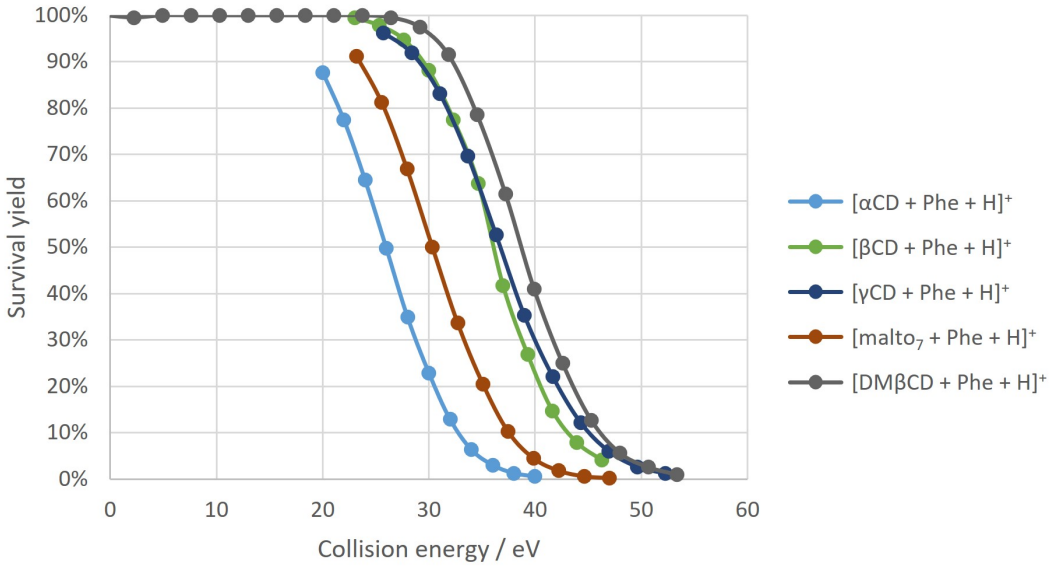

Figure 3.12: Survival yield curves of obtained from the decomposition of phenylalanine complexes. For all complexes except $[\alpha CD + Phe + H]^+$ only the region of interest for the determination of the CE_{50} values are displayed.

Table 3.1: CE_{50} values in center-of-mass (laboratory) frame of reference of HCD experiments.

	αCD	βCD	γCD	$malto_7$	DMβCD
+ Phe + H	0.62 (25.96)	0.76 (36.09)	0.69 (36.73)	0.63 (30.36)	0.71 (38.73)
+ Cp2Ti - H	0.77 (32.18)	0.85 (40.60)	0.80 (44.63)	0.75 (36.24)	

Comparison of the data obtained from the interaction of titanocene with cyclodextrins, methylated cyclodextrins, and linear saccharides revealed the effect of the hydroxy groups on the interaction. The formation of covalent bonds between titanium and these hydroxy-groups was supported by the fragment ions occurring as a result of collisional dissociation, which did not indicate a separation of the two complounds.

The results on the interaction of titancoene with β-cyclodextrins were published in the *International Journal of Molecular Sciences* in 2021.

International Journal of
Molecular Sciences

MDPI

Article

Mass Spectrometric Evaluation of β-Cyclodextrins as Potential Hosts for Titanocene Dichloride

Pia S. Bruni and Stefan Schürch *

Department of Chemistry, Biochemistry and Pharmaceutical Sciences, University of Bern, 3012 Bern, Switzerland; pia.bruni@unibe.ch
* Correspondence: stefan.schuerch@unibe.ch

Abstract: Bent metallocene dichlorides (Cp_2MCl_2, M = Ti, Mo, Nb, ...) have found interest as anti-cancer drugs in order to overcome the drawbacks associated with platinum-based therapeutics. However, they suffer from poor hydrolytic stability at physiological pH. A promising approach to improve their hydrolytic stability is the formation of host-guest complexes with macrocyclic structures, such as cyclodextrins. In this work, we utilized nanoelectrospray ionization tandem mass spectrometry to probe the interaction of titanocene dichloride with β-cyclodextrin. Unlike the non-covalent binding of phenylalanine and oxaliplatin to β-cyclodextrin, the mixture of titanocene and β-cyclodextrin led to signals assigned as $[\beta CD + Cp_2Ti–H]^+$, indicating a covalent character of the interaction. This finding is supported by titanated cyclodextrin fragment ions occurring from collisional activation. Employing di- and trimethylated β-cyclodextrins as hosts enabled the elucidation of the influence of the cyclodextrin hydroxy groups on the interaction with guest structures. Masking of the hydroxy groups was found to impair the covalent interaction and enabling the encapsulation of the guest structure within the hydrophobic cavity of the cyclodextrin. Findings are further supported by breakdown curves obtained by gas-phase dissociation of the various complexes.

Keywords: metallocene; gas-phase reaction; cyclodextrin; mass spectrometry; host-guest complex

Citation: Bruni, P.S.; Schürch, S. Mass Spectrometric Evaluation of β-Cyclodextrins as Potential Hosts for Titanocene Dichloride. *Int. J. Mol. Sci.* **2021**, *22*, 9789. https://doi.org/10.3390/ijms22189789

Academic Editor: Alexander O. Chizhov

Received: 3 August 2021
Accepted: 6 September 2021
Published: 10 September 2021

1. Introduction

Good solubility and stability in a physiological aqueous environment are essential prerequisites of a pharmaceutically active compound in order to develop its therapeutic activity. Within this context, low bioavailability due to high hydrophobicity, fast degradation, or deactivation as a result of rapid reaction with unspecific targets represent a continuous challenge in drug formulation [1,2]. Organometallic anti-cancer drugs based on transition metal complexes, such as cisplatin and its analogs and bent metallocene complexes, which are known to target nucleic acids as well as proteins, are severely suffering these difficulties [3].

Cisplatin exhibits a planar structure with a platinum(II) coordination center surrounded by two ammine and two chloride ligands in cis configuration (Figure 1) [4]. It is widely used in cancer treatment but suffers from severe side-effects due to its toxicity and accruing drug resistance [5]. By alteration of the ligands, alternative drugs (e.g., carboplatin, oxaliplatin) were developed to overcome these drawbacks [4]. In addition, transition metal centered bent metallocenes emerged as a promising alternative to platinum-based drugs [5].

1.1. Bent Metallocenes

Bent metallocene dichlorides (Cp_2MCl_2) are built of a transition metal center M, often Ti, Mo, Nb, or V, two η^5-cyclopentadienyl ligands (Cp) and two chloride ligands (Figure 1) [3,6,7]. In contrast to the platinum-based compounds, the transition metal is generally in the +IV oxidation state, and the overall structure resembles a distorted tetrahedron [6]. Among these metallocenes, titanocene had entered clinical trials in the 1990s, but

was finally rejected due to insufficient response to metastatic cancers [8,9]. Nevertheless, the proven antiproliferative activity of metallocenes encourages further investigation of their interaction with potential biological targets.

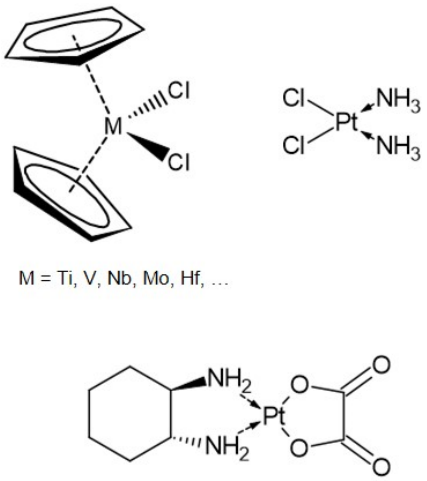

Figure 1. Structure of bent metallocene dichlorides (M = Ti, V, Nb, Mo, Hf, . . .), cisplatin, and its derivative oxaliplatin.

A key step for the development of the anti-cancer activity of these compounds is the exchange of the chloride ligands for hydroxy ions in an aqueous environment [4,10]. Hydrolysis of the first chloride ligand occurs rapidly, whereas the exchange of the second chloride ligand is dependent on the metal species and the pH of the solution. For titanocene dichloride, the half-life of the second chloride ligand is ~50 min [11]. In consequence of this hydrolysis, the pH of the solution drops significantly, resulting in substantial difficulties in the application in biological systems due to increased side effects [6]. In the case of titanocene, raising the pH to physiological conditions leads to hydrolysis of the two Cp-ligands and the formation of insoluble titanium oxide species [6,7,12]. In contrast, molybdenocene shows increased hydrolytic stability of the Cp-ligands at higher pH [3,13]. Although some metallocene dichlorides exhibit higher stability than others, their aqueous stability is generally poor and represents a major challenge for their administration and necessitates the processing of the drug prior to usage [5,7]. One approach is the replacement of one or both chloride ligands by different halogenides or organic ligands [6,14,15], while other studies aimed at a more targeted drug delivery by functionalization of the Cp-ligands (e.g., titanocene Y) or alteration of the metal center [5–7,14–18].

Another approach to prevent metallocenes from extensive hydrolysis in an aqueous environment is the encapsulation within a host molecule [12,19]. Additional advantages of this approach are the increased aqueous solubility and bioavailability and a lowered toxicity [1,4,12,13,15,20,21]. Host molecules typically combine a rather hydrophobic inner cavity, which undergoes non-covalent interaction with the guest molecules (or parts of it) with a more polar outer surface that promotes better solubility in an aqueous environment [1,22,23]. Examples of host molecules successfully applied in drug delivery are cyclodextrins, cucurbiturils, pillarenes, and calixarenes [24,25].

1.2. Cyclodextrins as Host Molecules

Due to their low toxicity [1,23,26], cyclodextrins are considered safe excipients when administered orally. In addition, they have found widespread applications as hosts of poorly soluble therapeutic agents, as summarized in recent review articles [2,22,23,26,27]. Cyclodextrins are a family of cyclic oligosaccharides composed of (1,4)-linked α-D-glucopyranose units. The naturally occurring α-, β-, and γ-cyclodextrins, comprising 6, 7, or 8 subunits, respectively,

are the result of the enzymatic degradation of starch. Due to the chair conformation of the glucopyranose monomer, cyclodextrins adopt the shape of a truncated cone, with the hydroxy groups located at the rim and the skeletal carbon atoms providing the hydrophobic character of the cavity (Figure 2) [1,2,22,23,26–30]. The ability to form a host-guest system depends on various factors. The size of the cavity of the host molecule has to fit the size of the guest structure. In the case of bent metallocenes, the cavity size of β-cyclodextrin (6.0–6.5 Å) is suitable for accommodating the Cp-ligands of titanocene dichloride with a diameter of 5.8 Å [1,22,24]. The driving forces of the interaction between the host and guest structures include hydrophobic interactions, electrostatic, van der Waals, as well as hydrogen bonding [1,2,25,30,31]. A key criterion that defines host-guest complexes is that no covalent bonds are broken nor newly formed [22,23,25,26]. Consequently, the host-guest complex is in equilibrium with the free cyclodextrin and its guest molecules in solution [23,26,27].

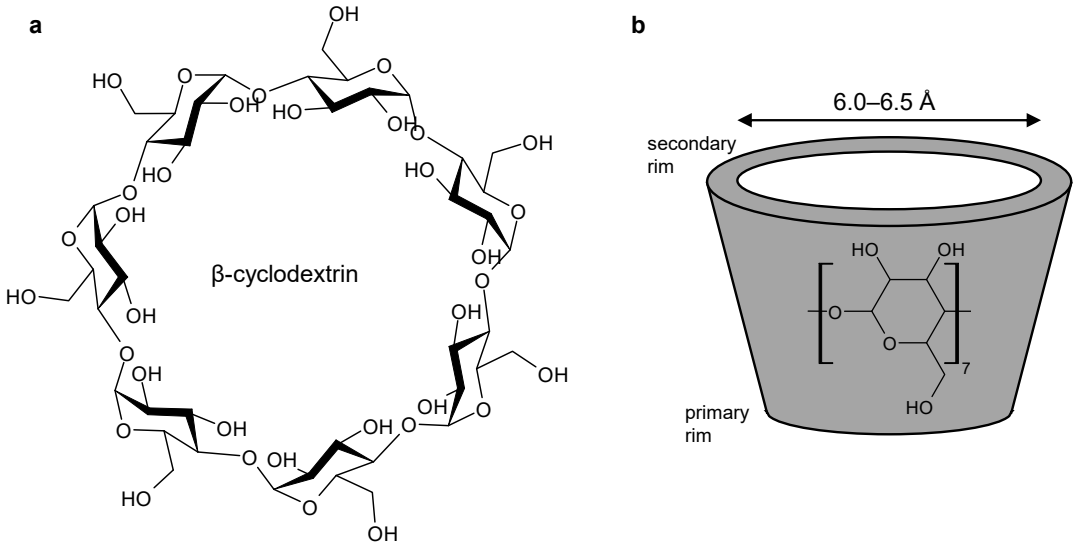

Figure 2. (**a**) Structural formula of β-cyclodextrin; (**b**) sketch of the truncated cone formed by β-cyclodextrin with the size of the cavity.

The formation of hydrogen bonds between adjacent hydroxy groups at the rim of cyclodextrins leads to a rather rigid structure and lowers their solubility, as the interaction with the surrounding water is decreased [22]. By modification of the hydroxy groups, e.g., by conversion into methyl-, hydroxypropyl-, sulfobutyl ether-, or acetyl-moieties, the regular hydrogen-bonding within the natural cyclodextrins is disrupted, thus, enabling better interaction with the surrounding water molecules and increasing the solubility [2,22,26,27].

1.3. Investigation of Complexes

Common techniques used to investigate the stability of cyclodextrin-substrate complexes are calorimetric analysis, nuclear magnetic resonance spectroscopy (NMR), X-ray diffraction, fluorescence spectroscopy, and FTIR. Phase solubility studies and conductometry titration are alternative methods suitable for the investigation of the efficiency of cyclodextrin complexation [2,13,26,31,32]. Furthermore, theoretical approaches and computational modeling have been applied to predict the structure of complexes [4,33].

Using these methods, the encapsulation of organic molecules including amino acids [2,31,34] and platinum compounds [4,35] has been described, and evidence for the inclusion of bent metallocenes with confirmed antitumor activity (M = Ti, Mo, Nb, V) in cyclodextrins was provided by various authors [12,13,15,29,33,36–39]. Depending on the metallocene, its orientation and hydrolysis state for encapsulation was found to be different. Based on an experimental and theoretical study, Braga et al. suggested molybdenocene dichloride entering the β-cyclodextrin cavity

preferably with only one Cp-ligand [33], whereas Morales et al. proposed niobocene to be incorporated as Cp_2NbCl_2OH, with the inclusion of one or both Cp-ligands occurring [12]. Theoretical considerations by Riviş et al. led to the conclusion that the formation of titanocene/cyclodextrin inclusion compounds is feasible and enhances the cytotoxic activity of titanocene as it enables controlled release of the drug and diminishes the hydrolysis of ligands [19].

1.4. Mass Spectrometry

Although inclusion complexes with cyclodextrins have been studied using various techniques, mass spectrometry contributed only rarely. With soft-ionization techniques such as matrix-assisted laser desorption/ionization and electrospray ionization, mass spectrometry has become a useful tool for the elucidation of molecular weights, stoichiometries, and even non-covalent interactions within supramolecular assemblies [25,32,34,39,40]. Mass spectrometry may provide advantages over different analytical techniques in terms of sensitivity and speed [32], and tandem mass spectrometric experiments employing collisional activation have successfully been applied to the evaluation of the relative stabilities of host-guest complexes [25]. The technique has been applied to provide information on the encapsulation of organic structures [25,34,41], ferrocene and its derivatives [39], as well as bent metallocenes [38] in cyclodextrins.

Mass spectrometric data on the inclusion of bent metallocenes have been published only sparsely. The scope of this investigation is to provide further insight into the interaction of titanocene dichloride with β-cyclodextrin and methylated cyclodextrin derivatives to assess the potential of these carbohydrate macrocycles as excipients in the formulation of bent metallocene-based drugs.

2. Results

Despite electrospray being a soft ionization technique, the decomposition of analyte ions due to collision with residual gas in the interface region may occur and potentially compromise the results. To probe the extent of such interfering effects and to demonstrate the capability of mass spectrometry to visualize host-guest interactions of cyclodextrin with organic compounds as well as transition metal complexes, phenylalanine, and the anti-cancer agent oxaliplatin, were chosen as guests. In a second step, the study was extended to the interaction of cyclodextrin with the bent metallocene titanocene dichloride.

Initial experiments aimed at the identification of peaks originating from the individual host and guest molecules, as besides the generation of molecular ions, adduct formation and in-source decomposition were expected, resulting in rather complex mass spectra. Based on high-resolution accurate mass analysis with deviations in the low parts per million (ppm) range and the detected isotopic pattern, the elemental composition of molecular as well as fragment ions can be determined. The full scan mass spectrum of β-cyclodextrin shows the protonated species $[\beta CD + H]^+$ (m/z 1135.3798, 2.5 ppm), the ammonium adduct $[\beta CD + NH_4]^+$ (m/z 1152.4060, 2.1 ppm), and the alkali metal-adducts $[\beta CD + Na]^+$ (m/z 1157.3599, 0.8 ppm) and $[\beta CD + K]^+$ (m/z 1173.3340, 0.9 ppm). Furthermore, in-source fragmentation products due to the loss of glucopyranose subunits $[glc_n + H]^+$ (n = 2–6; m/z 325.1128, −0.3 ppm; m/z 487.1653, −0.8 ppm; m/z 649.2186, 0.0 ppm; m/z 811.2720, 0.7 ppm; m/z 973.3255, 1.3 ppm) were identified (Supplementary Materials Table S1) [42].

Electrospray ionization mass spectrometry of guest species primarily results in their protonation and the formation of the corresponding sodium adducts. Additionally, fragment ions originating from in-source decomposition were detected. In the case of phenylalanine, the protonated form $[Phe + H]^+$ (m/z 166.0856, −4.8 ppm), the alkali adducts $[Phe + Na]^+$ (m/z 188.0676, −3.2 ppm) and $[Phe + K]^+$ (m/z 204.0416, −2.5 ppm), as well as the immonium ion $[Imm(Phe)]^+$ (m/z 120.0803, −4.2 ppm) were identified (Supplementary Materials Table S2). Comparable signals appeared for oxaliplatin, where $[oxaliPt + H]^+$ (m/z 395.0695, 5.3 ppm) and $[oxaliPt + Na]^+$ (m/z 420.0514, 4.8 ppm) were detected (Supplementary Materials Table S3). The mass spectra of titanocene dichloride show signals corresponding to $[Cp_2TiCl]^+$ (m/z 212.9940, −2.3 ppm) and the hydrolysis products $[Cp_2Ti(OH)]^+$ (m/z 195.0278, −3.1 ppm), $[CpTi(OH)_2 + H_2O]^+$ (m/z 165.0021, −3.0 ppm),

$[CpTi(OH)_2]^+$ (m/z 146.9915, −3.4 ppm), and $[Ti(OH)_3 + H_2O]^+$ (m/z 116.9657, −4.3 ppm), as well as $[Cp_2Ti(COOH)]^+$ (m/z 223.0227, −2.7 ppm), which was formed due to the presence of formic acid (Supplementary Materials Table S4). Though the samples were subjected to mass spectrometric analysis immediately after getting in contact with water, rapid hydrolysis of the chloride ligands could not be prevented. Experiments performed in pure MeOH resulted in comparable peaks, with the difference that complexes comprising not only hydroxo-, but also methoxo-ligands, such as $[CpTi(OH)(OMe)(H_2O)]^+$ at m/z 179.0178 (−2.2 ppm), were detected as well (Supplementary Materials Table S5).

2.1. Phenylalanine and Oxaliplatin Complexes

Beside the previously described ions, analysis of mixtures of β-cyclodextrin with phenylalanine and oxaliplatin revealed signals referring to the protonated inclusion complexes [βCD + Phe + H]$^+$ (m/z 1300.4575, 1.2 ppm) and [βCD + oxaliPt + H]$^+$ (m/z 1532.4389, 1.1 ppm), as well as the sodium adducts [βCD + Phe + Na]$^+$ (m/z 1322.4392, 0.9 ppm) and [βCD + oxaliPt + Na]$^+$ (m/z 1554.4207, 1.0 ppm), respectively (Supplementary Materials Tables S6 and S8).

A higher energy collision induced dissociation (HCD) experiment with [βCD + Phe + H]$^+$ as the precursor ion gave rise to signals referring to protonated phenylalanine [Phe + H]$^+$ (m/z 166.0863, 0.0 ppm), protonated β-cyclodextrin [βCD + H]$^+$ (m/z 1135.3777, 0.6 ppm), and protonated cyclodextrin fragments $[glc_n + H]^+$ (n = 1–6; m/z 163.0601, 0.0 ppm; m/z 325.1131, 0.6 ppm; m/z 487.1655, −0.4 ppm; m/z 649.2187, 0.2 ppm; m/z 811.2717, 0.4 ppm; m/z 973.3250, 0.8 ppm), indicating complete separation of host and guest along with the simultaneous decomposition of the host structure (Figure 3, Supplementary Materials Table S7). Fragmentation of the oxaliplatin inclusion complex [βCD + oxaliPt + H]$^+$ resulted in abundant signals of protonated oxaliplatin [oxaliPt + H]$^+$ (m/z 398.0681, 1.8 ppm) and protonated cyclodextrin fragments still interacting with oxaliplatin $[glc_n + oxaliPt + H]^+$ (n = 3–6; m/z 884.2279, 2.3 ppm; m/z 1046.2812, 2.4 ppm; m/z 1208.3344, 2.4 ppm; m/z 1370.3872, 2.1 ppm), whereas fragments of β-cyclodextrin without oxaliplatin were of very low intensity (Supplementary Materials Table S9). The molecular formula determined by accurate mass analysis of this singly charged ion hints at neutral β-cyclodextrin fragments interacting with neutral oxaliplatin in a non-covalent manner with the positive charge provided by an additional proton, whose exact location is not defined. Despite the fact that separation of the host and guest structures was not detected as for phenylalanine, the non-covalent interaction between oxaliplatin and the macrocycle indicates the formation of an inclusion complex.

2.2. Titanocene Complex

Analysis of a 1:1 stoichiometric mixture of β-cyclodextrin and titanocene dichloride showed the ions arising from titanocene, mainly in hydrolyzed form as $[Cp_2Ti(OH)]^+$ (m/z 195.0286, 1.0 ppm), and from β-cyclodextrin (Figure 4, Supplementary Materials Table S10). In addition, the isotopic distribution of the ion appearing at m/z 1311.3913 indicates an interaction between the titanium compound and β-cyclodextrin. Based on the accurate mass determination, the elemental composition of this ion was found to be $C_{52}H_{79}O_{35}Ti^+$, which corresponds to [βCD + Cp_2Ti–H]$^+$. Since the combination of β-cyclodextrin ($C_{42}H_{70}O_{35}$) and Cp_2Ti^{2+} ($C_{10}H_{10}Ti^{2+}$) would result in a doubly charged complex with an elemental composition of $C_{52}H_{80}O_{35}Ti^{2+}$, one of the two charges must have been compensated for by the lack of a proton, presumably at a hydroxy group at either the primary or the secondary rim of β-cyclodextrin. More detailed localization of the deprotonation site, however, was not accomplishable by means of mass spectrometry.

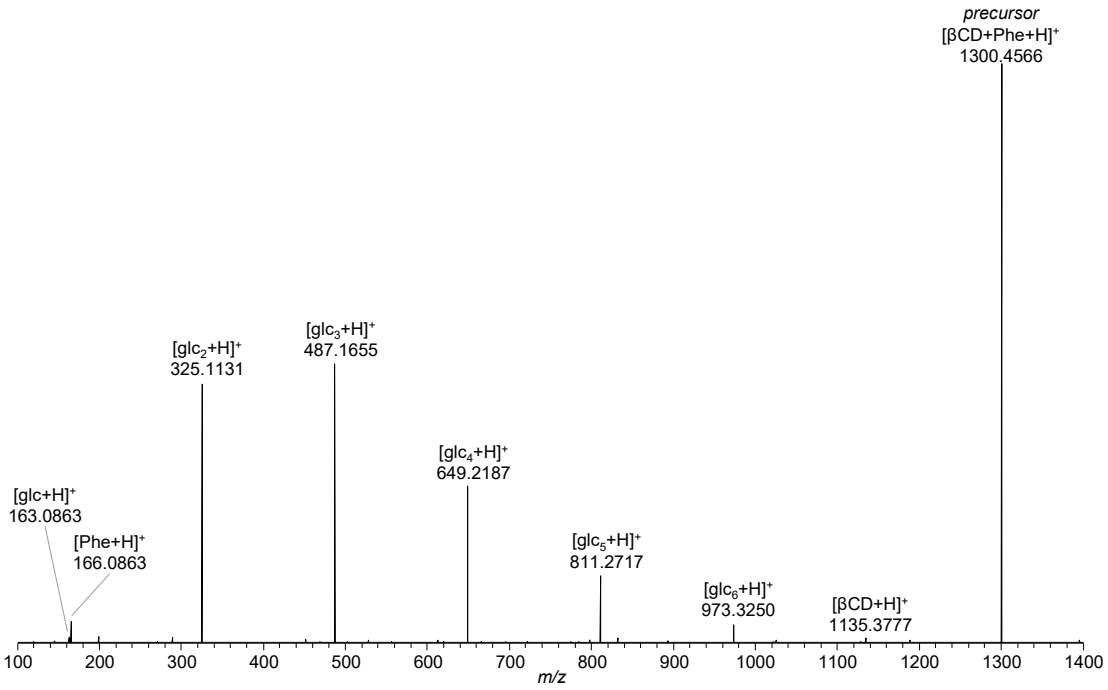

Figure 3. Higher energy collision induced dissociation (HCD) spectrum of [βCD + Phe + H]$^+$ (m/z 1300.48) at 37 eV (16% normalized collision energy (NCE)) showing the separation of the precursor ion into [Phe + H]$^+$, [βCD + H]$^+$, and β-cyclodextrin fragment ions [glc$_n$ + H]$^+$ (n = 1–6).

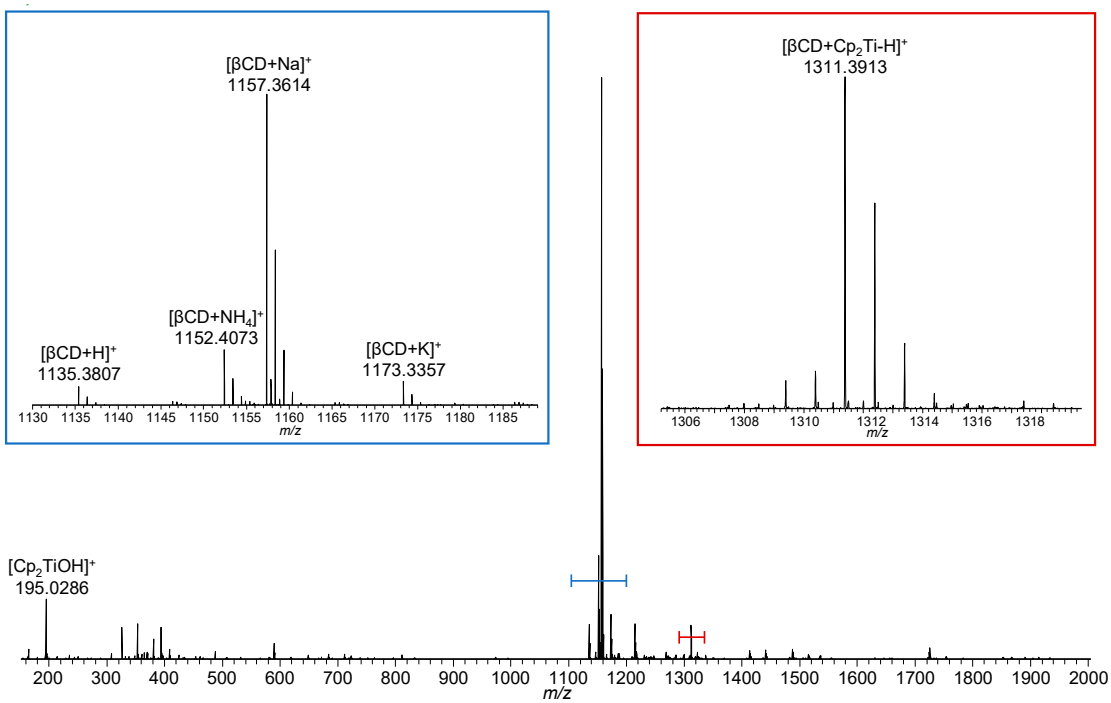

Figure 4. Full scan mass spectrum of the mixture of β-cyclodextrin and titanocene dichloride showing the peak indicating an interaction between the two compounds (red inset), as well as the hydrolyzed titanocene, and cationized β-cyclodextrin (blue).

Collisional activation of [βCD + Cp_2Ti–H]$^+$ (m/z 1311.3859, −1.3 ppm) resulted in the loss of a neutral cyclopentadiene (C_5H_6) moiety, leading to [βCD + CpTi–2H]$^+$ (m/z 1245.3391, −1.2 ppm). With increasing energy, the loss of neutral glucose subunits from β-cyclodextrin occurred, but the titanium species was still bound to the cyclodextrin fragment ions, as indicated by the [glc_n + Cp_2Ti–H]$^+$ (n = 1–6; m/z 339.0699, −2.1 ppm; m/z 501.1221, −2.8 ppm; m/z 663.1747, −2.4 ppm; m/z 825.2277, −1.7 ppm; m/z 987.2802, −1.7 ppm; m/z 1245.3391, −1.2 ppm) and [glc_n + CpTi–2H]$^+$ (n = 1–6; m/z 273.0233, −1.5 ppm; m/z 435.0754, −2.5 ppm; m/z 597.1281, −2.0 ppm; m/z 759.1808, −1.8 ppm; m/z 921.2335, −1.6 ppm; m/z 1083.2862, −1.5 ppm) fragment ions. Loss of the second cyclopentadiene moiety in combination with the decomposition of β-cyclodextrin resulted in [glc_n + Ti–3H]$^+$ (n = 2–6; m/z 369.0287, −2.4 ppm; m/z 531.0811, −2.4 ppm; m/z 693.1339, −1.9 ppm; m/z 855.1866, −1.6 ppm; m/z 1017.2391, −1.8 ppm) fragment ions (Figure 5, Supplementary Materials Table S11). In contrast to β-cyclodextrin complexes with phenylalanine and oxaliplatin, separation of the host and guest structures was not observed as neither the intact β-cyclodextrin nor free titanocene-derived ions (e.g., [$Cp_2Ti(OH)$]$^+$) were detected and all fragment ions were found to contain titanium. These results indicate that the interaction of titanocene dichloride with cyclodextrin differs from the situation observed for the phenylalanine and oxaliplatin guest species.

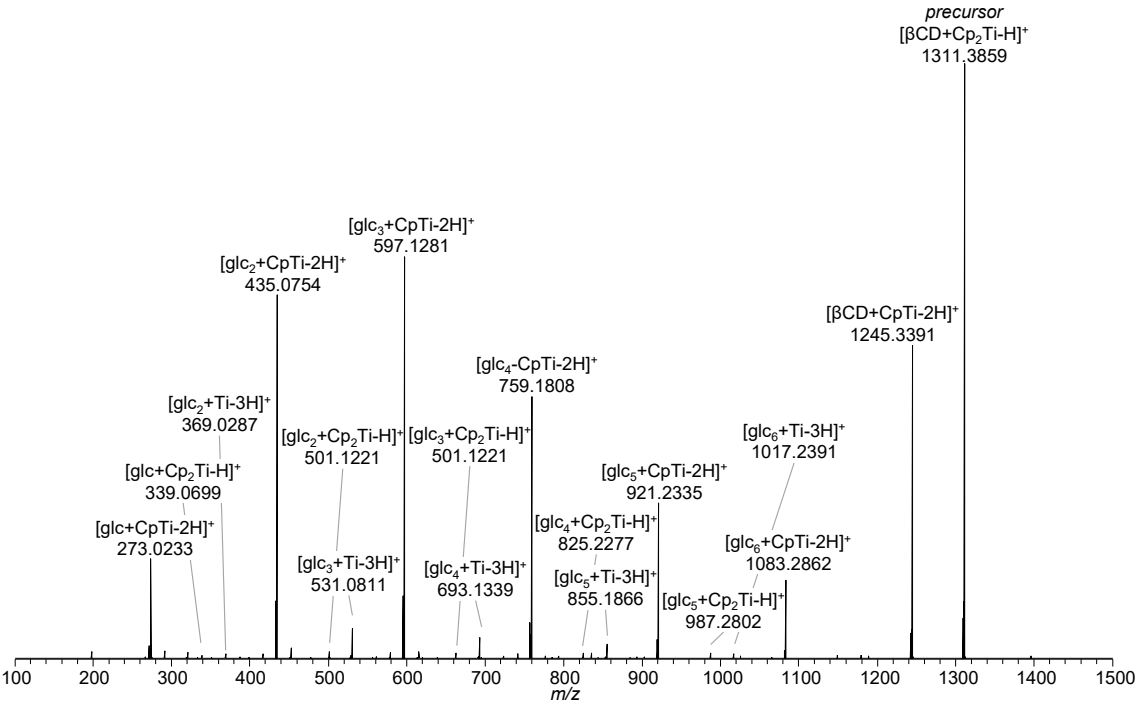

Figure 5. HCD mass spectrum of [βCD + Cp_2Ti–H]$^+$ (m/z 1311.40) at 47 eV (20% NCE) showing the loss of one or two cyclopentadiene moieties (C_5H_6) and the decomposition of β-cyclodextrin into its subunits, still interacting with titanocene species.

Additional experiments probing the interaction of titanocene dichloride with the disaccharides sucrose and maltose gave evidence for the formation of singly charged [sugar + Cp_2Ti–H]$^+$ ions (m/z 519.1314, −5.1 ppm and m/z 519.1325, −3.1 ppm; Supplementary Materials Tables S12 and S14), which is in agreement with the interaction observed for the titanocene with cyclodextrin. Collisional activation of this ion resulted in metallated fragment ions, such as [$C_6H_{10}O_5$ + Cp_2Ti–H]$^+$ (m/z 339.0696, −3.2 ppm) and [$C_6H_{12}O_6$ + Cp_2Ti–H]$^+$ (m/z 357.0800, −3.4 ppm) due to glycosidic bond cleavage and loss of one of the sugar moieties as a neutral (Supplementary Materials Tables S13 and S15).

2.3. Methylated β-Cyclodextrins

The di- and trimethylated cyclodextrin analogs heptakis(2,6-di-*O*-methyl)-β-cyclodextrin (DMβ-cyclodextrin) and heptakis(2,3,6-tri-*O*-methyl)-β-cyclodextrin (TMβ-cyclodextrin) served as host structures for probing their interaction mode with titanocene and deciphering the role of the hydroxy groups. Full scan MS analyses of the host structures showed several peaks spaced by 14 mass units, indicating different degrees of methylation. Consequently, the spectral complexity was increased and the peak intensities were significantly reduced (Supplementary Materials Tables S16 and S17) [42]. Nevertheless, the analysis of phenylalanine in the presence of the two methylated host structures revealed comparable interaction as with unmodified β-cyclodextrin, resulting in signals assigned as $[DM\beta CD + Phe + H]^+$ (m/z 1496.6749, −0.1 ppm) and $[TM\beta CD + Phe + H]^+$ (m/z 1594.7865, 1.1 ppm) (Supplementary Materials Tables S18 and S22). The masking of the hydroxy groups at the rim of β-cyclodextrin does not prevent the interaction with phenylalanine and gives proof for the ability of methylated β-cyclodextrin to act as a host for hydrophobic structures.

Collisional activation of the protonated $[DM\beta CD + Phe + H]^+$ complexes led to fragmentation of the host structures, as demonstrated by Figure 6 for the complex with the dimethylated cyclodextrin (Supplementary Materials Table S19). Though the product ion spectrum of $[DM\beta CD + Phe + H]^+$ did not show the peaks of separated $[Phe + H]^+$ and $[DM\beta CD + H]^+$ ions, the lack of any signals referring to cyclodextrin fragments still bound to phenylalanine indicates a host-guest character of the interaction. A similar situation was encountered for trimethylated cyclodextrin as host for phenylalanine $[TM\beta CD + Phe + H]^+$ (Supplementary Materials Table S23).

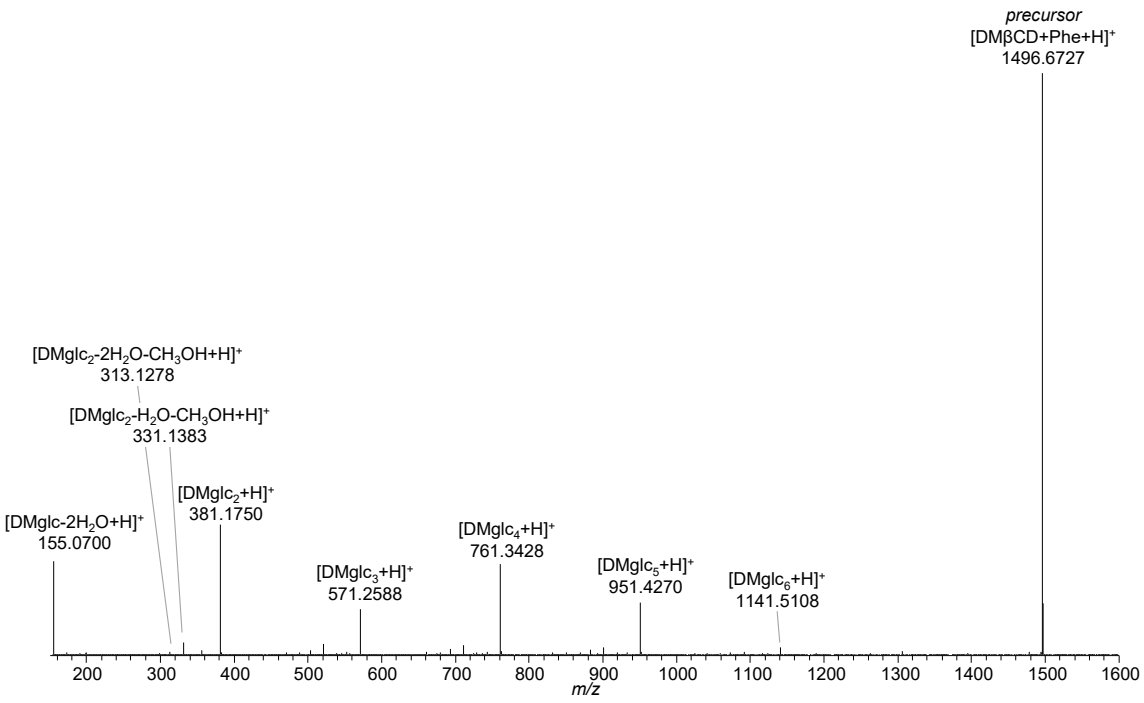

Figure 6. HCD mass spectrum of $[DM\beta CD + Phe + H]^+$ (m/z 1496.70) at 40 eV (15% NCE) showing the separation of the precursor ion and subsequent decomposition of DMβ-cyclodextrin into its subunits $[DMglc_n + H]^+$.

The data obtained from mixtures of titanocene with methylated cyclodextrins significantly differ from previous results on unmodified cyclodextrin. As soon as all hydroxy groups at the rim of β-cyclodextrin are methylated, as in the case of trimethylated β-cyclodextrin, a peak referring to a $[TM\beta CD + Cp_2Ti–H]^+$ interaction product was not observed. This is in contrast to the experiments with unmodified β-cyclodextrin,

which revealed the peak of $[\beta CD + Cp_2Ti–H]^+$. However, the peaks of the putative host-guest complexes $[TM\beta CD + Cp_2Ti(OH)_2 + H]^+$ (m/z 1641.7401, 1.6 ppm) and $[TM\beta CD + Cp_2Ti(OH)]^+$ (m/z 1623.7297, 1.8 ppm) could be detected, though with minor abundance only, which hampered precursor ion isolation for tandem mass spectrometric analysis (Supplementary Materials Table S24).

A different picture was seen for dimethylated and incompletely trimethylated cyclodextrins. The analysis of the mixture of titanocene dichloride with dimethylated β-cyclodextrin resulted in signals assigned as $[DM\beta CD + Cp_2Ti–H]^+$ (m/z 1507.6043; −1.6 ppm) as well as $[DM\beta CD + Cp_2Ti(OH)_2 + H]^+$ (m/z 1543.6249, −1.9 ppm) (Supplementary Materials Table S20). As previously observed for the β-cyclodextrin complex, the energy provided by collisional activation of $[DM\beta CD + Cp_2Ti–H]^+$ promotes the loss of a Cp-ligand (C_5H_5) yielding the $[DM\beta CD + CpTi–H]^+$ (m/z 1442.5635, −2.8 ppm) fragment ion. Further fragment ions were found to correspond to titanium bound to glucose subunits, e.g., $[DMglc_2 + Cp_2Ti–H]^+$ (m/z 557.1843, −3.2 ppm) (Supplementary Materials Table S21).

The hydroxy groups occurring in incompletely trimethylated β-cyclodextrins (e.g., macrocycles bearing 19 (TMβCD*) or 20 (TMβCD$^{\#}$) instead of 21 methoxy groups only) represent targets for the interaction with titanocene. The peaks at m/z 1577.6880 and m/z 1591.7036, corresponding to $[TM\beta CD^* + Cp_2Ti–H]^+$ (2.0 ppm) and $[TM\beta CD^{\#} + Cp_2Ti–H]^+$ (1.9 ppm), respectively, clearly indicate that the lack of one or two methyl-groups is sufficient to form small amounts of covalently-bound titanocene adducts (Supplementary Materials Tables S23–S26).

2.4. Breakdown Curves

To obtain a measure for the strength of the interaction between the host and guest molecules, breakdown curves were recorded by an incremental increase of the collision energy from 0% to 50% normalized collision energy (NCE) in HCD experiments. For each identified ion, the proportion of its intensity (I_n) in the sum of the intensities of the precursor (I_p) and all fragment ions (I_f) is plotted against the collision energy ($y_n = I_n / \left(I_p + \sum I_f \right) \cdot 100$) [43]. CE_{50} values (50% of the precursor ion decomposed into fragments) of 36.2 eV (E_{COM} = 0.78 eV) and 38.7 eV (E_{COM} = 0.72 eV) were obtained for phenylalanine as guest in β-cyclodextrin, and for the interaction of phenylalanine with DMβ-cyclodextrin, respectively (Figure 7a,b, Supplementary Materials Figures S1 and S2). The CE_{50} value of 34.9 eV (E_{COM} = 0.64 eV), determined for the decomposition of $[\beta CD + oxaliPt + H]^+$, is on the same scale, thus, strengthening the hypothesis of host-guest complex formation (Supplementary Materials Figure S4).

The breakdown curve of $[\beta CD + Cp_2Ti–H]^+$ shows a CE_{50} value of 41.3 eV (E_{COM} = 0.88 eV, Figure 7c, Supplementary Materials Figure S3), which is significantly higher than for the host-guest complexes formed between phenylalanine and DMβ- or β-cyclodextrin. Due to the loss of the first Cp-ligand occurring at low collision energies prior to the decomposition of the cyclodextrin, the slope of the precursor decomposition curve is rather flat.

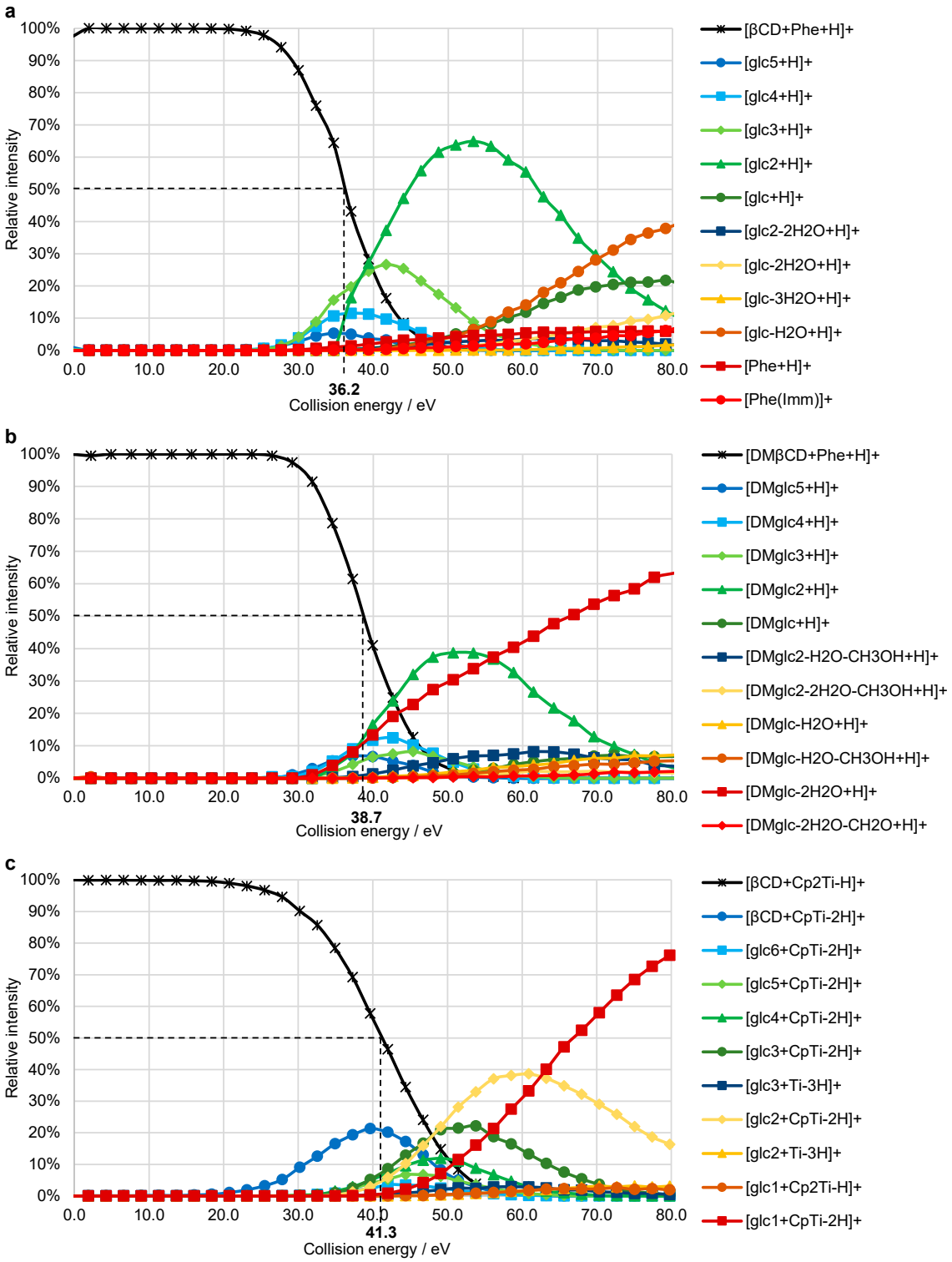

Figure 7. Breakdown curves recorded for HCD experiments of: (**a**) $[\beta CD + Phe + H]^+$ (m/z 1300.48), (**b**) $[DM\beta CD + Phe + H]^+$ (m/z 1496.70), (**c**) $[\beta CD + Cp_2Ti–H]^+$ (m/z 1311.40). Fragment ions with a maximum relative intensity < 2% are not displayed. The dashed lines indicate the CE_{50} values.

3. Discussion

Experiments with phenylalanine and oxaliplatin demonstrated the ability of electrospray ionization mass spectrometry to detect host-guest complexes. Though the literature suggests the formation of an inclusion complex of titanocene dichloride with β-cyclodextrin [19,38], mass spectrometric experiments did not give evidence for the generation of the corresponding $[\beta CD + Cp_2TiCl_2 + H]^+$ ion at m/z 1383.3409. Titanocene dichloride is known to rapidly undergo hydrolysis of the chloride ligands upon contact with water. Nevertheless, the inclusion of these hydrolysis products in β-cyclodextrin was not detected, but the corresponding peaks were observed with low abundance in the spectra with DMβ- and TMβ-cyclodextrin hosts. On the other hand, experiments with β-cyclodextrins bearing unmodified hydroxy groups and disaccharides resulted in similar ions of the type $[\text{sugar} + Cp_2Ti–H]^+$, clearly indicating the significance of hydroxy groups on the interaction of titanocene with saccharides.

Based on the elemental composition determined for the titanocene-cyclodextrin assembly $[\beta CD + Cp_2Ti–H]^+$, two interaction modes are possible: (i) formation of a single covalent bond between the titanium center and a hydroxy group of the primary or secondary rim of β-cyclodextrin with the charge residing on the titanium (Figure 8a), and (ii) formation of two covalent bonds to hydroxy groups while the charge is provided by an additional proton (Figure 8b). Elucidation of the elemental composition does not provide any further details about the mode of interaction, nor the position and number of the hydroxy groups involved. Electrospray mass spectrometric analysis of cyclodextrin, even in a mixture with the metallocene, resulted in the signal of the protonated macrocycle (m/z 1135.3807, 3.3 ppm) and additionally, in the highly abundant peak of the cyclodextrin-sodium adduct (m/z 1157.3614, 2.1 ppm). Sodium adduct formation ($[\beta CD + Cp_2Ti–2H + Na]^+$, m/z 1333.3695), however, was never observed for the titanocene-cyclodextrin assembly. In the case of interaction mode ii, this peak is anticipated, as any cation might provide the charge for the assembly. The lack of this ion suggests the formation of a single covalent bond between any deprotonated hydroxy group of β-cyclodextrin and the titanium coordination center as the most plausible mode of interaction, where the excess positive charge resides on the titanium (Figure 8a). This finding is supported by the results from collisional activation experiments of $[\beta CD + Cp_2Ti–H]^+$, which gave evidence for cyclodextrin fragments still interacting with titanium. According to our previous work [42], bond cleavage between the glucopyranose units as the predominant mechanism for the decomposition of β-cyclodextrin is independent of the hydroxy groups and, therefore, not affected by the interaction with titanocene.

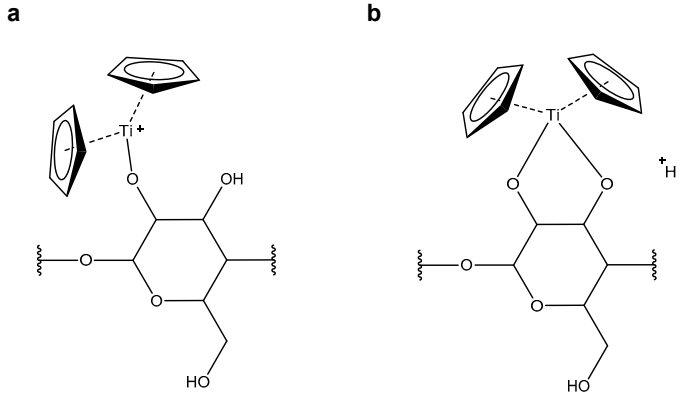

Figure 8. Possible interaction modes between titanocene and β-cyclodextrin: (**a**) formation of one covalent bond and the positive charge residing on the titanium; (**b**) formation of two covalent bonds with the charge emerging from an additional proton.

The CE_{50} values determined for $[\beta CD + Phe + H]^+$, $[DM\beta CD + Phe + H]^+$, and $[\beta CD + Cp_2Ti–H]^+$ are significantly higher than the 15.3 eV obtained for $[\beta CD + H]^+$ in a previous study [42]. Likewise, Dossmann et al. [44] reported values ranging between 15 and 23 eV for doubly charged metallated β-cyclodextrin ions $[\beta CD + M]^{2+}$ ($M = Fe^{2+}$, Co^{2+}, Ni^{2+}, Cu^{2+}, Zn^{2+}). At first sight, these results are unexpected as the dissociation of a covalent bond requires more energy than the disruption of a non-covalent interaction. However, a proton or metal ion bound to glycosidic oxygen significantly destabilizes the corresponding glycosidic bond, thereby inducing dissociation. Protonation of the phenylalanine inclusion complex, on the other hand, occurs most likely at the *N*-terminal amino group of the amino acid, therefore not affecting the integrity of the host structure, which is reflected by the higher CE_{50} value.

The hypothesis of the formation of titanocene dichloride inclusion complexes with β-cyclodextrin, as previously proposed from NMR experiments [38] and theoretical approaches [19], could not be confirmed by our mass spectrometric results, as the formation of a host-guest complex without the involvement of covalent bonds would result in disintegration of the complex, as shown for the interaction of β-cyclodextrin with phenylalanine and oxaliplatin. Therefore, unmodified cyclodextrins are not expected to considerably improve the hydrolytic stability and bioavailability of titanocene dichloride.

4. Materials and Methods

D-L-Phenylalanine (Sigma Aldrich, Buchs, Switzerland) was dissolved in 50/50 water/acetonitrile + 0.5% formic acid (water: MilliQ, in house; acetonitrile: Biosolve, Valkenswaard, the Netherlands; formic acid: Sigma Aldrich, Buchs, Switzerland) to give a 50 mM solution and further diluted to 1 mM in 50/50 water/acetonitrile. Oxaliplatin and titanocene dichloride (Sigma Aldrich, Buchs, Switzerland) were dissolved in ULC-MS grade acetonitrile (Biosolve, Valkenswaard, the Netherlands) and ultrasonicated for 30 min to give a 1 mM stock solution. Heptakis(2,3,6-tri-*O*-methyl)-β-cyclodextrin (TMβ-cyclodextrin), heptakis(2,6-di-*O*-methyl)-β-cyclodextrin (DMβ-cylclodextrin) (Sigma Aldrich, Buchs, Switzerland), β-cyclodextrin (Fluka, Sigma Aldrich, Buchs, Switzerland), sucrose (Merck, Darmstadt, Germany), and maltose (Sigma Aldrich, Buchs, Switzerland) were dissolved in MilliQ water to a final concentration of 1 mM by shaking for 1 h at 21 °C and 12,000 rpm on a thermomixer (Eppendorf, Schönenbuch, Switzerland).

For measurement, samples at a concentration of 0.02 mM were prepared either in 50/50 water/acetonitrile, 50/50 water/acetonitrile + 0.5% formic acid, or methanol (Sigma Aldrich, Bruchs, Switzerland), either of the host and guest structures solely, or mixed in a 1:1 molar ratio.

Mass Spectrometry

Nano electrospray-ionization mass spectrometric experiments were performed on an LTQ Orbitrap XL instrument (Thermo Fisher Scientific, Bremen, Germany) with Econo12 Glass PicoTips (New Objective, Littleton, MA, USA) as electrospray emitters. Mass spectrometry was performed in positive ionization mode with spray voltages ranging from 0.8 to 1.3 kV, tube lens voltage of 250 V, capillary voltage of 20 V, and a capillary temperature of 200 °C. The mass spectrometer was used in FTMS mode at a resolution of 100,000. HCD experiments were performed with precursor ion isolation windows in the range of 3 to 8 m/z. Collision energies ranged between 0% and 50% NCE and were converted to eV [45,46]. Data processing was performed using the Xcalibur software suite (Thermo Fisher Scientific, Bremen, Germany).

Supplementary Materials: Supplementary Materials can be found at https://www.mdpi.com/article/10.3390/ijms22189789/s1.

Author Contributions: Conceptualization, methodology, project administration, validation, writing—review and editing, P.S.B. and S.S.; formal analysis, data curation, investigation, visualization,

writing—original draft preparation, P.S.B.; resources, supervision, S.S. All authors have read and agreed to the published version of the manuscript.

Funding: This research received no external funding.

Data Availability Statement: Data are contained within the Supplementary Materials.

Conflicts of Interest: The authors declare no conflict of interest.

References

1. Gidwani, B.; Vyas, A. A Comprehensive Review on Cyclodextrin-Based Carriers for Delivery of Chemotherapeutic Cytotoxic Anticancer Drugs. *Biomed. Res. Int.* **2015**, *2015*, 198268. [CrossRef]
2. di Cagno, M. The Potential of Cyclodextrins as Novel Active Pharmaceutical Ingredients: A Short Overview. *Molecules* **2017**, *22*, 1. [CrossRef] [PubMed]
3. Waern, J.B.; Harding, M.M. Bioorganometallic Chemistry of Molybdocene Dichloride. *J. Organomet. Chem.* **2004**, *689*, 4655–4668. [CrossRef]
4. Anconi, C.P.A.; Da Silva Delgado, L.; Alves Dos Reis, J.B.; De Almeida, W.B.; Costa, L.A.S.; Dos Santos, H.F. Inclusion Complexes of α-Cyclodextrin and the Cisplatin Analogues Oxaliplatin, Carboplatin and Nedaplatin: A Theoretical Approach. *Chem. Phys. Lett.* **2011**, *515*, 127–131. [CrossRef]
5. Causey, P.W.; Baird, M.C.; Cole, S.P.C. Synthesis, Characterization, and Assessment of Cytotoxic Properties of a Series of Titanocene Dichloride Derivatives. *Organometallics* **2004**, *23*, 4486–4494. [CrossRef]
6. Harding, M.M.; Mokdsi, G. Antitumour Metallocenes: Structure-Activity Studies and Interactions with Biomolecules. *Curr. Med. Chem.* **2000**, *7*, 1289–1303. [CrossRef] [PubMed]
7. Abeysinghe, P.M.; Harding, M.M. Antitumour Bis(Cyclopentadienyl) Metal Complexes: Titanocene and Molybdocene Dichloride and Derivatives. *Dalt. Trans.* **2007**, 3474–3482. [CrossRef]
8. Lümmen, G.; Sperling, H.; Luboldt, H.; Otto, T.; Rübben, H. Phase II Trial of Titanocene Dichloride in Advanced Renal-Cell Carcinoma. *Cancer Chemother. Pharmacol.* **1998**, *42*, 415–417. [CrossRef]
9. Kröger, N.; Kleeberg, U.R.; Mross, K.; Edler, L.; Hossfeld, D.K. Phase II Clinical Trial of Titanocene Dichloride in Patients with Metastatic Breast Cancer. *Onkologie* **2000**, *23*, 60–62. [CrossRef]
10. Chen, X.; Zhou, L. The Hydrolysis Chemistry of Anticancer Drug Titanocene Dichloride: An Insight from Theoretical Study. *J. Mol. Struct. Theochem* **2010**, *940*, 45–49. [CrossRef]
11. Toney, J.H.; Marks, T.J. Hydrolysis Chemistry of the Metallocene Dichlorides M(H5-C5H5)2Cl2, M = Titanium, Vanadium, or Zirconium. Aqueous Kinetics, Equilibria, and Mechanistic Implications for a New Class of Antitumor Agents. *J. Am. Chem. Soc.* **1985**, *107*, 947–953. [CrossRef]
12. Morales, A.; Struppe, J.; Meléndez, E. Host-Guest Interactions between Niobocene Dichloride and α-, β-, and γ-Cyclodextrins: Preparation and Characterization. *J. Incl. Phenom. Macrocycl. Chem.* **2008**, *60*, 263–270. [CrossRef]
13. Braga, S.S.; Marques, M.P.M.; Sousa, J.B.; Pillinger, M.; Teixeira-Dias, J.J.C.; Gonçalves, I.S. Inclusion of Molybdenocene Dichloride (Cp2MoCl2) in 2-Hydroxypropyl- and Trimethyl-β-Cyclodextrin: Structural and Biological Properties. *J. Organomet. Chem.* **2005**, *690*, 2905–2912. [CrossRef]
14. Meléndez, E. Metallocenes as Target Specific Drugs for Cancer Treatment. *Inorganica Chim. Acta* **2012**, *393*, 36–52. [CrossRef]
15. Meléndez, E. Bioorganometallic Chemistry of Molybdenocene Dichloride and Its Derivatives. *J. Organomet. Chem.* **2012**, *706–707*, 4–12. [CrossRef]
16. Erxleben, A.; Claffey, J.; Tacke, M. Binding and Hydrolysis Studies of Antitumoural Titanocene Dichloride and Titanocene Y with Phosphate Diesters. *J. Inorg. Biochem.* **2010**, *104*, 390–396. [CrossRef]
17. Vessières, A.; Plamont, M.-A.; Cabestaing, C.; Claffey, J.; Dieckmann, S.; Hogan, M.; Müller-Bunz, H.; Strohfeldt, K.; Tacke, M. Proliferative and Anti-Proliferative Effects of Titanium- and Iron-Based Metallocene Anti-Cancer Drugs. *J. Organomet. Chem.* **2009**, *694*, 874–879. [CrossRef]
18. Cini, M.; Bradshaw, T.D.; Woodward, S. Using Titanium Complexes to Defeat Cancer: The View from the Shoulders of Titans. *Chem. Soc. Rev.* **2017**, *46*, 1040–1051. [CrossRef]
19. Riviş, A.; Hădărugă, N.G.; Gârban, Z.; Hădărugă, D.I. Titanocene/Cyclodextrin Supramolecular Systems: A Theoretical Approach. *Chem. Cent. J.* **2012**, *6*, 129–139. [CrossRef] [PubMed]
20. Jambhekar, S.S.; Breen, P. Cyclodextrins in Pharmaceutical Formulations II: Solubilization, Binding Constant, and Complexation Efficiency. *Drug Discov. Today* **2016**, *21*, 363–368. [CrossRef] [PubMed]
21. Plumb, J.A.; Venugopal, B.; Oun, R.; Gomez-Roman, N.; Kawazoe, Y.; Venkataramanan, N.S.; Wheate, N.J. Cucurbit[7]Uril Encapsulated Cisplatin Overcomes Cisplatin Resistance via a Pharmacokinetic Effect. *Metallomics* **2012**, *4*, 561–567. [CrossRef] [PubMed]
22. Saokham, P.; Muankaew, C.; Jansook, P.; Loftsson, T. Solubility of Cyclodextrins and Drug/Cyclodextrin Complexes. *Molecules* **2018**, *23*, 1161. [CrossRef] [PubMed]
23. Jambhekar, S.S.; Breen, P. Cyclodextrins in Pharmaceutical Formulations I: Structure and Physicochemical Properties, Formation of Complexes, and Types of Complex. *Drug Discov. Today* **2016**, *21*, 356–362. [CrossRef]

24. Senthilnathan, D.; Solomon, R.V.; Kiruthika, S.; Venuvanalingam, P.; Sundararajan, M. Are Cucurbiturils Better Drug Carriers for Bent Metallocenes? Insights from Theory. *J. Biol. Inorg. Chem.* **2018**, *23*, 413–423. [CrossRef]
25. Ramanathan, R.; Prokai, L. Electrospray Ionization Mass Spectrometric Study of Encapsulation of Amino Acids by Cyclodextrins. *J. Am. Soc. Mass Spectrom.* **1995**, *6*, 866–871. [CrossRef]
26. Jansook, P.; Ogawa, N.; Loftsson, T. Cyclodextrins: Structure, Physicochemical Properties and Pharmaceutical Applications. *Int. J. Pharm.* **2018**, *535*, 272–284. [CrossRef]
27. Davis, M.E.; Brewster, M.E. Cyclodextrin-Based Pharmaceutics: Past, Present and Future. *Nat. Rev. Drug Discov.* **2004**, *3*, 1023–1035. [CrossRef]
28. Loftsson, T.; Saokham, P.; Sá Couto, A.R. Self-Association of Cyclodextrins and Cyclodextrin Complexes in Aqueous Solutions. *Int. J. Pharm.* **2019**, *560*, 228–234. [CrossRef]
29. Hapiot, F.; Tilloy, S.; Monflier, E. Cyclodextrins as Supramolecular Hosts for Organometallic Complexes. *Chem. Rev.* **2006**, *106*, 767–781. [CrossRef] [PubMed]
30. Lee, J.U.; Lee, S.S.; Lee, S.; Oh, H.B. Noncovalent Complexes of Cyclodextrin with Small Organic Molecules: Applications and Insights into Host–Guest Interactions in the Gas Phase and Condensed Phase. *Molecules* **2020**, *25*, 4048. [CrossRef]
31. Rudolph, S.; Riedel, E.; Henle, T. Studies on the Interaction of the Aromatic Amino Acids Tryptophan, Tyrosine and Phenylalanine as Well as Tryptophan-Containing Dipeptides with Cyclodextrins. *Eur. Food Res. Technol.* **2018**, *244*, 1511–1519. [CrossRef]
32. Silion, M.; Fifere, A.; Lungoci, A.L.; Marangoci, N.L.; Ibanescu, S.A.; Zonda, R.; Rotaru, A.; Pinteală, M. Mass Spectrometry as a Complementary Approach for Noncovalently Bound Complexes Based on Cyclodextrins. In *Advances in Experimental Medicine and Biology*; Woods, A.G., Darie, C.C., Eds.; NLM (Medline); Springer: Berlin/Heidelberg, Germany, 2019; Volume 1140, pp. 685–701. [CrossRef]
33. Braga, S.S.; Gonçalves, I.S.; Pillinger, M.; Ribeiro-Claro, P.; Teixeira-Dias, J.J. Experimental and Theoretical Study of the Interaction of Molybdenocene Dichloride (Cp2MoCl2) with β-Cyclodextrin. *J. Organomet. Chem.* **2001**, *632*, 11–16. [CrossRef]
34. Guo, M.; Song, F.; Liu, Z.; Liu, S. Characterization of Non-Covalent Complexes of Rutin with Cyclodextrins by Electrospray Ionization Tandem Mass Spectrometry. *J. Mass Spectrom.* **2004**, *39*, 594–599. [CrossRef]
35. Zhang, D.; Zhang, J.; Jiang, K.; Li, K.; Cong, Y.; Pu, S.; Jin, Y.; Lin, J. Preparation, Characterisation and Antitumour Activity of β-, γ- and HP-β-Cyclodextrin Inclusion Complexes of Oxaliplatin. *Spectrochim. Acta Part A Mol. Biomol. Spectrosc.* **2016**, *152*, 501–508. [CrossRef]
36. Morales, A.; Weber, R.T.; Melendez, E. Spectroscopic and Thermal Characterization of the Host–Guest Interactions between A-, B- and Γ-cyclodextrins and Vanadocene Dichloride. *Appl. Organomet. Chem.* **2008**, *22*, 440–450. [CrossRef]
37. Morales, A.; Santana, A.; Althoff, G.; Melendez, E. Host–Guest Interactions between Calixarenes and Cp2NbCl2. *J. Organomet. Chem.* **2011**, *696*, 2519–2527. [CrossRef]
38. Turel, I.; Demšar, A.; Košmrlj, J. The Interactions of Titanocene Dihalides with α-, β- and γ-Cyclodextrin Host Molecules. *J. Incl. Phenom. Macrocycl. Chem.* **1999**, *35*, 595–604. [CrossRef]
39. Bakhtiar, R.; Kaifer, A.E. Mass Spectrometry Studies on the Complexation of Several Organometallic Complexes by α- and β-Cyclodextrins. *Rapid Commun. Mass Spectrom.* **1998**, *12*, 111–114. [CrossRef]
40. Lebrilla, C.B. The Gas-Phase Chemistry of Cyclodextrin Inclusion Complexes. *Acc. Chem. Res.* **2001**, *34*, 653–661. [CrossRef]
41. Barylyuk, K.; Balabin, R.M.; Grünstein, D.; Kikkeri, R.; Frankevich, V.; Seeberger, P.H.; Zenobi, R. What Happens to Hydrophobic Interactions during Transfer from the Solution to the Gas Phase? The Case of Electrospray-Based Soft Ionization Methods. *J. Am. Soc. Mass Spectrom.* **2011**, *22*, 1167–1177. [CrossRef] [PubMed]
42. Bruni, P.S.; Schürch, S. Fragmentation Mechanisms of Protonated Cyclodextrins in Tandem Mass Spectrometry. *Carbohydr. Res.* **2021**, *504*, 108316. [CrossRef] [PubMed]
43. Memboeuf, A.; Jullien, L.; Lartia, R.; Brasme, B.; Gimbert, Y. Tandem Mass Spectrometric Analysis of a Mixture of Isobars Using the Survival Yield Technique. *J. Am. Soc. Mass Spectrom.* **2011**, *22*, 1744–1752. [CrossRef]
44. Dossmann, H.; Fontaine, L.; Weisgerber, T.; Bonnet, V.; Monflier, E.; Ponchel, A.; Przybylski, C. First Steps to Rationalize Host-Guest Interaction between α-, β-, and γ-Cyclodextrin and Divalent First-Row Transition and Post-Transition Metals (Subgroups VIIB, VIIIB, and IIB). *Inorg. Chem.* **2021**, *60*, 930–943. [CrossRef] [PubMed]
45. Przybylski, C.; Bonnet, V. Discrimination of Cyclic and Linear Oligosaccharides by Tandem Mass Spectrometry Using Collision-Induced Dissociation (CID), Pulsed-Q-Dissociation (PQD) and the Higherenergy C-Trap Dissociation Modes. *Rapid Commun. Mass Spectrom.* **2013**, *27*, 75–87. [CrossRef] [PubMed]
46. Szabó, D.; Schlosser, G.; Vékey, K.; Drahos, L.; Révész, Á. Collision Energies on QTof and Orbitrap Instruments: How to Make Proteomics Measurements Comparable? *J. Mass Spectrom.* **2021**, *56*, e4693. [CrossRef]

4 Effect of Source Parameters

In-source fragmentation is the cause of a considerable part of the ions detected in full scan mass spectra. With proper adjustment of the instrumental parameters, this unspecific dissociation can be reduced. The schematic setup of the LTQ Orbitrap XL instrument used for our experiments is shown in figure 4.1A. The source interface region is shown in more detail in figure 4.1B. It is located in the first vacuum region of the instrument and is composed of an ion sweep cone, a spray cone, the ion transfer tube (also referred to as capillary), a heater block, the tube lens, and the skimmer. Easily adjustable parameters in this source interface potentially affecting the ionization process are the capillary voltage, the capillary temperature, and the tube lens voltage [193]. The capillary is a metal tube responsible for transferring the ions from the atmospheric pressure ionization (API) ion source into the tube lens region and assists in their desolvation, aided by the temperature applied by the surrounding heater block. The voltage applied to the tube lens accelerates the ions exiting the capillary into the skimmer region, where the ions collide with the background gas. These collisions further aid in desolvating the ions and reducing analyte clusters. This process increases sensitivity, but a too high voltage can lead to extensive collisions and, consequently, analyte dissociation [259]. With the following experiments, the effect of the capillary voltage, the capillary temperature, and the tube lens voltage on the full scan mass spectra of a mixture of phenylalanine and β-cyclodextrin have been evaluated, especially their effect on the detection of the non-covalent complex.

4.1 Experimental Setup

As previously observed, the signal intensity is not very stable in nano-electrospray experiments. For more reliable results, continuous sample flow (14 µL/min) was achieved by using the standard electrospray source equipped with a syringe pump. The analyzed samples contained a 1:1 stoichiometric mixture of phenylalanine and β-cyclodextrin in 50/50 (v/v) H_2O/MeCN or 50/50 (v/v) H_2O/MeCN + 1% FA. The effect of the parameters were evaluated by varying the tube lens voltage in the range from 50–250 V, the capillary voltage from 20–140 V, and the capillary temperature from 100–350 °C. In 1D experiments, two parameters are kept constant

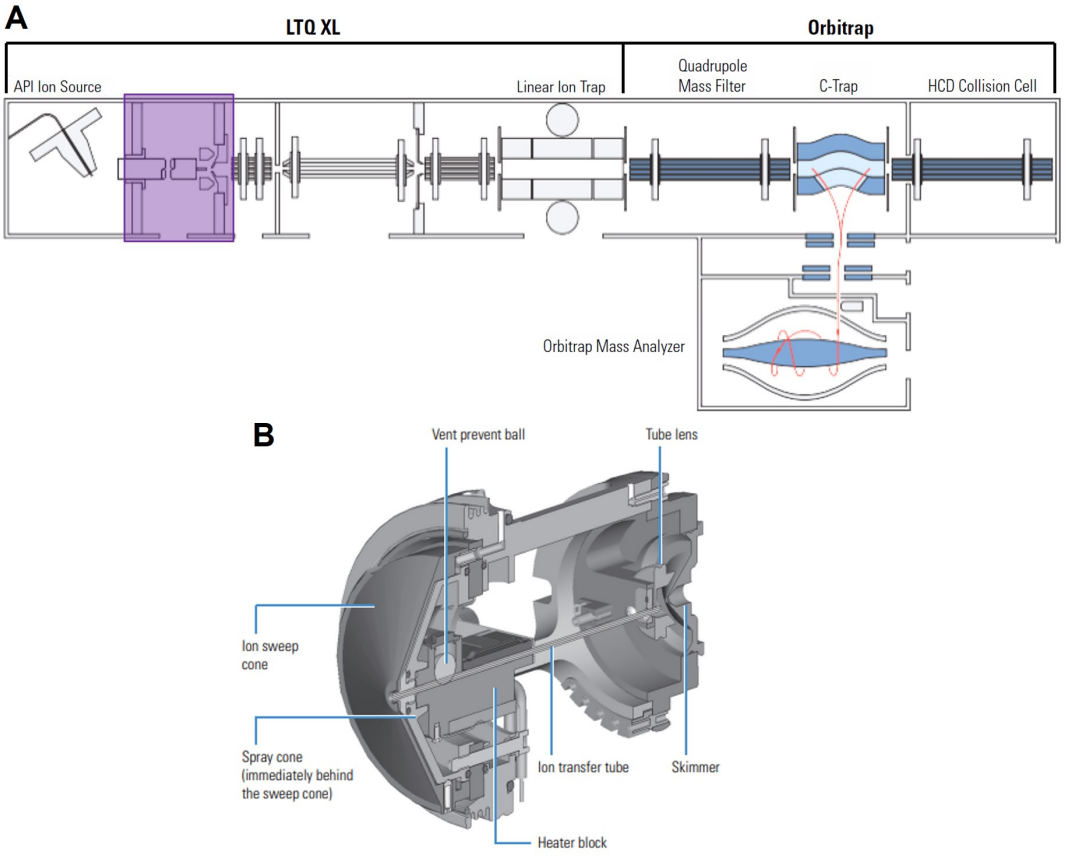

Figure 4.1: A) Schematic setup of the Thermo Fisher Orbitrap XL mass spectrometer with the source interface region highlighted in purple [260]. B) Cross-sections of the source interface region [259].

at their base value while the range of the remaining parameter was scanned. In 2D experiments, one parameter remained at its base value while the two others were changed. These base values have been set to 200 V for the tube lens voltage, 50 V for the capillary voltage, and 200 °C for the capillary temperature. In all experiments, the potential applied to the spray capillary was set to 5 kV.

4.1.1 Data Evaluation

For better evaluation of the quality of the recorded full scan mass spectra, several properties that characterize a "good" mass spectrum are discussed in the following section. First of all, high total ion current and little signal related to undefined compounds and noise are preferred. In this context, the signals of undefined compounds and noise means the difference between the total ion current and the sum of the intensities of the assigned ions. The higher the fraction of the assignable ions of the total ion current, the better the mass spectra. For the following experiments, a minimum fraction at which a spectrum is considered as

Table 4.1: Definition of the ion groups of the mixture of phenylalanine and β-cyclodextrin used for the data interpretation.

Group	A) Host	B) Guest	E) Complex
Ions	$[\beta CD + H]^+$ $[\beta CD + Na]^+$ $[\beta CD + K]^+$ $[\beta CD + NH_4]^+$ $[\beta CD + Ca]^{2+}$	$[Phe + H]^+$ $[Phe + Na]^+$ $[Phe + K]^+$	$[\beta CD + Phe + H]^+$ $[\beta CD + Phe + Na]^+$
Group	C) Host Fragments	D) Guest Fragments	
Ions	$[glc_4 + H]^+$ $[glc_3 + Na]^+$ $[glc_2 - H_2O + H]^+$ $\cdots$	$[Imm(Phe)]^+$	

good was set to 10% for the subsequent data evaluation. For proper assignment of an ion, its absolute intensity has to be of appropriate intensity. For the following evaluation, this threshold was set to 3'000 counts. In order to draw a conclusion on the detection of the host and guest compounds and the non-covalent complex in the sample mixture, the identified ions are assigned to the five groups A) to E) (table 4.1). Group A and B contain the ions assigned to intact β-cyclodextrin and phenylalanine, respectively. Group C and D cover the respective fragment ions, whereas group E contains the non-covalent complexes of phenylalanine and β-cycldoextrin. Thereafter, the effect of the source parameters on the intensities of these ion groups is determined. The intensity of the complex ions (group E) should be as high as possible. Additionally, higher intensities of intact host and guest ions (groups A and B) are preferred over extensive in-source fragmentation (high intensity of groups C and D ions), as this simplifies the data interpretation due to fewer signals occurring in the mass spectra.

4.2 1D Experiments

In the following 1D experiments, two parameters have been set to the base value and one has been changed. This led to a first overview of the potential of each parameter to improve the mass spectra.

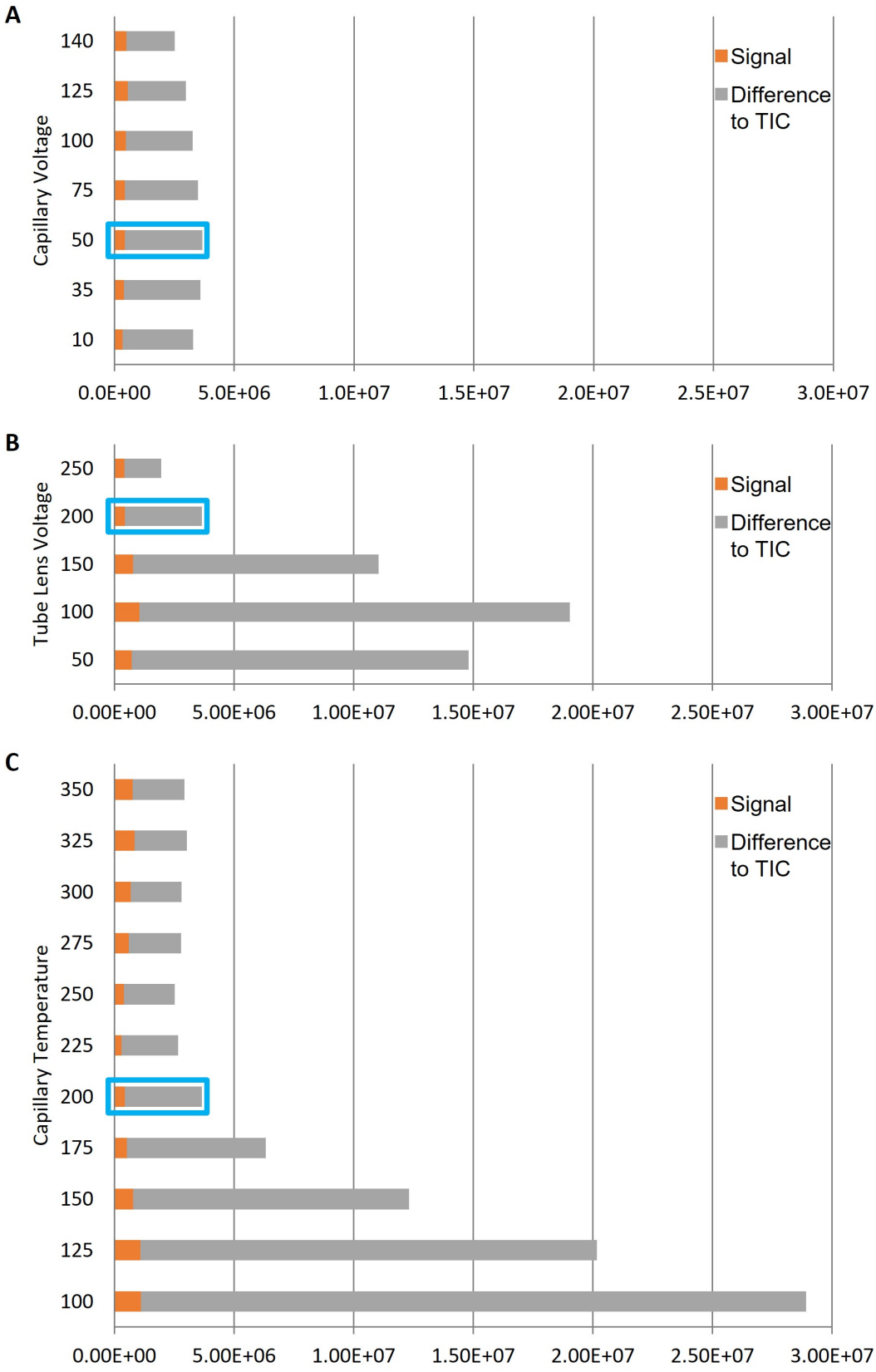

Figure 4.2: Depiction of the signal intensities and the intensity of unassigned signals obtained from 1D experiments. The base conditions are indicated in blue (capillary voltage 50 V, tube lens voltage 200 V, and capillary temperature 200 °C).

Capillary Voltage

The capillary voltage was set to 10, 35, 50, 75, 100, 125, and 140 V while the tube lens voltage was kept at 200 V and the capillary temperature at 200 °C. As displayed by figure 4.2A, the capillary voltage has only little effect on the total ion current and the total signal intensity. While at 10 V only 10.3% of the total ion current was assignable to the five groups of ions, the maximum fraction was 20.2% obtained at 140 V capillary voltage (table 4.2). The composition of the detected ions showed a decrease of the intact guest and the guest fragments. The intensity of the host and the host fragment ions both increased with higher capillary voltage. With an increase by a factor of 1.5 in the absolute intensity of the complex ions, the capillary voltage has only a minor effect on the detection of the non-covalent complex.

Table 4.2: Absolute and relative signal intensities detected for different capillary voltages at a tube lens voltage of 200 V and a capillary temperature of 200 °C.

Capillary Voltage	Ion Group A	B	C	D	E	Signal (% of TIC)
10	1.8×10^5 (54.4%)	5.4×10^4 (16.0%)	1.6×10^4 (4.8%)	7.9×10^4 (23.5%)	4.3×10^3 (1.3%)	3.4×10^5 (10.3%)
35	2.1×10^5 (53.2%)	6.7×10^4 (16.8%)	1.3×10^4 (3.3%)	1.0×10^5 (25.2%)	5.9×10^3 (1.5%)	4.0×10^5 (11.0%)
50	2.3×10^5 (52.4%)	6.2×10^4 (14.2%)	2.1×10^4 (4.8%)	1.2×10^5 (27.2%)	6.2×10^3 (1.4%)	4.3×10^5 (11.8%)
75	2.4×10^5 (55.4%)	4.6×10^4 (10.7%)	2.3×10^4 (5.3%)	1.2×10^5 (27.2%)	6.0×10^3 (1.4%)	4.3×10^5 (12.4%)
100	2.8×10^5 (59.4%)	4.0×10^4 (8.4%)	4.3×10^4 (8.9%)	1.0×10^5 (21.7%)	7.6×10^3 (1.6%)	4.8×10^5 (14.5%)
125	3.3×10^5 (58.4%)	3.4×10^4 (6.1%)	1.2×10^5 (22.3%)	6.3×10^4 (11.2%)	1.0×10^4 (1.9%)	5.6×10^5 (18.7%)
140	2.8×10^5 (55.3%)	2.6×10^4 (5.1%)	1.6×10^5 (30.6%)	3.7×10^4 (7.2%)	8.9×10^3 (1.8%)	5.1×10^5 (20.2%)

A) Host, B) Guest, C) Host Fragments, D) Guest Fragments, E) Complex;
TIC: Total ion current.

Tube Lens Voltage

Changes in the tube lens voltage showed a significantly higher effect on the total intensity of the signals and the total ion current detected in the full scan mass

Table 4.3: Absolute and relative signal intensities detected for different tube lens voltages at a capillary voltage of 20 V and a capillary temperature of 200 °C.

Tube Lens Voltage	Ion Group A	B	C	D	E	Signal (% of TIC)
50	7.5×10^4 (10.3%)	6.0×10^5 (82.7%)	4.7×10^3 (0.6%)	4.4×10^4 (6.0%)	1.9×10^3 (0.3%)	7.3×10^5 (4.8%)
100	1.3×10^5 (12.1%)	8.2×10^5 (78.8%)	6.6×10^3 (0.6%)	8.6×10^4 (8.3%)	2.3×10^3 (0.2%)	1.0×10^6 (5.5%)
150	1.9×10^5 (23.4%)	4.3×10^5 (54.8%)	8.0×10^3 (1.0%)	1.6×10^5 (20.1%)	5.4×10^3 (0.7%)	7.9×10^5 (7.2%)
200	2.3×10^5 (52.4%)	6.2×10^4 (14.2%)	2.1×10^4 (4.8%)	1.2×10^5 (27.2%)	6.2×10^3 (1.4%)	4.3×10^5 (11.8%)
250	2.8×10^5 (66.9%)	2.2×10^4 (5.3%)	8.3×10^4 (20.1%)	2.3×10^4 (5.5%)	9.0×10^3 (2.2%)	4.1×10^5 (21.1%)

A) Host, B) Guest, C) Host Fragments, D) Guest Fragments, E) Complex;
TIC: Total ion current.

spectra (figure 4.2B). With 50 V tube lens voltage, the assigned ion intensities represented only 4.9% of the total ion current. With increasing voltage, their relative intensity increased by a factor of 4.3 (to 21.1% at 250 V), but the absolute value did indicate a slight decrease from 1.6×10^6 at 100 V to 4.1×10^5 at 150 V (table 4.3). Therefore, the increased percentage of the signal resulted from a significant decrease in the total ion current, caused by less noise. Also, the composition of the detected ions showed significant changes. The absolute and relative signal intensities of the intact host and host fragment ions increased, whereas the intensity of the guest ions decreased. The relative and absolute intensities of the guest fragment ions first increased up to a tube lens voltage of 200 V and decreased significantly at an applied tube lens voltage of 250 V. The intensity of the complex increased with higher tube lens voltages.

Capillary Temperature

At low capillary temperature, the total ion current is high, but the percentage of the intensity of the detected ions is $< 10\%$ up to 175 °C but the absolute intensity decreases from 1.1×10^6 to 5.1×10^5. From 200 °C to 325 °C, the relative intensity of the signal increases from 11.8% to 28.2%. The intensity of the signals corresponding to host ions first increases from an absolute intensity of 5.5×10^4 at 100 °C to 2.3–2.5×10^5 at 200–250 °C and decreases again to 5.5×10^4 at 350 °C.

The intensity of the host fragment ion signals increases with increased temperature. Therefore, a higher temperature promotes the ionization of the host and its degradation at even higher temperatures. The absolute intensity of the guest ions decreases continuously from 9.7×10^5 at 100 °C to 1.2×10^4 at 350 °C, and their fragment ion intensity increases slightly from 6.4×10^4 (100 °C) to 1.2×10^5 (175–200 °C), to decrease again with higher temperature. The complex was not detected at all at a capillary temperature of 100 °C. The intensity of the signals belonging to this ion group increased to a maximum of 7.5×10^3 at 275–325 °C.

Table 4.4: Absolute and relative signal intensities detected for different capillary temperatures at a tube lens voltage of 200 V and a capillary voltage of 50 V.

Capillary Temperature	Ion Group A	B	C	D	E	Signal (% of TIC)
100	5.5×10^4 (5.0%)	9.7×10^5 (88.4%)	8.4×10^3 (0.8%)	6.4×10^4 (5.8%)	0.0 (0.0%)	1.1×10^6 (3.8%)
125	1.2×10^5 (10.7%)	8.7×10^5 (80.7%)	3.2×10^3 (0.3%)	8.7×10^4 (8.1%)	2.4×10^3 (0.2%)	1.1×10^6 (5.4%)
150	1.5×10^5 (18.9%)	5.3×10^5 (67.3%)	3.5×10^3 (0.4%)	1.0×10^5 (12.9%)	3.4×10^3 (0.4%)	7.9×10^5 (6.4%)
175	1.8×10^5 (34.2%)	2.1×10^5 (40.0%)	3.9×10^3 (0.8%)	1.2×10^5 (24.0%)	5.0×10^3 (1.0%)	5.1×10^5 (8.1%)
200	2.3×10^5 (52.4%)	6.2×10^4 (14.2%)	2.1×10^4 (4.8%)	1.2×10^5 (27.2%)	6.2×10^3 (1.4%)	4.3×10^5 (11.8%)
225	1.9×10^5 (64.4%)	1.6×10^4 (5.4%)	3.7×10^4 (12.5%)	4.9×10^4 (16.5%)	3.5×10^3 (1.2%)	3.0×10^5 (11.1%)
250	2.5×10^5 (62.8%)	1.9×10^4 (4.7%)	9.7×10^4 (24.4%)	2.6×10^4 (6.5%)	6.2×10^3 (1.6%)	4.0×10^5 (15.8%)
275	3.1×10^5 (52.6%)	2.0×10^4 (3.4%)	2.3×10^5 (39.1%)	2.2×10^4 (3.7%)	7.5×10^3 (1.3%)	5.9×10^5 (21.3%)
300	2.2×10^5 (31.4%)	1.6×10^4 (2.2%)	4.4×10^5 (6.0%)	1.6×10^4 (2.2%)	7.5×10^3 (1.1%)	6.9×10^5 (24.7%)
325	1.3×10^5 (14.7%)	1.5×10^4 (1.7%)	6.9×10^5 (81.1%)	1.4×10^4 (1.6%)	7.5×10^3 (0.9%)	8.5×10^5 (28.2%)
350	5.5×10^4 (7.2%)	1.2×10^4 (1.6%)	6.8×10^5 (89.0%)	1.2×10^4 (1.6%)	4.6×10^3 (0.6%)	7.7×10^5 (26.1%)

A) Host, B) Guest, C) Host Fragments, D) Guest Fragments, E) Complex;
TIC: Total ion current.

In conclusion, all three parameters show an effect on the detected full scan mass spectra. However, the capillary voltage only showed minor effects. Too mild conditions lead to little signal intensity compared to the total ion current and are generally favored for detecting intact phenylalanine. On the other hand, the signals of intact β-cyclodextrin are detected with higher intensities under moderate conditions, while signals originating from its decomposition are detected to a greater extent under harsh conditions. The same effect is observed for the detection of the complex ions. Therefore, a compromise has to be found for proper detection of intact phenylalanine, β-cyclodextrin, and the complex, whereas extensive decomposition of these compounds should be prevented.

4.3 2D Experiments

As the capillary voltage has only minor effects on the detected ions, it was kept constant at 50 V while the tube lens voltage and the capillary temperature were scanned in the range of 50–250 V and 100–350 °C, respectively. The total ion current shows a similar trend as in 1D experiments: Low capillary temperature and tube lens voltage lead to higher intensity (figure 4.3). The intensity of the signals of identified ions shows two local maxima around (100–150 °C; 100–125 V) and (300 °C; 250 V). The relative intensity of the sum of the identified ions of the total ion current reaches its maximum at 300 °C and 250 V. The total intensity of the signal of intact guest ions reaches its maximum at 275 °C and 200 V. Generally, suitable signal intensities ($> 1.0 \times 10^5$) of the intact guest ions are detected for a tube lens voltages of 100 V and capillary temperatures in the range of 150–300 °C. At temperatures > 225 °C and tube lens voltages of 200 V and 250 V, extensive fragmentation of β-cyclodextrin was indicated by high intensities of signals assigned as host fragments (group C ions). In contrast, peaks of intact phenylalanine were detected most intensively at temperatures < 150 °C. At higher temperatures (150–200 °C), lower tube lens voltages (~ 100 V) were required for sufficient prevention of decomposition of the guest. Decomposition of phenylalanine at harsher conditions first led to an increase in the signal intensity of group D ions, and further to a decrease, forming a ridge from 150 °C; 200 V to 350 °C; 100 V. Beyond this ridge, the phenylalanine fragment ion is further decomposed into smaller fragments that are not identified anymore.

The complex ion signals are detected at the highest intensity (9.0×10^3) at a capillary temperature of 200 °C and a tube lens voltage of 250 V. The defined requirement of a signal intensity $> 3'000$ was not fulfilled with a tube lens voltage

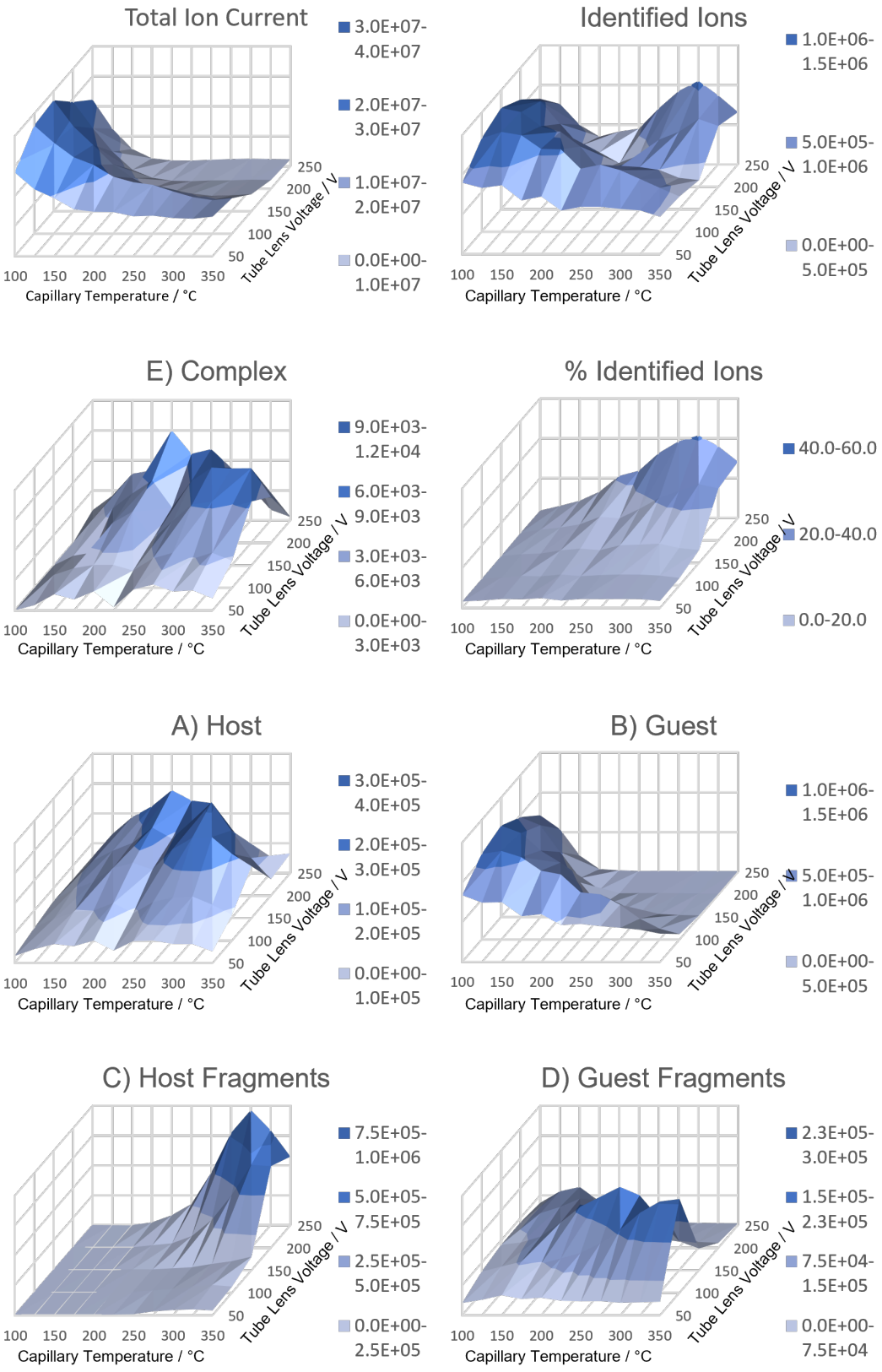

Figure 4.3: Surface charts showing the intensities of the total ion current, the total identified ions, and the ion groups A to E.

of 50 V, independent of the capillary temperature. Also, capillary temperatures $< 150\,^{\circ}\mathrm{C}$ do not allow for the detection of the complex ion signals at sufficient intensities. Additionally, lower tube lens voltages require higher capillary temperatures for sufficient signal intensity, whereas temperatures between 150 °C and 300 °C are sufficient if the tube lens voltage is set to 250 V.

These 1D and 2D experiments show the minor effect of the capillary voltage and the significant impact of the capillary temperature and tube lens voltage on the recorded full scan mass spectra. If the conditions are not selected appropriately for each experiment, essential ions might remain undetected, such as complex ions. Furthermore, noise can crowd the mass spectrum, exacerbating the identification of signals. Finally, extensive in-source fragmentation leads to the separation of the complex and decomposition of the host and guest compounds. In conclusion, proper adjustment of the instrumental parameters for each experiment is mandatory for the recording of convincing data.

5 Conclusion & Outlook

In this thesis, several aspects of the mass spectrometric behavior of cyclodextrins and their host-guest complexes have been successfully investigated. First, the fragmentation mechanism of protonated β-cyclodextrin has been elucidated based on the fragmentation patterns obtained by a combination of in-source fragmentation, ion-trap CID, and HCD experiments. Afterward, the potential of cyclodextrins to improve the aqueous stability of antitumor metallocenes has been evaluated. The interaction of titanocene dichloride with β-cyclodextrin has been compared to that of phenylalanine, which was used as reference. In contrast to the non-covalent interaction detected for the assembly of phenylalanine and cyclodextrin, titanocene has been found to form a covalent bond to a deprotonated hydroxy group at the rim of cyclodextrin. Tandem mass spectrometric experiments of the interaction products have further supported the formation of a covalent bond. Comparing these findings with data obtained from the interaction of titanocene and phenylalanine with linear saccharides also indicated different interaction characteristics for these two assemblies. Determination of the CE_{50} values of the dissociation of the assemblies provided further proof for the covalent interaction occurring between titanocene and cyclodextrins. Additionally, increasing the pH of the sample solution of titanocene and β-cyclodextrin to seven showed reduced signal intensities of titanium-containing species. Thus, the desired effect of increasing the hydrolytic stability of titanocene by interaction with cyclodextrins was not achieved. Finally, the effect of three source parameters on the recorded full scan mass spectra of a mixture of phenylalanine and β-cyclodextrin has been evaluated. While the capillary voltage has been found to have only minor effects, the tube lens voltage and the capillary temperature significantly affect the signal intensities of the host, guest, and complex ions and the respective fragment ions. Generally, mild conditions prevent adequate ionization, leading to the detection of a tremendous amount of undefined compounds and noise. On the other hand, harsh conditions induce extensive in-source fragmentation, which is also unfavorable.

The annual number of new cases of cancer is proposed to increase continuously to about 29–37 million new cases in 2040 globally [2]. Therefore, the development of new anticancer drugs and the implementation of advances in the treatment with current medication will have a huge impact on the improvement of the global health

situation.

Although cyclodextrins did not show the desired effect on the hydrolytic stability of titanocene, their potential for inclusion of other metallocenes represents a copious field for further research. Further macrocyclic structures, such as cucurbiturils or calixarenes, can be tested as hosts for metallocene anticancer drugs to improve their hydrolytic stability. The concept of host-guest complex formation in cancer treatment is not limited to metallocenes and bears also the potential to improve the pharmaceutical properties of a broad spectrum of drugs. The main idea of host-guest complex formation of drugs is the improvement of their bioavailability and control of their transport and release. Therefore, the release of drugs from the host cavity to their respective biological targets is crucial in their application [261]. Investigation of the release of metallocenes from host compounds in the presence of biological targets and their subsequent interaction represents a fascinating field for further research.

6 References

[1] Mary E. Miller. *Cancer*. Ed. by A. Malcolm Campbell. Momentum Press, 2018. ISBN: 1944749853.

[2] World Health Organization. *WHO report on cancer: setting priorities, investing wisely and providing care for all*. Tech. rep. Geneva: World Health Organization, 2020.

[3] Bernard Desoize. "Metals and metal compounds in cancer treatment". In: *Anticancer Res.* 24.3A (2004), pp. 1529–1544.

[4] Reza Bayat Mokhtari et al. "Combination therapy in combating cancer". In: *Oncotarget* 8.23 (2017), pp. 38022–38043. DOI: 10.18632/oncotarget.16723.

[5] James C. Dabrowiak. *Metals in Medicine*. John Wiley & Sons, Ltd, 2009. ISBN: 978-0-470-68196-1.

[6] Daisuke Namima et al. "The Effect of Gemcitabine on Cell Cycle Arrest and microRNA Signatures in Pancreatic Cancer Cells". In: *In Vivo (Brooklyn).* 34.6 (2020), pp. 3195–3203. DOI: 10.21873/INVIVO.12155.

[7] Linkui Bai et al. "Research progress in modern structure of platinum complexes". In: *Eur. J. Med. Chem.* 140 (2017), pp. 349–382. DOI: 10.1016/j.ejmech.2017.09.034.

[8] Claire S Allardyce and Paul J Dyson. "Metal-based drugs that break the rules". In: *Dalt. Trans.* 45.8 (2016), pp. 3201–3209. DOI: 10.1039/C5DT03919C.

[9] Melchior Cini, Tracey D Bradshaw, and Simon Woodward. "Using titanium complexes to defeat cancer: the view from the shoulders of titans". In: *Chem. Soc. Rev.* 46 (2017), pp. 1040–1051. DOI: 10.1039/C6CS00860G.

[10] Santiago Gómez-Ruiz et al. "On the Discovery, Biological Effects, and Use of Cisplatin and Metallocenes in Anticancer Chemotherapy". In: *Bioinorg. Chem. Appl.* 2012 (2012), pp. 1–14. DOI: 10.1155/2012/140284.

[11] S. R. McWhinney, R. M. Goldberg, and H. L. McLeod. "Platinum neurotoxicity pharmacogenetics". In: *Mol. Cancer Ther.* 8.1 (2009), pp. 10–16. DOI: 10.1158/1535-7163.MCT-08-0840.

[12] Timothy C Johnstone, Kogularamanan Suntharalingam, and Stephen J Lippard. "The Next Generation of Platinum Drugs: Targeted Pt(II) Agents, Nanoparticle Delivery, and Pt(IV) Prodrugs". In: *Chem. Rev.* 116.5 (2016), pp. 3436–3486. DOI: 10.1021/acs.chemrev.5b00597.

[13] Frank A Blommaert et al. "Formation of DNA Adducts by the Anticancer Drug Carboplatin: Different Nucleotide Sequence Preferences in Vitro and in Cells". In: *Biochemistry* 34.26 (1995), pp. 8474–8480. DOI: 10.1021/bi00026a031.

[14] Viktor Brabec, Ondrej Hrabina, and Jana Kasparkova. "Cytotoxic platinum coordination compounds. DNA binding agents". In: *Coord. Chem. Rev.* 351 (2017), pp. 2–31. DOI: 10.1016/j.ccr.2017.04.013.

[15] Younes Ellahioui, Sanjiv Prashar, and Santiago Gómez-Ruiz. "Anticancer Applications and Recent Investigations of Metallodrugs Based on Gallium, Tin and Titanium". In: *Inorganics* 5.1 (2017), p. 4. DOI: 10.3390/inorganics5010004.

[16] Ronald P. Miller et al. "Mechanisms of Cisplatin Nephrotoxicity". In: *Toxins (Basel).* 2 (2010), pp. 2490–2518. DOI: 10.3390/toxins2112490.

[17] Cleber P.A. Anconi et al. "Inclusion complexes of α-cyclodextrin and the cisplatin analogues oxaliplatin, carboplatin and nedaplatin: A theoretical approach". In: *Chem. Phys. Lett.* 515.1-3 (2011), pp. 127–131. DOI: 10.1016/j.cplett.2011.09.005.

[18] Gilles Gasser, Ingo Ott, and Nils Metzler-Nolte. "Organometallic Anticancer Compounds". In: *J. Med. Chem.* 54 (2011), pp. 3–25. DOI: 10.1021/jm100020w.

[19] Frauke Hackenberg and Matthias Tacke. "Benzyl-substituted metallocarbene antibiotics and anticancer drugs". In: *Dalt. Trans.* 43 (2014), pp. 8144–8153. DOI: 10.1039/C4DT00624K.

[20] Gregory S. Smith and Bruno Therrien. "Targeted and multifunctional arene ruthenium chemotherapeutics". In: *Dalt. Trans.* 40 (2011), p. 10793. DOI: 10.1039/c1dt11007a.

[21] P. Manohari Abeysinghe and Margaret M. Harding. "Antitumour bis (cyclopentadienyl) metal complexes: Titanocene and molybdocene dichloride and derivatives". In: *Dalt. Trans.* (2007), pp. 3474–3482. DOI: 10.1039/b707440a.

[22] Michael J Clarke, Fuchun Zhu, and Dominic R Frasca. "Non-Platinum Chemotherapeutic Metallopharmaceuticals". In: *Chem. Rev.* 99 (1999), pp. 2511–2534. DOI: 10.1021/cr9804238.

[23] Christian G. Hartinger, Nils Metzler-Nolte, and Paul J. Dyson. "Challenges and Opportunities in the Development of Organometallic Anticancer Drugs". In: *Organometallics* 31 (2012), pp. 5677–5685. DOI: 10.1021/om300373t.

[24] Pingyu Zhang and Peter J. Sadler. "Advances in the design of organometallic anticancer complexes". In: *J. Organomet. Chem.* 839 (2017), pp. 5–14. DOI: 10.1016/j.jorganchem.2017.03.038.

[25] Oscar A Lenis-Rojas et al. "Ru II (p -cymene) Compounds as Effective and Selective Anticancer Candidates with No Toxicity in Vivo". In: *Inorg. Chem.* 57.21 (2018), pp. 13150–13166. DOI: 10.1021/acs.inorgchem.8b01270.

[26] Enrique Meléndez. "Metallocenes as target specific drugs for cancer treatment". In: *Inorganica Chim. Acta* 393 (2012), pp. 36–52. DOI: 10.1016/j.ica.2012.06.007.

[27] Margaret M Harding and George Mokdsi. "Antitumour metallocenes: structure-activity studies and interactions with biomolecules." In: *Curr. Med. Chem.* 7 (2000), pp. 1289–1303. DOI: 10.2174/0929867003374066.

[28] Laura Vidal et al. "Phase i clinical and pharmacokinetic study of trabectedin and carboplatin in patients with advanced solid tumors". In: *Invest. New Drugs* 30.2 (2012), pp. 616–628. DOI: 10.1007/s10637-010-9559-3.

[29] Gerd Lümmen et al. "Phase II trial of titanocene dichloride in advanced renal-cell carcinoma". In: *Cancer Chemother. Pharmacol.* 42.5 (1998), pp. 415–417. DOI: 10.1007/s002800050838.

[30] N. Kröger et al. "Phase II Clinical Trial of Titanocene Dichloride in Patients with Metastatic Breast Cancer". In: *Onkologie* 23.1 (2000), pp. 60–62. DOI: 10.1159/000027075.

[31] Andrea Erxleben, James Claffey, and Matthias Tacke. "Binding and hydrolysis studies of antitumoural titanocene dichloride and Titanocene Y with phosphate diesters". In: *J. Inorg. Biochem.* 104.4 (2010), pp. 390–396. DOI: 10.1016/j.jinorgbio.2009.11.010.

[32] Jorge R. Güette-Fernández et al. "A molecular docking study of the interactions between human transferrin and seven metallocene dichlorides". In: *J. Mol. Graph. Model.* 75 (2017), pp. 250–265. DOI: 10.1016/j.jmgm.2017.05.005.

[33] C V Christodoulou et al. “Anti-proliferative activity and mechanism of action of titanocene dichloride”. In: *Br. J. Cancer* 77.12 (1998), pp. 2088–2097.

[34] Idainés Feliciano, Jaime Matta, and Enrique Meléndez. “Water-soluble molybdenocene complexes with both proliferative and antiproliferative effects on cancer cell lines and their binding interactions with human serum albumin”. In: *J. Biol. Inorg. Chem.* 14 (2009), pp. 1109–1117. DOI: 10.1007/s00775-009-0554-0.

[35] Xiomara Narváez-Pita et al. “Water soluble molybdenocene complexes: Synthesis, cytotoxic activity and binding studies to ubiquitin by fluorescence spectroscopy, circular dichroism and molecular modeling”. In: *J. Inorg. Biochem.* 132 (2014), pp. 77–91. DOI: 10.1016/j.jinorgbio.2013.10.014.

[36] Jan Honzíček and Jaromír Vinklárek. “Bioinorganic chemistry of vanadocene dichloride”. In: *Inorganica Chim. Acta* 437 (2015), pp. 87–94. DOI: 10.1016/j.ica.2015.08.008.

[37] Patrick W. Causey, Michael C. Baird, and Susan P. C. Cole. “Synthesis, characterization, and assessment of cytotoxic properties of a series of titanocene dichloride derivatives”. In: *Organometallics* 23 (2004), pp. 4486–4494. DOI: 10.1021/om049679w.

[38] Karl Döppert. “Die Chemie der Cyclopentadienyltitan(IV)Verbindungen in wäßrigem Medium”. In: *Naturwissenschaften* 77.1 (1990), pp. 19–24. DOI: 10.1007/BF01131789.

[39] Enrique Meléndez. “Bioorganometallic chemistry of molybdenocene dichloride and its derivatives”. English. In: *J. Organomet. Chem.* 706-707 (2012), pp. 4–12. DOI: 10.1016/j.jorganchem.2012.02.006.

[40] Jenny B. Waern and Margaret M. Harding. “Bioorganometallic chemistry of molybdocene dichloride”. In: *J. Organomet. Chem.* Vol. 689. 25. Elsevier, 2004, pp. 4655–4668. DOI: 10.1016/j.jorganchem.2004.08.014.

[41] Jeffrey H. Toney and Tobin J. Marks. “Hydrolysis chemistry of the metallocene dichlorides M(η5-C5H5)2Cl2, M = titanium, vanadium, or zirconium. Aqueous kinetics, equilibria, and mechanistic implications for a new class of antitumor agents”. In: *J. Am. Chem. Soc.* 107.4 (1985), pp. 947–953. DOI: 10.1021/ja00290a033.

[42] Damian P Buck et al. “Inclusion complexes of the antitumour metallocenes Cp2MCl2 (M = Mo, Ti) with cucurbit[n]urils”. English. In: *Dalt. Trans.* (2008), pp. 2328–2334. DOI: 10.1039/b718322d.

[43] Anthony Deally et al. “Synthesis and Biological Evaluation of Achiral Indole-Substituted Titanocene Dichloride Derivatives”. In: *Int. J. Med. Chem.* 2012 (2012), pp. 1–13. DOI: 10.1155/2012/905981.

[44] Margaret M. Harding, Michael Prodigalidad, and Mark J. Lynch. “Organometallic Anticancer Agents. 2. Aqueous Chemistry and Interaction of Niobocene Dichloride with Nucleic Acid Constituents and Amino Acids”. In: *J. Med. Chem.* 39 (1996), pp. 5012–5016. DOI: 10.1021/jm9603678.

[45] Julia Schur et al. “A comparative chemical-biological evaluation of titanium(iv) complexes with a salan or cyclopentadienyl ligand”. In: *Chem. Commun.* 49.42 (2013), pp. 4785–4787. DOI: 10.1039/c3cc38604j.

[46] Olivia R. Allen et al. “Functionalized Cyclopentadienyl Titanium Organo-09:47 24.03.2022metallic Compounds as New Antitumor Drugs”. In: *Organometallics* 23 (2004), pp. 288–292. DOI: 10.1021/om030403i.

[47] Enrique Meléndez. “Titanium complexes in cancer treatment”. In: *Crit. Rev. Oncol. Hematol.* 42 (2002), pp. 309–315. DOI: 10.1016/S1040-8428(01)00224-4.

[48] Santiago Gómez-Ruiz et al. “Cytotoxic studies of substituted titanocene and ansa-titanocene anticancer drugs”. In: *J. Inorg. Biochem.* 102 (2008), pp. 1558–1570. DOI: 10.1016/j.jinorgbio.2008.02.001.

[49] Gregory D. Potter, Michael C. Baird, and Susan P.C. Cole. “A new series of titanocene dichloride derivatives bearing chiral alkylammonium groups: Assessment of their cytotoxic properties”. In: *J. Organomet. Chem.* 692 (2007), pp. 2508–3518. DOI: 10.1016/j.ica.2010.05.020.

[50] James Claffey et al. “Pseudo-halide derivatives of titanocene Y: Synthesis and cytotoxicity studies”. In: *Metallomics* 1.6 (2009), pp. 511–517. DOI: 10.1039/b911753a.

[51] James Claffey et al. “Synthesis and cytotoxicity studies of novel anion-exchanged Titanocene Y derivatives”. In: *Appl. Organomet. Chem.* 24.10 (2010), pp. 675–679. DOI: 10.1002/aoc.1665.

[52] Nigel Sweeney et al. “Heteroaryl substituted titanocenes as potential anticancer drugs”. In: *J. Inorg. Biochem.* 100.9 (2006), pp. 1479–1486. DOI: 10.1016/j.jinorgbio.2006.04.006.

[53] Ulrike Olszewski et al. “Anticancer activity and mode of action of titanocene C”. In: *Invest. New Drugs* 29.4 (2011), pp. 607–614. DOI: 10.1007/s10637-010-9395-5.

[54] Jeffrey H Toney, Carolyn P Brock, and Tobin J Marks. “Aqueous coordination chemistry of vanadocene dichloride with nucleotides and phosphoesters. Mechanistic implications for a new class of antitumor agents”. In: *J. Am. Chem. Soc.* 108.23 (1986), pp. 7263–7274.

[55] Maolin Guo, Zijian Guo, and Peter J Sadler. “Titanium(IV) targets phosphoesters on nucleotides: implications for the mechanism of action of the anticancer drug titanocene dichloride”. In: *JBIC J. Biol. Inorg. Chem.* 6 (2001), pp. 698–707. DOI: 10.1007/s007750100248.

[56] Rahel P Eberle, Yvonne Hari, and Stefan Schürch. “Specific Interactions of Antitumor Metallocenes with Deoxydinucleoside Monophosphates.” In: *J Am Soc Mass Spectrom* 28.9 (2017), pp. 1901–1909. DOI: 10.1007/s13361-017-1697-9.

[57] Dhurairajan Senthilnathan et al. “Antitumor activity of bent metallocenes: electronic structure analysis using DFT computations”. In: *J. Mol. Model.* 17 (2011), pp. 465–475. DOI: 10.1007/s00894-010-0734-4.

[58] George Mokdsi and Margaret M Harding. “Water soluble, hydrolytically stable derivatives of the antitumor drug titanocene dichloride and binding studies with nucleotides”. In: *J. Organomet. Chem.* 565 (1998), pp. 29–35. DOI: 10.1016/S0022-328X(98)00441-0.

[59] Rahel P Eberle, Yvonne Hari, and Stefan Schürch. “Transition Metal-based Anticancer Drugs Targeting Nucleic Acids: A Tandem Mass Spectrometric Investigation.” In: *Chim.* 71.3 (2017), pp. 120–123. DOI: 10.2533/chimia.2017.120.

[60] Rahel P Eberle and Stefan Schürch. “Titanocene binding to oligonucleotides.” In: *J Inorg Biochem* 184 (2018), pp. 1–7. DOI: 10.1016/j.jinorgbio.2018.03.014.

[61] Antonello Merlino, Tiziano Marzo, and Luigi Messori. “Protein Metalation by Anticancer Metallodrugs: A Joint ESI MS and XRD Investigative Strategy”. In: *Chem. - A Eur. J.* 23.29 (2017), pp. 6942–6947. DOI: 10.1002/chem.201605801.

[62] Christian G Hartinger et al. “Characterization of Platinum Anticancer Drug Protein-Binding Sites Using a Top-Down Mass Spectrometric Approach”. In: *Inorg. Chem.* 47 (2008), pp. 17–19. DOI: 10.1021/ic702236m.

[63] Enzo Cadoni et al. “Competitive reactions among glutathione, cisplatin and copper-phenanthroline complexes”. In: *J. Inorg. Biochem.* 173 (2017), pp. 126–133. DOI: 10.1016/j.jinorgbio.2017.05.004.

[64] George Mokdsi and Margaret M Harding. “A 1H NMR study of the interaction of antitumor metallocenes with glutathione”. In: *J. Inorg. Biochem.* 86 (2001), pp. 611–616. DOI: 10.1016/S0162-0134(01)00221-5.

[65] Arthur D Tinoco, Emily V Eames, and Ann M Valentine. “Reconsideration of serum Ti(IV) transport: albumin and transferrin trafficking of Ti(IV) and its complexes.” eng. In: *J. Am. Chem. Soc.* 130 (2008), pp. 2262–2270. DOI: 10.1021/ja076364+.

[66] Kate S. Campbell et al. “Radiotracer studies of the antitumor metallocene molybdocene dichloride with biomolecules”. In: *Polyhedron* 26 (2007), pp. 456–459. DOI: 10.1016/j.poly.2006.07.004.

[67] Maolin Guo et al. “TiIV Uptake and Release by Human Serum Transferrin and Recognition of TiIV-Transferrin by Cancer Cells: Understanding the Mechanism of Action of the Anticancer Drug Titanocene Dichloride”. In: *Biochemistry* 39 (2000), pp. 10023–10033. DOI: 10.1021/bi000798z.

[68] Maolin Guo and Peter J. Sadler. “Competitive binding of the anticancer drug titanocene dichloride to N,N’-ethylenebis(o-hydroxyphenylglycine) and adenosine triphosphate: A model for TiIVuptake and release by transferrin”. In: *J. Chem. Soc. Dalt. Trans.* (2000), pp. 7–9. DOI: 10.1039/a908759a.

[69] Hongzhe Sun et al. “The First Specific TiIV–Protein Complex: Potential Relevance to Anticancer Activity of Titanocenes”. In: *Angew. Chemie Int. Ed.* 37.11 (1998), pp. 1577–1579. DOI: 10.1002/(SICI)1521-3773(19980619)37:11<1577::AID-ANIE1577>3.0.CO;2-M.

[70] Bina Gidwani and Amber Vyas. “A Comprehensive Review on Cyclodextrin-Based Carriers for Delivery of Chemotherapeutic Cytotoxic Anticancer Drugs”. In: *Biomed Res. Int.* 2015 (2015). DOI: 10.1155/2015/198268.

[71] Jae Ung Lee et al. “Noncovalent complexes of cyclodextrin with small organic molecules: Applications and insights into host–guest interactions in the gas phase and condensed phase”. In: *Molecules* 25.18 (2020), p. 4048. DOI: 10.3390/molecules25184048.

[72] José Luis Casas-Hinestroza et al. “Recent advances in mass spectrometry studies of non-covalent complexes of macrocycles - A review”. In: *Anal. Chim. Acta* (2019). DOI: 10.1016/j.aca.2019.06.029.

[73] Lei Wang et al. “Host-guest supramolecular nanosystems for cancer diagnostics and therapeutics”. In: *Adv. Mater.* 25.28 (2013), pp. 3888–3898. DOI: 10.1002/adma.201301202.

[74] G. Astray, J. C. Mejuto, and J. Simal-Gandara. “Latest developments in the application of cyclodextrin host-guest complexes in beverage technology processes”. In: *Food Hydrocoll.* 106 (2020), p. 105882. DOI: 10.1016/j.foodhyd.2020.105882.

[75] Ana Maria Grigoriu, Constantin Luca, and Aurelia Grigoriu. “Cyclodextrins applications in the textile industry”. In: *Cellul. Chem. Technol.* 42.1-3 (2008), pp. 103–112.

[76] Song Li and William C Purdy. “Cyclodextrins and Their Applications in Analytical Chemistry”. In: *Chem. Rev.* 92.6 (1992), pp. 1457–1470. DOI: 10.1021/cr00014a009.

[77] Lajos Szente and Julianna Szemán. “Cyclodextrins in analytical chemistry: Host-guest type molecular recognition”. In: *Anal. Chem.* 85.17 (2013), pp. 8024–8030. DOI: 10.1021/ac400639y.

[78] Daniel W Armstrong, Wade DeMond, and Bronislaw P Czech. “Separation of Metallocene Enantiomers by Liquid Chromatography: Chiral Recognition Via Cyclodextrin Bonded Phases”. In: *Anal. Chem.* 57.2 (1985), pp. 481–484. DOI: 10.1021/ac50001a037.

[79] A A Zamani, A S Zarabadi, and M R Yaftian. “Water soluble crown ethers: selective masking agents for improving extraction-separation of zinc and lead cations”. In: *J. Incl. Phenom. Macrocycl. Chem.* 63 (2009), pp. 327–334. DOI: 10.1007/s10847-008-9526-1.

[80] Phennapha Saokham et al. “Solubility of cyclodextrins and drug/cyclodextrin complexes”. In: *Molecules* 23.5 (2018), p. 1161. DOI: 10.3390/molecules07:4424.03.202223051161.

[81] Massimiliano di Cagno. “The Potential of Cyclodextrins as Novel Active Pharmaceutical Ingredients: A Short Overview”. In: *Molecules* 22.1 (2017). DOI: 10.3390/molecules22010001.

[82] József Szejtli. “Past, present and futute of cyclodextrin research”. In: *Pure Appl. Chem.* 76.10 (2004), pp. 1825–1845. DOI: 10.1351/pac200476101825.

[83] Zhaofeng Li et al. “Alpha-cyclodextrin: Enzymatic production and food applications”. In: *Trends Food Sci. Technol.* 35.2 (2014), pp. 151–160. DOI: 10.1016/j.tifs.2013.11.005.

[84] Phatsawee Jansook, Noriko Ogawa, and Thorsteinn Loftsson. “Cyclodextrins: structure, physicochemical properties and pharmaceutical applications”. In: *Int. J. Pharm.* 535.1-2 (2018), pp. 272–284. DOI: 10.1016/j.ijpharm.2017.11.018.

[85] Sunil S. Jambhekar and Philip Breen. “Cyclodextrins in pharmaceutical formulations I: structure and physicochemical properties, formation of complexes, and types of complex”. In: *Drug Discov. Today* 21.2 (2016), pp. 356–362. DOI: 10.1016/j.drudis.2015.11.017.

[86] Thorsteinn Loftsson, Phennapha Saokham, and André Rodrigues Sá Couto. “Self-association of cyclodextrins and cyclodextrin complexes in aqueous solutions”. In: *Int. J. Pharm.* 560 (2019), pp. 228–234. DOI: 10.1016/j.ijpharm.2019.02.004.

[87] Goutam Chakraborty et al. “Does the degree of substitution on the cyclodextrin hosts impact their affinity towards guest binding?” In: *Photochem. Photobiol. Sci.* 19.7 (2020), pp. 956–965. DOI: 10.1039/d0pp00103a.

[88] Mark E. Davis and Marcus E. Brewster. “Cyclodextrin-based pharmaceutics: Past, present and future”. In: *Nat. Rev. Drug Discov.* 3 (2004), pp. 1023–1035. DOI: 10.1038/nrd1576.

[89] Rajeswari Challa et al. “Cyclodextrins in drug delivery: An updated review”. In: *AAPS PharmSciTech* 6.2 (2005), E329–E357. DOI: 10.1208/pt060243.

[90] Rebecca L. Carrier, Lee A. Miller, and Imran Ahmed. “The utility of cyclodextrins for enhancing oral bioavailability”. In: *J. Control. Release* 123 (2007), pp. 78–99. DOI: 10.1016/j.jconrel.2007.07.018.

[91] Kimoon Kim et al. “Functionalized cucurbiturils and their applications”. In: *Chem. Soc. Rev.* 36.2 (2007), pp. 267–279. DOI: 10.1039/B603088M.

[92] Woo Sung Jeon et al. “Complexation of Ferrocene Derivatives by the Cucurbit[7]uril Host: A Comparative Study of the Cucurbituril and Cyclodextrin Host Families”. In: *J. Am. Chem. Soc.* 127 (2005), pp. 12984–12989. DOI: 10.1021/ja052912c.

[93] Lyle Isaacs. “Cucurbit[n]urils: from mechanism to structure and function”. In: *Chem. Commun.* 6 (2009), pp. 619–629. DOI: 10.1039/B814897J.

[94] Eric Masson et al. “Cucurbituril chemistry: a tale of supramolecular success”. In: *RSC Adv.* 2 (2012), pp. 1213–1247. DOI: 10.1039/C1RA00768H.

[95] Tomoki Ogoshi et al. “Facile, Rapid, and High-Yield Synthesis of Pillar[5]arene from Commercially Available Reagents and Its X-ray Crystal Structure”. In: *J. Org. Chem.* 76 (2011), pp. 328–331. DOI: 10.1021/jo1020823.

[96] Guocan Yu and Xiaoyuan Chen. “Host–guest chemistry in supramolecular theranostics”. In: *Theranostics* 9.11 (2019), pp. 3041–3074. DOI: 10.7150/thno.31653.

[97] Alexis Morales et al. “Host–guest interactions between calixarenes and Cp2NbCl2”. In: *J. Organomet. Chem.* 696 (2011), pp. 2519–2527. DOI: 10.1016/j.jorganchem.2011.03.021.

[98] Anwen M. Krause-Heuer et al. “Substituted β-Cyclodextrin and Calix[4]arene As Encapsulatory Vehicles for Platinum(II)-Based DNA Intercalators”. In: *Inorg. Chem.* 47.15 (2008), pp. 6880–6888. DOI: 10.1021/ic800467c.

[99] Simin Maleknia and Jennifer Brodbelt. “Gas-Phase Selectivities of Crown Ethers for Alkali Metal Ion Complexation”. In: *J. Am. Chem. Soc.* 114.11 (1992), pp. 4295–4298. DOI: 10.1021/ja00037a038.

[100] Brian L. Williamson and Colin S. Creaser. “Noncovalent inclusion complexes of protonated amines with crown ethers”. In: *Int. J. Mass Spectrom.* 188.1-2 (1999), pp. 53–61. DOI: 10.1016/S1387-3806(98)14204-5.

[101] Thorsteinn Loftsson and Marcus E. Brewster. “Pharmaceutical Applications of Cyclodextrins. 1. Drug Solubilization and Stabilization”. In: *J. Pharm. Sci.* 85.10 (1996), pp. 1017–1025. DOI: 10.1021/js950534b.

[102] Sunil S. Jambhekar and Philip Breen. “Cyclodextrins in pharmaceutical formulations II: solubilization, binding constant, and complexation efficiency”. In: *Drug Discov. Today* 21.2 (2016), pp. 363–368. DOI: 10.1016/j.drudis.2015.11.016.

[103] E. M.Martin Del Valle. *Cyclodextrins and their uses: A review.* 2004. DOI: 10.1016/S0032-9592(03)00258-9.

[104] Paola Cescutti, Domenico Garozzo, and Roberto Rizzo. “Effect of methylation of β-cyclodextrin on the formation of inclusion complexes with aromatic compounds. An ionspray mass spectrometry investigation”. English. In: *Carbohydr. Res.* 302 (1997), pp. 1–6. DOI: 10.1016/S0008-6215(97)00110-9.

[105] Hyunmyung Kim et al. “Preference prediction for the stable inclusion complexes between cyclodextrins and monocyclic insoluble chemicals based on Monte Carlo docking simulations”. In: *J. Incl. Phenom.* 54 (2006), pp. 165–170. DOI: 10.1007/s10847-005-6288-x.

[106] Allan R. Hedges. “Industrial Applications of Cyclodextrins”. In: *Chem. Rev.* 98 (1998), pp. 2035–2044. DOI: 10.1021/cr970014w.

[107] Mihaela Silion et al. “Mass Spectrometry as a Complementary Approach for Noncovalently Bound Complexes Based on Cyclodextrins”. In: *Adv. Exp. Med. Biol.* Ed. by A. G. Woods and C. C. Darie. Vol. 1140. NLM (Medline), 2019, pp. 685–701. DOI: 10.1007/978-3-030-15950-4_41.

[108] Hang Li et al. “Inclusion complexes of cannabidiol with β-cyclodextrin and its derivative: Physicochemical properties, water solubility, and antioxidant activity”. In: *J. Mol. Liq.* 334 (2021), p. 116070. DOI: 10.1016/j.molliq.2021.116070.

[109] Walter Ferreira da Silva Júnior et al. “Inclusion Complexes of β and HPβ-Cyclodextrin with α, β Amyrin and In Vitro Anti-Inflammatory Activity”. In: *Biomolecules* 9.6 (2019), p. 241. DOI: 10.3390/biom9060241.

[110] Qing Tang et al. “Host-Guest Complexes of l-Borneol with Cucurbituril and Cyclodextrin and Its Potential Use in Analysis of Drugs”. In: *ChemistrySelect* 4.23 (2019), pp. 6924–6929. DOI: 10.1002/slct.201900913.

[111] Le Xin Song et al. “Formation, Structure, and Stability of α- and β-Cyclodextrin Inclusion Complexes of Phenol and Benzoic Acid Derivatives in Vacuo and in Water”. In: *Bull. Chem. Soc. Jpn.* 80.12 (2007), pp. 2313–2322. DOI: 10.1246/bcsj.80.2313.

[112] Yujuan Cao et al. “1H NMR titration and quantum calculation for the inclusion complexes of styrene and α-methyl styrene with α, β and γ -cyclodextrins”. In: *J. Mol. Struct.* 660 (2003), pp. 73–80. DOI: 10.1016/j.molstruc.2003.07.011.

[113] Yan Yang and Le Xin Song. “Study on the inclusion compounds of eugenol with α-, β-, γ- and heptakis (2,6-di-O-methyl)-β-cyclodextrins”. In: *J. Incl. Phenom.* 53 (2005), pp. 27–33. DOI: 10.1007/s10847-005-0247-4.

[114] Aun Raza et al. “Preparation, characterization, and in vitro anti-inflammatory evaluation of novel water soluble kamebakaurin/hydroxypropyl-β-cyclodextrin inclusion complex”. In: *J. Mol. Struct.* 1130 (2017), pp. 319–326. DOI: 10.1016/j.molstruc.2016.10.059.

[115] Thammarat Aree et al. “Fluorometric and theoretical studies on inclusion complexes of β-cyclodextrin and d-, l-phenylalanine”. English. In: *Spectrochim. Acta Part A Mol. Biomol. Spectrosc.* 96 (2012), pp. 736–743. DOI: 10.1016/j.saa.2012.07.049.

[116] Yinjuan Chen et al. “Gas-phase complexation of α-/β-cyclodextrin with amino acids studied by ion mobility-mass spectrometry and molecular dynamics simulations”. English. In: *Talanta* 186 (2018), pp. 1–7. DOI: 10.1016/j.talanta.2018.04.003.

[117] Xin Cong et al. “Structural relationships in small molecule interactions governing gas-phase enantioselectivity and zwitterionic formation”. English. In: *J. Am. Soc. Mass Spectrom.* 17 (2006), pp. 442–452. DOI: 10.1016/j.jasms.2005.11.015.

[118] C B Lebrilla. “The gas-phase chemistry of cyclodextrin inclusion complexes”. English. In: *Acc. Chem. Res.* 34 (2001), pp. 653–661. DOI: 10.1021/ar980125x.

[119] Ragulan Ramanathan and Laszlo Prokai. “Electrospray ionization mass spectrometric study of encapsulation of amino acids by cyclodextrins”. In: *J. Am. Soc. Mass Spectrom.* 6 (1995), pp. 866–871. DOI: 10.1016/1044-0305(95)00482-S.

[120] Javier Ramirez et al. “Evidence for the formation of gas-phase inclusion complexes with cyclodextrins and amino acids”. English. In: *J. Am. Chem. Soc.* 122 (2000), pp. 6884–6890. DOI: 10.1021/ja000717m.

[121] Mahendra Nath Roy et al. “Host-guest inclusion complexes of α and β-cyclodextrins with α-amino acids”. In: *RSC Adv.* 4.80 (2014), pp. 42383–42390. DOI: 10.1039/c4ra07877b.

[122] Steffi Rudolph, Edris Riedel, and Thomas Henle. “Studies on the interaction of the aromatic amino acids tryptophan, tyrosine and phenylalanine as well as tryptophan-containing dipeptides with cyclodextrins”. English. In: *Eur. Food Res. Technol.* 244.9 (2018), pp. 1511–1519. DOI: 10.1007/s00217-018-3065-9.

[123] Sung-Sik Lee et al. “Chiral differentiation of d- and l-alanine by permethylated β-cyclodextrin: IRMPD spectroscopy and DFT methods”. English. In: *Phys. Chem. Chem. Phys.* 19.22 (2017), pp. 14729–14737. DOI: 10.1039/C7CP01085K.

[124] Tetsumi Irie and Kaneto Uekama. "Cyclodextrins in peptide and protein delivery". In: *Adv. Drug Deliv. Rev.* 36 (1999), pp. 101–123. DOI: 10.1016/S0169-409X(98)00057-X.

[125] F.L. Aachmann et al. "Structural background of cyclodextrin-protein interactions". In: *Protein Eng. Des. Sel.* 16.12 (2004), pp. 905–912. DOI: 10.1093/protein/gzg137.

[126] S Cao et al. "The investigation of β-cyclodextrin noncovalent complex with protein or dipeptide by electrospray ionization mass spectrometry". English. In: *Anal. Lett.* 37.9 (2004), pp. 1871–1883. DOI: 10.1081/AL-120039432.

[127] Yulin Qi, Timon Geib, and Dietrich A Volmer. "Determining the Binding Sites of β-Cyclodextrin and Peptides by Electron-Capture Dissociation High Resolution Tandem Mass Spectrometry". English. In: *J. Am. Soc. Mass Spectrom.* 26.7 (2015), pp. 1143–1149. DOI: 10.1007/s13361-015-1118-x.

[128] Anna Balaji et al. "Synthesis and characterization studies of cisplatin/hydroxypropyl-β-cyclodextrin complex". In: *Pharmacologyonline* 1 (2009), pp. 1135–1143.

[129] Jane A. Plumb et al. "Cucurbit[7]uril encapsulated cisplatin overcomes cisplatin resistance via a pharmacokinetic effect". In: *Metallomics* 4.6 (2012), pp. 561–567. DOI: 10.1039/c2mt20054f.

[130] Young Jin Jeon et al. "Novel molecular drug carrier: Encapsulation of oxaliplatin in cucurbit[7]uril and its effects on stability and reactivity of the drug". In: *Org. Biomol. Chem.* 3 (2005), pp. 2122–2125. DOI: 10.1039/b504487a.

[131] Da Zhang et al. "Preparation, characterisation and antitumour activity of β-, γ- and HP-β-cyclodextrin inclusion complexes of oxaliplatin". In: *Spectrochim. Acta Part A Mol. Biomol. Spectrosc.* 152 (2016), pp. 501–508. DOI: 10.1016/j.saa.2015.07.088.

[132] Susana S Braga et al. "Experimental and theoretical study of the interaction of molybdenocene dichloride (Cp2MoCl2) with β-cyclodextrin". In: *J. Organomet. Chem.* 632 (2001), pp. 11–16. DOI: 10.1016/S0022-328X(01)00836-1.

[133] Susana S. Braga et al. "Inclusion of molybdenocene dichloride (Cp2MoCl2) in 2-hydroxypropyl- and trimethyl-β-cyclodextrin: Structural and biological properties". In: *J. Organomet. Chem.* 690 (2005), pp. 2905–2912. DOI: 10.1016/j.jorganchem.2005.03.012.

[134] Alexis Morales, Ralph T Weber, and Enrique Melendez. "Spectroscopic and thermal characterization of the host–guest interactions between α-, β- and γ-cyclodextrins and vanadocene dichloride". In: *Appl. Organomet. Chem.* 22 (2008), pp. 440–450. DOI: 10.1002/aoc.1420.

[135] Iztok Turel, Alojz Demšar, and Janez Košmrlj. "The Interactions of Titanocene Dihalides with α-, β- and γ-cyclodextrin Host Molecules". In: *J. Incl. Phenom. Macrocycl. Chem.* 35 (1999), pp. 595–604. DOI: 10.1023/A:1008026715964.

[136] Alexis Morales, Jochem Struppe, and Enrique Meléndez. "Host-guest interactions between niobocene dichloride and α-, β-, and γ-cyclodextrins: Preparation and characterization". In: *J. Incl. Phenom. Macrocycl. Chem.* 60 (2008), pp. 263–270. DOI: 10.1007/s10847-007-9374-4.

[137] Adrian Riviş et al. "Titanocene / cyclodextrin supramolecular systems: a theoretical approach". In: *Chem. Cent. J.* 6.1 (2012), pp. 129–139. DOI: 10.1186/1752-153X-6-129.

[138] Dhurairajan Senthilnathan et al. "Are cucurbiturils better drug carriers for bent metallocenes? Insights from theory". In: *J. Biol. Inorg. Chem.* 23.3 (2018), pp. 413–423. DOI: 10.1007/s00775-018-1547-7.

[139] Paola Mura. "Analytical techniques for characterization of cyclodextrin complexes in the solid state: A review". In: *J. Pharm. Biomed. Anal.* 113 (2015), pp. 226–238. DOI: 10.1016/j.jpba.2015.01.058.

[140] Kazuaki Harata. "The Structure of the Cyclodextrin Complex. XXII. Crystal Structures of Hexakis(2,6-di- O -methyl)-α-cyclodextrin Complexes with 1-Propanol and Iodine. Evidence for the Formation of Iodine-Host Charge-Transfer Complex". In: *Bull. Chem. Soc. Jpn.* 63.9 (1990), pp. 2481–2486. DOI: 10.1246/bcsj.63.2481.

[141] Camila Sampaio Mangolim et al. "Curcumin–β-cyclodextrin inclusion complex: Stability, solubility, characterisation by FT-IR, FT-Raman, X-ray diffraction and photoacoustic spectroscopy, and food application". In: *Food Chem.* 153 (2014), pp. 361–370. DOI: 10.1016/j.foodchem.2013.12.067.

[142] Hans-Jörg Schneider et al. "NMR Studies of Cyclodextrins and Cyclodextrin Complexes". In: *Chem. Rev.* 98 (1998), pp. 1755–1785. DOI: 10.1021/cr970019t.

[143] Jennifer S. Brodbelt. “Probing molecular recognition by mass spectrometry”. In: *Int. J. Mass Spectrom.* 200.1-3 (2000), pp. 57–69. DOI: 10.1016/S1387-3806(00)00302-X.

[144] Shibdas Banerjee and Shyamalava Mazumdar. “Electrospray Ionization Mass Spectrometry: A Technique to Access the Information beyond the Molecular Weight of the Analyte”. In: *Int. J. Anal. Chem.* 2012 (2012), pp. 1–40. DOI: 10.1155/2012/282574.

[145] Christoph A. Schalley. “Supramolecular chemistry goes gas phase: The mass spectrometric examination of noncovalent interactions in host-guest chemistry and molecular recognition”. In: *Int. J. Mass Spectrom.* 194.1 (2000), pp. 11–39. DOI: 10.1016/S1387-3806(99)00243-2.

[146] Michael Przybylski and Michael O Glocker. “Electrospray Mass Spectrometry of Biomacromolecular Complexes with Noncovalent Interactions—New Analytical Perspectives for Supramolecular Chemistry and Molecular Recognition Processes”. In: *Angew. Chemie Int. Ed. English* 35 (1996), pp. 806–826. DOI: 10.1002/anie.199608061.

[147] Marco Vincenti. “Special feature: Perspective. Host-guest chemistry in the mass spectrometer”. In: *J. Mass Spectrom.* 30.7 (1995), pp. 925–939. DOI: 10.1002/jms.1190300702.

[148] John B Cunniff and Paul Vouros. “False positives and the detection of cyclodextrin inclusion complexes by electrospray mass spectrometry”. In: *J. Am. Soc. Mass Spectrom.* 6 (1995), pp. 437–447. DOI: 10.1016/1044-0305(95)00053-G.

[149] Konstantin Barylyuk et al. “What Happens to Hydrophobic Interactions during Transfer from the Solution to the Gas Phase? The Case of Electrospray-Based Soft Ionization Methods”. English. In: *J. Am. Soc. Mass Spectrom.* 22 (2011), pp. 1167–1177. DOI: 10.1007/s13361-011-0118-8.

[150] Valérie Gabelica, Nives Galic, and Edwin De Pauw. “On the specificity of cyclodextrin complexes detected by electrospray mass spectrometry”. English. In: *J. Am. Soc. Mass Spectrom.* 13.8 (2002), pp. 946–953. DOI: 10.1016/S1044-0305(02)00416-6.

[151] Judit Sztáray et al. “Leucine enkephalin - A mass spectrometry standard”. In: *Mass Spectrom. Rev.* 30.2 (2011), pp. 298–320. DOI: 10.1002/mas.20279.

[152] Antony Memboeuf et al. “Size effect on fragmentation in tandem mass spectrometry”. In: *Anal. Chem.* 82.6 (2010), pp. 2294–2302. DOI: 10.1021/ac902463q.

[153] Antony Memboeuf et al. “Tandem mass spectrometric analysis of a mixture of isobars using the survival yield technique”. In: *J. Am. Soc. Mass Spectrom.* 22.10 (2011), pp. 1744–1752. DOI: 10.1007/s13361-011-0195-8.

[154] Héloïse Dossmann et al. “First Steps to Rationalize Host-Guest Interaction between α-, β-, and γ-Cyclodextrin and Divalent First-Row Transition and Post-transition Metals (Subgroups VIIB, VIIIB, and IIB)”. In: *Inorg. Chem.* 60.2 (2021), pp. 930–943. DOI: 10.1021/acs.inorgchem.0c03052.

[155] Cédric Przybylski, Véronique Bonnet, and Christine Cézard. “Probing the common alkali metal affinity of native and variously methylated β-cyclodextrins by combining electrospray-tandem mass spectrometry and molecular modeling”. In: *Phys. Chem. Chem. Phys.* 17.29 (2015), pp. 19288–19305. DOI: 10.1039/c5cp02895g.

[156] Xiaoxiao Ma et al. “Gas-phase fragmentation of host-guest complexes between β-cyclodextrin and small molecules.” In: *Talanta* 93 (2012), pp. 252–6. DOI: 10.1016/j.talanta.2012.02.029.

[157] Cédric Przybylski and Véronique Bonnet. “Discrimination of cyclic and linear oligosaccharides by tandem mass spectrometry using collision-induced dissociation (CID), pulsed-Q-dissociation (PQD) and the higherenergy C-trap dissociation modes”. In: *Rapid Commun. Mass Spectrom.* 27.1 (2013), pp. 75–87. DOI: 10.1002/rcm.6422.

[158] David J. Harvey. “Carbohydrate Analysis by ESI and MALDI”. In: *Electrospray and MALDI Mass Spectrometry: Fundamentals, Instrumentation, Practicalities, and Biological Applications: Second Edition*. Ed. by Richard B. Cole. John Wiley and Sons Inc., 2012. Chap. 19, pp. 723–769. ISBN: 9780471741077. DOI: 10.1002/9780470588901.ch19.

[159] David J. Harvey. “Analysis of carbohydrates and glycoconjugates by matrix-assisted laser desorption/ionization mass spectrometry: An update covering the period 1999-2000”. In: *Mass Spectrom. Rev.* 25.4 (2006), pp. 595–662. DOI: 10.1002/mas.20080.

[160] Anne Dell. “F.A.B.-Mass spectrometry of carbohydrates”. In: *Adv. Carbohydr. Chem. Biochem.* 45.C (1987), pp. 19–72. DOI: 10.1016/S0065-2318(08)60136-5.

[161] Liang Han and Catherine E. Costello. “Mass spectrometry of glycans”. In: *Biochem.* 78 (2013), pp. 710–720. DOI: 10.1134/S0006297913070031.

[162] Bo Xie and Catherine E. Costello. “Carbohydrate Structure Determination by Mass Spectrometry”. In: *Carbohydr. Chem. Biol. Med. Appl.* Elsevier Ltd, 2008, pp. 29–57. ISBN: 9780080548166. DOI: 10.1016/B978-0-08-054816-6.00002-1.

[163] L. P. Brüll et al. “Loss of internal 1 → 6 substituted monosaccharide residues from underivatized and per-O-methylated trisaccharides”. In: *J. Am. Soc. Mass Spectrom.* 8.1 (1997), pp. 43–49. DOI: 10.1016/S1044-0305(96)00134-1.

[164] Yuri E.M. Van Der Burgt et al. “FAB CIDMS/MS analysis of partially methylated maltotrioses derived from methylated amylose: A study of the substituent distribution”. In: *Carbohydr. Res.* 329.2 (2000), pp. 341–349. DOI: 10.1016/S0008-6215(00)00187-7.

[165] V. Kováčik et al. “Oligosaccharide characterization using collision-induced dissociation fast atom bombardment mass spectrometry: Evidence for internal monosaccharide residue loss”. In: *J. Mass Spectrom.* 30.7 (1995), pp. 949–958. DOI: 10.1002/jms.1190300704.

[166] Yu Liang Ma et al. “Internal glucose residue loss in protonated O-diglycosyl flavonoids upon low-energy collision-induced dissociation”. In: *J. Am. Soc. Mass Spectrom.* 11.2 (2000), pp. 136–144. DOI: 10.1016/S1044-0305(99)00133-6.

[167] James A. Carroll et al. “Liquid Secondary Ion Mass Spectrometry/Fourier Transform Mass Spectrometry of Oligosaccharide Anions”. In: *Anal. Chem.* 65.11 (1993), pp. 1582–1587. DOI: 10.1021/ac00059a017.

[168] James A. Carroll, Dale Willard, and Carlito B. Lebrilla. “Energetics of cross-ring cleavages and their relevance to the linkage determination of oligosaccharides”. In: *Anal. Chim. Acta* 307.2-3 (1995), pp. 431–447. DOI: 10.1016/0003-2670(94)00514-M.

[169] B.L. Gillece-Castro and A.L. Burlingame. *Oligosaccharide Characterization with High-energy Collision-induced Dissociation Mass Spectrometry.* Vol. 193. C. 1990, pp. 689–712. DOI: 10.1016/0076-6879(90)93445-Q.

[170] Vladimír Kováčik et al. “Liquid Secondary Ion Mass Spectrometry of Methyl Glycosides of Oligosaccharides Using Matrices Containing Carboxamides”. In: *Rapid Commun. Mass Spectrom.* 10.13 (1996), pp. 1661–1667. DOI: 10.1002/(SICI)1097-0231(199610)10:13<1661::AID-RCM680>3.0.CO;2-6.

[171] Guilherme L. Sassaki and Lauro Mera de Souz. “Mass Spectrometry Strategies for Structural Analysis of Carbohydrates and Glycoconjugates”. In: *Tandem Mass Spectrometry - Molecular Characterization*. Ed. by Ana Varela Coelho. InTech, 2013. DOI: 10.5772/55221.

[172] A. Dell et al. “Structure determination of carbohydrates and glycosphingolipids by fast atom bombardment mass spectrometry”. In: *Int. J. Mass Spectrom. Ion Phys.* 46 (1983), pp. 415–418. DOI: 10.1016/0020-7381(83)80140-5.

[173] Sajid Bashir et al. “Matrix-assisted laser desorption/ionisation time-of-flight mass spectrometry. A comparison of fragmentation patterns of linear dextran obtained by in-source decay, post-source decay and collision-induced dissociation and the stability of linear and cyclic”. In: *Eur. J. Mass Spectrom.* 10.1 (2004), pp. 109–120. DOI: 10.1255/ejms.544.

[174] Mark T. Cancilla et al. “Coordination of Alkali Metals to Oligosaccharides Dictates Fragmentation Behavior in Matrix Assisted Laser Desorption Ionization/Fourier Transform Mass Spectrometry”. In: *J. Am. Chem. Soc.* 118.28 (1996), pp. 6736–6745. DOI: 10.1021/ja9603766.

[175] Sung Seen Choi et al. “Comparison of ionization behaviors of ring and linear carbohydrates in MALDI-TOFMS”. In: *Int. J. Mass Spectrom.* 279.1 (2009), pp. 53–58. DOI: 10.1016/j.ijms.2008.10.007.

[176] Marion Rohmer et al. “Fragmentation of neutral oligosaccharides using the MALDI LTQ Orbitrap”. In: *Int. J. Mass Spectrom.* 305.2-3 (2011), pp. 199–208. DOI: 10.1016/j.ijms.2010.11.008.

[177] Bing Guan and Richard B. Cole. “MALDI Linear-Field Reflectron TOF Post-Source Decay Analysis of Underivatized Oligosaccharides: Determination of Glycosidic Linkages and Anomeric Configurations Using Anion Attachment”. In: *J. Am. Soc. Mass Spectrom.* 19.8 (2008), pp. 1119–1131. DOI: 10.1016/j.jasms.2008.05.003.

[178] Tohru Yamagaki, Hiroaki Suzuki, and Kazuo Tachibana. “Semiquantitative analysis of isomeric oligosaccharides by negative-ion mode UV-MALDI TOF postsource decay mass spectrometry and their fragmentation mechanism

study at N-acetyl hexosamine moiety". In: *J. Mass Spectrom.* 41.4 (2006), pp. 454–462. DOI: 10.1002/jms.1001.

[179] David J. Harvey. "Matrix-assisted laser desorption/ionization mass spectrometry of carbohydrates". In: *Mass Spectrom. Rev.* 18.6 (1999), pp. 349–450. DOI: 10.1002/(sici)1098-2787(1999)18:6<349::aid-mas1>3.3.co;2-8.

[180] David J. Harvey. "Analysis of carbohydrates and glycoconjugates by matrix-assisted laser desorption/ionization mass spectrometry: An update for 2013–2014". In: *Mass Spectrom. Rev.* 37.4 (2018), pp. 353–491. DOI: 10.1002/mas.21530.

[181] E.V. Da Costa et al. "Differentiation of isomeric pentose disaccharides by electrospray ionization tandem mass spectrometry and discriminant analysis". In: *Rapid Commun. Mass Spectrom.* 26.24 (2012), pp. 2897–2904. DOI: 10.1002/rcm.6415.

[182] Joseph Zaia. "Mass spectrometry of oligosaccharides". In: *Mass Spectrom. Rev.* 23.3 (2004), pp. 161–227. DOI: 10.1002/mas.10073.

[183] Muchena J. Kailemia et al. "Oligosaccharide analysis by mass spectrometry: A review of recent developments". In: *Anal. Chem.* 86.1 (2014), pp. 196–212. DOI: 10.1021/ac403969n.

[184] M. M. Gaye, R. Kurulugama, and D. E. Clemmer. "Investigating carbohydrate isomers by IMS-CID-IMS-MS: Precursor and fragment ion cross-sections". In: *Analyst* 140.20 (2015), pp. 6922–6932. DOI: 10.1039/c5an00840a.

[185] Christopher John Gray, Isabelle Compagnon, and Sabine L Flitsch. "Mass spectrometry hybridized with gas-phase InfraRed spectroscopy for glycan sequencing". In: *Curr. Opin. Struct. Biol.* 62 (2020), pp. 121–131. DOI: https://doi.org/10.1016/j.sbi.2019.12.014.

[186] Christopher J Gray et al. "Bottom-Up Elucidation of Glycosidic Bond Stereochemistry". In: *Anal. Chem.* 89.8 (2017), pp. 4540–4549. DOI: 10.1021/acs.analchem.6b04998.

[187] Eike Mucha et al. "In-depth structural analysis of glycans in the gas phase". In: *Chem. Sci.* 10.5 (2019), pp. 1272–1284. DOI: 10.1039/c8sc05426f.

[188] Salla Pasanen, Janne Jänis, and Pirjo Vainiotalo. "Cello-, malto- and xylooligosaccharide fragmentation by collision-induced dissociation using QIT and FT-ICR mass spectrometry: A systematic study". In: *Int. J. Mass Spectrom.* 263.1 (2007), pp. 22–29. DOI: 10.1016/j.ijms.2006.12.002.

[189] Lambert C. Ngoka, Carllto B. Lebrilla, and Jean Françols Gal. "Effects of Cations and Charge Types on the Metastable Decay Rates of Oligosaccharides". In: *Anal. Chem.* 66.5 (1994), pp. 692–698. DOI: 10.1021/ac00077a018.

[190] Benjamin J. Bythell et al. "Cationized Carbohydrate Gas-Phase Fragmentation Chemistry". In: *J. Am. Soc. Mass Spectrom.* 28.4 (2017), pp. 688–703. DOI: 10.1007/s13361-016-1530-x.

[191] Parisa Bayat, Denis Lesage, and Richard B. Cole. "Tutorial: Ion Activation In Tandem Mass Spectrometry Using Ultra-High Resolution Instrumentation". In: *Mass Spectrom. Rev.* 39.5-6 (2020), pp. 680–702. DOI: 10.1002/mas.21623.

[192] Sharron G. Penn, Mark T. Cancilla, and Carlito B. Lebrilla. "Collision-Induced Dissociation of Branched Oligosaccharide Ions with Analysis and Calculation of Relative Dissociation Thresholds". In: *Anal. Chem.* 68.14 (1996), pp. 2331–2339. DOI: 10.1021/ac960155i.

[193] Valérie Gabelica and Edwin De Pauw. "Internal energy and fragmentation of ions produced in electrospray sources". In: *Mass Spectrom. Rev.* 24.4 (2005), pp. 566–587. DOI: 10.1002/mas.20027.

[194] Federico Maria Rubino. "Center-of-mass iso-energetic collision-induced decomposition in tandem triple quadrupole mass spectrometry". In: *Molecules* 25.9 (2020). DOI: 10.3390/molecules25092250.

[195] C S Ho et al. "Electrospray ionisation mass spectrometry: principles and clinical applications." In: *Clin. Biochem. Rev.* 24.1 (2003), pp. 3–12.

[196] Bruno Domon and Catherine E. Costello. "A systematic nomenclature for carbohydrate fragmentations in FAB-MS/MS spectra of glycoconjugates". In: *Glycoconj. J.* 5.4 (1988), pp. 397–409. DOI: 10.1007/BF01049915.

[197] J.-L. Chen et al. "Collision-induced dissociation of sodiated glucose and identification of anomeric configuration". In: *Phys. Chem. Chem. Phys.* 19.23 (2017), pp. 15454–15462. DOI: 10.1039/c7cp02393f.

[198] Hsing Ling Cheng and Guor Rong Her. "Determination of linkages of linear and branched oligosaccharides using closed-ring chromophore labeling and negative ion trap mass spectrometry". In: *J. Am. Soc. Mass Spectrom.* 13.11 (2002), pp. 1322–1330. DOI: 10.1016/S1044-0305(02)00528-7.

[199] W. Tüting, R. Adden, and P. Mischnick. "Fragmentation pattern of regioselectively O-methylated maltooligosaccharides in electrospray ionisation-mass spectrometry/collision induced dissociation". In: *Int. J. Mass Spectrom.* 232.2 (2004), pp. 107–115. DOI: 10.1016/j.ijms.2003.12.004.

[200] D. T. Li and G. R. Her. "Structural analysis of chromophore-labeled disaccharides and oligosaccharides by electrospray ionization mass spectrometry and high-performance liquid chromatography/electrospray ionization mass spectrometry". In: *J. Mass Spectrom.* 33.7 (1998), pp. 644–652. DOI: 10.1002/(SICI)1096-9888(199807)33:7<644::AID-JMS667>3.0.CO;2-F.

[201] Sharron G. Penn, Mark T. Cancilla, and Carlito B. Lebrilla. "Fragmentation behavior of multiple-metal-coordinated acidic oligosaccharides studied by matrix-assisted laser desorption ionization Fourier transform mass spectrometry". In: *Int. J. Mass Spectrom.* 195-196 (2000), pp. 259–269. DOI: 10.1016/S1387-3806(99)00169-4.

[202] Balakumar Vijayakrishnan et al. "MSn of the six isomers of $(GlcN)_2(GlcNAc)_2$ aminoglucan tetrasaccharides (diacetylchitotetraoses): Rules of fragmentation for the sodiated molecules and application to sequence analysis of hetero-chitooligosaccharides". In: *Carbohydr. Polym.* 84.2 (2011), pp. 713–726. DOI: 10.1016/j.carbpol.2010.04.041.

[203] Tammy T. Fang and Brad Bendiak. "The Stereochemical Dependence of Unimolecular Dissociation of Monosaccharide-Glycolaldehyde Anions in the Gas Phase: A Basis for Assignment of the Stereochemistry and Anomeric Configuration of Monosaccharides in Oligosaccharides by Mass Spectrometry via". In: *J. Am. Chem. Soc.* 129.31 (2007), pp. 9721–9736. DOI: 10.1021/ja0717313.

[204] Jérôme Lemoine et al. "Collision-induced dissociation of alkali metal cationized and permethylated oligosaccharides: Influence of the collision energy and of the collision gas for the assignment of linkage position". In: *J. Am. Soc. Mass Spectrom.* 4.3 (1993), pp. 197–203. DOI: 10.1016/1044-0305(93)85081-8.

[205] Hsu Chen Hsu et al. "Simple Approach for De Novo Structural Identification of Mannose Trisaccharides". In: *J. Am. Soc. Mass Spectrom.* 29.3 (2018), pp. 470–480. DOI: 10.1007/s13361-017-1850-5.

[206] Jun Xue et al. “Determination of linkage position and anomeric configuration in Hex-Fuc disaccharides using electrospray ionization tandem mass spectrometry”. In: *Rapid Commun. Mass Spectrom.* 18.17 (2004), pp. 1947–1955. DOI: 10.1002/rcm.1573.

[207] Zhongrui Zhou, Sherri Ogden, and Julie A. Leary. “Linkage Position Determination in Oligosaccharides: MS/MS Study of Lithium-Cationized Carbohydrates”. In: *J. Org. Chem.* 55.20 (1990), pp. 5444–5446. DOI: 10.1021/jo00307a011.

[208] Yansheng Liu and David E. Clemmer. “Characterizing oligosaccharides using injected-ion mobility/mass spectrometry”. In: *Anal. Chem.* 69.13 (1997), pp. 2504–2509. DOI: 10.1021/ac9701344.

[209] M.R. Asam and G.L. Glish. “Tandem mass spectrometry of alkali cationized polysaccharides in a quadrupole ion trap”. In: *J. Am. Soc. Mass Spectrom.* 8.9 (1997), pp. 987–995. DOI: 10.1016/S1044-0305(97)00124-4.

[210] David Ashline et al. “Congruent Strategies for Carbohydrate Sequencing. 1. Mining Structural Details by MS n”. In: *Anal. Chem.* 77.19 (2005), pp. 6250–6262. DOI: 10.1021/ac050724z.

[211] Stefan König and Julie A. Leary. “Evidence for linkage position determination in cobalt coordinated pentasaccharides using ion trap mass spectrometry”. In: *J. Am. Soc. Mass Spectrom.* 9.11 (1998), pp. 1125–1134. DOI: 10.1016/S1044-0305(98)00096-8.

[212] Tammy T. Fang, Joseph Zirrolli, and Brad Bendiak. “Differentiation of the anomeric configuration and ring form of glucosyl-glycolaldehyde anions in the gas phase by mass spectrometry: isomeric discrimination between m/z 221 anions derived from disaccharides and chemical synthesis of m/z 221 standards”. In: *Carbohydr. Res.* 342.2 (2007), pp. 217–235. DOI: 10.1016/j.carres.2006.11.021.

[213] Chiharu Konda et al. “Assignment of the Stereochemistry and Anomeric Configuration of Sugars within Oligosaccharides Via Overlapping Disaccharide Ladders Using MSn”. In: *J. Am. Soc. Mass Spectrom.* 25.8 (2014), pp. 1441–1450. DOI: 10.1007/s13361-014-0881-4.

[214] T. Yamagaki, K. Fukui, and K. Tachibana. “Analysis of glycosyl bond cleavage and related isotope effects in collision-induced dissociation quadrupole-time-of-flight mass spectrometry of isomeric trehaloses”. In: *Anal. Chem.* 78.4 (2006), pp. 1015–1022. DOI: 10.1021/ac051334f.

[215] Messele A. Fentabil et al. “Blackbody infrared radiative dissociation of protonated oligosaccharides”. In: *J. Am. Soc. Mass Spectrom.* 22.12 (2011), pp. 2171–2178. DOI: 10.1007/s13361-011-0243-4.

[216] Manfred Wuhrer, André M. Deelder, and Yuri E.M. Van Der Burgt. “Mass spectrometric glycan rearrangements”. In: *Mass Spectrom. Rev.* 30.4 (2011), pp. 664–680. DOI: 10.1002/mas.20337.

[217] Manfred Wuhrer et al. “Mass spectrometry of proton adducts of fucosylated N-glycans: Fucose transfer between antennae gives rise to misleading fragments”. In: *Rapid Commun. Mass Spectrom.* 20.11 (2006), pp. 1747–1754. DOI: 10.1002/rcm.2509.

[218] David J. Harvey et al. ““Internal Residue Loss”: Rearrangements Occurring during the Fragmentation of Carbohydrates Derivatized at the Reducing Terminus”. In: *Anal. Chem.* 74.4 (2002), pp. 734–740. DOI: 10.1021/ac0109321.

[219] Eike Mucha et al. “Fucose Migration in Intact Protonated Glycan Ions: A Universal Phenomenon in Mass Spectrometry”. In: *Angew. Chemie - Int. Ed.* 57.25 (2018), pp. 7440–7443. DOI: 10.1002/anie.201801418.

[220] L. P. Brüll et al. “Sodium-cationized oligosaccharides do not appear to undergo ‘internal residue loss’ rearrangement processes on tandem mass spectrometry”. In: *Rapid Commun. Mass Spectrom.* 12.20 (1998), pp. 1520–1532. DOI: 10.1002/(sici)1097-0231(19981030)12:20<1520::aid-rcm336>3.3.co;2-n.

[221] N. Viseux, E. de Hoffmann, and B. Domon. “Structural Analysis of Permethylated Oligosaccharides by Electrospray Tandem Mass Spectrometry”. In: *Anal. Chem.* 69.16 (1997), pp. 3193–3198. DOI: 10.1021/ac961285u.

[222] Nelly Viseux, Edmond De Hoffmann, and Bruno Domon. “Structural assignment of permethylated oligosaccharide subunits using sequential tandem mass spectrometry”. In: *Anal. Chem.* 70.23 (1998), pp. 4951–4959. DOI: 10.1021/ac980443+.

[223] Hailong Zhang, Suddham Singh, and Vernon N. Reinhold. “Congruent Strategies for Carbohydrate Sequencing. 2. FragLib: An MS n Spectral Library”. In: *Anal. Chem.* 77.19 (2005), pp. 6263–6270. DOI: 10.1021/ac050725r.

[224] Maria Lorna et al. “Cross-Ring Fragmentation Patterns in the Tandem Mass Spectra of Underivatized Sialylated Oligosaccharides and Their Special Suitability for Spectrum Library Searching Experimental Spectrum Library Spectrum 2,4 A 3”. In: *J. Am. Soc. Mass Spectrom* 30 (2019), pp. 426–438. DOI: 10.1007/s13361-018-2106-8.

[225] Cheng Zhu et al. “Energetics of cellulose and cyclodextrin glycosidic bond cleavage”. In: *React. Chem. Eng.* 2.2 (2017), pp. 201–214. DOI: 10.1039/c6re00176a.

[226] Gretchen E. Hofmeister, Zhongrui Zhou, and Julie A. Leary. “Linkage Position Determination in Lithium-Cationized Disaccharides: Tandem Mass Spectrometry and Semiempirical Calculations”. In: *J. Am. Chem. Soc.* 113.16 (1991), pp. 5964–5970. DOI: 10.1021/ja00016a007.

[227] R. Orlando, C. Allen Bush, and C. Fenselau. “Structural analysis of oligosaccharides by tandem mass spectrometry: Collisional activation of sodium adduct ions”. In: *Biol. Mass Spectrom.* 19.12 (1990), pp. 747–754. DOI: 10.1002/bms.1200191202.

[228] Alexander O. Chizhov, Yury E. Tsvetkov, and Nikolay E. Nifantiev. “Gas-phase fragmentation of cyclic oligosaccharides in tandem mass spectrometry”. In: *Molecules* 24.12 (2019), p. 2226. DOI: 10.3390/molecules24122226.

[229] Jordan M. Rabus et al. “Unravelling the structures of sodiated β-cyclodextrin and its fragments”. In: *Phys. Chem. Chem. Phys.* 23.24 (2021), pp. 13714–13723. DOI: 10.1039/d1cp01058a.

[230] Wanghui Wei et al. “Quantifying non-covalent binding affinity using mass spectrometry: A systematic study on complexes of cyclodextrins with alkali metal cations”. In: *Rapid Commun. Mass Spectrom.* 29.10 (2015), pp. 927–936. DOI: 10.1002/rcm.7181.

[231] Rafał Frański et al. “Mass spectrometric decompositions of cationized β-cyclodextrin”. In: *Carbohydr. Res.* 340.8 (2005), pp. 1567–1572. DOI: 10.1016/j.carres.2005.03.014.

[232] Eric C. Huang and Jack D. Henion. “Characterization of cyclodextrins using ion-evaporation atmospheric-pressure ionization tandem mass spectrometry”. In: *Rapid Commun. Mass Spectrom.* 4.11 (1990), pp. 467–471. DOI: 10.1002/rcm.1290041103.

[233] Xiao Dan He et al. “Investigation on non-covalent complexes of cyclodextrins with Li + in gas phase by mass spectrometry”. In: *Chinese J. Chem. Phys.* 26.3 (2013), pp. 287–294. DOI: 10.1063/1674-0068/26/03/287-294.

[234] Soonmin Jang and Sung Seen Choi. “Characterization of the fragmentation behaviors of protonated α-cyclodextrin generated by electrospray ionization”. In: *Rapid Commun. Mass Spectrom.* 35.2 (2021), e8967. DOI: 10.1002/rcm.8967.

[235] McDonald Donkuru et al. “Multi-stage tandem mass spectrometric analysis of novel β-cyclodextrin-substituted and novel bis-pyridinium gemini surfactants designed as nanomedical drug delivery agents”. In: *Rapid Commun. Mass Spectrom.* 28.7 (2014), pp. 757–772. DOI: 10.1002/rcm.6827.

[236] Cristian Peptu et al. “Structural architectural features of cyclodextrin oligoesters revealed by fragmentation mass spectrometry analysis”. In: *Molecules* 23.9 (2018), p. 2259. DOI: 10.3390/molecules23092259.

[237] A. O. Chizhov et al. “Gas-phase fragmentation studies of cyclic oligo-β-(1→6)-D-glucosamines by electrospray ionization mass spectrometry using a hybrid high-resolution mass spectrometer”. In: *Russ. Chem. Bull.* 67.1 (2018), pp. 144–149. DOI: 10.1007/s11172-018-2050-6.

[238] Stefano Sforza et al. “ESI-mass spectrometry analysis of unsubstituted and disubstituted β-cyclodextrins: Fragmentation mode and identification of the AB, AC, AD regioisomers”. In: *J. Am. Soc. Mass Spectrom.* 14.2 (2003), pp. 124–135. DOI: 10.1016/S1044-0305(02)00853-X.

[239] David Bongiorno et al. “Guest-to-host proton transfer in melatonin-β-cyclodextrin inclusion complex by ionspray, fast atom bombardment and tandem mass spectrometry”. English. In: *J. Mass Spectrom.* 36 (2001), pp. 1189–1194. DOI: 10.1002/jms.226.

[240] Antonio Selva et al. “A study of β-cyclodextrin and its inclusion complexes with piroxicam and terfenadine by ionspray mass spectrometry”. In: *Org. Mass Spectrom.* 28.9 (1993), pp. 983–986. DOI: 10.1002/oms.1210280909.

[241] Arthur T. Blades, Michael G. Ikonomou, and Paul Kebarle. “Mechanism of Electrospray Mass Spectrometry. Electrospray as an Electrolysis Cell”. In: *Anal. Chem.* 63.19 (1991), pp. 2109–2114. DOI: 10.1021/ac00019a009.

[242] Royal Society of Chemistry. *Experimental reporting requirements.*

[243] David J. Harvey. "Collision-induced fragmentation of underivatizedN-linked carbohydrates ionized by electrospray". In: *J. Mass Spectrom.* 35.10 (2000), pp. 1178–1190. DOI: 10.1002/1096-9888(200010)35:10<1178::AID-JMS46>3.0.CO;2-F.

[244] Ayako Kurimoto et al. "Analysis of Energy-Resolved Mass Spectra at MS n in a Pursuit To Characterize Structural Isomers of Oligosaccharides". In: *Anal. Chem.* 78.10 (2006), pp. 3461–3466. DOI: 10.1021/ac0601361.

[245] Vivien F. Taylor et al. "A mass spectrometric study of glucose, sucrose, and fructose using an inductively coupled plasma and electrospray ionization". In: *Int. J. Mass Spectrom.* 243.1 (2005), pp. 71–84. DOI: 10.1016/j.ijms.2005.01.001.

[246] Pia S. Bruni and Stefan Schürch. "Fragmentation mechanisms of protonated cyclodextrins in tandem mass spectrometry". In: *Carbohydr. Res.* 504 (2021). DOI: 10.1016/j.carres.2021.108316.

[247] Thermo Fisher Scientific. *Normalized Collision EnergyTM Technology.* Tech. rep.

[248] Adrien Nyakas et al. "OMA and OPA - Software-supported mass spectra analysis of native and modified nucleic acids". In: *J. Am. Soc. Mass Spectrom.* 24.2 (2013), pp. 249–256. DOI: 10.1007/S13361-012-0529-1/FIGURES/10.

[249] Janna Anichina and Diethard K Bohme. "Mass-Spectrometric Studies of the Interactions of Selected Metalloantibiotics and Drugs with Deprotonated Hexadeoxynucleotide GCATGC". In: *J. Phys. Chem. B* 113 (2009), pp. 328–335. DOI: 10.1021/jp807034v.

[250] Tzipporah M Kertesz et al. "CE50: Quantifying Collision Induced Dissociation Energy for Small Molecule Characterization and Identification". In: *J. Am. Soc. Mass Spectrom.* 20.9 (2009), pp. 1759–1767. DOI: 10.1016/j.jasms.2009.06.002.

[251] Françoise Rogalewicz, Yannik Hoppilliard, and Gilles Ohanessian. "Fragmentation mechanisms of α-amino acids protonated under electrospray ionization: A collisional activation and ab initio theoretical study". In: *Int. J. Mass Spectrom.* 195-196 (2000), pp. 565–590. DOI: 10.1016/S1387-3806(99)00225-0.

[252] Charlotte Møller et al. "Determination of the binding sites for oxaliplatin on insulin using mass spectrometry-based approaches". In: *Anal. Bioanal. Chem.* 401.5 (2011), pp. 1623–1633. DOI: 10.1007/s00216-011-5239-1.

[253] Wenjiang Zhang, Lesley Seymour, and Eric X. Chen. "Determination of intact oxaliplatin in human plasma using high performance liquid chromatography-tandem mass spectrometry". In: *J. Chromatogr. B* 876.2 (2008), pp. 277–282. DOI: 10.1016/J.JCHROMB.2008.10.055.

[254] Ida Ritacco et al. "Fragmentation pathways analysis for the gas phase dissociation of protonated carnosine-oxaliplatin complexes". In: *Dalt. Trans.* 44.10 (2015), pp. 4455–4467. DOI: 10.1039/c4dt02217c.

[255] A. F. Hollemann and Egon Wiberg. *Lehrbuch der Anorganischen Chemie*. 102nd ed. Berlin: Walter de Gruyter & CO., 1960. ISBN: 978-3-11-017770-1.

[256] Lara Nadine Maeder. "Tandem mass spectrometry to compare different host-guest interactions with cyclodextrins as hosts". PhD thesis. University of Bern, 2020, p. 50.

[257] Pia S. Bruni and Stefan Schürch. "Mass spectrometric evaluation of β-cyclodextrins as potential hosts for titanocene dichloride". In: *Int. J. Mol. Sci.* 22.18 (2021), p. 9789. DOI: 10.3390/ijms22189789.

[258] Yannis Dotsikas and Yannis L. Loukas. "Efficient determination and evaluation of model cyclodextrin complex binding constants by electrospray mass spectrometry". In: *J. Am. Soc. Mass Spectrom.* 14 (2003), pp. 1123–1129. DOI: 10.1016/S1044-0305(03)00451-3.

[259] Thermo Fisher Scientific. *LTQ Series Hardware Manual*. Tech. rep. 2015.

[260] Thermo Fisher Scientific. *LTQ Orbitrap XL Hybrid FT Mass Spectrometer*. Tech. rep. 2016.

[261] Valentino J. Stella et al. "Mechanisms of drug release from cyclodextrin complexes". In: *Adv. Drug Deliv. Rev.* 36 (1999), pp. 3–16. DOI: 10.1016/S0169-409X(98)00052-0.

Erklärung

gemäss Art. 18 PromR Phil.-nat. 2019

Name/Vorname: Bruni Pia Simona

Matrikelnummer: 13-123-963

Studiengang: PhD of Science in Chemie und Molekulare Wissenschaften

Bachelor ☐ Master ☐ Dissertation ☑

Titel der Arbeit: Aspects of Cyclodextrin Host-Guest Complexes in Mass Spectrometry

LeiterIn der Arbeit: Prof. Dr. Stefan Schürch

Ich erkläre hiermit, dass ich diese Arbeit selbständig verfasst und keine anderen als die angegebenen Quel-len benutzt habe. Alle Stellen, die wörtlich oder sinn-gemäss aus Quellen entnommen wurden, habe ich als solche gekennzeichnet. Mir ist bekannt, dass andern-falls der Senat gemäss Artikel 36 Absatz 1 Buchstabe r des Gesetzes über die Universität vom 5. September 1996 und Artikel 69 des Universitätssta-tuts vom 7. Juni 2011 zum Entzug des Doktortitels be-rechtigt ist.
Für die Zwecke der Begutachtung und der Überprüfung der Einhaltung der Selbständigkeitserklärung bzw. der Reglemente betreffend Plagiate erteile ich der Univer-sität Bern das Recht, die dazu erforderlichen Perso-nendaten zu bearbeiten und Nutzungshandlungen vor-zunehmen, insbesondere die Doktorarbeit zu vervielfäl-tigen und dauerhaft in einer Datenbank zu speichern sowie diese zur Überprüfung von Arbeiten Dritter zu verwenden oder hierzu zur Verfügung zu stellen.

Bern, 11.03.2022

Ort/Datum

P. Bruni

Unterschrift